Mesozoic Detrital Zircon Provenance of Central Africa: Implications for Jurassic-Cretaceous Tectonics, Paleogeography and Landscape Evolution.

Thesis Submitted by

Prince C. Owusu Agyemang (BSc, MSc, BGeoHons)

December 2018

For the degree of:

Doctorate of Philosophy

In the:

Department of Geosciences

College of Science and Engineering

Statement of Access

I, the undersigned author of this thesis, understand that James Cook University will make this thesis available for use within the university library and allow access in other approved libraries after its submission. All users consulting this thesis will have to sign the following statement:

In consulting this thesis I agree not to copy or closely paraphrase it in whole or in part without the written consent of the author; and to make proper public written acknowledgement for any assistance which I have obtained from it.

Beyond this, I do not wish to place any restriction on access to this thesis.

Prince C. Owusu Agyemang

December 2018.

Declaration

I declare that this thesis is my own work and has not been submitted in any form for another degree or diploma at any university or other institution or tertiary education. Information derived from the published or unpublished work of others has been acknowledged in the text and a list of references is given.

Prince C. Owusu Agyemang

December 2018.

Every reasonable effort has been made to gain permission and acknowledge the owners of copyright material. I would be pleased to hear from any copyright owner who has been omitted or incorrectly acknowledged.

Statement on the contribution of others

Nature of Assistance	Contribution	Names & affiliations of co-contributors
Intellectual support	Supervision	Assoc. Prof. Eric M. Roberts, JCU Assoc. Prof. Carl J Spandler, JCU
	Proposal writing	Assoc. Prof. Eric M. Roberts, JCU
	Data analysis	Assoc. Prof. Eric M. Roberts, JCU Dr. Richard Wormald, JCU Assoc. Prof. Carl J Spandler, JCU Dr. Cassian Pirard, JCU Dr. Ioan Sanislov, JCU
	Editorial assistance	Assoc. Prof. Eric M. Roberts, JCU Dr. Ioan Sanislov, JCU
Financial support	Research funding	Assoc. Prof. Eric M. Roberts, JCU De Beers Group Exploration, Bowleven Oil Plc, Adamantine Energy
	Stipend	Australian Government Research Training Program Scholarship Bowleven Oil Plc, Adamantine Energy
Analytical support		Assoc. Prof. Eric M. Roberts, JCU Assoc. Prof. Carl J Spandler, JCU

Statement of Contribution

Chapter	Publication on which chapter is based	Nature and extent of intellectual input
2	Owusu Agyemang, P. C., Roberts, E. M., and Jelsma, H. A. (2016). Late Jurassic-Cretaceous fluvial evolution of central Africa: insights from the Kasai-Congo Basin, Democratic Republic Congo. *Cretaceous Research.*	Assoc. Prof. Eric M. Roberts contributed to the initial concept development, preliminary data analysis and provided editorial assistance. Dr. Hielke A. Jelsma contributed to the sample acquisition, primary discussion and provided editorial assistance.
3	Owusu Agyemang, P. C., Roberts, E. M., Joy, S., and Jelsma, H. A. (In prep). Detrital zircon provenance analysis of the diamondiferous mid-Cretaceous Calonda Formation, northeastern Angola.	Assoc. Prof. Eric M. Roberts contributed to the initial concept development, provided feedback on the discussion and provided editorial assistance.

		Dr. Hielke A. Jelsma contributed to the sample acquisition, primary discussion, data analysis and provided editorial assistance. Dr. Joy Sojen contributed to sample acquisition, data analysis and provided editorial assistance.
4	Owusu Agyemang, P. C., Roberts, E. M., Downie, B., and Sertich, J. J. W. (2018). Sedimentary provenance and maximum depositional age analysis of the Cretaceous? Lapur and Muruanachok sandstones (Turkana Grits), Turkana Basin, Kenya. *Geological Magazine*	Assoc. Prof. Eric M. Roberts contributed to the initial concept development, provided feedback on the discussion and provided editorial assistance. Mr. Bob Downie contributed to the fieldwork and sampling, primary discussion, data analysis and provided editorial assistance. Dr. Joseph J. W. Sertich contributed to the discussion of the vertebrate fossil record and provided editorial assistance.
5	Owusu Agyemang, P. C., Roberts, E. M., Bussert, R., Evans, D., and Müller, J. (accepted; *Cretaceous Research*). U-Pb detrital zircon constraints on the depositional age and provenance of the dinosaur-bearing mid-Late Cretaceous Wadi Milk Formation of Sudan.	Assoc. Prof. Eric M. Roberts contributed to the primary discussion, data analysis and provided editorial assistance. Dr. Robert Bussert contributed to the fieldwork, sampling and provided editorial assistance. Assoc. Prof. David Evans and Dr. Johannes Müller also contributed to the fieldwork, sampling and discussion of the vertebrate fossil record.
6	Owusu Agyemang, P. C., and Roberts, E. M. (*In prep*). Paleogeographic and drainage evolution of Mesozoic central Africa: Insights from U-Pb detrital zircon geochronology and Lu-Hf isotope geochemistry.	Assoc. Prof. Eric M. Roberts contributed to some of the data analysis and provided editorial assistance.

Acknowledgements

To God be the all the glory, great things he has done and greater things will he do. Amen. This thesis would not have been possible without the help and support of many people, especially my primary supervisor Assoc. Prof. Eric M. Roberts. I am most grateful to Eric, who is also the 'supreme' leader of the Gravel Monkeys Sedimentology Research Group at James Cook University for the opportunity, steadfast support and guidance throughout this thesis. I am also thankful to him for giving me the opportunity to teach and demonstrate for the undergraduate sedimentology and energy resources classes. I also thank all the gravelmonkeys, past and present for the discussion of ideas and friendship. My co-supervisor Assoc. Prof. Carl J Spandler is also gratefully acknowledged for providing insights into the meaning of the geochemistry data for this thesis.

This thesis also benefited from the Australian Government Research Training Program Scholarship, which was administered by the Graduate Research School and it is gratefully acknowledged. This project was also partly funded by industry colloborators, who provided samples and funds for analysis. De Beers Group Services are acknowledged for their collaboration and provision of samples for both the Democratic Republic of Congo and Angola chapters of this thesis. The Head of De Beers is especially thanked for permission to publish the results of these two chapters in peer-review journals. Bowleven Oil and Gas plc, and Adamantine Energy Limited are gratefully acknowledged for providing samples and funding for the Kenya chapter, and for permission to publish the results in peer-review journal.

Deutsche Forschungsgemeinschaft (DFG, Mu 1760/6-1) and the Royal Ontario Museum, are gratefully acknowledged for financially supporting fieldwork in Sudan on the Wadi

Milk Formation. Dr. Brigitte Cech of the Qatar-Sudan Archaeology Project (Mission 037) is gratefully acknowledged for collecting the Shendi (Sudan) Formation samples.

I am grateful to Dr. Cassian Pirrard (*formally of* JCU), for teaching me how to prepare petrographic thin sections for my Angola samples included in this thesis. I am also thankful to Michael S. Hayford and Teirmoor N. Dehkordi, both colleagues at JCU for sacrifing their time to sit with me during many after-hours LA-ICP-MS analysis. A big thank you also to the staff of the Advanced Analytical Centre also at JCU, especially Dr. Yi Hu, Dr. Kevin Blake and Dr. Shane Askew for their assistance with zircon imaging, U-Pb age dating, Lu-Hf isotope and trace elelment geochemistry. Dr. Richard Wormald (*formally of* JCU) is thanked for showing how to reduce my first U-Pb data files using Glitter software and for technical assistance with minerals separation. I acknowledge Dr. Rob Holm (JCU) for assisting with figure design for DRC manuscript. Dr. Ioan Sanislov is especially thanked for showing how to process the Lu-Hf isotope data. Dr. Isaac Corral Calleja, Jaime Poblete Alvarado and Dr. Yanbo Cheng (JCU) are acknowledged for their assistance in processing the zircon trace elements data used. I am also grateful to all the current and former staff of Geosciences, College of Science and Engineering, and the Graduate Research School, especially Prof. Paul Dirks, Dr. Jan Huizenga, Dr. Huang (Jeffrey) Huiqing, Rebecca Steele, Judy Botting, Jo Scheffler, Alaina Jones, Beth Moore, Melissa Norton and Andrew Norton for the technical, administrative and IT support.

I also want to acknowledge a number of collaborators I have worked with and come to admire for their expertise and love for the geosciences during the course of this thesis. Mr. Bob Downie (Bowleven Oil plc and Heritage Oil Ltd), whose critical questions and reviews gave me a deeper understanding of the geology of the Turkana Basin in Kenya. I

am grateful to Dr. Joseph J. W. Sertich (Denver Museum of Nature & Science) for providing some paleontological contex for the Lapur Sandstone in the Turkana Basin (Kenya). I am very thankful to Dr. Robert Bussert (Technical University of Berlin), for his timely response to my quries on the geology of the Wadi Milk and Shendi formations, and for his assistance on figure design for the Sudan manuscript. Dr. Hielke Jelsma (AngloGold American) is gratefully acknowledged for availing his technical expertise on the geology of the DRC and Angola to me during this thesis. I am also thankful to Dr. Sojen Joy of Debeers Group for facilitating a smooth running of Angola Project-1 (Angola Chapter) and for helping to secure samples and funds for Angola Project-2 (not part of this theis). I am also grateful to both Dr. David Evans (Royal Ontario Museum) and Dr. Johannes Müller (Museum für Naturkunde) for their constructive comments that helped to improve the quality of the Sudan manuscript, and for helping to put the new age of the Wadi Milk Formation in the proper paleontological context.

Finally, I say a big thank you to my family and friends for their immense sacrifice and support. To my brother and friend Dr. Collins Ameyaw (Kumasi Technical University), I say thank you for your great help to me. To my sweet wife, Mrs Rebecca E. Owusu Agyemang, I say '*many women do noble things, but you surpass them all*' *Proverbs 31:29.* Thank you Esi for your support and sacrifice, I am forever grateful. To my children: Michelle Abena Owusu Agyemang, Sophie Akosua Owusu Agyemang and Joshua Kwaku Owusu Agyemang, thank you very much for your love and support. I love you all.

Thesis Abstract

Jurassic-Cretaceous tectonics, paleogeography and sedimentary provenance of central Africa are poorly constrained and continue to be debated. The lack of constraints on the timing and controls on late Mesozoic sedimentary basin development, drainage evolution and paleoenvironments is problematic because central Africa is well endowed with natural resources, and good understanding of these issues is fundamental to a better assessment of hydrocarbon and alluvial diamond exploration targeting. Moreover, by improving our understanding of Mesozoic strata across this vast region, we can also help to contextualise the ecological and evolutionary relationships of floras and faunas from central Africa with contemporary floras and faunas from different parts of Africa and throughout Gondwana. In particular, refining the depositional age of late Mesozoic units is key to understanding and reconstructing regional paleogeography and drainage patterns during this poorly resolved time period in Africa, which also furthers our understanding of the origins and dispersal pathways for Mesozoic, Cenozoic and modern African floras and faunas, as well as economically significant alluvial mineral resources, such as diamonds, that are important to the economies of this part of the world.

To address these issues a detailed and multifaceted sedimentary provenance analysis of 14 late Mesozoic units from seven sedimentary basins across central Africa (spanning seven different countries) was conducted. This integrated sedimentological approach incorporated sandstone petrography, paleocurrent analysis, U-Pb detrital zircon geochronology, Lu-Hf isotope and trace element geochemistry to investigate Jurassic and Cretaceous continental deposits from central Africa. The main objective was to investigate late Mesozoic sedimentary basin development, drainage evolution and provide

constraints on the age of deposition, sediment source and paleofluvial drainage patterns, using core and outcrop samples from across the region; including Democratic Republic of Congo (DRC), Kenya, Angola, Sudan, Tanzania, Zimbabwe and Malawi.

Sandstone petrography and paleocurrent data indicate mixed sediment sources mainly to the south of study areas. Maximum depositional age analyses performed on U-Pb detrital zircon sample results demonstrate that most of the late Mesozoic units in central Africa are younger than previously accepted. Detrital zircon provenance analysis points to primary contributions from Neoproterozoic Pan-African Mobile Belts (e.g., Mozambique and Zambezi belts), which were probably exposed at this time are the dominant (>75%). The Lu-Hf isotope geochemistry results also show a mixed sediment provenance consisting of juvenile mantle and reworked crustal sources, which corroborates the sandstone petrography results. Western areas of central Africa (e.g. DRC and Angola) are dominated by sediments from reworked crustal sources, whereas eastern parts of central Africa (e.g. Sudan, Kenya and Tanzania) are dominated by sediments of juvenile mantle sources. The results further suggest a pattern of large ephemeral lakes in the Middle Jurassic to Early Cretaceous in the Congo and Zambezi basins, followed by the development of a large, dominantly north directed fluvial systems across central Africa in the middle Cretaceous. The results are supportive of a uniform northward continental drainage pattern throughout late Mesozoic, which supports the assertion that the paleo-Congo drainage system was likely north flowing, rather than east flowing out of the Congo Basin and into Indian Ocean as previously suggested. The results of this thesis are also supportive of the hypothesis of a major drainage divide between southern and central Africa during the late Mesozoic and the concept of a major NW trending fluvial drainage pattern into the shear zones within the Central African Rift System, although the ultimate

depocentre still remains uncertain. The maximum depositional age of three Cretaceous sedimentary units, including the dinosaur-bearing Wadi Milk Formation of Sudan has been constrained. The new ages shows a generally much younger age of deposition than previous assignations, calling into question the reliability of these overly broad biostratigraphic age for these important sedimentary units.

Table of Contents

Contents of Digital Appendices

Chapter 2

Appendix 2S1 – Detrital modes for the Kasai sandstones (DRC)

Appendix 2S2 – All U-Pb age data for the Kasai sandstones (DRC)

Appendix 2S3 – Lu–Hf isotopic data for Kasai sandstones (DRC)

Chapter 3

Appendix 3S1 – All U-Pb age data for the Calonda Formation, Angola

Appendix 3S2 – Lu–Hf isotopic data for the Calonda Formation, Angola

Appendix 3S3 - Zircon trace element data for the Calonda Formation, Angola

Chapter 4

Appendix 4S1 – All U-Pb age data for the Lapur and Muruanachok sandstones, Kenya

Appendix 4S2 – Lu–Hf isotopic data for the Lapur and Muruanachok sandstones, Kenya

Appendix 4S3 - Zircon trace element data for the Lapur and Muruanachok sandstones, Kenya

Chapter 5

Appendix 5S1 – All U-Pb age data for the Wadi Milk and Shendi formations, Sudan

Appendix 5S2 – Lu–Hf isotopic data for the Wadi Milk and Shendi formations, Sudan

Appendix 5S3 - Zircon trace element data for the Wadi Milk and Shendi formations, Sudan

Chapter 6

Appendix 6S1A – All U-Pb age data for the detrital samples from Tendaguru Formation, Tanzania,

Appendix 6S1B –Cuvette Centrale and Kwango Area, DRC from Linol et al. (2016)

Appendix 6S1C – U-Pb age data for the detrital samples from Zimbabwe

Appendix 6S1D – U-Pb age data for the detrital samples from Malawi.

Appendix 6S2 – Lu–Hf isotopic data for Tendaguru Formation, Tanzania.

List of figures

List of Tables

List of Published Papers

Appendix 1

Late Jurassic-Cretaceous fluvial evolution of central Africa: Insights from the Kasai-Congo Basin, Democratic Republic Congo (*Cretaceous Research, 2016*)

Appendix 2

Sedimentary provenance and maximum depositional age analysis of the Cretaceous? Lapur and Muruanachok sandstones (Turkana Grits), Turkana Basin, Kenya (*Geological Magazine, 2018*)

1. CHAPTER ONE

Thesis introduction

1.1 Background and introduction

Late Mesozoic tectonics, sedimentary provenance and drainage evolution in Africa is a topic of considerable interest (e.g. Partridge and Maud, 1987; Thomas and Shaw, 1988; Shaw and Thomas, 1992; Shaw et al., 1992; Partridge, 1998; Moore, 1999; Moore and Larkin, 2001; Goudie, 2005; Stankiewicz and de Wit, 2006; Moore et al., 2009, 2012; Roberts et al., 2012). The quest to resolve the timing and controls on late Mesozoic tectonics, sedimentary basin development, drainage patterns and paleoenvironments in Africa is particularly important for evaluating regional hydrocarbon prospectivity and for identifying the sources and genesis of kimberlites and alluvial diamonds, particularly in central Africa (Burke, 1996, 2003; Mathu and Davies, 1996; Censier and Lang 1999; Moore, 1999; Moore and Larkin, 2001; Goudie, 2005; Guiraud et al., 2005; Mahaney et al., 2012). Better constraints on drainage patterns can also improve our understanding of the paleogeography of Africa during this time, and in effect help us to contextualise ecological, biogeographic and evolutionary relationships between floras and faunas in different parts of Africa and Gondwana (e.g., Jacobs et al., 2009; O'Connor et al., 2006, 2010, and 2011).

The evolution of late Mesozoic to Cenozoic drainage patterns in southern Africa is generally well understood (e.g. Goudie, 2005). Landscape and paleodrainage evolution studies in southern Africa have largely centred on the roles played by mantle hot spots and far-field stresses resulting from plate tectonics (e.g. Partridge and Maud, 1987; Partridge, 1998; Moore and Blenkinsop, 2002; Goudie, 2005; Moore et al., 2009). However, paleodrainage evolution of central Africa remains less well-constrained, as highlighted by two contrasting drainage models (Stankiewicz and de Wit, 2006; Roberts et al., 2012).

In central Africa, investigations in the Congo Basin by Stankiewicz and de Wit (2006) found evidence for two remnant peneplain surfaces, which they used to propose an eastward flowing paleo-Congo River that emptied into the Indian Ocean. They propose this paleo-Congo River was flowing out of the Congo Basin through the present Lualabua River drainage, which then cut across the Rukwa Rift system, linking up with northward tributaries coming out of the modern Chambeshi and Luangwa drainages, and ultimately exiting through the Ruaha Gorge into Rufiji delta during the Late Cretaceous-Paleogene. This hypothesis was in part developed as an explanation for why the Rufiji Delta is too large to be explained by modern drainage patterns. In contrast to the east flowing paleo-Congo River model, Roberts et al. (2012), who examined provenance and paleocurrent data from the northern Malawi and Rukwa Rift basins, found little support for eastward flow out of the Congo Basin. Instead, they found strong evidence for consistent NW paleoflow. They interpreted the Rukwa Rift Basin (formed along the Ubendian Shear zone) to have been the axis for a major trans-continental drainage system extending from northern Malawi and ultimately draining into the Congo Basin. They utilised detrital zircon provenance to demonstrate dominantly Irumide Belt and Pan-African Mozambique belt sources in the southern highlands of Zambezi and Malawi, which were drained by a long-lived fluvial system that flowed along the axes of the Rukwa and southern Tanganyika rifts. This trans-continental river, they posited, may have emptied into a paleo-lake or continued flowing across the Congo Basin and probably into the Doba Trough. Moreover, they demonstrated a complete lack of Kibaran Belt (~1400 Ma) provenance in the Cretaceous Red Sandstone Group, as would be expected from the East flowing Congo River model. Although both Stankiewicz and de Wit (2006) and Roberts et al. (2012) have each provided lines of evidence to interpret late Mesozoic-Cenozoic

paleo-river drainage evolution in central Africa, the paucity of data from other portions of central Africa has limited efforts to fully interrogate these hypotheses.

The lack of constraints on drainage evolution in central Africa can largely be linked to the poor age and stratigraphic control of continental sedimentary units of late Mesozoic age. The limited understanding of the late Mesozoic stratigraphy and poor age control of sedimentary units in central Africa continues to pose a major challenge for the exploration and mining of precious metals and gems, as it makes it difficult to track sediments to their sources (Marshall and Baxter-Brown, 1995; Patyk-Kara, 2002; Pervov et al., 2011; Bata et al., 2016). The lack of understanding of Mesozoic and Cenozoic strata has also hampered hydrocarbon exploration of rift basins in central Africa (e.g. Bosworth, 1992; Burke, 1996, Burke et al, 2003). Furthermore, the dispersion and paleobiogeographic relationships of Mesozoic floras and faunas, with respect to other Gondwanan floras and faunas, is limited by poor age control and stratigraphy.

Most of the previous attempts to understand drainage evolution on the African continent are largely based on the concepts of long-lived erosional surfaces, present-day geomorphology and timing of tectonic events (e.g. King 1963; Partridge and Maud, 1987; Moore and Larkin, 2001), however, geological methods for evaluating sedimentary provenance and reconstructing drainage patterns, involving framework petrography, facies and paleocurrent analysis, and U-Pb detrital zircon geochronology has only seen limited application in central Africa to date (e.g., Roberts et al., 2012; Linol et al., 2016). Reconstruction of Mesozoic drainage evolution of central Africa has proven difficult for a number of other reasons including lack of access to proprietary industry data, and limited outcrop exposure in key regions (e.g. Daly et al, 1992). Moreover, much of the existing

work on Mesozoic tectonics and paleodrainage evolution is based on geomorphic concepts and the identification of peneplain surfaces suggesting that the African landscape is very old and experienced periods of long quiescence and deep weathering; a product of Cretaceous erosion (i.e., African Erosion Surfaces concepts of King, 1963). However, outside of southern Africa,, limited sedimentologic investigations of these rare Jurassic and Cretaceous exposures across central Africa have been performed since the early colonial geological survey investigations in the early to mid-1900's (Giresse, 2005). Hence, modern approaches to sedimentology and sedimentary provenance analysis (e.g. U-Pb geochronology), as presented in this thesis, have yet to be applied to many of the sedimentary basins and deposits across central Africa.

Attempts to provide constraints on the stratigraphy of sedimentary units dates back to the 1920s, which commenced from survey style work and paleontological exploration in Tanzania, Malawi, Cameroon and Kenya. This was followed by more focused hydrocarbon explorations in the 1980s and 1990s and alluvial diamond and kimberlite investigation (e.g. Partridge, 1998; Purcell, 2014, 2017). Thus, the geological data arising from such investigations are largely proprietary (e.g. Purcell, 2017). Moreover, the age of the sedimentary units where these important fossils were recovered remains vaguely characterized in many cases (e.g. Klitzsch & Wycisk, 1987; Flynn et al., 1988; Jacobs et al., 1990; Gomani, 1997; Kruse et al., 1997; Heinrich, 1999; O'Connor et al., 2006, Roberts et al., 2010; Gorscak et al., 2014). These fossils although limited are important as they have played a significant role in our understanding of the geological, biological and paleontological history of Mesozoic Africa (e.g. Sereno, 1994). Mateer et al. (1992) presented an inter-regional correlation of non-marine Cretaceous units across the Africa and the Middle East in an attempt to correlate similar units. One of the main

challenges for these authors was that the ages of most of the Cretaceous strata are vague due mainly to imprecise biostratigraphy.

The main aim of this thesis was to investigate the Mesozoic detrital zircon provenance of central Africa and its implications to Jurassic-Cretaceous tectonics, paleogeography and landscape evolution. In order to accomplish this objective, an integrated approach incorporating a combination of sandstone petrography, paleocurrent analysis, U-Pb detrital zircon geochronology, Lu-Hf isotope and trace element geochemistry to investigate Jurassic and Cretaceous continental deposits from central Africa. Core and outcrop samples from across the region, including DRC, Kenya, Angola Sudan, Tanzania, Zimbabwe and Malawi were investigated. Specific objectives and detailed methodology are listed in the individual data chapters.

Advances in U-Pb detrital zircon geochronology and its applications to geologic problems over the last two decades, has proved particularly useful in solving geologic problems, particularly stratigraphy and tectonic reconstructions (Fedo et al., 2003; Griffin et al., 2003, 2004; Carrapa, 2010; Cawood, et al., 2012; Gehrels, 2014). The application of U-Pb detrital zircon geochronology to estimate the maximum depositional age of different stratigraphic units has proven invaluable, especially for continental sedimentary strata with dearth of fossils or vague biostratigraphy (Dickinson and Gehrels, 2009; Jinnah et al., 2009). Dating of detrital minerals such as zircon is extremely useful for obtaining geologic and tectonic information about source rocks from which the zircons were derived, such as age, unknown magmatic and metamorphic events (e.g. Griffin et al. 2004; Carrapa, 2010). U-Pb zircon geochronology has been used extensively for sedimentary basin analysis and reconstructing ancient paleodrainage patterns for large

areas in North America (e.g. Sears 2014; Blum and Pecha, 2014), South America (e.g. Solari et al., 2014), Europe (e.g. Samuelsson et al 1997; Fernández-Suárez et al., 2014) and Asia-Pacific (e.g. Tucker et al., 2013; Tang et al, 2014). However, with the exception of the Karoo Basin of South Africa (e.g. Fildani et al., 2009), few detrital zircon geochronology studies have been done on Phanerozoic sedimentary basins in Africa, except for isolated samples from outside the central African sub-region (Mozambique and Madagascar: Kroner et al., 1996, 1997; Tanzania: Roberts et al., 2012). Hence, this project represents the first systematic detrital zircon provenance analysis of the late Mesozoic strata across central Africa.

The detailed late Mesozoic sedimentary provenance of central Africa presented in this thesis is expected to help fill some of these gaps and provide new information on the age of strata and dispersal pathways for these sediments. The new information provided by this research is also designed to help refine and improve economic exploration of placer minerals deposits and their primary sources; for instance by helping to refine the stratigraphic and temporal relationships of primary alluvial diamond-bearing placer deposits in DRC (Chapter 2) and Angola (Chapter 3). Secondly, it will significantly improve oil and gas exploration and prospectivity analysis through refining of the age relationships and stratigraphy of different Mesozoic units (chapters 4-5). Thirdly, detailed sedimentary provenance of central Africa is expected to help understand the role of regional paleogeography and tectonics (chapter 6) and how it may have affected paleodrainage of Africa (e.g. Bosworth, 1992; Moore, 1999; Moore and Larkin, 2001; Guiraud et al., 2005; Roberts et al., 2012). Finally, this thesis is expected to improve our understanding of ancient terrestrial ecosystems through time in central Africa, and lead to a better understanding of the paleobiogeography and possible ecological and evolutionary

connections between the faunas in the different parts of Africa and more broadly western Gondwana.

1.2 Thesis structure

This research attempts a regional detrital zircon investigation of late Mesozoic strata across central Africa, and provides new constraints on age, sedimentary provenance and drainage evolution. The U-Pb age analysis of detrital zircons in a sandstone provides us with the opportunity to match detrital zircon ages with crystallization ages of potential source rocks. The identification and documentation of probable sediment dispersal pathways is critical to understanding the evolution of river systems that transported these sediments to their depocentres. The exercise of understanding the late Mesozoic paleogeography in central Africa was carried out by reconciling the detrital zircon data and other provenance information with respect to their respective stratigraphic, sedimentologic and tectonic frameworks (e.g. Thomas 2011).

The thesis is structured so that each data chapter is a stand-alone manuscript intended for journal publication. This format was agreed upon by the advisory committee and the candidate at the initial stages of the research. Although each chapter is an individual body of work, it is worth noting that, they complement each other, and are all related to the central theme of this thesis: reconstructing late Mesozoic sedimentary provenance and drainage patterns with a particular focus on constraining the age (stratigraphy) and provenance of late Mesozoic continental sedimentary units in central Africa. The thesis includes seven chapters, which are made up of: (Chapter 1) an introductory chapter with a short background, problem definition, the purpose and

justification of the study; (Chapters 2-5) four discrete data chapters, each investigating a unique basin or area of central Africa; (Chapters 6) a “big picture” synthesis chapter focused on integrating the results from the four data chapters, plus some additional new data and published data from central Africa; and finally, (Chapter 7) a brief conclusion.

Two chapters have already been published, including Chapter 2 which was published in *Cretaceous Research* and focuses on the Late Jurassic-Cretaceous fluvial evolution of the Kasai portion of the Congo Basin (Democratic Republic of Congo) in central Africa. This chapter builds on the previous works of Roberts et al. (2015), Linol (2013), Linol et al. (2016) and others in the Congo Basin. Samples and support for Chapter 2 was provided by DeBeers. Chapter 4 is published in *Geological Magazine,* and focuses on the sedimentary provenance and maximum depositional age analysis of the Cretaceous Lapur and Muruanachok sandstones (Turkana Grits), in the Turkana Basin of north western Kenya. The findings from this study are particularly important, as they have implications for hydrocarbon exploration in the region, better age resolution of this important central African dinosaur bearing formation, and potentially for documenting the initiation of volcanism in the East African Rift System. Support for this research was provided by Bowleven Oil and Adamantine Energy.

Chapter 3 is now formatted and ready for submission to the *Journal of African Earth Sciences*; and will proceed following final approval from DeBeers, who provided support for this work. This chapter presents on the detrital zircon provenance of the diamondiferous mid-Cretaceous Calonda Formation of northeastern Angola. The objective of this chapter was to refine the depositional age and sedimentary provenance of

the Calonda Formation, as well as to establish Cretaceous paleofluvial drainage patterns for that part of central Africa.

Chapter 5 has been submitted to *Cretaceous Research* for publication and now in press. This chapter provides important new constraints on the depositional age and provenance of the dinosaur-bearing mid-Late Cretaceous Wadi Milk and Shendi formations of Sudan using U-Pb detrital zircon geochronology and geochemistry. The new Campanian maximum depositional age presented in this chapter conclusively shows that the Wadi Milk Formation (and its dinosaur fauna) is considerably younger than previously suggested. This work was performed in collaboration with paleontological research conducted by Royal Ontario Museum with support from Deutsche Forschungsgemeinschaft.

Finally, Chapter 6 presents a summarized synthesis of the results from the four data chapters, in addition to other new results and a synthesis of data on central Africa from the literature. Samples analysed and presented in this chapter come from a variety of sources. My published thesis chapters and other published manuscripts from my PhD are included at the end as appendices.

2. CHAPTER TWO

Late Jurassic-Cretaceous fluvial evolution of central Africa: insights from the Kasai-Congo Basin, Democratic Republic Congo

ABSTRACT

The Congo Basin in central Africa is one of the largest intracratonic sedimentary basins in the world. The geological knowledge of Congo Basin is mainly based on studies from the central part of the basin ("Cuvette Centrale"). In this study, we present the results of sedimentary provenance investigations of the Jurassic–Cretaceous strata from the southwestern part of the basin, called the Kasai region. This study combines sandstone petrography with U-Pb and Lu-Hf analyses of detrital zircons to assess the stratigraphy, sedimentary provenance and drainage history of the Upper Jurassic-Cretaceous strata in the Kasai region. The stratigraphy is subdivided into a single Jurassic unit (J1) and four Cretaceous units (C1-C4). Petrographically, sandstones from all units except the conglomeratic C3 are texturally and compositionally mature, dominated by quartzarenite and subarkosic compositions. These characteristics are attributed to considerable recycling of older sedimentary strata and crustal sources, along with long distance fluvial and aeolian processes. U-Pb analyses of fifteen detrital zircon samples from the Upper Jurassic–Cretaceous strata yielded mainly Archean and Proterozoic zircons. This result suggests that sandstones are sourced from the underlying Archean-Paleoproterozoic Congo–Kasai Craton, and from nearby Proterozoic mobile belts, particularly the Irumide and Lufilian Belts to the south of the basin. The dominance of Archean and Proterozoic detrital zircons in Upper Jurassic–Cretaceous strata suggests that the Kasai portion of the Congo Basin experienced exhumation and erosion, which is possibly associated with far-field reactivation of Archean and Proterozoic structures during Gondwana rifting in the late Mesozoic. A large fluvial drainage network, sourced from the south of the basin, is interpreted to have developed across central Africa during the Late Jurassic–Cretaceous. This fluvial system is believed to have flowed northward across the Congo Basin and ultimately drained into a wrench fault system

called the Central African Shear Zone, which extends in an ENE direction from the Gulf of Guinea through Cameroon into Sudan and Kenya.

Citationn for this chapter:
Owusu Agyemang, P.C., Roberts, E. M., and Jelsma, H. A. (2016). Late Jurassic-Cretaceous fluvial evolution of central Africa: Insights from the Kasai-Congo Basin, Democratic Republic Congo. Cretaceous Research, doi:10.1016/j.cretres.2016.06.013.

Keywords:

Cretaceous; Kasai-Congo; Detrital zircon; Provenance; Paleodrainage; Lu-Hf.

2.1 Introduction

The intracratonic Congo Basin in central Africa is among the largest continental sedimentary basins in the world, covering ~1.8 million km^2 of Africa's landmass (Fig. 2-1: Kadima et al., 2011; Linol et al., 2016; Raveloson et al., 2015). This near-circular basin occupies most of the Democratic Republic of Congo (DRC, formerly Zaire), portions of the Republic of Congo, the Central African Republic (CAR) and Angola. The Congo Basin contains up to 9 km of sedimentary strata ranging in age from late Precambrian to Recent (Daly et al., 1992; Roberts et al., 2015). The basin is typically subdivided into a central portion called the Cuvette Centrale and discrete thick strata (depocentres) around the periphery of the basin, including the Kwango, Kasai and Lundas (Figs. 2-1 and 2-2: Daly et al., 1992; Giresse, 2005).

Despite its size and resource potential (Milesi et al., 2006), the Congo Basin has received comparatively little detailed scientific attention until recently, which is largely attributed to thick vegetation cover and recurring socio-political instability in the central Africa region (Cahen et al., 1984). Moreover, the geological knowledge of the basin is mainly limited to the investigations of the Cuvette Centrale, where four deep exploration well cores have provided a means of deciphering the basin's history (e.g., Samba #1[S], Dekese #1[D], Mbandaka #1[M] and Gilson #1[G] wells; Giresse, 2005; Fig. 2-1). Recent studies of these well cores from the Cuvette Centrale, coupled with limited investigation of the Kasai and Kwango portions of the basin have increased our knowledge of the Congo Basin, however much work remains to be done (e.g., Myers et al., 2011; Delpomdor et al., 2013; Gartner et al., 2014; Linol et al., 2016; Roberts et al., 2015). The scarcity of precise radiometric age data

particularly from outside the Cuvette Centrale, makes stratigraphic correlation of the Congo Basin units difficult (De Wit and Linol, 2015).

Two competing hypotheses have been proposed in an attempt to explain the origin and timing of putative Mesozoic erosion surfaces and drainage evolution in central Africa (*see* Stankiewicz and De Wit, 2006; Roberts et al*.,* 2012). Stankiewicz and De Wit (2006) identified a possible basin-scale erosional surface, which they interpreted as evidence of a possible east-flowing Cretaceous Congo River system out of the Congo Basin and towards the Indian Ocean via the Rufiji delta (Fig. 2-2).

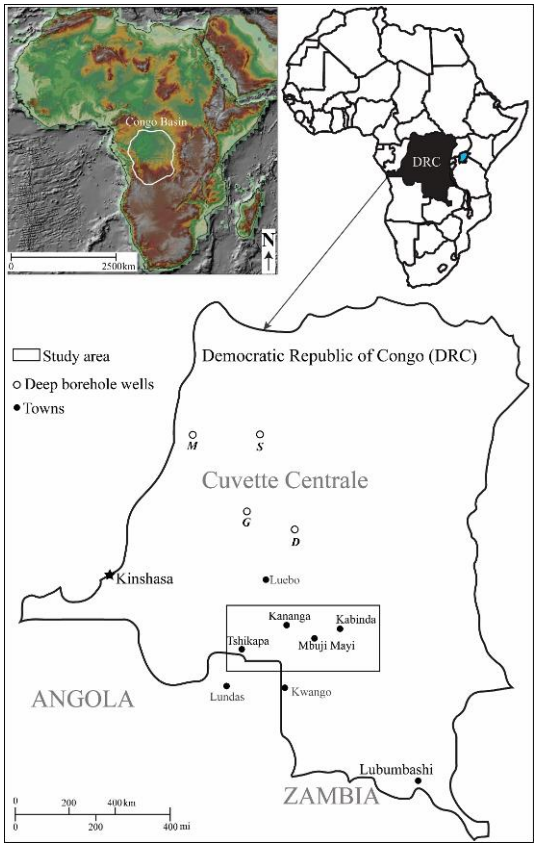

Figure 2-1. Geographical location of the Congo Basin in central Africa

The white outline is the Congo Basin and the study area is shown by the rectangle.

In contrast, Roberts et al. (2012) documented paleocurrent and detrital zircon evidence for a large transcontinental river system that flowed northwest into the Congo Basin during the Cretaceous. Roberts et al. (2012) argue that at least up until the Late Cretaceous, this river system flowed out of the northern Malawi Rift, through the axis of the Rukwa Rift and into the Congo Basin (Fig. 2-2).

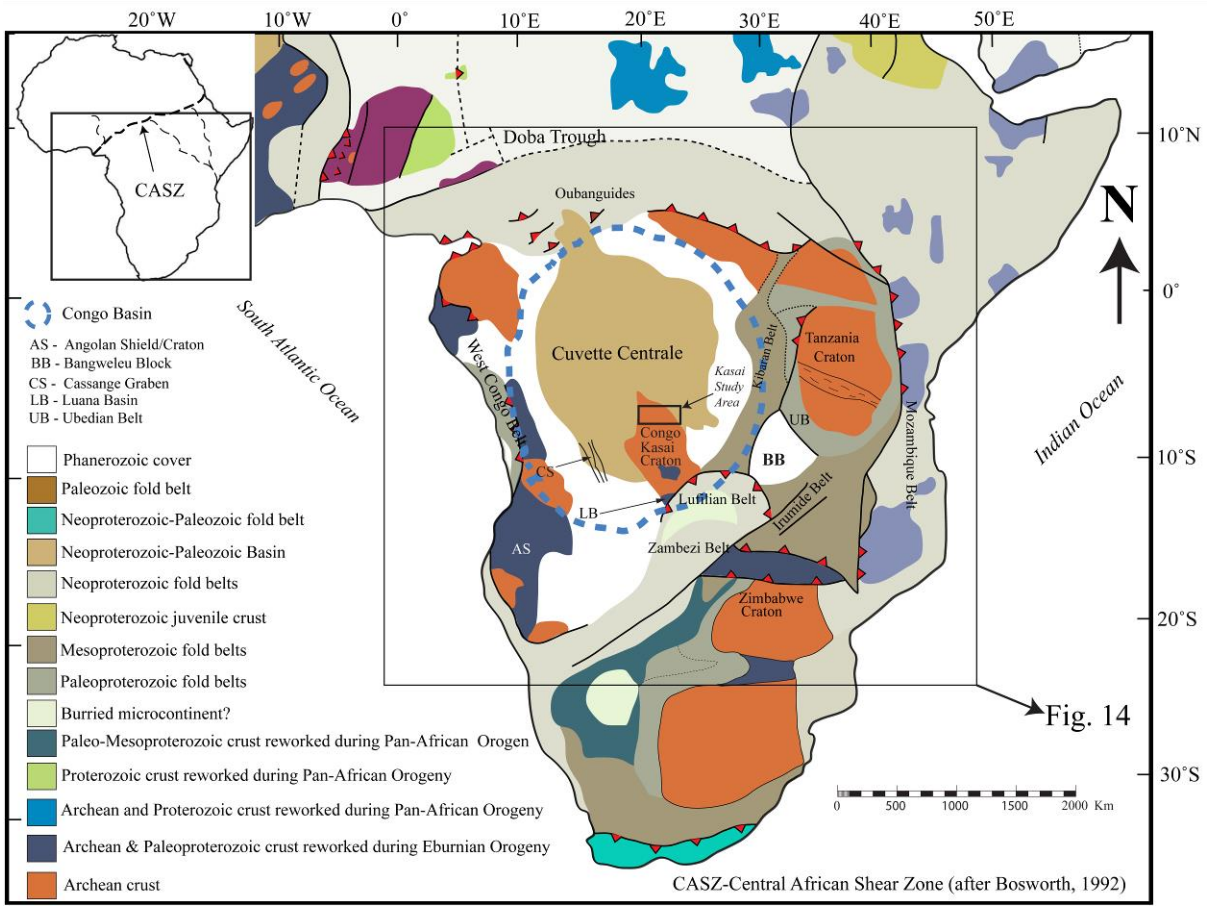

Figure 2-2. Generalized Basement rock map of central and southern Africa.

Map shows the main cratonic blocks and mobile belts (Modified from Begg et al., 2009 and Foster et al., 2015).

The timing and origin of southern and eastern Africa's unusually high–elevation topography has been the focus of considerable attention for many years (e.g., King, 1963; Meadows, 2001; Moore and Larkin, 2001; Grab et al., 2015). Researchers have sought to identify the connections between surface uplift and topography, and their link to fluvial (drainage)

transport and sediment dispersion (e.g., Moore and Larkin, 2001). Understanding Mesozoic drainage evolution or patterns in central Africa has major implications for tracking of alluvial diamonds to their sources, as well as for reconstructing the tectonic, evolutionary and ecological patterns that set the stage for modern African flora and fauna (O'Connor et al., 2006). The southern margin of the Congo Basin is known for alluvial diamonds, particularly in the Mbuji-Mayi area and the Lundas region in Angola (Fig. 2-1). The alluvial diamonds from these areas are hosted in Mesozoic strata and understanding their provenance history is important for tracing the sources of primary and secondary alluvial diamond-bearing deposits in the region (Davis 1977; Partridge, 1998; Robles-Cruz et al. 2012).

Here, the results of a detailed sedimentary provenance investigation of the Upper Jurassic–Cretaceous strata in the Kasai portion of the Congo Basin (i.e. Kasai–Congo Basin). This study combines petrography with U-Pb and Lu-Hf detrital zircon analyses on a suite of sandstone borehole well core samples from exploration boreholes drilled across the Kasai Region by De Beers Exploration Limited between 2006 and 2008. In addition, paleocurrent datasets from across central Africa were compiled to assist in provenance analysis and to help develop a regional drainage model for central Africa during the Cretaceous. The results of this study allow for testing of current hypotheses regarding the initiation and tectonic control on large–scale drainage patterns in central Africa during the Late Jurassic–Cretaceous.

2.2 Geologic setting and stratigraphy of the Congo Basin

2.2.1 Geologic setting

The Congo Basin is bounded by the Mesozoic passive Atlantic continental margin to the west and the Cenozoic East African Rift System on the east (Daly et al., 1992; Linol et al., 2016). Kadima et al. (2011) and Linol et al. (2016) each describe the basin's location as the centre of the African plate and central Gondwana. The Congo Basin sits on the Archean–Paleoproterozoic Congo-Kasai Craton (Cahen et al., 1984). The basin has a near-circular shape with a thicker central part (Cuvette Centrale) and thinner margins (Daly et al., 1992). The basin is also surrounded by a number of Proterozoic mobile belts (Fig. 2-2; Cahen et al., 1984; Kampunzu and Cailteux, 1999; De Waele et al., 2008; Tack et al., 2010). Repeated deformation along the margins of the Congo-Kasai Craton have uplifted these Proterozoic mobile belts, causing them to become important provenance sources for sediments in the Congo Basin (Milesi et al., 2006).

The Congo Basin is an intracratonic sedimentary basin that evolved through different geodynamic processes including extension and subsidence related to stretching over 800 Ma (Kadima et al., 2011). Isostatic rebound and surface uplift of the western margin of central Africa during and following Gondwana breakup resulted in the formation of the western margin of the Congo Basin (e.g. Van Balen et al., 1995; Fairhead et al., 2013). The uplift of the western margin of central Africa is believed to have contributed much of the sediment to the basin as a result of continued basin margin flexure and active tectonics (e.g., Jelsma et al., 2009). Additionally, far-field stresses associated with Mesozoic tectonic events in central Africa are thought to have influenced local sedimentation patterns as a result of reactivation of Proterozoic extensional faults within the Congo Basin (Roberts et al., 2015; Linol et al.,

2016). In particular, Roberts et al. (2015) identified evidence for Cretaceous reactivation of the Cassange Graben (Fig. 2-2) and the formation of thick, syndepositional alluvial fans along reactivated fault segments. These different geodynamic processes in the Congo Basin's evolution influenced sediment deposition patterns and stratigraphy of the different parts of the basin (Kadima et. al., 2011). The Central African Shear Zone (Fig. 2-2) is a wrench fault system, which extends in an ENE direction from the Gulf of Guinea through Cameroon into Sudan and Kenya (Ibrahim et al., 1996; Schl ter and Trauth, 2008). The displacement along the Central African Shear Zone during Gondwana breakup could have helped to accommodate sediment from the south (Ibrahim et al., 1996; Censier and Lang, 1999).

2.2.2 Stratigraphy

The Phanerozoic Congo Basin is characterized by the Cretaceous-Cenozoic Cuvette Centrale as well as Jurassic and Cenozoic sediment-fill in the eastern margins (Daly et al., 1992; Linol et al., 2016). Stratigraphic correlation in the basin is limited by a number of factors, including lack of well-constrained biostratigraphic and radiometric age data from across the whole basin (Kadima et al., 2011). Correlation of stratigraphic units is also limited by the considerable lateral disparity between similar units across large areas of the basin (e.g., Daly et al., 1992; Linol, 2013). Thus, the stratigraphy of the Congo Basin has largely been compiled from seismic data and boreholes drilled in the Cuvette Centrale (Daly et al., 1992; Kadima et al., 2011). The seminal works on the stratigraphy of the Congo Basin by Cahen (1954) and others in the Cuvette Centrale are summarized by Linol et al. (2016) and Roberts et al. (2015). The contributions of Cahen, and more recently, Linol (2013), Delpomdor et al.

(2013) and De Wit et al. (2015) have greatly improved our understanding of the Congo Basin's evolution and stratigraphy; however, the picture is still far from complete (Fig. 2-3).

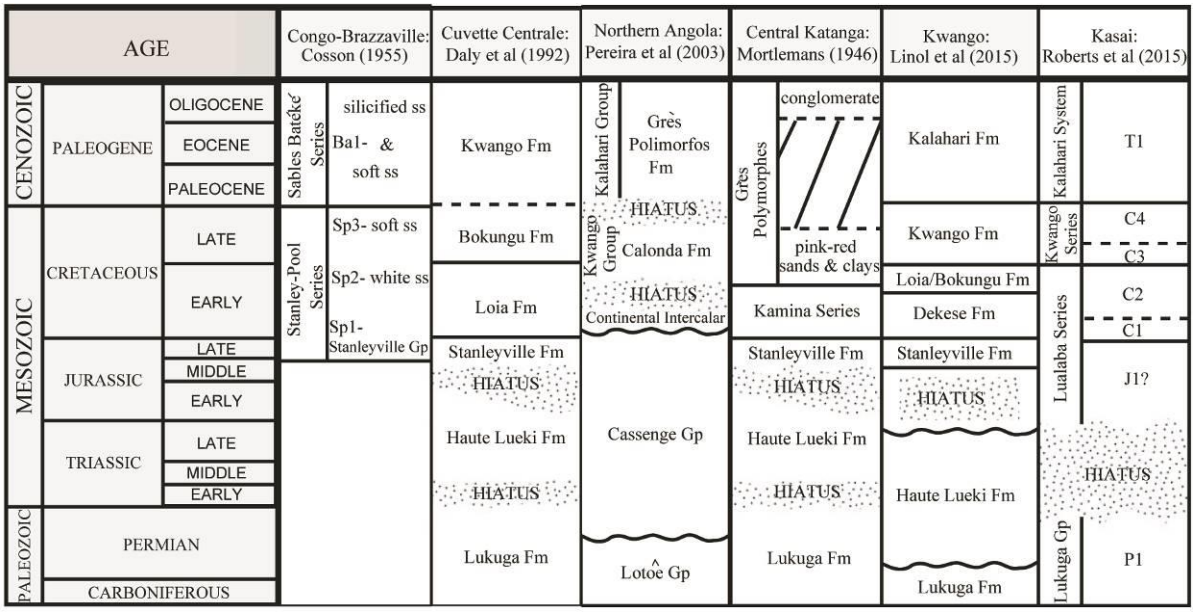

Figure 2-3. Phanerozoic stratigraphy of different depocentres in the Congo Basin.

In the Cuvette Centrale, Daly et al. (1992) identified five depositional sequences (successions) using seismic and borehole data (Kadima et al., 2011). The ages of these sequences range from Neoproterozoic to Cenozoic (see Kadima et al., 2011 and Roberts et al., 2015 for detailed discussion). The first succession is the Vendian of late Neoproterozoic age and is composed of shallow marine stromatolitic limestones and subordinate evaporites. The second succession is of Cambrian age and is composed of marine clastic deposits, whereas the overlying third succession of Ordovician-Devonian age is interpreted as a transgressive-regressive marine cyclothem across the whole Congo Basin. The fourth succession, which is also exposed on the eastern margin of the Congo Basin, is of Permian age and considered correlative to the lower part of the Karoo System of South Africa (Daly et al., 1992). The last succession in the Cuvette Centrale consists of Triassic-Cenozoic

continental clastic units. This succession consists of four Mesozoic and one Cenozoic units. The Mesozoic units include the Stanleyville, Dekese, Loia/Bokungu and Kwango Groups (Fig. 2-3), which were recently characterized together as the Congo Supergroup by Linol et al. (2016). Linol et al. (2016) suggested that a regional peneplanation event occurred after the deposition of the Congo Supergroup before the Cenozoic Kalahari succession was deposited (Linol, 2013).

In the Kwango region only three main successions were identified and mapped by Linol (2013). These three successions are the Karoo Supergroup, the Mesozoic Kwango Group and Cenozoic Kalahari Group. The Karoo Supergroup is mainly composed of conglomerates, red siltstones and sandstones, whereas the Kwango Group is composed of large-scale cross-bedded white and red sandstones. The Kalahari Group is also composed of sandstones (Linol et al., 2016).

U-Pb detrital zircon provenance analysis of the Phanerozoic sequences from the Kwango region and the Cuvette Centrale by Linol et al. (2016) yielded five main age populations. These include Archean to early Paleoproterozoic (3.1 Ga and 2.9–2.4 Ga), Paleoproterozoic (Eburnean: 2.1–1.8 Ga), Mesoproterozoic (Kibaran: 1.4–1.0 Ga) and Neoproterozoic (Pan-African: 750–500 Ma). Linol et al. (2016) interpreted each of these age populations as important sediment sources during the Mesozoic and Cenozoic depositional cycles. Linol et al. (2016) identified the Archean – Paleoproterozoic Congo-Kasai Craton as the principal provenance source in the Kwango region, likely due to tectonic uplift and coeval erosional processes (Batumike et al., 2009). Batumike et al. (2009) also recognized the Congo-Kasai Craton as the main source of sediments in the Luebo part of the Congo Basin (Fig. 2-1). These findings are consistent with those of Roberts et al. (2015), who documented localized

Mesozoic reactivation of basement structures in the Kasai region, which would have exposed Archean basement. Each of these studies suggest uplift and reactivation of Archean crystalline basement during the Mesozoic, which may help to explain why regional stratigraphic correlation of the Congo Basin strata (Fig. 2-3), particularly on the periphery of the basin, has been so difficult to achieve (De Wit and Linol, 2015).

2.2.2.1 Kasai Region Stratigraphy

Seven lithostratigraphic units have been identified in the Kasai-Congo Basin by Roberts et al. (2015). Roberts et al. (2015) refined the lithostratigraphy, following the seminal work of Cahen (1954). This revised Kasai stratigraphy includes locally restricted basal Permo-Carboniferous glacio-lacustrine deposits of the Dwyka equivalent Lukugu Group referred to as P1 (Fig. 2-3). No deposits of the Triassic Haute-Leki sequence were unequivocally identified by Roberts et al. (2015) in the Kasai–Congo Basin; however, continental deposits correlative to the Upper Jurassic Stanleyville Formation were identified from the Tshikapa area and termed J1. They interpreted J1 units as being deposited by fluvial and aeolian processes.

The most widespread sedimentary unit in the Kasai–Congo Basin is the Lower Cretaceous Loia equivalent strata termed C1/C2, which is composed of alluvial fan, braided fluvial and isolated aeolian strata. Roberts et al. (2015) differentiated C1 as the conglomeratic alluvial fan facies found at the base of the Cretaceous section in some areas, whereas C2 is restricted to the dominantly fluvial and isolated aeolian units. The Kwango Group equivalent strata were also identified above C1/C2 deposits across the Kasai region. They include basal alluvial fans, termed C3, and overlying fluvial strata termed C4 (Roberts et al., 2015).

Capping the stratigraphic succession in the Kasai region are Paleogene deposits correlative to the Kalahari Group, which Roberts et al. (2015) termed T1. Although uncertainties in the correlation and age of sedimentary successions in the Congo Basin still exist, for the purposes of this study the revised stratigraphy presented in Roberts et al. (2015) is utilized (Fig. 2-3).

2.3 Samples and methods

Detrital zircon and sandstone petrography samples presented in this manuscript were selected from borehole cores drilled by De Beers (Democratic Republic of Congo) Exploration Limited. De Beers explored the Congo Basin and cored 196 exploration boreholes in the Tshikapa, Kananga, Mbuji Mayi and Kabinda areas of the Kasai region, southwest of the Congo Basin from 2005 to 2008 in partnership with Société Minière de Bakwanga (MIBA) and Bugeco. Subsets of these borehole well cores were studied by Hansen (2007) and by Roberts et al. (2015). Small fractions of the studied well cores were preserved for further studies. These preserved samples form the focus of this manuscript. Detailed sample descriptions can be found in Hansen (2007) and Roberts et al. (2015). Due to the vegetative cover of the study area only a small suite of paleocurrent directions (n = 9) was recorded in the field. A combination of sandstone petrography, U-Pb detrital zircon geochronology and Lu-Hf isotope geochemistry was applied in this study.

2.4 Sandstone petrography

Fifty thin sections were prepared from selected well core samples taken from Upper Jurassic and Cretaceous units for point-counting following Gazzi-Dickinson methodology using a

transmitted-light polarizing microscope (Dickinson, 1970; Ingersoll et al., 1984). The point-counting dataset from Hansen (2007, N=64) was recalibrated to take into account the revised stratigraphy of Roberts et al. (2015), and combined with point count data from the 50 thin sections analysed during this study. Note that a number of replicate QFL results were performed on the samples of Hansen (2007), to ensure that results were comparable with the methods of this study, thus indicating data reproducibility (Howarth, 1998).

Of the 114 point counted sandstones, eight samples are from the Upper Jurassic J1 beds, 20 samples are from the Lower Cretaceous C1/C2 units, 18 samples are from the Upper Cretaceous C3 beds and 68 samples were selected from the Upper Cretaceous C4 beds (see Appendix 2S1). Units J1 and C1/C2 beds are restricted to the western side of the Kasai study area, near Tshikapa, whereas C3 beds are limited to the central and eastern areas of Kasai between Kananga, Mbuji Mayi and Kabinda areas. Unit C4 beds are widely distributed across the entire Kasai area (Fig 2-1).

2.5 U-Pb detrital zircon geochronology

In addition to the sandstone petrography, 17 samples from eight cores were selected for U-Pb and Lu-Hf detrital zircon analyses. The samples for detrital zircon analyses were limited, so sample selection was designed to maximize the stratigraphic and geographic coverage based on the availability. Moreover, the number of zircon grains recovered from some samples was small and so samples from similar portions of the same well core were combined to produce large enough datasets for provenance interpretations (Table 2-1).

2.5.1 Detrital zircon sample preparation

Detrital zircons samples were prepared for age dating using U-Pb laser ablation inductively coupled mass spectrometry (U-Pb LA-ICP-MS), following methods outlined in Gehrels et al. (2008). The detrital zircon samples were crushed, milled, sieved, washed and decanted to remove clay-sized fraction. Heavy minerals were separated using lithium polytungstate adjusted to a specific gravity of ~2.85. Concentrates were washed, dried and further treated by a hand magnet and Frantz magnetic separator, set progressively at higher magnetic currents of 0.4 A, 0.8 A, 1.0 A and 1.2 A, at a constant 5° side slope to separate the magnetic from non-magnetic fractions. All zircons were then handpicked from the >1.0 A non-magnetic fractions (≥ 100/sample) and mounted in a 25 mm epoxy resin puck. The puck was polished to reveal the mid-sections of zircons for imaging using a Jeol JSM5410LV scanning electron microscope with an attached cathodoluminescence detector. Cathodoluminescent images were used to document and avoid microstructures, including cracks, inclusions and complex zoning during the U-Pb laser ablation analyses (Gehrels et al., 2008). Care was taken to avoid contamination during all stages of mineral separation processes and bias during hand-picking of zircons (Slma and Koler, 2012). All mineral separation work, cathodoluminescence imaging U-Pb dating and Lu–Hf analysis were conducted at the James Cook University, Townville, Australia.

2.5.2 U-Pb LA-ICP-MS dating of detrital zircons

All U-Pb LA-ICP-MS dating analyses were conducted using a Coherent GeolasPro 193 nm ArF Excimer laser ablation system connected to a Bruker 820-MS (formerly Varian 820-MS). Details of analytical techniques are described in Tucker et al. (2013). The ablation cell was connected to the Bruker 820-MS via Tygon tubing and a 3-way mixing bulb with volume

~5 cm^3, but with a custom-designed polycarbonate insert to reduce the effective volume to 4 cm^3. The Bruker 820-MS uses an ion mirror design, which reflects the ion beam exiting the skimmer cone by 90° and focusses this into the mass analyser. All U-Pb age data from this study are listed in Appendix 2S2

Table 2-1. Summarize U-Pb detrital zircon results from the Kasai Congo Basin.

Core ID	Sample #	Bed/Unit	#Zircons recovered	Age span	Location
169-X020	1	J1	23 (18)	2728 – 375 Ma	Tshikapa
	2	C1&C2	0 (0)	-	
	3	C4	6 (6)	1901 – 254 Ma	
157-X015	2	C4	40 (30)	2645 – 243 Ma	Kananga
	6&7	C4	23 (11)	2936 – 609 Ma	
	9	C3	78 (26)	2983 – 585 Ma	
171-X031	11&12	C4	55 (42)	3204 – 252 Ma	
	19	C3	75 (51)	2970 – 509 Ma	
172-X050	50	C4	64 (39)	3186 – 150 Ma	Mbuji-Mayi
	59	C3	58 (28)	3204 – 475 Ma	
172-X146	61&62	C4	5 (4)	3345 – 2764 Ma	
	73	C4	- (-)	-	
186-X004	32&33	C4	51 (22)	3228 – 1074 Ma	
159-027	20	C3	19 (8)	2834 – 362 Ma	Kabinda
	26&27	C3	24 (17)	2004 – 728 Ma	
173-X009	3B	C3	59 (57)	2930 – 76 Ma	
	6	C3	37 (37)	2905 - 559	

Notes: The number of concordant zircons are shown in parenthesis. *(Zircons from sample 172-X146-73 was excluded from analysis with the exception of only 4 zircons from sample 172-X146-61/62 due to suspected Common Pb contamination).*

Total analysis time was 70 seconds, including the first 30 seconds for measuring background intensities followed by 40 seconds of sample ablation. Standard bracketing was used to correct for remaining elemental fractionation, mass bias, down-hole fractionation variation and instrumental drift (Gehrels et al., 2008). On average, two analyses each of a primary

zircon standard (GJ-1, 609 Ma, Jackson et al., 2004) and secondary zircon standard (Temora-2, 416.8 Ma, Black et al., 2003) were conducted before and after analysis of 10–12 unknown sample zircons. NIST 612 standard glass (50ppm glass USGS working values, 2009) was analysed before and after each U-Pb laser ablation session and at least once between sessions for calibrating thorium and uranium concentrations. Zircon grains were ablated using a 24 – 32 μm diameter beam due to the small size of most of the zircons.

Data reduction and age determination was performed using GLITTER 4.0 software (Van Achterbergh et al., 2001). The reduced data was exported to Microsoft Excel for the calculation of discordancy, which is a ratio of $^{206}Pb/^{238}U$ and $^{207}Pb/^{206}Pb$ ages. The majority of zircons in this study are of Paleoarchean to Neoproterozoic age and generally discordant if a tight discordant cut-off (e.g. 10% or less) is applied. Thus, a discordance cut-off of 15% was applied. Tighter discordance cut-off was avoided for two reasons: 1) to prevent biasing sediment provenance trends; and 2) to capture the greatest number of sources, which proved particularly important for evaluating the provenance impact of abundant Paleoarchean to Neoproterozoic zircon grains in this study. The discordance filter was not applied to zircon grains younger than 300 Ma, because their $^{207}Pb/^{206}Pb$ ages cannot be reliably determined (Gehrels, 2012).

The concordant zircon data was then used to plot Concordia diagrams (2σ error ellipses) and probability density plots using the Concordia features of Isoplot /Ex 3.75 (Ludwig, 2012). The $^{207}Pb/^{206}Pb$ age was selected for zircon grains older than 1.0 Ga as they are more reliable for older zircons, whereas the $^{206}Pb/^{238}U$ age was selected for zircons younger than 1.0 Ga because $^{206}Pb/^{238}U$ ages are reliable for younger zircons (e. g. Gehrels et al., 2009). Errors for the U-Pb age data described in this manuscript are all at 1σ level for $^{206}Pb/^{238}U$, $^{206}Pb/^{207}Pb$

and $^{206}Pb/^{204}Pb$. Reported uncertainties were propagated by linear addition of the external reproducibility obtained from primary standard zircon GJ-1 during individual analytical sessions.

2.6 Lu-Hf isotopic systematics

Zircon grains from eight dated samples were analysed for their Lu-Hf isotope ratios. The laser ablation Hf isotope analyses were done at the Advanced Analytical Centre at James Cook University, Townsville, Australia, using a GeoLas 193-nm ArF laser and a Thermo Scientific Neptune multicollector (MC) ICP-MS. The Lu-Hf isotopic ratios were derived from a 60-s ablation period, comprising 60 cycles of one-second integration time. A repetition rate of 4 Hz and power density of sample maintained around 6–7 Jcm^{-2} that translates into an estimated ablation rate of ~0.5 μms^{-1} using helium as a carrier gas. Background gas was measured at the beginning of every analysis. The mass spectrometer cup configuration for this study is shown in the Appendix 2S3. The isotopic data was acquired using a uniform laser spot size of 60 μm, usually overlapping the same spot of concordance where the zircon grain was ablated for the U-Pb age data (e.g., Fisher et al., 2014).

Detrital zircon grains (n = 97) with discordance ≤ 10% were selected for the determination of their initial εHf (t) values, with the exception of grains younger than 300 Ma. The Lu-Hf datasets were subsequently processed offline to check for the homogeneity of all ablated zircons. Corrections for the isobaric interference of lutetium and ytterbium (Yb) on ^{176}Hf was performed by monitoring ^{175}Lu ($^{176}Lu/^{175}Lu = 0.026549$) and ^{171}Yb ($^{176}Yb/^{171}Yb = 0.897145$) respectively. Both ^{171}Yb and ^{173}Yb were measured in order to correct for the mass bias and subsequently corrected by exponential law (e.g. Fisher et al., 2011).

The measured average $^{176}Hf/^{177}Hf$ from three standard zircons; Mud Tank zircon (MTZ), Temora-2 and Geo-standard FC1 zircon, were used to monitor the instrumental state and analytical accuracy (Fisher et al., 2014). The measured Temora-2 zircon standard (n =2) yielded a normalized $^{176}Hf/^{177}Hf$ value of 0.282158 ± 8 and a 'true' (solution) value of 0.282686±8 (Woodhead and Hergt, 2005). The measurement of FC1 zircon standard (n = 10) also yielded a normalized $^{176}Hf/^{177}Hf$ value of 0.282158 ± 8 and a 'true' (solution) value of 0.282184 ±16 (Woodhead and Hergt, 2005). Finally, the measured average $^{176}Hf/^{177}Hf$ from MTZ obtained over all analytical sessions was calculated as 0.282486 ± 7; (n=14) and compared with the 'true' (solution) value of 0.282507 ± 6 (Woodhead and Hergt, 2005), where uncertainties of the measurements are two standard deviations. Based on the analyses of the MTZ, a $^{176}Hf/^{177}Hf$ normalization factor of *1.000075* was applied to the unknown sample zircons from the Kasai region (Woodhead and Hergt, 2005).

2.7 Results

2.7.1 Sandstone petrography results and interpretation

In thin section, feldspars are generally uncommon, but those that exist typically appear fresh, with minimal evidence of intense weathering or alteration (Fig. 2-4). The investigation revealed a relatively high concentration of labile mafic minerals in Unit C3, including pyroxenes and amphiboles, which would be expected to break down quickly in wet paleo-environments (e.g., Hoefen et al., 2003). The preservation of these minerals is consistent with sedimentologic interpretations of arid to semi-arid conditions in the Congo Basin during the Late Jurassic to Cretaceous (Myers et al., 2011). Slow generation of accommodation and reworking by fluvial and aeolian processes contributed to sediment recycling, mechanical

weathering and the elevated maturity throughout the Jurassic and Cretaceous units observed in this study (*see* Linol, 2013).

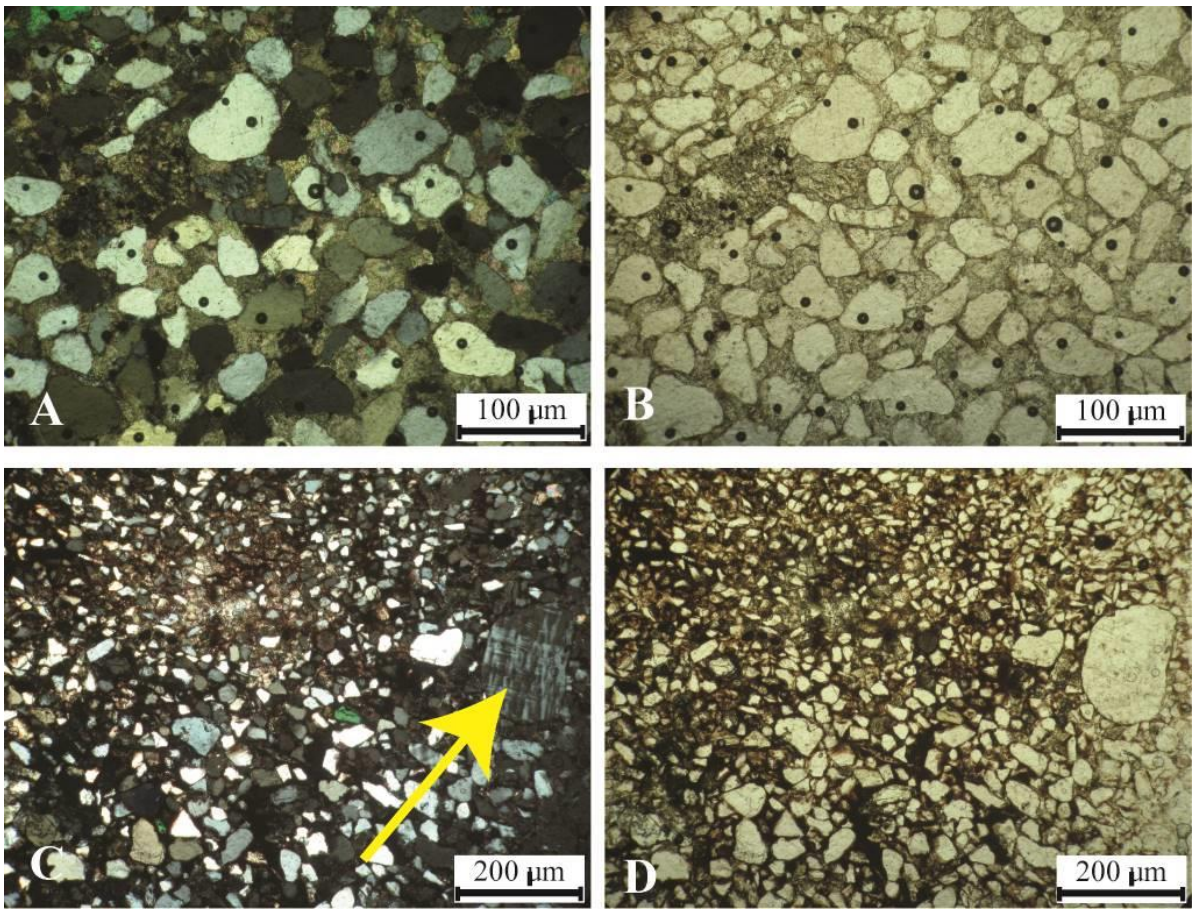

Figure 2-4 Thin section photomicrographs of selected samples from the Kasai – Congo Basin.

Left column photos were taken with cross polarized light, whereas the right column photos were taken with plane polarized light. Photomicrographs showing mostly sub angular to rounded quartz grains. Yellow arrow pointing to fresh feldspar in sample C.

Samples from Upper Jurassic J1 beds cluster together on both the Q_tFL and Q_mFL_t ternary diagrams (Fig. 2-5a) and plot as quartzarenite from a continental block tectonic provenance source (Dickinson, 1970; Dickinson and Suczek 1979). The overlying Lower Cretaceous C1/C2 beds fall into the quartzarenite and subarkosic petrofacies, and plot within the recycled orogen tectonic field (Fig. 2-5a). A provenance variation is observed in the conglomeratic Upper Cretaceous C3 beds, which remain subarkosic, but show significantly greater

proportions of feldspar and lithic grains, and plot within the recycled orogen tectonic field. The Upper Cretaceous C4 beds, however, trend towards the quartzose end of the subarkose petrofacies and show a mixed provenance between the continental block and recycled orogen tectonic fields (Fig. 2-5a).

In general, each of the stratigraphic units (J1 to C4) shows a tight clustering of samples within discrete petrofacies domains. These domains are consistent with their characterisation as discrete stratigraphic units by Roberts et al. (2015). The limited amount of scatter between samples suggests that climatic variations were not intense and major provenance shifts are unlikely to have occurred throughout the Jurassic-Cretaceous (Myers et al., 2011).

Overall, the Kasai sandstones show a tighter clustering in the east than in the west. The Tshikapa and Kananga area samples plot as quartzarenite to lithic arkoses. Sandstones from Tshikapa predominantly plot within the recycled orogen tectonic fields, whereas Kananga area sandstones plot as mixed provenance of continental block and recycled orogen sources (Fig. 2-5b).

The Mbuji Mayi and Kabinda sandstones from the eastern side of the study area plot as subarkoses with mixed tectonic sources (Fig. 2-5b). In summary, J1-C4 units, with the minor exception of a number of proximal alluvial fan facies of C3, represent mature to super mature sandstones. Evidence for arid to semi-arid depositional settings, combined with a lack of chemical weathering in the feldspars, indicates that the mature provenance is dominantly the result of recycling of older sedimentary and metasedimentary provenance sources and probably high-energy fluvial and aeolian processes, perhaps involving both proximal and distal source areas.

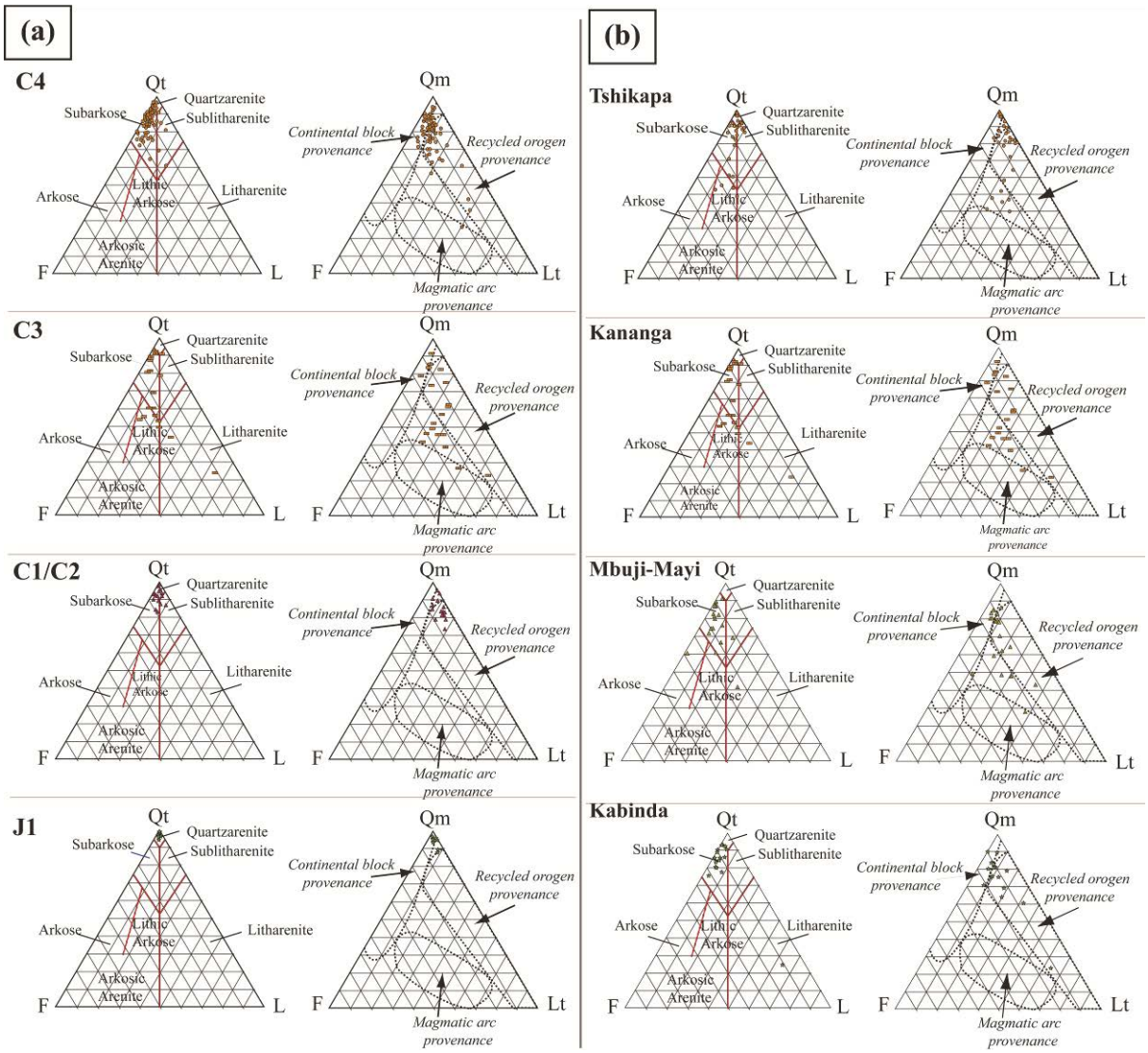

Figure 2-5. Detrital modes for the Kasai-Congo Basin sandstones.

(a). Detrital modes of Late Jurassic (J1) and Cretaceous (C1-C4) sandstones from Kasai-Congo Basin. Unit J1 samples plot as quartzarenites within the continental block provenance fields. Unit C1/C2 samples plot between quartzarenites and subarkose compositions, within the continental block and recycled orogen fields. Unit C3 samples plot as subarkosic with recycled orogen provenance respectively, whereas Unit C4 samples plot on the quartzose end of the subarkose petrofacies with a and a mixed provenance between the continental block and recycled orogen fields. (b). Detrital modes of Late Jurassic–Cretaceous Sandstones from the four areas in the Kasai region of the Congo Basin. Samples from the Tshikapa and Kananga areas mostly plot as quartzarenites to lithic arkoses whereas the Mbuji Mayi and Kabinda samples plot as quartzarenites sandstones. Detrital modes from all the four areas plot as mixed provenance. Qt – total Quartz; Qm – monocrystalline Quartz; F – feldspar; L – lithics; Lt – total lithics

2.7.2 Detrital zircon Geochronology

All samples with significant zircon yield were collected from the Upper Cretaceous units C3 and C4 in the Kananga, Mbuji Mayi and Kabinda areas (Fig. 2-6). A single Upper Jurassic J1 sample (*169-X020-1*) yielded datable zircons and no zircons were recovered from the Lower Cretaceous CI/C2 sample (Table 2-1). Thus, all the detrital zircon geochronology results (n = 617) reported in this manuscript originate from only three of the units investigated (J1, C3 and C4).

The single Upper Jurassic J1 sample yielded 18 concordant zircons out of 23 analyses. Zircons from J1 are euhedral to sub-rounded compositionally zoned and translucent in appearance. The age of J1 zircons range from Neoarchean (~2.7 Ga) to Late Devonian (~375 Ma). Archean and Paleoproterozoic zircons accounts for ~26% of all analyses of J1 and they are represented by two main peaks around 2.7 Ga and 2.0 Ga. Neoproterozoic grains account for ~48% of J1 analyses and form two main peaks around 730 Ma and 600 Ma (Fig. 2-6).

Seven samples from the Upper Cretaceous C3 beds yielded 224 concordant zircons out of 350 analyses. Unit C3 zircons are euhedral to sub-rounded, mostly translucent and reveal quite variable zonation patterns. The ages of zircon grains from Unit C3 samples range from Mesoarchean (~3.2 Ga) to Late Cretaceous (~77 Ma), with a dominant Neoproterozoic age populations (~38%) (Fig. 7). Archean zircons are represented by three main populations with peaks between 3.2 Ga and 2.5 Ga (Fig. 2-6). Paleoproterozoic zircons (2.47 – 1.7 Ga) account for ~23% of analyses, with a major peak around 1.9 Ga, whereas Mesoproterozoic zircons (n = 20) are represented by a prominent peak at ~1.0 Ga. Finally, the Phanerozoic age zircons from C3 samples range from Cambrian (~509 Ma) to Late Cretaceous (~77 Ma) and they account for 5% of analyses.

Seven samples from the Upper Cretaceous C4 beds yielded 154 concordant zircons out of 244 analyses. Zircons from unit C4 vary significantly in size, shape and clarity. The ages of C4 zircons span from Paleoarchean (~3.3 Ga) to Late Jurassic (~150 Ma). The Archean age zircons account for the largest proportion of C4 analyses (~26%), and fall into five main populations with two prominent peaks around 3.0 Ga and 2.65 Ga (Fig. 2-6). Paleoproterozoic and Mesoproterozoic zircons represent ~23% each of C4 analyses and show a concentration of ages between 2.4 Ga and 1.1 Ga. Neoproterozoic zircons account for ~15% of analyses with peaks around 950 Ma, 650 Ma and 550 Ma. The Phanerozoic age zircons from C4 beds also account for ~13% with a significant Permian population (n = 6).

2.7.3 Lu-Hf isotope geochemistry

Lu–Hf isotopic data for eight samples from Kasai study area, along with data for the three standard zircons are listed in Appendix 2S3. Twenty-three zircons from the Kananga area, 18 zircons from the Mbuji Mayi area and 56 zircons from the Kabinda were analysed in this study for their Lu-Hf isotope ratios. No zircon grains were analysed from the Tshikapa area due to a lack of zircons of suitable size for the analyses. The initial εHf (t) values for all the 97 zircons range from –28.2 to +9.3 (Fig. 2-7). The results indicate mixed provenance sources with both juvenile mantle derived components and older reworked crustal sources, which is supported by the Hf model age plot (Fig. 2-7: Kinny and Maas, 2003). Archean zircons (~3.3 – 2.6 Ga; n = 20) yielded Initial εHf (t) values from –12.7 to +4.9; Paleoproterozoic grains (n = 20) also yielded values between –16.1 and +2.4, –25.5 to +9.0 for Mesoproterozoic grains (n = 17), and –28.2 to +9.3 for Neoproterozoic grains (n=30).

Finally, the initial εHf (t) values for Paleozoic–Mesozoic (≤ 0.5 Ga; n=10) zircons range between –12.8 to +5.7.

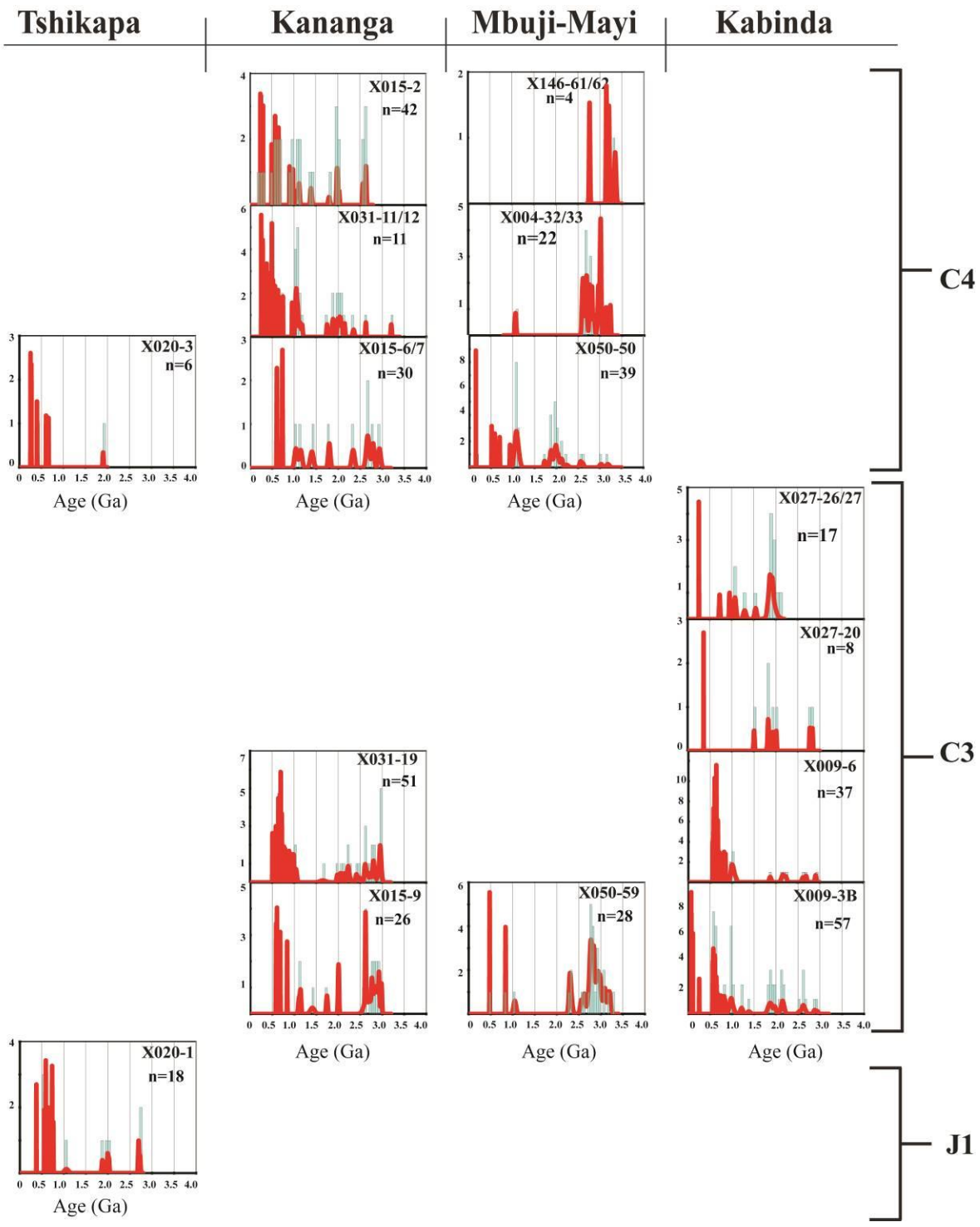

Figure 2-6. Probability density of detrital zircon grains from three Late Jurassic-Cretaceous units (J1, C3 and C4).

Precambrian age populations are dominant in all units. $^{207}Pb/^{206}Pb$ age is preferred for zircons older than 1Ga, whereas 206Pb/238U age is preferred for zircons younger than 1Ga

Overall, the $^{176}Hf/^{177}Hf$ isotopic ratios for the four areas in Kasai are consistent with a mixed provenance that represents a dominantly reworked component with a minor juvenile mantle or crustal addition.

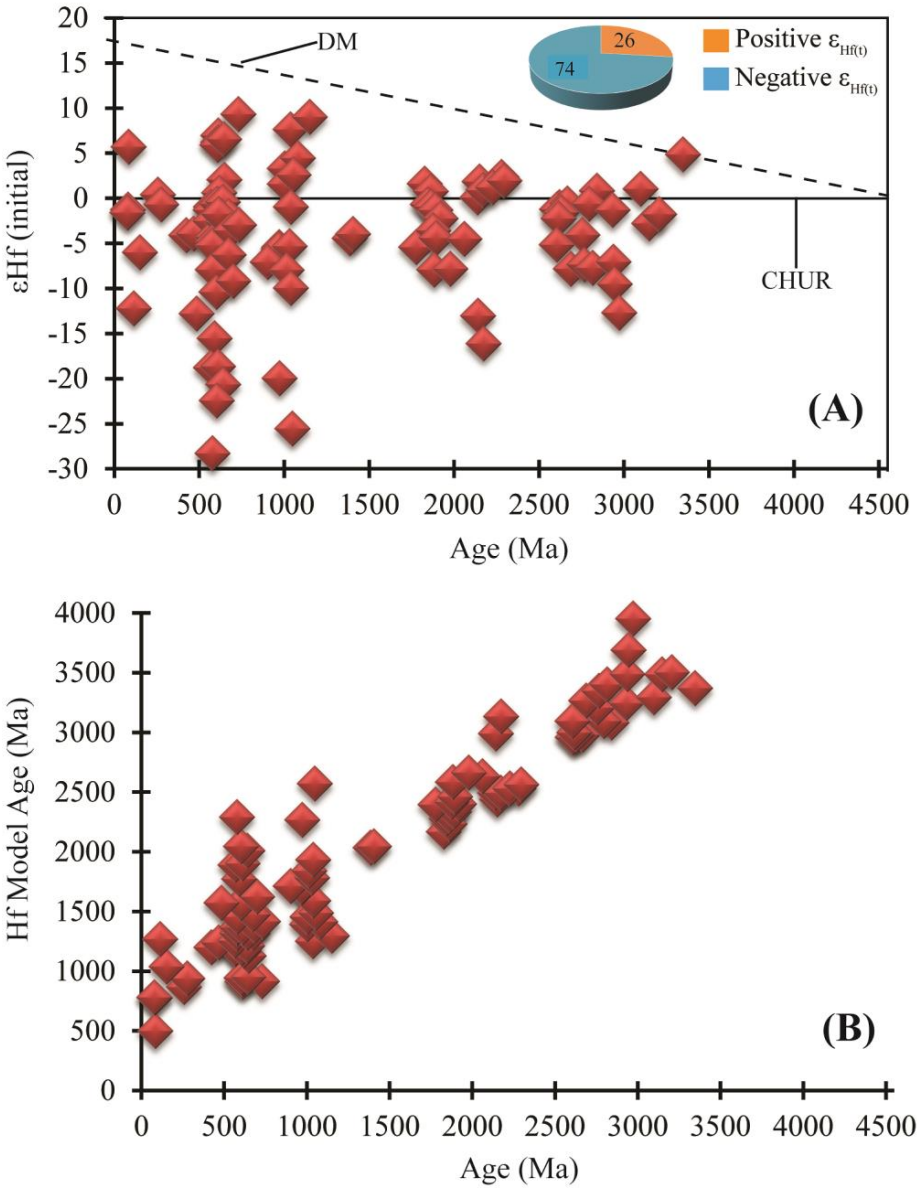

Figure 2-7 Lu-Hf plots for the detrital zircons from the Kasai Congo Basin.

(a) Plot of initial εHf vs U-Pb age of concordant detrital zircons from the Late Jurassic–Cretaceous units in the Kasai–Congo Basin (N = 97). (b) Plot of Hf model ages vs U-Pb age. The plot shows that most of the zircons in this study were derived from older crustal sources (The depleted mantle (DM) evolution curve is for linear evolution from a Chondritic Uniform Reservoir (CHUR) value at the Earth's formation (i.e., 0 at 4.56 Ga) to εHf = 17 at the present for the DM Dhuime et al. (2011)).

2.8 Discussion

Detrital zircon data reported here shed new light on Upper Jurassic-Cretaceous sediment sources and drainage patterns in the Kasai-Congo Basin, and more regionally within central Africa. This study demonstrates a wide range of detrital zircon populations and highlights the predominance of Precambrian source rocks in all four areas and throughout the stratigraphy in the Kasai region of the Congo Basin. Archean and Proterozoic zircons account for nearly 93% of all concordant analyses (n = 396) and ~94% of all discordant grains (n = 221). The discordant zircons were rejected from further investigation; however, the large proportion of discordant grains from this study does confirm the significance of Precambrian sources in the Kasai-Congo Basin. All provenance discussions are based on concordant zircon grains that pass the discordant 15% filter test.

2.8.1 Provenance of Jurassic-Cretaceous strata in the Kasai-Congo Basin

This section discusses the main zircon populations from the Kasai–Congo Basin in an attempt to place their provenance into a regional paleogeographic and tectonic context. The inspection of the combined probability density plot (Fig. 2-8) for the 15 analysed samples reveals five main population clusters from the Kasai–Congo Basin. The main population clusters include: 1) Paleoarchean to early Paleoproterozoic (3.3–2.4 Ga); 2) middle to late Paleoproterozoic (Eburnian Orogeny: 2.3–1.7 Ga); 3) Mesoproterozoic–early Neoproterozoic

(1.6–0.9 Ga); 4) middle – late Neoproterozoic (Pan-African Orogeny: 0.85–0.55 Ga); and 5) Paleozoic-Mesozoic (520–77 Ma). In general, the detrital zircon data have a wide Precambrian spread of crystallization ages (Fig. 2-8); yet there are significant age variations geographically from east to west (Fig. 2-6).

The age spectra of the detrital samples (N = 9) show dissimilarities (Fig. 2-9). This disparity in the age spectra even between samples of the same stratigraphic unit (e.g. Units C3) could be an artefact of small number of analysis for certain samples (Table 2-1). Drainage reversal and associated complexities in the central Africa (Congo Basin) during late Mesozoic times (Goudie, 2005; Stankiewicz and De Wit, 2006) could also explain the variabilities observed between samples. We used Kolmogorov-Smirnov (K-S) statistics to test the similarities between the nine samples that yielded a statistically viable number of analyses (i.e., $n \geq 20$) (e.g. Amidon et al., 2005; Solari et al., 2014). The results of the K-S tests (Fig. 2-10 and Table 2-2) show obvious differences even between samples from the same stratigraphic unit, suggesting that the nine samples are not similar and therefore not likely to have come from the same source area.

2.8.1.1 Paleoarchean–early Paleoproterozoic (3.3–2.4 Ga) zircons

The Paleoarchean to early Paleoproterozoic zircon grains from this study account for ~28% of the U-Pb analyses. Nonetheless, the actual proportion of the Paleoarchean to early Paleoproterozoic sources in the Kasai–Congo Basin is likely higher than 28% due to the high proportion (~70%) of discordant Paleoarchean to early Paleoproterozoic zircons. The large proportion of Archean – Paleoproterozoic zircons recovered in this study is noteworthy as only a fraction of the Congo-Kasai Craton is actually exposed at the surface today (Goodwin, 2013).

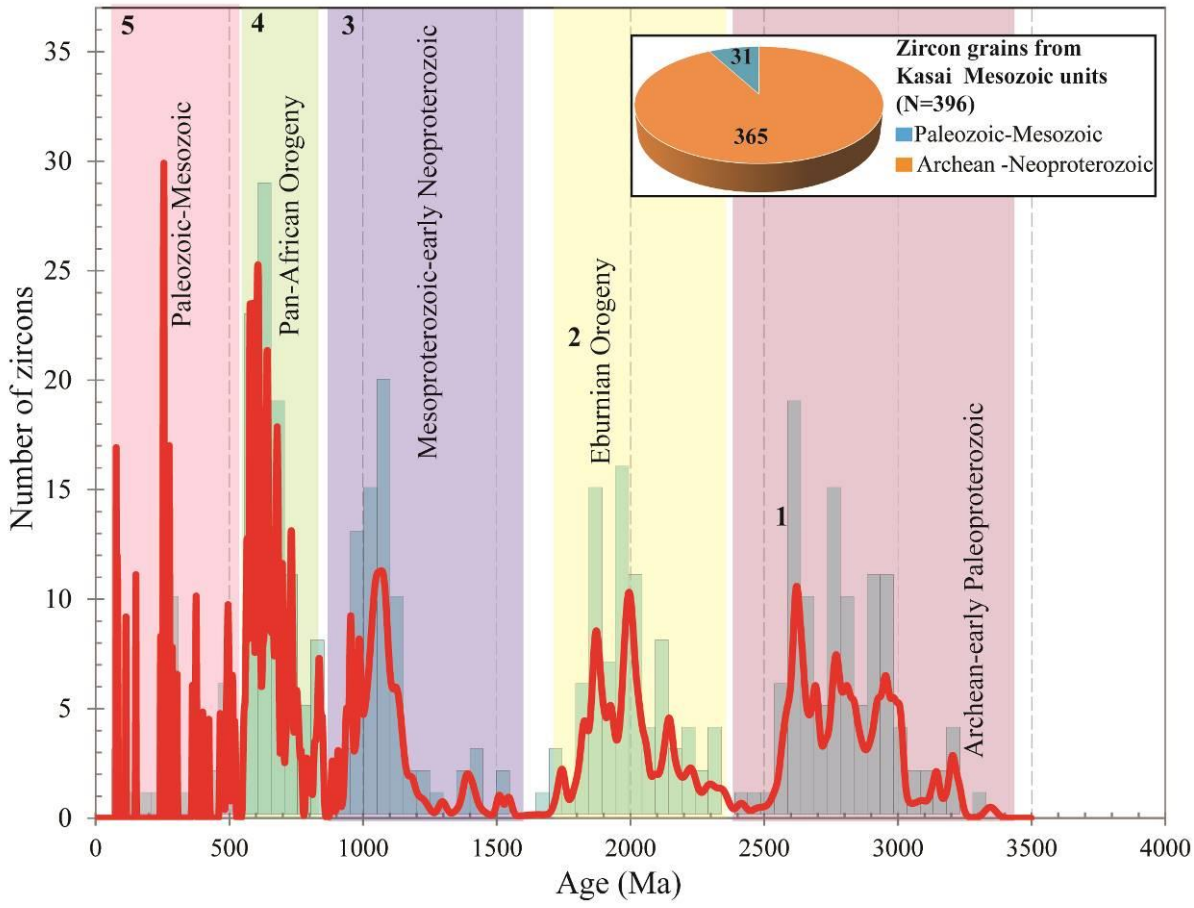

Figure 2-8 Probability density plots of all concordant analysis (n=396) from the Kasai–Congo Basin.

The plot shows five main detrital zircon populations from the zircons in the Kasai region; 1. Archean to early Paleoproterozoic (3.3–2.4 Ga); 2. Middle to late Paleoproterozoic (Eburnian: 2.3–1.7 Ga); 3). Mesoproterozoic–early Neoproterozoic (1.6–0.9 Ga); 4. Middle to late Neoproterozoic (Pan-African: 0.85–0.55 Ga) and 5. Paleozoic - Mesozoic (520–77 Ma).

This finding suggests that most of these very old zircon grains could have been sourced from other Archean cratons in the region. Existing age dates for the Congo-Kasai Craton suggest that crustal growth was focused between 3.1–3.0 Ga (Walraven and Rumvegeri, 1993) and 2.9-2.7 Ga (Delhal and Liegeois, 1982; Delpomdor et al., 2013). However, the U-Pb detrital zircon ages documented in this study and from recent analysis of sediments in modern drainages in the Congo Basin indicate a broader temporal range of Archean crustal growth (e.g., Batumike et al., 2009; Iizuka et al., 2013).

Paleoarchean to early Paleoproterozoic zircons recovered from the Kasai field area appear fresh and mostly euhedral or angular, with a major age peak centred on ~2.6 Ga. These Archean – Paleoproterozoic zircons in the Kasai-Congo Basin could have come from a number of cratonic sources in the region, including the Congo – Kasai Craton, the Zimbabwe Craton (3.57 – 2.57 Ga) or the Tanzania Craton (3.5 – 2.65 Ga), which are all known to host zircons of similar age (e.g. Muhongo et al., 2001; Jelsma and Dirks, 2002; Rollinson and Whitehouse, 2011; Kabette et al., 2012). The typically fresh and euhedral morphology of many of these Archean - Paleoproterozoic zircon grains are inconsistent with long distance sediment transport across the continent or multi-phase recycling from older sedimentary units. The predominantly negative initial εHf (t) values and older Hf model ages (Fig. 2-7) from our Lu-Hf analyses of zircons indicate that a high proportion of sediment in the Kasai – Congo Basin were derived from reworked older crustal sources. Furthermore, Batumike et al. (2009) reported previously unrecognised older crust (~ 3.6 Ga) in the central part of the Congo – Kasai Craton that underwent late Archean reworking. They interpreted this older crust as undergoing partial melting in the late Archean, which was successively reworked during the Paleoproterozoic, Mesoproterozoic and Neoproterozoic tectonic episodes. Moreover, whole rock studies by De Waele et al. (2008) on the Tanzania Craton indicated that this craton is mainly composed of juvenile mantle with minimal input from older crustal basement rocks. Findings by De Waele et al. (2008) indicate that the Tanzania Craton an unlikely source of Archean zircons in the Kasai area. The Permian glaciation and glacial transport of sediments into the basin from distal regions could explain the deposition of these very old zircons in the Kasai–Congo Basin, as well as the euhedral and fresh morphology of the grains. This scenario is unlikely, as only a single well core 171-X031 with any appreciable Permian strata was identified in the Kasai Region during our investigations. It

would be expected that the subjacent Unit J1 should have received more Archean – Paleoproterozoic zircons as it is closer to the crust than C3 or C4. However, only a single small core sample of Unit J1 was available for detrital zircon analyses compared to seven samples each of units C3 and C4. The low yield of Archean – Paleoproterozoic zircons from Unit J1 could be an artefact of the small number of analysis. The dominant 2.6 Ga peak coincides with magmatic events in the Kasai region and is also consistent with the age of the Kwanza Horst in northern Angola. The Kwanza Horst that sits on Congo-Kasai Craton may account for sediments of this age in the study area (e.g., Cahen et al., 1984; Batumike et al, 2009; Pearson et al., 2013). Similarly, the ~2.9 – 2.7 Ga peaks were likely derived from a portion of the Congo–Kasai Craton, which is exposed in the Kwango area southwest of Tshikapa (Figs. 2-1; Cahen et al., 1984; Delhal, 1991; Linol et al., 2016). These proposed sources are consistent with the limited paleocurrent data (n = 9) from outcrops of J1-C2 in the Tshikapa area. Detrital zircon grains >3.0 Ga, identified in this study are also likely to have come from the Congo-Kasai Craton as they are consistent with the age of crustal rocks identified by Batumike et al. (2009) from the southern part of the Congo Basin.

2.8.1.2 Middle to late Paleoproterozoic (Eburnian: 2.3–1.7 Ga) zircons

The middle to late Paleoproterozoic zircon population accounts for ~21% of the analyses that pass the discordance filter, with a primary peak at 2.0 Ga (Fig. 2-8). This peak coincides with the maximum depositional age of the Luana Formation (in the Luana Basin: Fig. 2-2), which developed between 2.03 Ga and 1.9 Ga on the Congo-Kasai Craton (Doucouré et al., 1999; Pereira et al, 2003). may have contributed to the sediments in the Kasai–Congo Basin. For instance, ~2.0 Ga grains are limited in the east, but are increasingly abundant in the central and western side of the basin (Fig. 2-6).

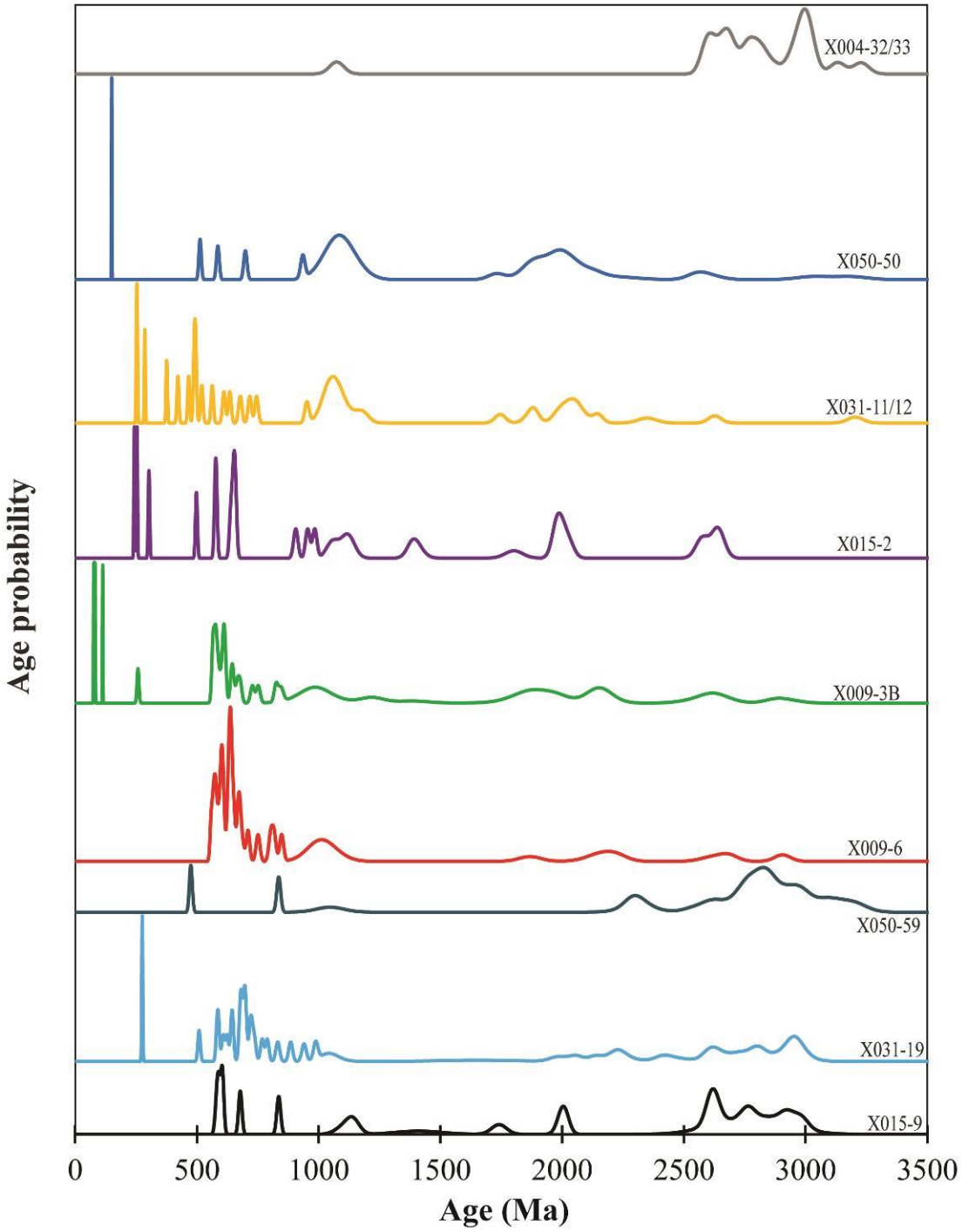

Figure 2-9. Relative age probability plots of detrital zircon samples (N = 9).

This plots shows similarities and differences between the different samples in the Kasai-Congo Basin.

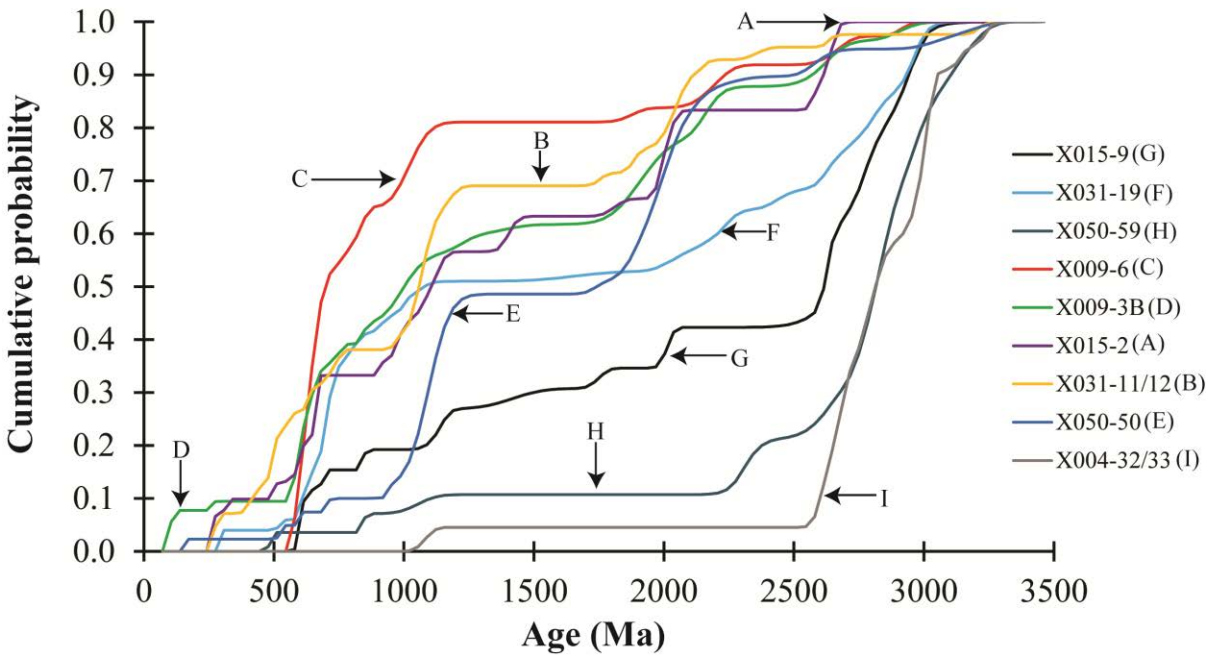

Figure 2-10. Cumulative distribution frequency diagram detrital zircon samples studied in the Kasai–Congo Basin

Table 2-2. K-S Test results for Kasai-Congo Basin samples (n = 9).

	K-S P-values using error in the CDF								
	X015-9	X031-19	X050-59	X009-6	X009-3B	X015-2	X031-11/12	X050-50	X004-32/33
X015-9		**0.087**	**0.130**	0.000	0.001	0.015	0.000	0.002	**0.050**
X031-19	**0.087**		0.000	0.037	**0.057**	**0.126**	0.011	0.017	0.000
X050-59	**0.130**	0.000		0.000	0.000	0.000	0.000	0.000	**0.808**
X009-6	0.000	0.037	0.000		**0.129**	**0.072**	**0.064**	0.000	0.000
X009-3B	0.001	**0.057**	0.000	**0.129**		**0.990**	**0.644**	0.009	0.000
X015-2	0.015	**0.126**	0.000	**0.072**	**0.990**		**0.951**	**0.153**	0.000
X031-11/12	0.000	0.011	0.000	**0.064**	**0.644**	**0.951**		**0.087**	0.000
X050-50	0.002	0.017	0.000	0.000	0.009	**0.153**	**0.087**		0.000
X004-32/33	**0.050**	0.000	**0.808**	0.000	0.000	0.000	0.000	0.000	

Notes: The bold p-values obtained are > 0.05, indicates that these samples passed the K-S test. The results show that the samples are more dissimilar than similar. Quantitative K-S tests were not conducted for the rest of the samples due to low or no zircon yield (Table 2-1).

The Paleoproterozoic age spectra show variability (Fig. 2-6) from Kabinda (east) to Tshikapa (west). These differences in the age spectra suggest that multiple Paleoproterozoic sources This pattern makes the Paleoproterozoic Ubendian Belt to the east of the basin an unlikely source for the ~2.0 Ga population in the Kasai–Congo Basin although portions of the

Ubendian Belt have been found to be dominated by reworked Archean crust (Fig. 2-11; Lawley et al., 2013; Linol et al, 2016). Instead, this population could have come from localized sources including from the south of the Kananga area or from the Paleoproterozoic granitoid intrusions within the Angolan Shield south of study area (Batumike et al., 2009; Pearson et al., 2013).

A different age variability is also seen in samples from east to the west of the study area. For example, 1.9 - 1.8 Ga zircon peaks are common in samples from the Kabinda area but limited in samples from the Mbuji Mayi and Kananga and absent in Tshikapa. This pattern suggests that the Ubendian Belt or the Bangweulu Block (Fig. 2-11) may be the main source for the dominant younger Paleoproterozoic population (1.9 - 1.8 Ga) in the eastern areas of Kasai–Congo Basin where most (N = 4) of the C3 samples were selected (De Waele et al., 2008; Kadima et al., 2011; Roberts et al., 2012). A dominant younger Paleoproterozoic population in the eastern part of the study area is consistent with Roberts et al. (2012) findings, who proposed long-lived Mesozoic paleo-drainage system that flowed along the NW trending Rukwa Rift (along the Ubendian Belt) and into the Congo Basin. Thus, it is possible that a paleo-river system drained the Ubendian Belt into the Cuvette Centrale, and then turned south into the Kasai–Congo Basin. The Lufubu Metamorphic Complex, which stretches from Namibia to the southern extent of the Democratic Republic of Congo also hosts grains of similar Paleoproterozoic age and could have sourced the middle Paleoproterozoic zircon grains recovered from the Kasai – Congo Basin (Rainaud et al., 2005).

2.8.1.3 Mesoproterozoic–early Neoproterozoic (1.6–0.9 Ga) zircons

Well-rounded Mesoproterozoic to early Neoproterozoic zircon grains account for ~19% of the total analyses with two main peaks at ~1.1 Ga and ~1.4 Ga (Figs. 2-6 and 2-8). The ~ 1.1 Ga peak is consistent with magmatic activity recorded in the Irumide and Lufilian Belts at that time (Fig. 2-2; Kampunzu and Cailteux, 1999; DeWaele and Mapani, 2002; De Waele et al., 2008). The recycling of local sedimentary units, such as the Upper Congo Supergroup or the Mbuji Mayi Supergroup, which has a maximum depositional age of ~1174 Ma could also account for the Mesoproterozoic zircons in this study (Jelsma et al., 2011; Delpomdor et al., 2013). However, this scenario is considered less likely than the former option, as a follow-on effect from a late Mesoproterozoic tectonism in the Irumide Belt is believed to have contributed to the extensive reworking along the southern margin of the Congo-Kasai Craton (De Waele et al., 2008).

The second peak around 1.4 Ga (n = 4) were documented from well core X015 in the Kananga area (Fig. 2-6). These ages are consistent with U-Pb zircon ages from the Kibaran Belt located to the northeast of the study area (Fig. 2-11; Tack et al., 2010). However, the preponderance of evidence for dominantly southern source areas suggests that these few grains are probably recycled from older sedimentary units in the study region, such as the Roan Group or Kundelungu Supergroup (Armstrong et al. 2005; Batumike et al., 2007).

2.8.1.4 Middle–late Neoproterozoic (Pan-African: 0.85–0.55 Ga) zircons

Middle to late Neoproterozoic zircons account for the second largest population of grains (~24%) in this study. They are represented by different populations between 850–550 Ma (Figs. 2-6 and 2-8), which are particularly common in the samples from the Kabinda and Kananga areas (Fig. 2-6).

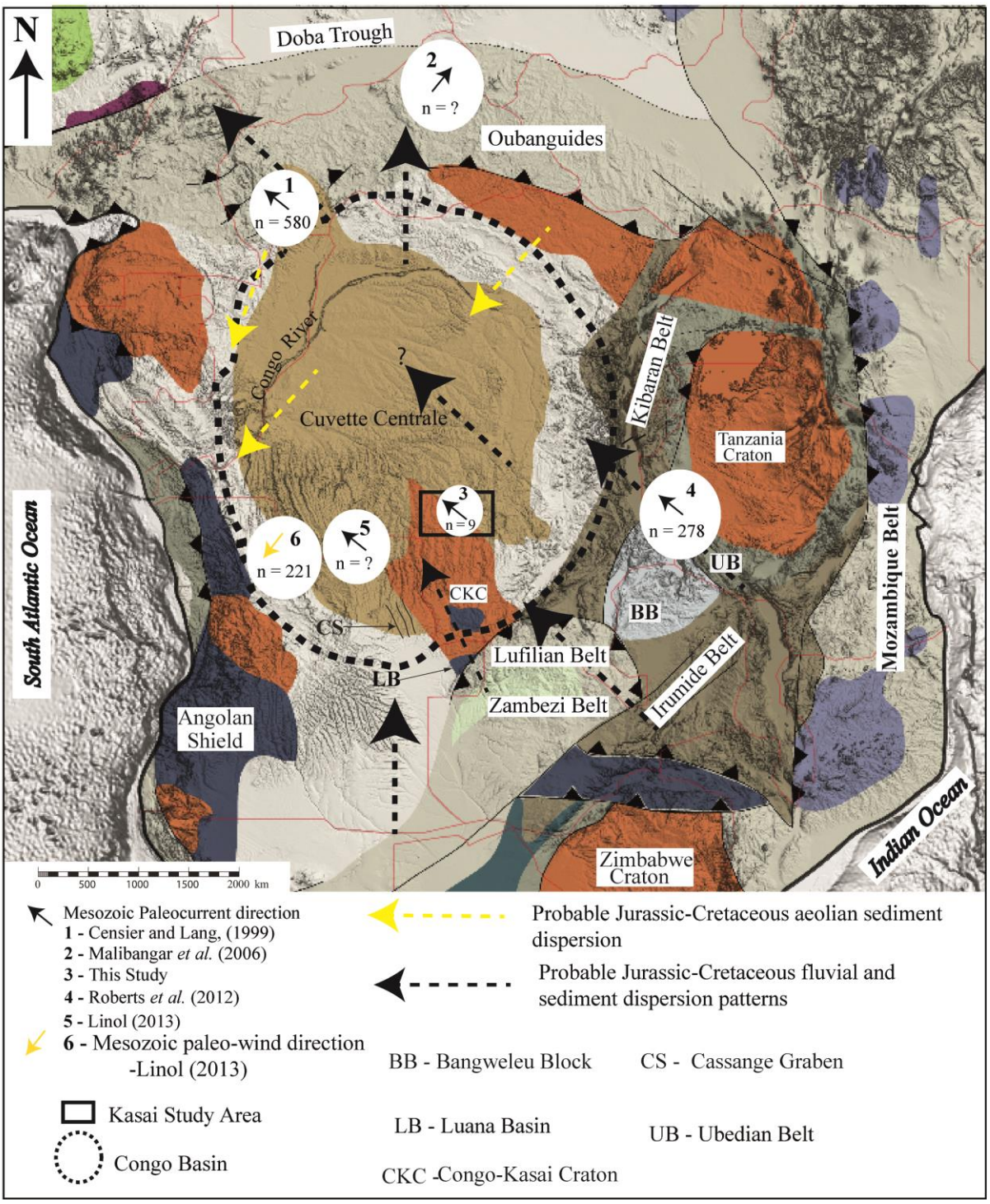

Figure 2-11. Probable Late Jurassic-Cretaceous sediment pathways and drainage patterns in central Africa.

The blue arrow river shows the probable sediment dispersion paths into the Kasai-Congo Basin (Map modified from Begg et al., 2009 and Foster et al., 2015).

The range of ages is typical of the Pan-African orogenic mobile belts around the Congo Basin (Fig. 2-11). These include the West Congo (~700-500 Ma), the Mozambique (~700-550 Ma), the Lufilian (~883-550 Ma) and the Zambezi belts (~795-530 Ma; Kampunzu and Cailteux, 1999; Hargrove et al 2003; Kröner and Stern, 2004; Armstrong et al. 2005; Frimmel et al., 2006). The Tshikapa area recorded the 12 Pan-African grains from a single well core 169-X020, which makes the West Congo Belt a likely source for the Pan-African age sediments in the Kasai-Congo Basin. However, a southern source, probably linked to the Lufilian Belt, is also a possibility and would be consistent with the well-rounded morphology of these grains and the limited north directed paleocurrents in the Tshikapa (e.g. Linol et al., 2016). Given the limited number of paleocurrents and lack of diagnostic ages linking these grains to either source, the provenance of these populations cannot be distinguished with certainty.

2.8.1.5 Paleozoic to Mesozoic (520–77 Ma) zircons

Paleozoic to Mesozoic zircons only account for ~8% of total grain population, yet they represent very important provenance sources and in some cases, help refine the depositional age of units. Permian-age peaks around 275 Ma and 255 Ma (Figs. 2-7 and 2-9) are the main peaks in this range, and they can be linked to a series of kimberlites and lamproites in Angola and Zambia (Smith et al., 1986), or possibly from within the Congo Kasai Craton as reported by Batumike et al. (2009). A suite of Cambrian (540–490 Ma) and Ordovician-Devonian (480-365 Ma) zircons is likely associated with recycled Paleozoic sedimentary strata in the Congo Basin, possibly within the Cassange Graben (Fig. 2-11; Roberts et al., 2015).

One of the most important populations identified in this study is represented by one Early Cretaceous and three Late Cretaceous zircon grains that were reported by Roberts et al.

(2015) from well core 173-X009 in the Kabinda area. The mean age of the three Late Cretaceous zircons (~79.8 Ma) is consistent with the maximum depositional age of the Kwango Series in the Congo Basin (Roberts et al., 2015). Furthermore, the Early Cretaceous grain (113 Ma) and a single Late Jurassic grain (150 Ma) recovered from well core 172-X050 in the Mbuji Mayi area, coincide with dates obtained for kimberlite magmatism in Mbuji Mayi and Lundas region of the Democratic Republic of Congo and north-eastern Angola respectively (Davis 1977; Schärer et al., 1997; Kerschhofer et al., 2000; Eley et al., 2008; Robles-Cruz et al., 2012;).

2.8.2 Jurassic-Cretaceous drainage patterns of the Congo Basin

Jurassic-Cretaceous drainage patterns in the Congo Basin are broadly reconstructed here based on the U-Pb geochronology data and a compilation of available paleocurrent data from the central Africa. The U-Pb age data presented here, as well as in other recent provenance studies, coupled with paleocurrent datasets from central Africa, consistently demonstrate north-directed rivers from southern sources into (and possibly back out) of the Congo Basin (Figs. 2-11; Censier and Lang, 1999; Malibangar et al., 2006; Roberts et al., 2012; Linol, 2013; Linol et al., 2016).

Paleo-wind patterns measured from Mesozoic aeolian strata along the Kwango River points to south-southwest wind flow (Linol et al., 2016). Linol et al. (2016) suggested that these aeolian sandstones may have sourced from volcanic dust originating from volcanoes above the Andean subduction margin of Gondwana. In contrast, the cross-stratified fluvial sandstones of the Kalahari Group they studied in the Kwango region indicate NNW directed paleoflow directions. This NNW paleocurrent direction is consistent with the limited

paleocurrent data from outcrops of J1-C2 in the Tshikapa area and detrital zircon provenance interpretations for the Kasai region. Both the Kwango and Kasai fluvial paleocurrents match the northwest oriented paleocurrent orientation documented for the Mesozoic strata in the Rukwa Rift Basin by Roberts et al. (2012), who suggested that a large trans-continental river system flowed northwest out of the Rukwa Rift into the Congo Basin. However, Roberts et al. (2012) were not clear whether this fluvial system emptied into a "paleo-lake" Congo or whether it joined other stream systems and continued across the basin.

The direction of fluvial systems in central Africa may be understood by examining paleocurrent data from other parts of the Congo Basin or central Africa. Although such data is limited, paleocurrent analyses of the Cretaceous Carnot and Mouka-Ouadda Sandstone formations on the northern flank of the Congo Basin in the Central African Republic, both indicate north directed flows (Censier and Lang, 1999; Malibangar et al., 2006). In the Carnot Sandstone Formation located southwest of the Central African Republic, investigations by Censier and Lang (1999) identified a NNW flowing braided fluvial system that apparently flowed out of the Congo Basin through Central African Republic and into the Doba Trough in Chad and the Touboro Basin in Cameroon, which are both part of the Central African Shear Zone (Fig. 2-11). Similar investigations of the Mouka-Ouadda Formation on the north-eastern margin of the Central African Republic also apparently indicate a braided stream with proximal conglomerates and distal fine-grained sandstones with NNE-NE directed paleoflows, which Malibangar et al. (2006) argued were sourced from within the Congo Basin.

The majority of provenance and paleocurrent data for Upper Jurassic-Cretaceous fluvial deposits across the Kasai region, and indeed much of the Congo Basin, suggest north directed

fluvial systems during this time. Tributaries likely originated from highlands to the south of the Congo Basin in the Lufilian and Irumide Belts, along with minor point sources in the Ubendian Belt to the southeast. These rivers flowed into the Kasai region, where they received considerable local sediment input from the Archean Congo-Kasai Craton, which was likely exposed at this time (Godwin, 2013) due to reactivation and faulting of Precambrian basement structures as reported by Roberts et al. (2015). These river systems likely then flowed north into the Cuvette Centrale, where they probably coalesced with large fluvial systems coming out of the Kwango region, as well as from the Rukwa Rift System via the Luama Trough. It is hypothesised that, at certain times, these north directed rivers fed large, ephemeral lake systems and possibly a marine embayment in the Cuvette Centrale (see Roberts et al., 2012). However, it seems likely that at other times, this hypothetical Mesozoic trunk river system likely transported sediment across the basin, into the CAR and then emptied into the Doba Trough and Touboro Basin as suggested by Censier and Lang (1999). This scenario is consistent with thick sedimentary successions reported for portions of the Central African Shear Zone by Ibrahim et al. (1996), which was reactivated during the break-up of Gondwana in the late Mesozoic and became a major sediment depocentre.

2.9 Conclusions

This study provides the first detailed detrital zircon investigation of the Mesozoic strata in the Kasai–Congo Basin. The results of sandstone petrography, paleocurrent analysis, and U-Pb and Lu-Hf analyses of detrital zircons suggest that the most significant provenance sources for the Kasai region are the Archean-Proterozoic Congo–Kasai Craton and Proterozoic Irumide and Lufilian mobile Belts located to the south – southeast of the Congo Basin. The

dominance of Precambrian zircon populations in Upper Jurassic–Cretaceous strata suggests exhumation and erosion of these mobile belts to the south of the basin, as well as local structural uplifts and basement highs in the Congo–Kasai Craton.

Based on these patterns we proposed that a north-directed transcontinental paleoriver system developed in central Africa during the Late Jurassic-Cretaceous. This fluvial system is believed to have originated from the southern highlands in Malawi, Zambia, and southern Democratic Republic of Congo and flowed into the Congo Basin and potentially converged with another large channel system from the east (Rukwa Region). This hypothetical transcontinental river system may have periodically flowed entirely across the basin, combining with channel systems in Central African Republic, before emptying into the Central African Shear Zone. From here, this channel system may have formed an inland delta system, or fluvial transport may have continued westward through the Central African Shear Zone and into the Proto-Atlantic Ocean via the Benue Trough. The new data from this study can help us to better understand the sediment dispersion in the Kasai–Congo Basin, including primary and secondary sources of alluvial diamonds.

3. CHAPTER THREE

Detrital zircon provenance analysis of the diamondiferous mid-Cretaceous Calonda Formation, northeastern Angola.

Abstract

The middle-Cretaceous Calonda Formation was deposited within a series of SW-NE trending grabens and half-grabens in the northeastern part of Angola and the southwestern part of the Democratic Republic of Congo. The Calonda Formation, a first collector of diamonds resulting from erosion of primary and weathered, Cretaceous kimberlite sources is assigned a middle-Cretaceous age based primarily on fish macrofossils and palynomorphs, and on the observation that it was deposited synchronously with kimberlite magmatism sometime between 145 Ma and 113 Ma. In this study, constraints were put on the depositional age and sedimentary provenance of the Calonda Formation . Sandstone petrography and U-Pb geochronology coupled with Lu-Hf isotope geochemistry and trace elements of detrital zircons from four Calonda Formation core samples were analysed. All four samples are dominated by quartz reflective of recycled orogen and/or craton interior provenance fields. U-Pb detrital zircon age spectra show that the sediments are largely derived from Neoproterozoic (20%) and Permian (26%) basement sources. The reminder of the zircons have ages spread across the Archean to Mesozoic time periods, including eight Cretaceous grains. The Lu-Hf isotope compositions from the zircon populations are dominated by negative initial εHf (t) values accounting for 71% of analyses, suggesting a dominant input from older reworked crustal sources. Trace element results on selected grains indicate depleted HREE, enriched LREE, strong negative Eu and positive Ce anomalies, which are all consistent with felsic magmatic sources within Kasai Craton, with input from the Lufilian Arc and recycled Permian sedimentary strata of the Karoo Supergroup, to the south of the study area. These results, coupled with the fluvial facies characteristics of the Calonda Formation, indicate that sediment delivery into the Lucapa area was dominated by localized north-directed fluvial channels. The maximum depositional age for the Cretaceous

Calonda Formation is interpreted as 130.3 ± 3.4 Ma (MSWD = 0.87; prob. = 0.48; n = 5) based on the weighted mean age for the youngest coherent population.

Key words

Calonda Formation, Lunda, kimberlite, detrital zircon, U-Pb dating, Lu-Hf isotopes, trace element, provenance, paleodrainage, tectonics, Africa

3.1 Introduction

Angola is located in southern Africa and is bordered on the north and northeast by the Democratic Republic of Congo (DRC), to the west by the South Atlantic Ocean, Zambia to the east and Namibia to the south (Fig. 3-1). The country is well endowed with natural resources such as oil and gas, diamonds, iron ore, copper and rare earth metals. After oil and gas, diamonds are the most important export commodity (Dietrich, 2000). The diamonds produced from the Lunda Provinces have made Angola the fifth largest producer by value and the sixth largest in the world by volume (Real, 1959; Boyd and Danchin, 1980; Janse and Sheahan, 1995; Faure, 2010; Chambel et al., 2013; Zimnisky, 2017). The Lunda Norte Province (Fig. 3-1) in particular is noted as the place in Angola where the first alluvial diamond was recovered from the Mussulala River in 1912, and the subsequent discovery of the first kimberlite pipe in the Chicapa River in 1952 (De Kun, 1987; Janse and Sheahan, 1995).

The kimberlite and carbonatite occurrences in Angola are concentrated along the Lucapa Corridor (Fig. 3-1), a fault system stretching from the southwest to northeast of the country through to the southern DRC (e.g. Reis, 1972). The concentrated alluvial diamonds in the Lunda and Kasai provinces are typically thought to have been sourced through downwasting of diamond-bearing, most likely deeply weathered, kimberlite pipes mostly within the Lucapa Corridor, with sediments redeposited by northward flowing river systems in migrating river beds, alluvial flats alongside the rivers, terrace deposits, or proximal eluvial deposits (Davis, 1977; Helmore, 1984) during Cretaceous as well as post-Miocene times. The northeastern Angola kimberlites are considered to have formed synchronously with the opening of the South Atlantic beginning at ~145 Ma in the Kwanza graben of Luanda, and possibly continuing until 70 Ma in the Kasai Province of DRC (Jelsma et al., 2009).

A good constraint on the age of kimberlite in Angola is critical to both exploration and mining of the diamonds. Particularly, it can confirm the existence of kimberlite magmatism in a certain area (e.g. Heaman et al., 2003). The ages of kimberlites in Angola are still poorly constrained but appear to get younger from SW to NE of the country (Eley et al. 2008; Robles-Cruz et al., 2012; Jelsma et al., 2013). The ages of kimberlites have been variously posited, between unconfirmed possibly Devonian times in southwestern Angola (Egorov et al., 2009); Triassic times in central Angola (252 to 216 Ma: Jelsma et al., 2013) and Early Cretaceous times in northeastern Angola (145-113 Ma, Eley et al. 2008; Robles-Cruz et al., 2012; Castillo-Oliver et al. 2016). However, the older ages reported for Angola kimberlites are largely questionable. For instance the Devonian (372 Ma) age for the Chicuatite kimberlite in SW Angola did not result from radiometric methods but was calculated using constants (Egorov et al., 2009). Additionally, the 145 Ma and 136 Ma older ages documented by Eley et al. (2008) are both single point perovskite ages. However, the 115-113 Ma ages from Eley et al. (2008) and the 121-118 Ma ages by Robles-Cruz et al. (2012) for Catoca kimberlites are not single point but representative ages of kimberlites in the northeast of Angola. Moreover, the more recent 133-116 Ma ages by Castillo-Oliver et al. (2016) on perovskites from four areas in the NE Angola support the earlier findings of both Eley et al. (2008) and Robles-Cruz et al. (2012), and the cross-cut relationships kimberlite pipes and local rock units. The kimberlite pipes in northeastern Angola clearly cross-cut the Carboniferous-Permian Lutôe and Permian-Triassic Cassange groups, indicating Mesozoic emplacement (Fig. 3-2).

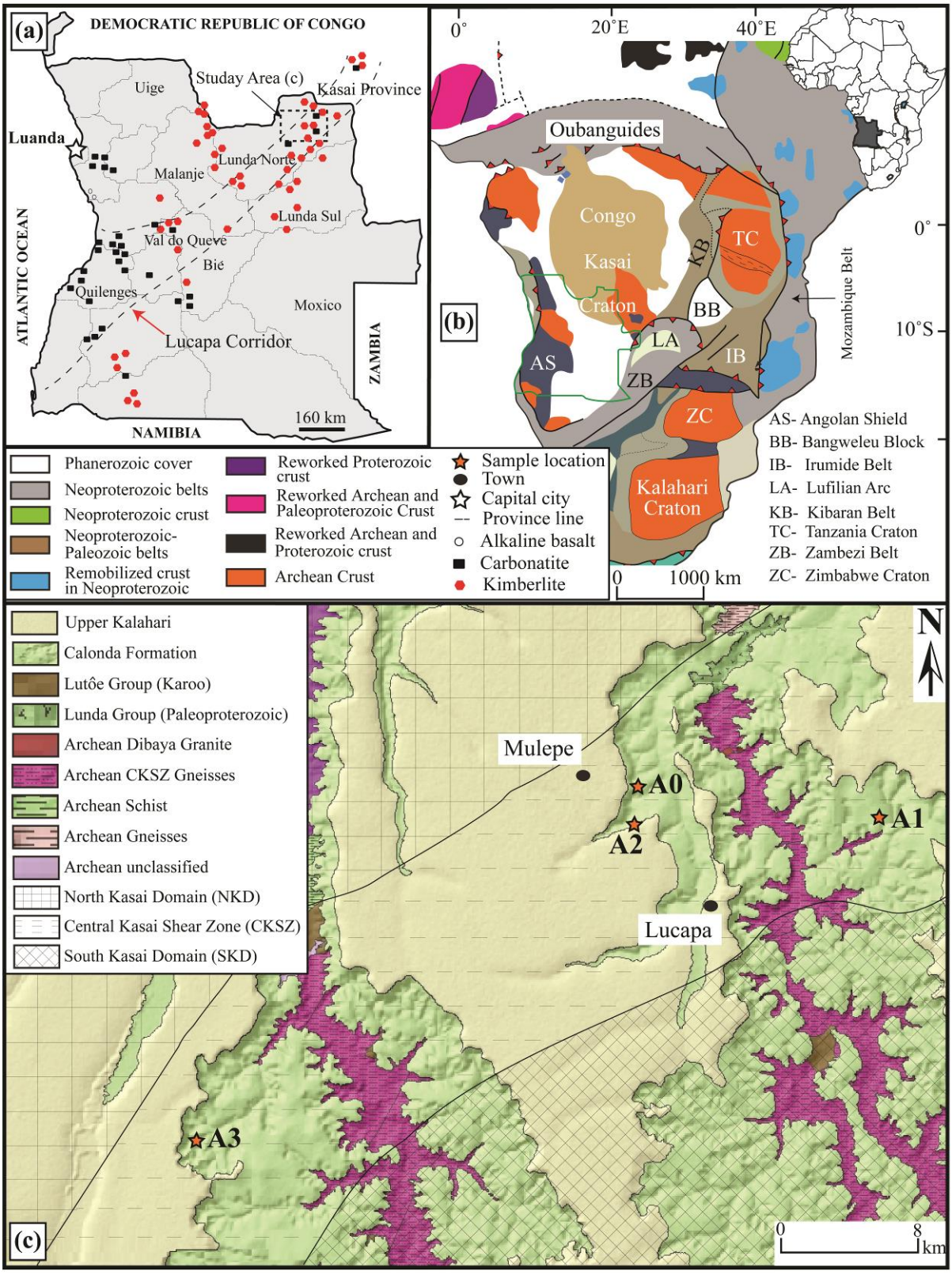

Figure 3-1 Geographic location of the study area in NE Angola.

(a). Simplified map of Angola showing the Lucapa Corridor with dominant kimberlite and carbonatite locations. (b). Generalized bedrock map of central and souther Africa after Begg et al. (2009). (c). The three tectonic domains

within the Kasai Craton discussed by Jelsma et al. (2015) are superimposed on the local geology of the study area in Lucapa, in the Lunda Norte Province, showing the different units in the area and the four sample locations.

The majority of these kimberlite pipes have been eroded away or remain covered, leaving considerable uncertainty with respect to the true timing and distribution of pipes in the Lucapa Corridor. However, the presence of widespread alluvial diamond bearing deposits in northeastern Angola and southern DRC provides important clues to unravelling these questions. In particular, the Cretaceous Calonda Formation or Calonda 'Gravel' widely recognized as one of the most significant sources of alluvial diamonds in the world (e.g. Janse and Sheahan, 1995) could give information on the timing and distribution of these kimberlite pipes.

This unit has been characterized as the first collector of alluvial diamonds generated from continental diastrophism, supergenic destruction and erosion of kimberlites in the NE Angola and the SW of the DRC during the late Mesozoic (Pereira et al., 2003; op. cit.). The Calonda Formation is also widely regarded to have been eroded and reworked in many places, providing the source for much of the younger diamondiferous post-Miocene terrace deposits mined in the region. However, the stratigraphy and age of this important diamond-bearing unit is still weakly constrained and interpreted to be between Albian and Cenomanian times based on the emplacement ages of kimberlites thought to be pre- or syn-depositional (Eley et al. 2008); and on fish macrofossils and palynomorphs (Davis, 1977). Refining the stratigraphy, age and sedimentary provenance is expected to help exploration and discovery of both primary kimberlites and secondary alluvial diamonds sources in the Lunda Province of Angola. The aim of this study was to put constraints on the age of deposition and source of sediment for the Calonda Formation and to provide better controls on the temporal

stratigraphic relationships, depositional history, and tectonic evolution of the Lucapa Corridor (NE Angola), and more broadly the Congo Basin.

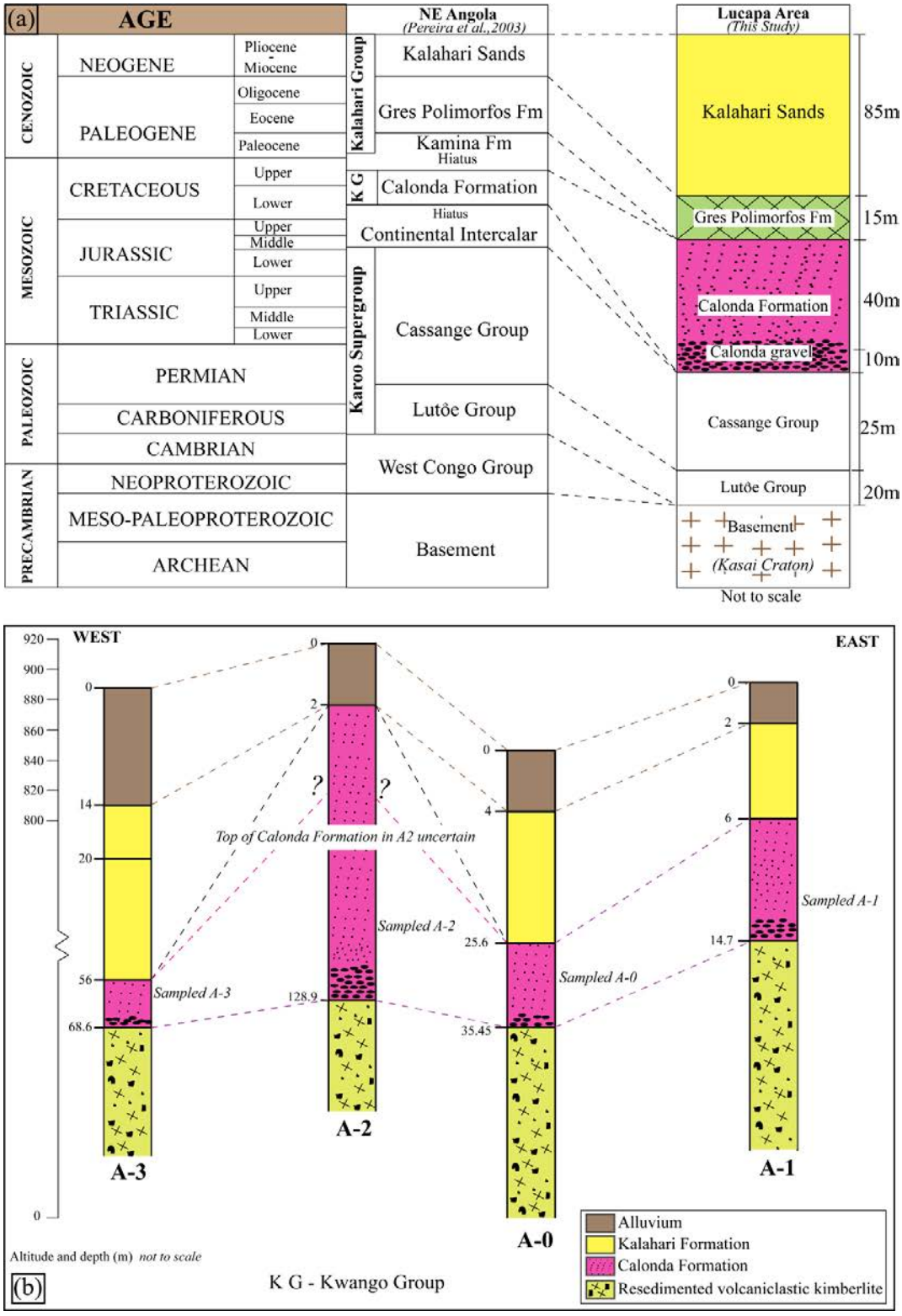

Figure 3-2. Stratigraphy of Calonda Formation.

(a). Simplified stratigraphy of the Lunda Norte Province after Pereira et al. (2003) and (b) Simplified stratigraphic correlation between the four Calonda Formation samples used in this study.

To accomplish this, sandstone petrography was combined with U-Pb geochronology, Lu-Hf geochemistry, and zircon trace element analysis of the Calonda Formation samples from different stratigraphic intervals (Fig. 3-2). Analysis was performed on four exploration core samples recovered from the type area by De Beers Group Exploration near the town of Lucapa in the Lunda Norte Province (Fig. 3-1c).

3.2 Geological setting and stratigraphy of the Lunda Province

3.2.1 Geologic setting.

The basement architecture of Angola is dominated by the Angolan Shield in the west and the Kasai Craton to the east. The Angolan Shield and the Kasai Craton represents the Congo-Kasai Craton in Angola (Jelsma et al., 2018). The Congo-Kasai Craton of central Africa extends from Angola through the DRC into South Sudan (e.g. De Waele et al. 2008; McCourt et al. 2013; De Wit and Linol, 2015; Jelsma et al., 2018). The basement rocks are dominated by Archean and Paleoproterozoic ages (De Carvalho et al., 2000; Jelsma et al., 2015). Archean lithologies include gneisses, migmatites and granulites, granitoids, gabbros and norites, schists, amphibolites and quartzites (De Carvalho et al., 2000). Paleoproterozoic lithologies have been related to the Eburnean times (2.1-1.9 Ga) development of continental arc complexes along the western edge of the craton. They are mainly comprised of gneisses and granitoids and associated supracrustal lithologies. Following the Pan-African orogeny (600 – 540), large parts of the basement were covered by Cambrian-Ordovician red-bed sediments. During the Phanerozoic, the Gondwana supercontinent was subjected to far-field

stresses resulting in the formation of the Karoo-age Cassange Graben and Cretaceous-age grabens and half-grabens. The formation of rift basins was accompanied by intraplate magmatism including of alkaline basalt, carbonatite and kimberlite types (Reis 1972; De Boorder, 1982; White et al., 1995; Campeny et al., 2014, 2015).

Amongst these is the Lucapa Corridor, which is a deep-seated, long-lived extensional fault system that is up to 90 km wide in the Lunda Provinces, and stretches over 1600 km in length from Quilenges in the southwestern part of Angola to Mbuji-Mayi in southern DRC (e.g. Sykes, 1978; Jelsma et al., 2009; Perritt et al., 2011; Pervov et al., 2011). This Corridor boasts of a long history of magmatic and tectonic activities dating back to the Paleoproterozoic, and with discrete episodes in reactivation from the Permian-Triassic and in the Cretaceous (Jelsma et al., 2009). During the Cretaceous a series of N-S faults and WSW-ENE trending grabens and half-grabens were formed. The tectonic evolution of the Lucapa Corridor is still poorly understood because of paucity of geological and geophysical data and presence of widespread Kalahari sedimentary cover (e.g. De Boorder, 1982; White et al., 1995), but is beyond the scope of this study.

3.2.2 Stratigraphy of the Lunda Province

The Kasai Craton forms the basement of the Lunda Provinces in northeastern Angola, with up to 7 km of Phanerozoic cover sediments of the Congo Basin in places preserved (Linol et al., 2015a,b; Roberts et al., 2015; Jelsma et al., 2015: Fig. 3-1). Jelsma et al. (2015) identified three key crustal tectonic domains within the Kasai Craton (Fig. 3-1). First is the Northern Kasai Domain (NKD), which they interpreted as a juvenile Neoarchean magmatic arc complex with ages ranging between 3.0–2.7 Ga. Southern Kasai Domain (SKD) is the

second domain, which Jelsma et al. (2015) interpreted as the old nucleus of the Kasai Craton with ages ranging between 3.6–2.8 Ga. The third domain described by Jelsma et al. (2015) is the Central Kasai Shear Zone (CKSZ), which connects the other two, and is comprised of a complex assemblage of terranes and sedimentary basins (Fig. 3-1).

The Paleozoic Karoo Supergroup in the Lunda Provinces unconformably overlies Archean and Proterozoic basement lithologies of the Kasai Craton. The Karoo Supergroup is divided into two groups, including: the Lutôe Group and the Cassange Group. The Carboniferous-Permian Lutôe Group is deposited directly on basement rocks of the Kasai Craton (Fig. 3-2), and generally considered to be stratigraphically similar to the Dwyka and Ecca Groups of Southern Africa (e.g. Bangert et al., 1999).The Lutôe Group is composed of tillites, conglomerates, sandstones and shales, and is mainly preserved at the base of down faulted grabens in the study area, cropping out in the Chicapa, Luachimo and Luembe rivers valleys. The overlying Upper Permian to Triassic age Cassange Group is mainly composed of fine-grained, thinly bedded sandstones with fossilized plant and fish remains (Antunes et al., 1990), which are exposed in the Cassange Graben and catchment of the Cuango (alt. Kwango) River (Fig. 3-2). The late Mesozoic stratigraphy in the Lunda provinces includes the Upper Jurassic-Lower Cretaceous Continental Intercalar and the Cretaceous Calonda and Kwango formations that have been assigned to the Kwango Group (Fig. 3-2). The basal conglomerates of the Calonda and Kwango Formations in northern Angola and adjoining parts of the DRC are assumed to be of the same age and together form the Kwango Group (Roberts et al., 2015). The Kwango Group is overlain by the Upper Cretaceous to Neogene Kalahari Goup, which is comprised of the Grés Polimorfos and the Kalahari Sands (Pereira et al., 2003). The Grés Polimorfos are characterized by calcretised gravels with well-rounded

quartz and quartzite clasts, whereas the Kalahari Sands are generally of Aeolian origin, and largely comprised of unlithified well sorted sand of varying thickness (Ward, 1998).

3.2.3 Stratigraphy and sedimentology of the Calonda Formation

The Cretaceous stratigraphy in the Lucapa region is quite variable, with Aeolian Continental Intercalar locally present (e.g., along the Kasai river in the DRC, Ward, 1998). Overlying the Continental Intercalar, and in some cases directly above basement or the Lutôe Group is the Calonda Formation (Fig. 3-2), comprising of a prominent basal diamondiferous conglomerate and overlain by red bed sandstones, minor conglomerates, silcretes, and mudstones (Pereira et al., 2003). The colour of the Calonda strata are affected by the presence of iron and manganese. The stratigraphy of the Calonda Formation is characterised by a fining upward succession. The Calonda gravel is a matrix-supported pebble to cobble size gravel with intraformational and extra-basinal clasts (Roberts et al., 2015). The Calonda Formation is thought to have been deposited shortly after or possibly syndepositional with kimberlite magmatism in the Lunda Provinces between ~145 and 113 Ma (Eley et al. 2008; Robles-Cruz et al., 2012), and on correlation with the Loia Group in the DRC (Roberts et al., 2015). The transition between the Calonda Formation and the overlying Kalahari Group is defined as a disconformity produced by a weak erosional event or hiatus, which is represented by the basal Grés Polimorfos. Kalahari Sands (or Ochre Sands) make up the top of the Kalahari Group in the Lucapa area (e.g. Cahen et al., 1984).

3.3 Study area and sampling

The topography of the Lucapa area is characterised by flat interfluves and deep river valleys formed by prominent alluvial diamond-bearing rivers such as the Lumange, Chicapa (alt.

Tshikapa), Luachimo (alt. Longatshimo) and Chiumbe (alt. Tshiumbe) that incise through the Paleogene, Cretaceous cover deposits and the underlying basement rocks (Cahen et al., 1984). The Kalahari surface in the Lucapa area slopes NE-ward suggesting post-Miocene tilting of the land surface. This tilt is associated with slope erosion, which allowed drainage channels to cut through the Kalahari and Calonda sediments (and in places Karoo) into the crystalline basement, redepositing sediments in river terraces (Helmore, 1984).

Table 3-1. Location details of the four core samples

Sample #	Formation	Elevation (m)	Latitude	Longitude
A-0	Calonda	847	8°22'7.44"S	20°41'39.07"E
A-1	Calonda	891	8°22'41.10"S	20°49'55.07"E
A-2	Calonda	918	8°22'50.57"S	20°41'34.77"E
A-3	Calonda	887	8°33'40.84"S	20°26'51.00"E

Note: Sample locations are shown on Figure 3-1c.

The study samples were selected from four cores drilled through the Calonda Formation near the town of Lucapa in Lunda Norte Province, northeastern Angola (Fig. 3-1). Lucapa is located ~800 km to the east of Luanda (Fig. 3-1). The area has a large number of reported kimberlites intruding the basement lithologies and the Karoo Supergroup sediments (Figs. 3-1 and 3-2). Four core samples of the alluvial diamond-bearing Calonda Formation were selected at different depths (Fig. 3-2B; Table 3-1) from sites drilled as part of kimberlite exploration programme of De Beers Group Exploration in Angola. All the four drill holes are located within the Central Kasai Shear Zone (see Jelsma et al., 2015).

3.4 Analytical methods

3.4.1 Sandstone petrography

Sandstone petrographic investigations was done to help infer parent rock characteristics of the four samples. Four thin sections were prepared to the standard thickness and point-counted following the Gazzi-Dickinson method (Ingersoll et al*.,* 1984), at James Cook University (JCU), Townsville, Australia. The point-counted data consisting of 350 points counted per sample were used to estimate the compositional percentages of quartz (Q), feldspar (F) and lithic (L) grain fragments (Ingersoll et al*.,* 1984; Dickinson, 1985), using transmitted-light polarizing Leica DMRXP microscope. Details of analytical methods are outlined in Owusu Agyemang et al., 2016, 2018)

3.4.2 U-Pb detrital zircon geochronology

Four detrital zircon samples typically weighing between 1.5-2.5 kg were separated at JCU, following standard procedures (e.g. Gehrels et al*.,* 2008) and then handpicked (≥ 100 grains for each sample) under a stereomicroscope and mounted in a 25 mm diameter transparent epoxy resin puck with pieces of zircon standards GJ-1 (609 Ma, Jackson et al*.,* 2004) and Temora-2 (416.8 Ma, Black et al*.,* 2003). Detailed sample preparation, zircon mounting and U-Pb dating analyses are outlined in Owusu Agyemang et al. (2016) presented in chapter two of this thesis. Zircon grains were ablated using a 32 beam diameter. Data reduction and age determination was performed using the GLITTER 4.0 software program (Van Achterbergh et al*.,* 2001). The reduced data was exported to Microsoft Excel with Isoplot/Ex 4.15 (Ludwig, 2012) for data analysis and display. A discordance cut-off of 15% was used for all grains >300 Ma as younger $^{207}Pb/^{206}Pb$ ages are not reliable (Gehrels, 2012). Kolmogorov-Smirnov

(K-S) statistical tests were used to compare the age distributions for provenance interpretations (see Owusu Agyemang et al., 2018 for detailed discussion).

3.4.3 Lu-Hf isotopic systematics

Detrital zircon grains from the four Calonda Formation samples were first dated and subsequently analysed for their Lu-Hf isotope ratios. Only zircon grains from the main populations from all four samples that passed the discordance filters were selected for Lu-Hf analyses. The Lu-Hf isotope analyses were conducted using a GeoLas 193-nm ArF laser and a Thermo Scientific Neptune multicollector (MC) ICP-MS. The isotopic data was acquired following procedures outlined by Kemp et al. (2009) and Næraa et al. (2012) using a uniform laser spot size of 60 μm, usually overlapping the same spot of concordance where the zircon grain was ablated during the U-Pb analysis.

The Lu-Hf datasets were subsequently processed offline to check for the homogeneity of all ablated zircons. Corrections for the isobaric interference of lutetium (Lu) and ytterbium (Yb) on ^{176}Hf was performed by monitoring ^{175}Lu (^{176}Lu/^{175}Lu = 0.026549) and ^{171}Yb (^{176}Yb/^{171}Yb = 0.897145), respectively. Both ^{171}Yb and ^{173}Yb were measured in order to correct for the mass bias and subsequently corrected by exponential law (Fisher et al., 2011). The measured average ^{176}Hf/^{177}Hf ratio from two standard zircons; Mud Tank zircon (MTZ) and Geo-standard FC1 zircon, were used to monitor the instrumental state and analytical accuracy (Fisher et al., 2014). The FC1 zircon standard was repeatedly measured, for which normalized ^{176}Hf/^{177}Hf values was 0.282189 ± 16 (n = 11) and the 'true' (solution) value is 0.282184 ± 16 (Woodhead and Hergt, 2005). The measured average ^{176}Hf/^{177}Hf from MTZ obtained over all analytical sessions is 0.282480 ± 6; (n = 17) and was compared with the 'true' (solution) value of 0.282507 ± 6 (Woodhead and Hergt, 2005), where the uncertainties

are two standard deviations. Based on the analyses of the MTZ, a $^{176}Hf/^{177}Hf$ normalization factor of *1.000094* was applied to the unknown sample zircons from this study (Næraa et al., 2012; Fisher et al., 2014). The ^{176}Lu decay constant of $1.867 \pm 0.008 \times 10^{-11}$ $year^{-1}$ reported by Söderlund et al. (2004) and the Chondritic Uniform Reservoir (CHUR) values of $^{176}Hf/^{177}Hf$ (0.282785) and $^{176}Lu/^{177}Hf$ (0.0336) reported by Bouvier et al. (2008) were used in the calculation of initial εHf(t) values and model ages.

3.4.4 Zircon trace elements analysis

Zircon trace element analyses were also conducted on a subset of grains from the main populations for each sample that had been analysed for U-Pb and or Lu-Hf isotopes. The trace element analysis was done to get more information on source region characteristics (e.g. Pearce et al., 1984; Heaman et al., 1990). The trace element analysis was conducted via LA-ICP-MS following procedures outlined in Kovacs et al. (2009), using a uniform spot size of 44 μm throughout the analysis. Detailed operating conditions and analytical procedure are listed in Chapter two and Owusu Agyemang et al. (2018).

3.5 Results and interpretation

3.5.1 Sandstone petrography

Modal QFL compositions and photomicrographs of the four thin sections are shown in Figure 3-3. All samples dominated by monocrystalline quartz grains with little to no feldspar. The only appreciable difference between the samples is the slightly higher concentration of polycrystalline quartz and lithics in A-1. Sample A-2 is much finer grained with a higher

proportion of clay matrix and hematite cement; however each of the samples are considered to be texturally immature, ranging from poorly- to moderately-sorted and composed of a range of both angular and rounded grains except A-2, which is more mature. Samples have minor to major amounts of clay matrix and are moderately indurated by hematite and kaolin cement. The samples can be classified in the quartz arenite to sub-arkose petrofacies and all plot within the quartzose recycled subfield (Fig. 3-3) tectonic provenance of Dickenson et al. (1983).

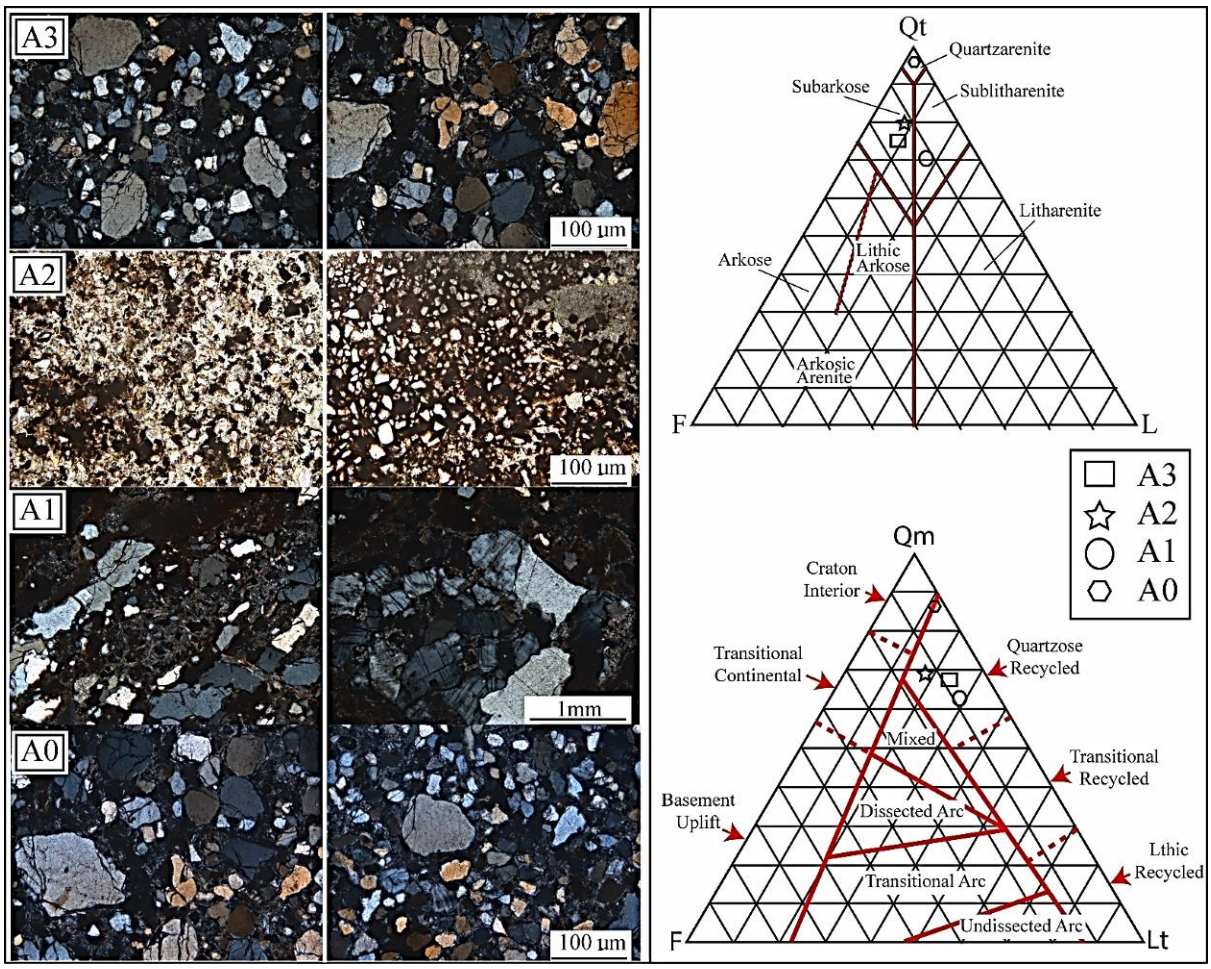

Figure 3-3. Thin section photomicrographs and detrital modes of Calonda Formation samples.

Left column is a selection of photomicrographs from the four samples (A0-A3), investigated in this study. The right column is the detrital modes of the four samples. Three of the samples plots as quartzarenite sandstones with quartzose recycled orogeny provenance except A1, which plots as sublitharenite sandstone with mixed provenance sources. Where quartz-feldspar-lithic is QFL respectively, Qt is total quartz grains, Qm is monocrystalline quartz and Lt is total lithics).

3.5.2 U-Pb detrital zircon

The cathodoluminescence images of selected zircon grains and Th/U ratio plot from the Calonda Formation is presented in Figure 3-4 and Figure 3-5 respectively. Probability density and corresponding Concordia plots are shown in Figure 3-6. The description and interpretation of the U-Pb results are based only on concordant or semi-concordant grains in each sample. The four Calonda Formation samples yielded 284 concordant grain ages out of the 405 single grains analyses. Summarized U–Pb age dating results are presented in Table 3-2 and full data is listed in Appendix 3S1.

In general, each of the four detrital zircon samples are similar, and show that the Calonda Formation has seven broad provenance sources, including; 1) Archean (9%); 2) Paleoproterozoic (6%); 3) Mesoproterozoic (8%); 4) Neoproterozoic-early Paleozoic (Pan-African) (33%); 5) middle-late Paleozoic (Ordovician-Carboniferous: 10%); 6) Permian (26%); and 7) Mesozoic component (8%). The modest Archean component is primarily limited to a population of 2900-3000 Ma grains, whereas the minor Paleoproterozoic population is characterised by a scattering of grains with a peak ~1800 Ma.

The Mesoproterozoic grains cluster around 1000-1100 Ma with relatively similar proportions from all four samples. The Neoproterozoic-early Paleozoic population shows a scattering of ages between 500 Ma and 1000 Ma, but are dominated by a grains between 500 Ma and 550 Ma with a peak around 540 ma. In contrast, the late Paleozoic population is characterised by a small number of grains between ~380 and 450 Ma. Perhaps the most interesting and unexpected grain population is the prominent Permian population characterised by a peak age around 277 Ma. The minor Mesozoic population is particularly interesting as they include both Jurassic and Cretaceous grains ranging from 190-75 Ma with a prominent cluster around 130 Ma.

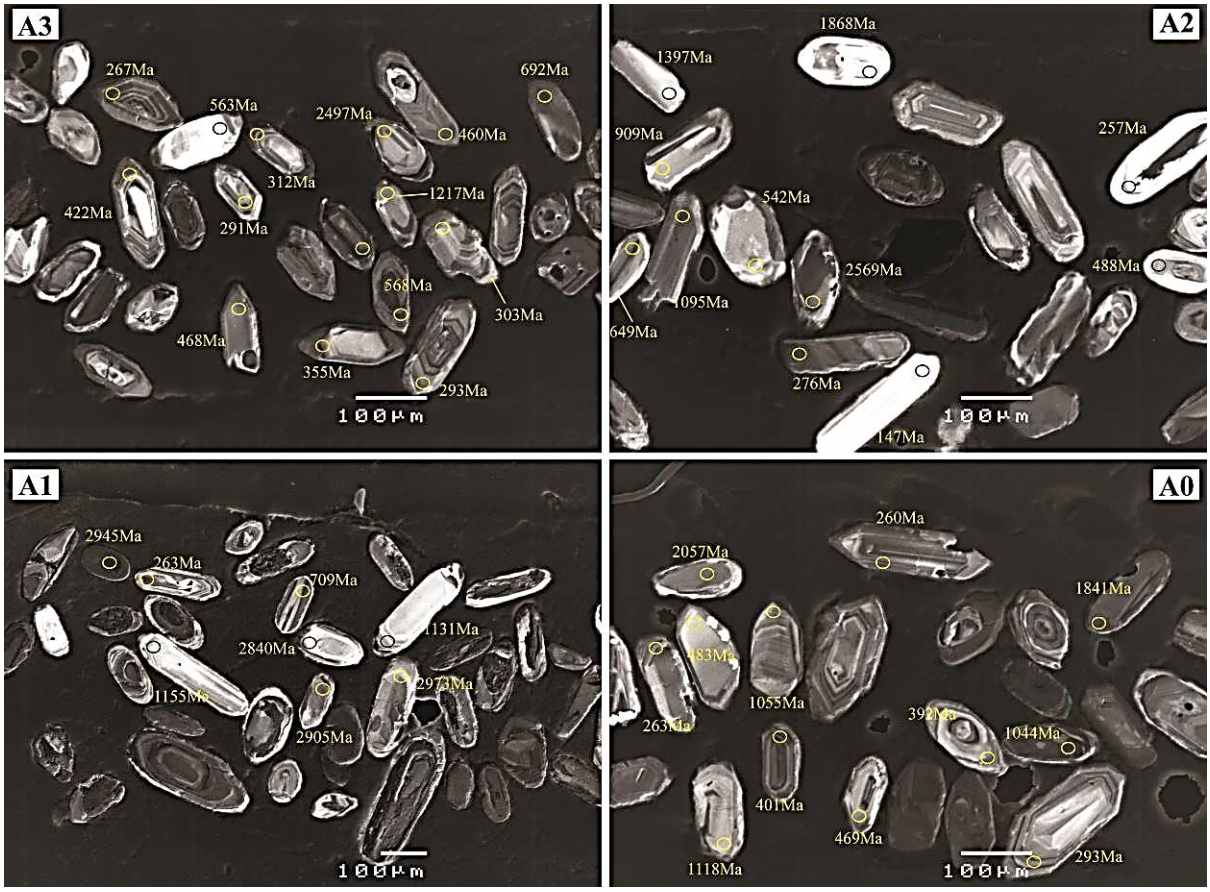

Figure 3-4. Representative CL images of the Calonda Formation.

The morphology of the Calonda Formation zircons is varied and ranges from euhedral prismatic to subhedral and rounded with grain lengths ranging from 50-µm to 300-µm and grain widths between 20-µm to 100-µm. The zircons range from very bright to dark with dominantly oscillatory zoning in cathodoluminescence. Significant amount of zircons are metamict, probably affected by kimberlitic emplacement in the Calonda Formation.

Table 3-2. Summarized U-Pb results of Calonda Formation

Sample	Total Analysis	Number of Concordant Analysis	Youngest grain (Ma)	Oldest grain (Ma)
A-0	90	85	125	3089
A-1	95	86	263	3292
A-2	110	102	75	2700
A-3	110	90	117	2954

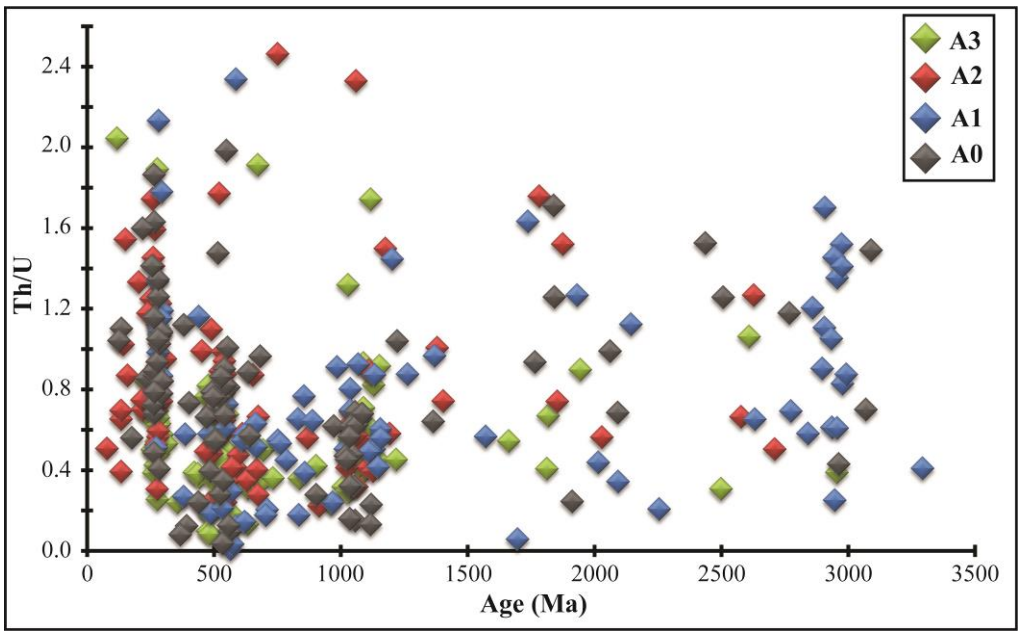

Figure 3-5. Th to U ratios detrital zircons from the Calonda Formation.

This figure shows that most (98%) grains have high Th/U ratios (> 0.1), which is typical of igneous or magmatic sources (Rubatto, 2002). The 2% grains with low Th/U ratios may have been affected by localized hydrothermal fluid interactions at depth as a result of kimberlite emplacement in the study area, or by metamorphism as recognized by complex internal structures of recrystallized domains and fluid-induced recrystallization and metamictization (Kröner et al., 2014) in some of the zircons especially from sample A-1, as shown in Figure 3-4.

Provenance of three of the samples are generally similar with ages ranging from Archean to Cretaceous, except sample A-1, which yielded a cosmopolitan age spectra with no Mesozoic age grains (Fig. 3-6). Sample A-0 is dominated by Neoproterozoic (~16%) and Permian (~28%) age grains but also yielded two Cretaceous (~125 and ~134 Ma) and two Jurassic (~175 and 190 Ma) zircons. Sample A-2 is also dominated by Neoproterozoic (~20 %) and Permian (~27%) age grains, but also yielded five Cretaceous grains (~75 – 139 Ma) and two Late Jurassic age grains (~147 Ma and ~156 Ma). Sample A-3 is dominated by Mesoproterozoic (~20%) and Permian (~28%) age grains, but also yielded a Cretaceous grain (~117 Ma). However, sample A-1 (Fig. 3-6) is different as it shows a major Archean (~25%) contribution in addition to the dominant Neoproterozoic (~19%) and Permian (~19%) age populations with no Mesozoic age zircons.

The four samples when compared using age probability plot (Fig. 3-7a) and cumulative distribution frequency plot (Fig. 3-7b) derived from the K-S statistical test (Table 3-3) shows sample A-1 fails the test and may have a different provenance to the other samples. However, when the four samples are compared without the Mesozoic and the Archean age grains (Fig. 3-7c; Table 3-3b), they all pass the K-S test suggestive of a common provenance. The second K-S test results indicate that the absence of Mesozoic and the presence of large Archean component of sample A-1 caused it to fail the K-S test (Fig. 3-7b; Table 3-3a). The K-S statistical test was also used to compare the large Permian grains from each sample, and the result (Fig. 3-7d; Table 3-3c) show that the Permian population from each sample pass the test and may have a common provenance. Overall, the four Calonda Formation samples are similar and appears to have a common provenance, and the difference in provenance is attributed to the lack of Mesozoic grains and a prominent Archean population from sample A-1.

3.5.3 Lu-Hf isotope geochemistry

In order to better understand the source of sediment for the different populations within the Calonda Formation, the Lu-Hf isotope ratios of subsets of the major U-Pb age populations (Fig. 3-8) were analysed for their Lu-Hf isotope ratios (initial εHf(t) values) to help constrain their tectonic provenance (Table 3-6). Particular attention was focused on the Mesozoic grains. Zircons with positive initial εHf(t) values are mainly sourced from juvenile mantle, whereas zircons with negative εHf(t) values are indicative of reworked crustal sources (Morag et al*.,* 2011).

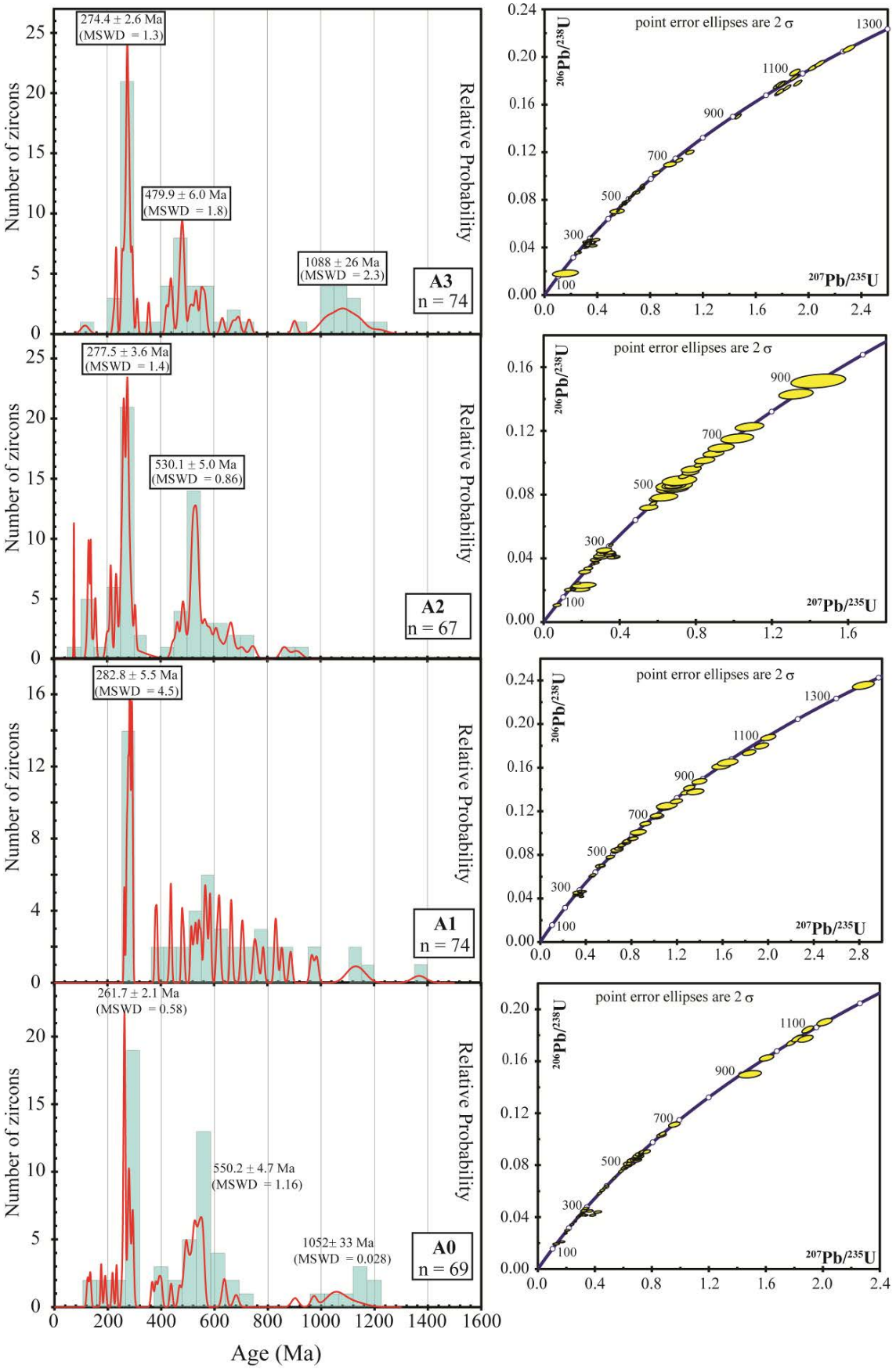

Figure 3-6. Probability density and Concordia plots for the Calonda Formation.

This plot shows the dominance of Neoproterozoic and Permian age zircons from the Calonda Formation (N = 4). Reported results are single zircon concordant analyses. The 207Pb/206Pb age was selected for zircon grains older than 1.0 Ga as they are more reliable for older zircons, whereas the 206Pb/238U age was selected for younger zircons with age less than 1.0 Ga, because 206Pb/238U ages are reliable for younger zircons (Gehrels et al., 2008; Gehrels, 2012).

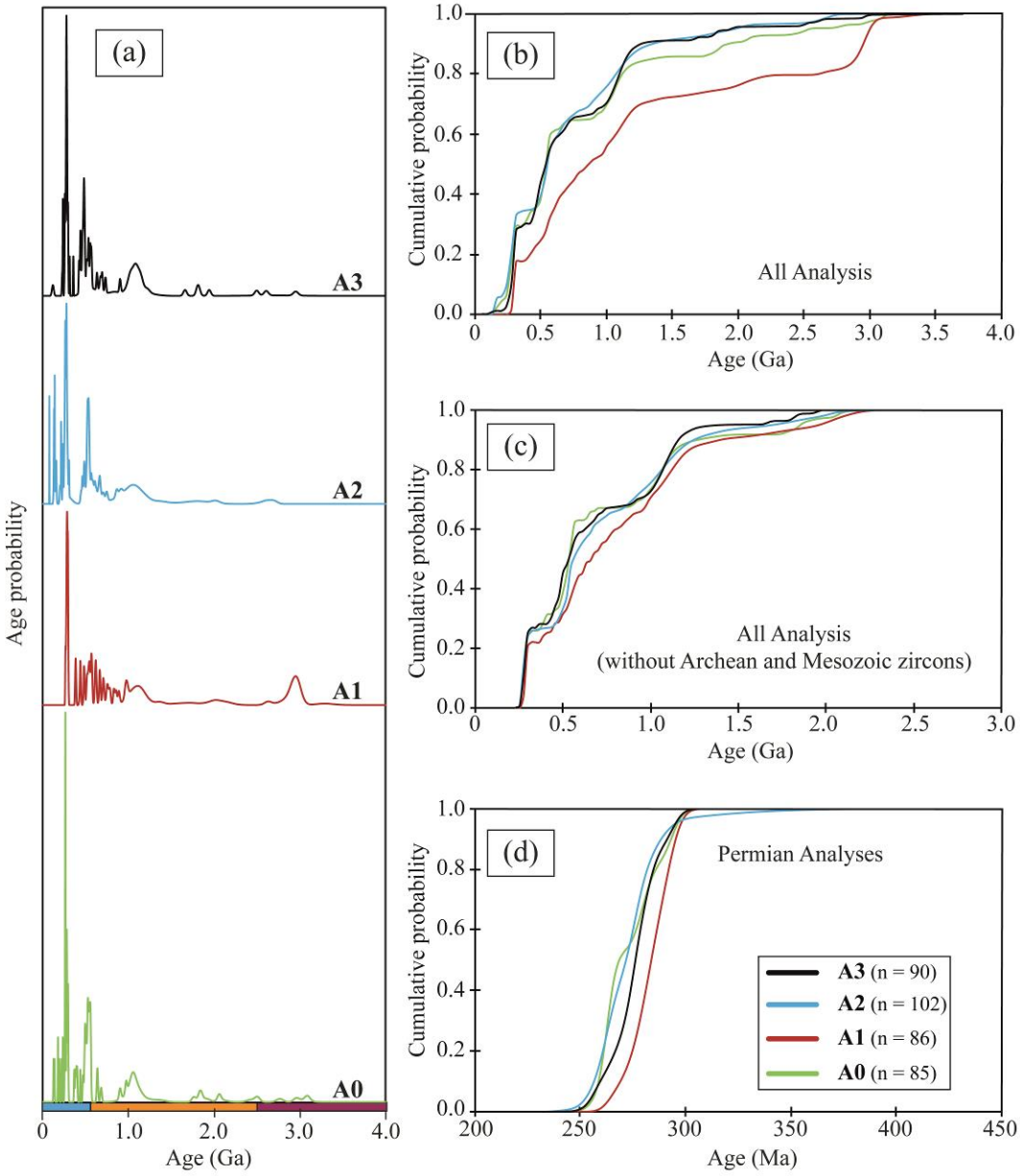

Figure 3-7. Age probability and Cumulative probability plots.

(a) Cumulative age distribution curves from the Kolmogorov-Smirnov (K-S) statistical tests used to detect potential similarities and or differences between the sediments of the Calonda Formation. (b). Age probability plot highlighting the similarities and difference between the four Calonda samples.

Table 3-3. K-S test results four Calonda samples

(a) K-S test results of all Analysis. P-values using errors in the CDF

	A-0	A-1	A-2	A-3
A-0		0.004	**0.978**	**0.989**
A-1	0.004		0.016	0.024
A-2	**0.978**	0.016		**0.571**
A-3	**0.989**	0.024	**0.571**	

(b) K-S test results of all Analysis except Mesozoic and Archean zircons. P-values using errors in the CDF

	A-0	A-1	A-2	A-3
A-0		**0.099**	**0.696**	**0.990**
A-1	**0.099**		**0.809**	**0.390**
A-2	**0.696**	**0.809**		**0.585**
A-3	**0.990**	**0.390**	**0.585**	

(c) K-S test results of Permian zircons. P-values using errors in the CDF

	A-0	A-1	A-2	A-3
A-0		**0.136**	**1.000**	**0.481**
A-1	**0.136**		**0.124**	**0.450**
A-2	**1.000**	**0.124**		**0.861**
A-3	**0.481**	**0.450**	**0.861**	

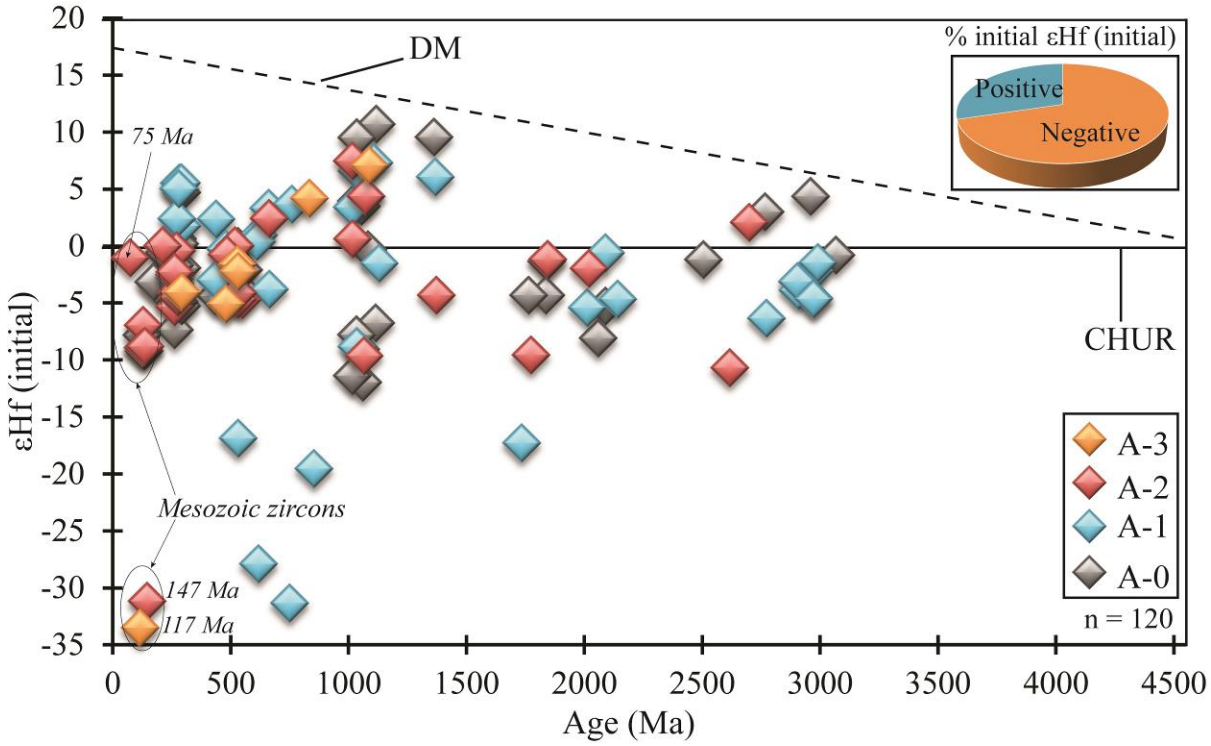

Figure 3-8. Plot of initial εHf vs U-Pb age of concordant detrital zircons.

The plot shows that most of the zircons from the Calonda Formation (n = 120) were derived from old reworked crustal sources. (The depleted mantle (DM) evolution curve is for linear evolution from a Chondritic Uniform Reservoir (CHUR) value at the Earth's formation (i.e., 0 at 4.56 Ga) to εHf (t) = 17 at the present for the DM; Dhuime et al., 2011). The εHf (t) values from this study (Fig. 3-7 and Table 3-6) indicate mixed provenance comprising of a dominant (n = 85) input from older reworked crustal sources and a minimum contribution (n = 35) from the juvenile mantle components.

Table 3-4. Summarized Lu-Hf isotope analysis for Calonda Formation

Formation	Zircon population	Initial εHf (t) values	Model Age DM	Source
Mesozoic	217.7-75.5 Ma (n = **12**/13)	(-33.5 to +0.1)	2085.9-760.5 Ma	Reworked Crust
Permian	295.3-254.5 Ma (n = **19**/27)	(-7.4 to +5.5)	1190.4-683.3 Ma	Reworked Crust
Neoproterozoic-early Paleozoic	854.2-519.8 Ma (n = **15**/23)	(-31.3 to +4.2)	2514.4-1101.0 Ma	Mixed
Mesoproterozoic	1373.5-1016.8 Ma (n = **15**/25)	(-12.0 to +10.7)	2039.5-1180.9 Ma	Mixed
Paleoproterozoic	2142.4-1735.6 Ma (n = **12**/12)	(-17.3 to -0.6)	2836.9-2298.4 Ma	Reworked Crust
Archean	3068.3-2506.5 Ma (n =**11**/14)	(-10.7 to +4.4)	3399.4-2867.8 Ma	Reworked Crust

Notes: This table shows the main detrital zircon populations in the studied zircons from the Calonda Formation. The table shows the dominant contributing source of sediment in each population. All populations from the Calonda Formation were sourced from reworked crustal sources or from a mixed provenance of both juvenile mantle and reworked crustal sources. The number of analysis for each population is shown as n = a (b); where a, is the dominant number of zircons with either positive or negative initial εHf (t) values. 'b' is the total number of analysis for a particular population. The population is described as sourced from a juvenile mantle or reworked crustal source when 'a' represents positive or negative values respectively.

The initial εHf (t) values are presented in Figure 3-8 and listed in Appendix 3S2, including the mass spectrometer cup configuration and normalization factor(s). The Lu-Hf isotope ratios from the 120 Calonda zircons analysed show a wide spread of initial $^{176}Hf/^{177}Hf$ ratios from 0.280758 to 0.282765, with εHf (t) values ranging from –33.5 to + 10.7; divided into 71% negative and 29% positive (Fig. 3-8), indicative of mixed provenance dominated by sources from the reworked crust. The negative initial εHf (t) values are mainly from the Archean, Paleo- to Meosproterozoic, Permian and Mesozoic populations, with the Mesozoic age zircons grains yielding the highest proportion of negative initial εHf (t) values after the Paleoproterozoic age grains (see Table 3-4). With exception of one Triassic age grains (213 Ma), all the Mesozoic zircons including the youngest Cretaceous grains -33.5 (~116.9 Ma), -1.0 (~75 Ma), -7.8 (~125 Ma) and -9.0 (~130 Ma), yielded negative initial εHf (t) values.

3.5.4 Zircon trace elements results

Summarized zircon trace element data are shown in Figure 3-9 and Table 3-5, and full results are listed in Appendix 3S3. The trace element analysis was performed on a subset of 38 grains, which included eight Mesozoic, eight Permian, six Neoproterozoic, seven Mesoproterozoic, two Paleoproterozoic and seven Archean zircons in a further attempt to better define discrete source characteristics (Taylor and McLennan, 1985; Hoskin, 2005). However, the similarity of REE patterns from different rock types makes trace element a difficult provenance indicator (e.g. Hoskin and Ireland, 2000), is recognised and the amount of Nb in zircons, which is usually depleted in Arc-related compared to within-plate settings is used to infer the magma source (e.g. Yang et al., 2012). The zircon trace element results from the Calonda Formation show that the main populations have similar chondrite-normalised REE patterns; strongly enriched LREE and depleted in HREE with strong negative Eu anomalies (Fig. 3-9a and Table 3-5). The zircon trace element results also show high Sc, U and Th concentrations (Fig. 3-9 b-e), all of which are consistent with weathering of continental sources for the Calonda Formation (Grimes et al., 2007, 2015). For instance, zircon grains with U/Yb < 0.1 are generally derived from within Mid-Ocean Ridge Basalt (MORB) type setting; which was not observed in this study for any of the zircon populations. The strong Ce and Eu anomalies observed (Table 3-5) is consistent with the magmatic source characterization (Fig. 3-9f) of Hoskin (2005), and supports the interpretations of the Th/U ratios (Fig. 3-5). Plots of Th/Nb vs Hf/Th and Th/U vs Nb/Hf (Fig. 3-9 g-h) also indicate that the Calonda samples were mainly sourced from arc-related settings (Hawkesworth and Kemp, 2006; Yang et al., 2012). Overall, the Calonda zircons have depleted Gd_N/Yb_N between 0.11 and 0.30, with strong negative Eu (Eu/Eu^* = 0.2–0.6) and positive Ce anomalies (Ce/Ce* = 61–202) characteristic of a felsic magmatic origin (e.g. Eu/Eu* < 1) for

the majority of the studied zircons. Significantly, none of the Mesozoic grains showed trace element ratios suggestive of strongly alkaline affinities or from within plate sources.

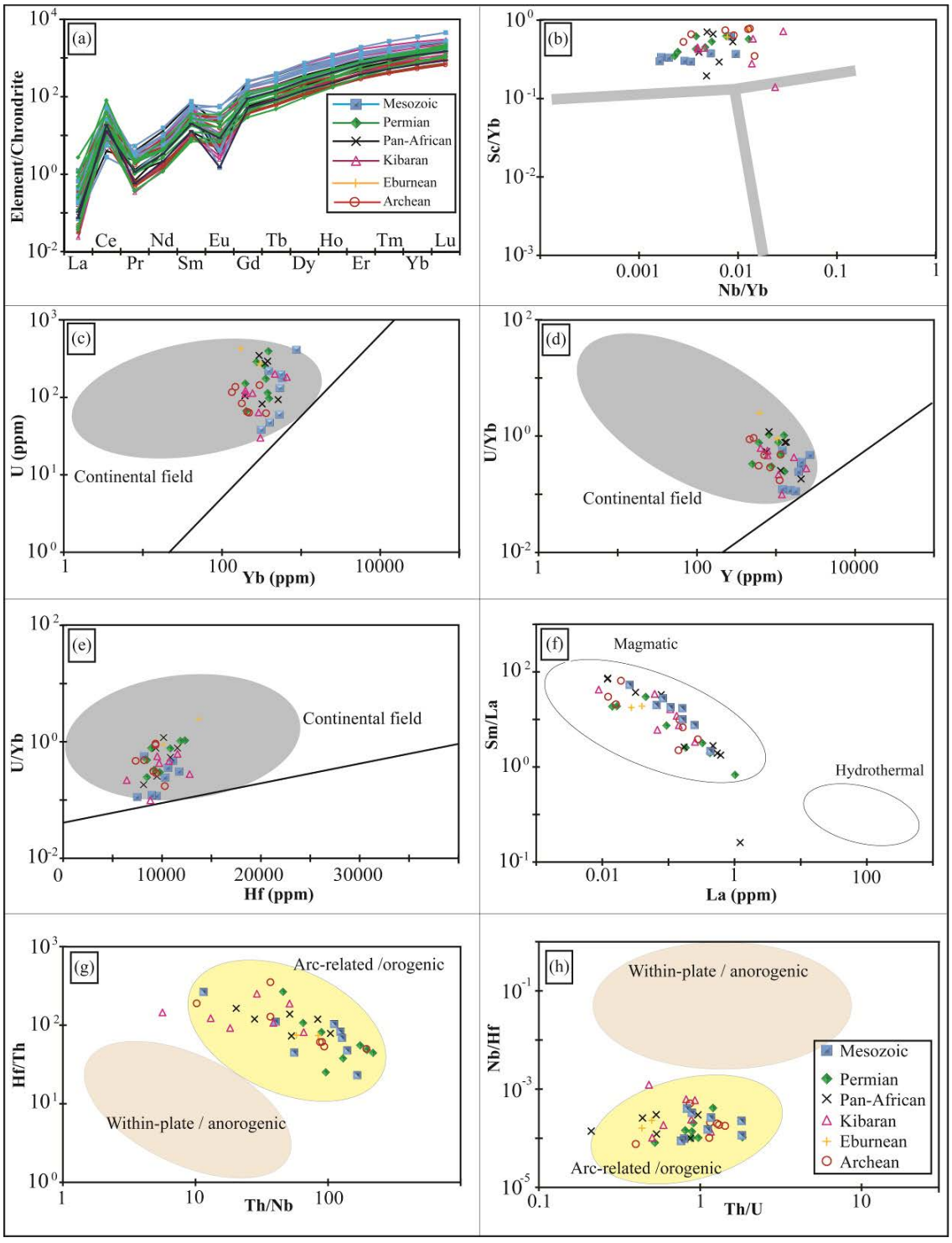

Figure 3-9. Zircon trace element plots for Calonda Formation samples.

(a). Chondrite-normalized rare earth element concentrations for major populations within the Calonda Formation. (b-e). Plot of ratios showing the continental origins of the Calonda Formation sediments. (f). Discrimination plots for magmatic and hydrothermal zircons. (g-h). Plots of trace element ratios showing a dominant Arc-related / orogenic as possible source terrain for the Calonda Formation sediments. Zircons sourced from dominantly Arc-related settings with higher Th/Nb and lower Nb/Hf ratios relative to within-plate settings, assuming magmatic fractionation were similar for both settings (e.g. Yang et al., 2012). Chondrite nationalization values were from Taylor and McLennan (1985).

Table 3-5. Ratios of chondrite-normalized zircon REE patterns.

Ratio /Population	Mesozoic	Permian	Neoproterozoic-early Paleozoic	Mesoproterozoic	Paleoproterozoic	Archean
(Sm/La)N	531(194)	300(104)	739(250)	422(174)	190(184)	653(198)
(Lu/Gd)N	23(15)	54(27)	28(27)	24(16)	17(17)	20(17)
Eu/Eu*	0.6(0.30)	0.51(0.42)	0.58(0.21)	0.34(0.20)	0.20(0.13)	0.55(0.36)
Ce/Ce*	61(23)	131(54)	82(24)	144(40)	92(65)	202(93)
(Gd/Yb)N	0.11(0.09)	0.08(0.06)	0.12(0.08)	0.12(0.09)	0.08(0.08)	0.13(0.09)
n	8	8	6	7	2	7

Note: Chondrite normalizing values from Taylor and McLennan (1985). n = the number of analyses contributing to the mean. The first number in each column represent the highest ratio for that population, whereas the number in parenthesis is the average value for the population. Eu and Ce anomalies were calculated as Eu/Eu* = EuN/(sqrt(SmN * GdN)) and Ce/Ce* = CeN/(sqrt(LaN * PrN)).

3.6 Discussion

3.6.1 Maximum depositional age of the Calonda Formation.

The first objective of this study was to refine the age of the diamond-bearing Calonda Formation through maximum depositional age calculation of the youngest zircon population. The youngest coherent cluster of grain ages ($n \geq 3$) in a detrital zircon population is usually used to assess the maximum depositional age of a unit (Dickinson and Gehrels, 2009). This approach of estimating the maximum depositional age is particularly useful in continental sedimentary successions like the Calonda Formation with limited fossils and vague biostratigraphic age. Numerous workers using different approaches and techniques for estimating the maximum depositional age of stratigraphic units (e.g. Dickinson and Gehrels, 2009, Tucker et al., 2013), have highlighted the importance of incorporating the geology of the area to develop the best interpretation for the given sample (e.g. Dickinson and Gehrels, 2009).

In this study, five such techniques were used to arrive at a maximum depositional age interpretation for the Calonda Formation and the preferred interpretation is discussed in light of other existing geological evidence. All the five techniques used here can be accessed via Microsoft Excel using isoplot macros of Ludwig (2012), and the use of these techniques have been discussed extensively by Dickinson and Gehrels (2009) and Tucker et al. (2013). The techniques include (i) youngest single grain age (YSG); (ii) youngest graphical peak age (YPP); (iii) youngest detrital zircon age (YDZ); (iv) the Weighted Average (WA) of a coherent cluster ($n \geq 3$); and (v) TuffZirc (Zircon Age Extractor, (+6 grains). The YSG age of sample A-2 of 75 Ma (Fig. 3-9, Table 3-6) coincides with kimberlite magmatism in the Mbuji-Mayi region of the DRC (Davis, 1977, Schärer et al., 1997). This age is also within error of Late Cretaceous detrital zircons (mean age = 79.8 ± 1.6 Ma; n = 3) reported by Roberts et al. (2015) from the potentially correlative Kwango Group in the Kasai Province of the DRC, some 400 km to the north-west of the study area. If the two units are indeed correlative, then the YSG from this sample may well reflect the best interpretation for the maximum depositional age for the Calonda Formation. The YSG age from sample A-3 (~117 Ma) is older, but coincides with age dates reported for kimberlite magmatism in the nearby Lunda Norte Province of Angola (Eley et al., 2008; Robles-Cruz et al., 2012) and could also be inferred as the maximum depositional age. The third YSG age from sample A-0 (~125Ma), collected from a core near Mulepe (Fig. 3-10) is also in agreement with the U-Pb age dates of perovskites for the Mulepe kimberlites (Mulepe 2: 123 ± 3.6 Ma) reported by Castillo-Oliver et al. (2016). Although the YSG ages from three samples are each consistent with kimberlite magmatism within the Lunda Norte and nearby Mbuji-Mayi in DRC, the ages should be used with caution as they only represent single grains with no reproducibility and may have been affected by Pb loss leading to artificially young ages. However, the YSG ages

could be accepted as the maximum depositional age(s) if each zircon grain were dated multiple times within the same age zone to demonstrate reproducibility and arrived at the same age (e.g. Spencer et al., 2016). Unfortunately, none of these Cretaceous grains were large enough to accommodate multiple analyses; and so the YSG ages cannot be supported at this time. The weighted average and tuffZirc techniques provide the most robust, but conservative maximum depositional age estimates for the Calonda Formation in this study. Both techniques estimated the maximum depositional age using a population ($n \geq 3$), which yielded a weighted average of 130.3 ± 3.4 Ma (MSWD = 0.87; prob. = 0.48; n = 5) and a tuffzirc age of 130.3 ± (+4.0/-13.4) at 96.9 % confidence level (n = 6; Table 3-6). The two techniques treated the two youngest zircons (75.3 Ma and 116.9 Ma) as anomalous, rejecting them from the age calculations.

Hence the weighted average and tuffZirc results provide excellent maximum depositional age control that confidently demonstrate that the Calonda Formation is no older than ~130 Ma, however the preponderance of geological information support a younger maximum depositional age that is likely more consistent with one of the YSG ages between 125-75 Ma. Moreover, existing fish fossils and palynological data suggest an Albian-Cenomanian (~94 – 113 Ma) age for the Calonda Formation (Pereira et al., 2003). Considered together, the most realistic age interpretation favours the YSG ages between 116-125 Ma, although the 75 Ma YSG age from sample A-2 may indicate that the Calonda Formation has a considerably longer depositional history than previous estimates. This study highlights the importance of further work with a larger number of samples.

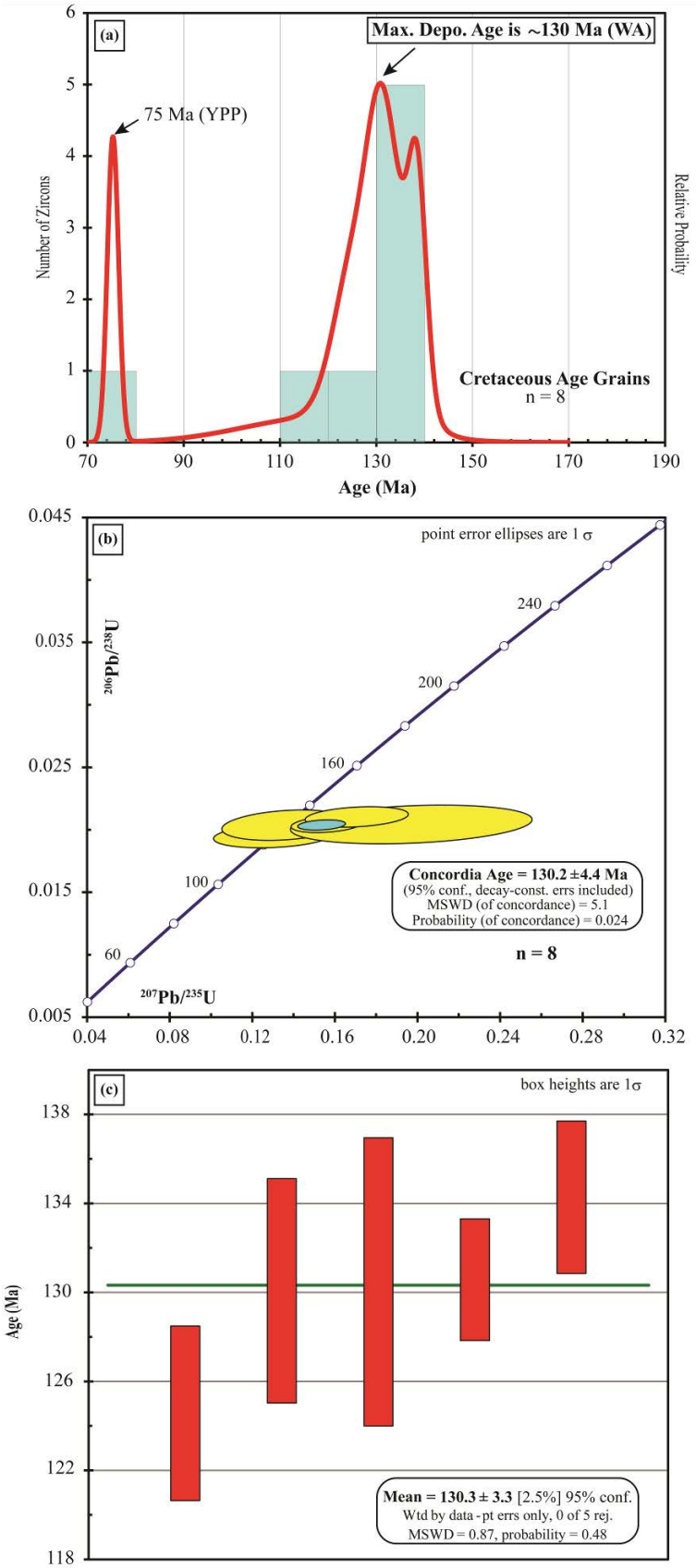

Figure 3-10. Maximum depositional age estimate for the Calonda Formation.

(a). Probability density plot of eight Cretaceous age zircons recovered from the Calonda Formation samples. (b). Concordia Age of Cretaceous zircons investigated in this study (c). The weighted average age of four zircons from samples A-0 and A-2 gives the maximum depositional age of ~130 Ma.

Table 3-6. Estimation of maximum depositional age for the Calonda Formation

	Analysis/ Samples	A0	A1	A2	A3	Composite (A0-A3)
1	**YSG**					
	Age	124.6	263.3	75.3	116.9	75.3
	Error	3.92	3.88	1.17	14.9	1.17
2	**YPP**					
	Age	125	264	75	117	75
3	**YDZ**					
	Age	124.58	262.92	75.5	118.33	75.25
	Range (±)	8.2/8.8	7.6/8.3	2.4/2.8	32/35	1.4/1.3
	Confidence	0.95	95	0.95	0.95	0.95
4	**Weighte Average (+3)**					
	Age	262.3 (±2.2)	275.8 (±4.7)	130.5 (±2.2)	232.8 (±8.6)	130.3 (±3.4)
	Confidence	0.95	0.95	0.95	95	95
	Rejection	0 of 9	0 of 4	0 of 3	0 of 3	0 of 5
	MSWD	0.12	0.39	0.02	1.2	0.87
	Probability	0.99	0.76	0.98	0.29	0.48
5	**TuffZirc (+6)**					
	Age	262.6	284.4	276	275.6	130.3
	Error (±)	1.1/1.4	5.8/5.9	7.5/4.0	6.5/2.4	4.0/13.4
	Confidence	0.961	93.5	96.1	97.8	96.9
	Group size	9	11	12	13	6

3.6.2 Provenance of the Calonda Formation

The second objective of this study was to reconstruct the sedimentary provenance and paleo-fluvial drainage patterns to provide additional information for alluvial diamonds vectoring in northeast Angola. All four samples are quartz dominated, but show a small variability ranging from quartzarenitic to subarkosic and sublitharenitic petrofacies, and plot in the Quartzose Recycled tectonic subfield of Dickinson et al. (1983). The sandstone

petrography result suggests that the Calonda Formation is likely derived, at least in part from recycling of older sedimentary strata. The presence of moderately well rounded and angular monocrystalline quartz grains in the Calonda samples is supportive of recycled source, but also points to input of fresh basement sources. K-S tests indicate that all samples except A-1 have a common source. This interpretation is supported by both quantitative and qualitative results of the sandstone petrography, which indicate that this sample is generally more immature and contains a higher proportion of lithic grains than the other samples. In terms of detrital zircons, the most significant variations between A-1 and the other samples are the lack of Mesozoic grains, the greater spread in Mesoproterozoic grain ages, and the significantly elevated abundance of Archean grains relative to the other samples (Fig. 3-6).

The presence of both angular and rounded detrital zircon grains (Fig. 3-3) from these samples also corroborates the supply of sediements from multiple sources. Moreover, the dominantly negative Lu-Hf initial εHf (t) values (Fig. 3-8), from the main zircon populations within the Calonda Formation also indicate a major recycled source component and a minor juvenile mantle source for the zircons in the study area. The negative Lu-Hf signatures from the Calonda Formation (Lucapa) is similar to that observed from the sediments within the Congo-Kasai Craton in central Africa investigated in the Luebo (Batumike et al., 2009) and the Kasai Province (Owusu Agyemang et al., 2016) both in the southwestern part of the Congo Basin, and north of the current study area. Overall, the results presented here strongly suggest that the Calonda sediments were predominantly derived from sources within the Congo-Kasai Craton and nearby reworked crustal sources, which may have resulted from continental arc-related magmatism as indicated by the zircon trace element results (Fig. 3-9). The main zircon populations are discussed further with respect to their possible provenance.

3.6.2.1 Archean-Mesoproterozoic zircons

The Archean-Paleoproterozoic zircons recovered from the Calonda Formation account for 15% of concordant analysis, with a significant peak age around ~2.9 Ga (Fig. 3-11). This peak age are consistent with Archean basement sources within the Congo-Kasai Craton as it coincides with the age of late Archean (2.9-2.5 Ga) reworking of the Southern Kasai Domain of Jelsma et al. (2015). The Paleoproterozoic zircons are also from localized sources of the Lunda Group (Figs. 3-11) within the Congo-Kasai Craton (e.g. Cahen et al., 1984; Owusu Agyemang et al., 2016) or from rocks resulting from the Eburnean orogeny in western Angola (De Carvalho et al., 2000), where these age grains are abundant. The limited representation of the Paleoproterozoic age population (6%) however, suggest that this population were more likely sourced locally from within the Congo-Kasai Craton and not transported from the west.

The Mesoproterozoic age grains (8%) may have come from any of the Pan-African mobile belts to the east and south of Angola (e.g. Kampunzu and Cailteux, 1999; Rainaud et al., 2003; Armstrong et al., 2005). The extension of the Congo-Kasai Craton runs through northeast to southeast of Angola, where it encounters the Lufilian Arc (De Carvalho et al., 2000). This craton could have served as a conduit for the transport of Mesoproterozoic age grains from either the Lufilian Arc (Kampunzu and Cailteux, 1999) or the Katanga Belt (e.g. Rainaud et al., 2003; Armstrong et al., 2005), which are known to host zircons of similar age. Again, the limited number of Paleoproterozoic (Eburnean) zircons in the Calonda samples does support provenance from the south or southeast of the study area.

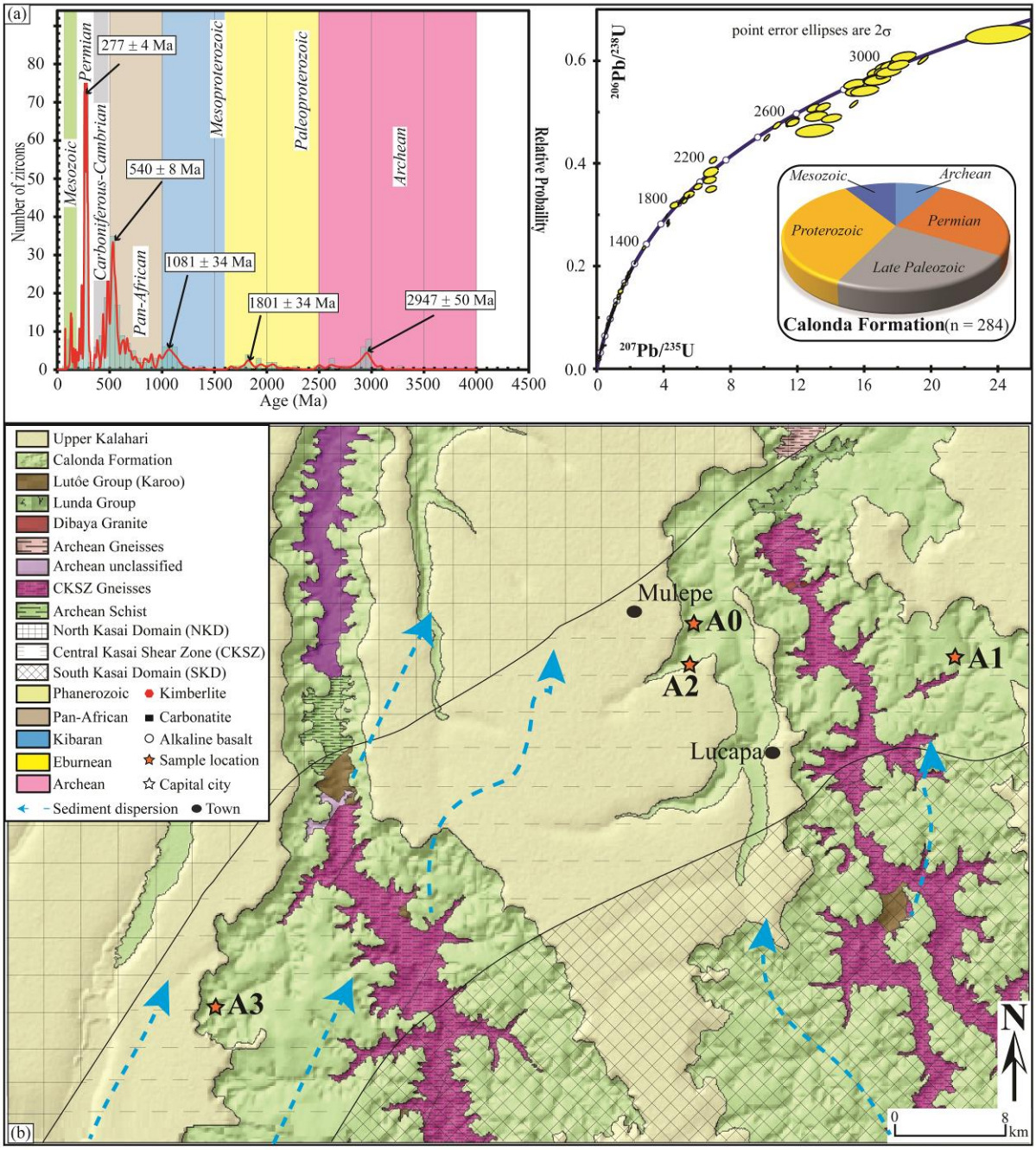

Figure 3-11. Provenance of Calonda Formation sediments.

(a). Composite probability density plot and corresponding Concordia plots for the Calonda Formation samples (N = 4). The plot shows the dominance of Neoproterozoic and Permian age zircons from the Calonda Formation. (b). Probable sediment pathways for the Calonda Formation

3.6.2.2 late Neoproterozoic-late Paleozoic

The late Neoproterozoic-early Paleozoic grains accounts for the largest population (25%). The late Neoproterozoic population were likely sourced from bedrock overlying the Congo-Kasai Craton (e.g. De Carvalho et al., 2000) or from nearby Pan-African age mobile belts such as the Lufilian Arc or the Katanga Belt as indicated for the Mesoproterozoic age population. The late Paleozoic (450-380 Ma) may represent a recycled sedimentary source within the Cassange Graben (Oesterlen, 1976, 1979), which has been reported to host zircons of similar age. Additionally, the kimberlite pipes of northeastern Angola, which cut across the Carboniferous-Permian Lutôe and Permian-Middle Jurassic Cassange groups of the Karoo Supergroup (Jelsma et al., 2009), may have sampled these zircon grains of this age on their ascent.

3.6.2.3 Permian zircons

The Permian zircons recovered from the Calonda Formation is the largest proportion (26%) after the Pan-African population (Neoproterozoic-early Paleozoic; 33%). This result is significant as detrital samples analyses from both the Carboniferous-Permian Lukugu Group and the Triassic Haute-Lueki Group units selected from the Samba and Dekese wells (Congo Basin) did not find any Permian age zircons out of 157 analyses (Linol et al., 2015a). Additionally, detrital zircon analyses (n = 214) of three samples from the Mesozoic Lower Kwango Group by Linol et al. (2015b) only yielded a single early Permian zircon grain (286 ± 7 Ma: Linol et al., 2016).

The age of the Calonda Permian zircons (n = 73) cluster into three distinct peaks, including ~262 Ma, ~277 Ma and ~292 Ma. These age peaks are consistent with Permian age population from the detrital zircon database from Africa (e.g. Puetz, 2017), and arc-related volcanic ash beds that have yielded Permian zircon ages from the Ecca Group of the Karoo

Basin in southern Africa (e.g. Fildani et al., 2007, 2009; Rubidge et al., 2013; Belica et al., 2017). The Karoo sources within the Permian-Jurassic Cassange Graben (Malanje Province; Fig. 3-1), which likely extends through southern Angola into Namibia (e.g. Oesterlen, 1976, 1979; Cairncross, 2001; Catuneanu et al., 2005) is also possible provenance source for the Permian zircons in the Calonda Formation. Although these Permian age zircons could also have come from the late Paleozoic-Jurassic Choiyoi volcanic province in South America as air-fall tuffs (Kay et al., 1989; Linol et al., 2015b). The Permian age spectra is also in agreement with the minor zircon populations (n = 11) reported from Jurassic-Cretaceous strata in the Kasai Province (Congo Basin) of the DRC (Owusu Agyemang et al. 2016). These authors attributed their Permian zircon grains to magmatism related kimberlite and lamproite sources from Angola and Zambia (Jelsma et al., 2013; Smith et al., 1986).

The paucity of Paleo- and Mesoproterozoic zircons in Calonda samples suggest that the provenance was more likely from the south in the Kalahari (e.g. Haddon, 2005) and not west due to the lack of abundant Paleoproterozic grains (Fig. 3-11). Such a distal provenance source, largely to the south of the study area, is consistent with the presence of mostly subhedral and sub-rounded zircons indicating some amount of recycling or transport by localized north directed fluvial systems.

3.6.2.4 Mesozoic zircons

The presence of minor Mesozoic (8%) zircon populations represents minor contributions from Mesozoic magmatic sources within the region. The age spectra from these Mesozoic zircons, which range from Triassic to Early Cretaceous are all consistent with kimberlite sources within Angola and nearby DRC (Eley et al., 2008; Jelsma et al., 2013; Robles-Cruz et al., 2012). Arc-related magmatism as indicated by the zircon trace element data (Fig. 3-9) in central Africa and South America (Jelsma et al., 2013; Smith et al., 1986) is

more likely to have sourced the Mesozoic zircons within the Calonda Formation. However, the dominance of negative initial εHf (t) values (Fig. 3-7) especially for Cretaceous zircons indicate a reworked source from a much older crustal material, which again points to the Congo-Kasai Craton.

3.7 Conclusions

The detrital zircon data presented in this study provide new insights into the age and provenance of the Calonda Formation. The recovery of a robust Early Cretaceous zircon population confirms the age of the Calonda Formation as Cretaceous, no older than 130.3 Ma. However, the presence of isolated younger grains, including a single Campanian zircon at 75 Ma, suggests that the unit may actually be considerably younger than previously thought. The confirmation of a Late Cretaceous depositional age requires further work, as the younger zircon age may indicate a reworked Kalahari component. The age spectra of the detrital zircon populations from the Calonda Formation suggests that the most likely source for these sediments are the immediate Archean and Proterozoic sources within the Kasai Craton, nearby mobile belts (e.g. Lufilian Arc) and recycled Karoo rocks and associated volcanics from the south. This indicates that sediment delivery into the Lucapa area was mainly from local north directed fluvial systems from the south, which suggest that kimberlite sources of alluvial diamonds within the Calonda Formation are to the south.

4. CHAPTER FOUR

Sedimentary provenance and maximum depositional age analysis of the Cretaceous? Lapur and Muruanachok sandstones (Turkana Grits), Turkana Basin, Kenya.

Abstract

The Turkana Basin of northwestern Kenya is well known for its rich Neogene-Quaternary vertebrate fossil record; however, it also represents one of the few locations in sub-Saharan Africa where Cretaceous vertebrate fossils, including dinosaurs and other archosaurs, are preserved. These Cretaceous deposits are colloquially referred to as the 'Turkana Grits', and assumed to be Cretaceous in age based on their limited biostratigraphy. The 'Turkana Grits' are overlain by Paleogene volcanics (<35 Ma), which are widely considered to record the earliest evidence of plume-related volcanism in the East African Rift System. In this study, the results of an integrated sedimentary provenance investigation of two units within the 'Turkana Grits' called the Lapur and Muruanachok sandstones are presented. Analysis of U-Pb ages and Lu-Hf initial εHf (t) values from 1106 detrital zircons demonstrate that sediments are primarily derived from Neoarchean and Neoproterozoic basement sources, except for six Paleogene grains from the upper Lapur Sandstone, which are of unknown provenance. Considered together, these data point to the Mozambique Belt, which makes up the nearby rift flanks, as the primary provenance source. This is consistent with paleocurrent data, and suggests localized sediment input by alluvial fans, which fed into north-directed fluvial systems. Perhaps the most surprising finding is the identification of the late Paleocene detrital zircons, which not only demonstrate that the depositional age for the top of the formation is Paleocene rather than Cretaceous, but also provides possible evidence for the oldest Paleogene volcanic activity within the East African Rift System.

Key words

Turkana Basin and Grits, Provenance, detrital zircon geochronology, East African Rift, Paleocene volcanism

Citation for this chapter:

Owusu Agyemang, P. C., Roberts, E. M., Downie, B., and Sertich, J. J. (2018). Sedimentary provenance and maximum depositional age analysis of the Cretaceous? Lapur and Muruanachok sandstones (Turkana Grits), Turkana Basin, Kenya. *Geological Magazine*, 1-23.

4.1 Introduction

The Turkana Basin of northwestern Kenya is well known for its rich Neogene-Quaternary vertebrate fauna including one of the richest records of hominin fossils in Africa (e.g. HB Boschetto, 1988; Feibel et al., 1989; Fleagle and Leakey, 2011; Ducrocq et al., 2010; Fortelius et al., 2016). The Turkana Basin is also known for its long-lived sedimentary history, with fossiliferous deposits extending back into the Upper Cretaceous (Brown and McDougall, 2011; O'Connor et al., 2011). Interest in the petroleum geology of the East African Rift basins has been stimulated through discoveries of commercial quantities of hydrocarbons in the Neogene of the Lokichar area of the Turkana Basin (Ngamia-1 discovery well drilled 2008; Purcell, 2014), as well as similar major discoveries in the Neogene deposits of the Albertine Rift in Uganda (Fig. 4-1) a few years earlier (e.g. Neumaier et al., 2014; Purcell, 2014). The economic significance of such discoveries has led to a regional renewal of interest and exploration for hydrocarbons in Mesozoic and Cenozoic (Oligocene – Miocene) basins throughout eastern and central Africa (e.g. Genik, 1993; Morley et al., 1999; Wescott et al., 1999; Tiercelin et al., 2004; 2012a, b; Muia, 2015; Tullow Oil plc, unpublished presentation 2017 half year results). The Turkana Basin is located within the Turkana Depression between the Ethiopian and Kenyan domes, and is generally associated with the formation of the East African Rift System (Dunkelman et al., 1989; Chorowicz, 2005; Purcell, 2017). The Turkana Basin is one of several N-S trending rift basins within the Kenya Rift (Tiercelin et al., 2004; 2012a, b; Purcell, 2017). The complexity of structures and stratigraphic framework within the basin has led to many challenges and uncertainties with subdivision and correlation of different sedimentary units (Bosworth, 1992; Figs 4-1 and 4-2). However, many workers have attempted to describe these sedimentary deposits (e.g. Murray-Hughes, 1933; Arambourg, 1943).

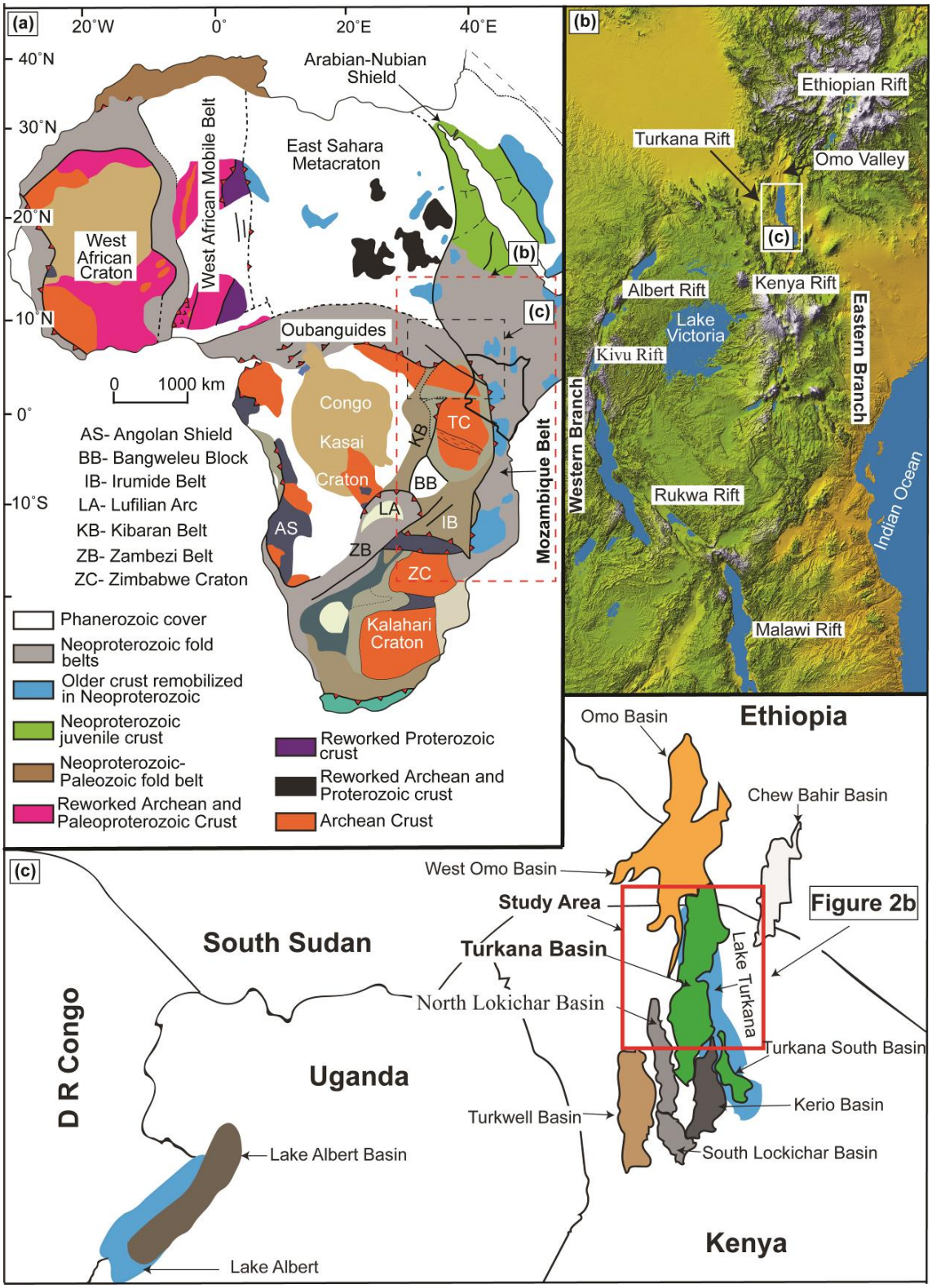

Figure 4-1. Map of the Kenya study area.

(a) Generalized basement map of Africa showing the main cratonic blocks and mobile belts. (Map modified from Begg et al., 2009 and Foster et al., 2015). (b) EARS showing the various rifts/basins in the region (Landsat image taken from the NASA Shuttle Radar Topography Mission collection and modified after Roberts et al., 2012). (c) Location of the Kenya Rift (Turkana Basin) showing some of the sub-basins within area. (Map modified after Tullow Oil plc, unpub. presentation, 2017 half year results).

The entire lower sedimentary successions in the basin overlying Precambrian basement rocks has previously been collectively called the 'Turkana Grits', and they are generally assumed to be Cretaceous in age based primarily on the presence of isolated dinosaur, crocodyliform and other vertebrate fossil remains (Murray-Hughes, 1933; Tiercelin et al., 2004; O'Connor et al., 2011; Fig. 4-2a, 4-3a). The term 'Turkana Grits' has previously been used as a 'catch-all' phrase for any outcrop of pre-Miocene, fluvial dominated, coarse-grained sandstone in the Turkana Basin/Anza Rift (e.g. Wescott et al., 1993; Thuo, 2009). The age and stratigraphic relationships of the different units within the 'Turkana Grits' are poorly understood, and are assumed to be primarily Cretaceous in age, although considerable uncertainty still exists (Bellieni et al., 1981; Zanettin et al., 1983; Morley et al., 1992; McDougall and Brown, 2009, O'Connor et al., 2011). The rift systems from central Sudan through to southern Kenya are believed to be the same, and oil production from southern Sudan has primed the Turkana region for exploration (Bosworth, 1992; Thuo, 2009). A refined age and provenance of the Turkana Grits could significantly improve exploration efforts in the area. The two most prominent subaerially exposed and presumed lateral equivalent units of the 'Turkana Grits' are the Lapur and the Muruanachok sandstones (Fig. 4-2), and together, they form the focus of this study.

The aim of this study is to constrain the age and sediment provenance of the Lapur and Muruanachok sandstones using framework petrography coupled with U-Pb geochronology, Lu-Hf isotope analysis and trace element geochemistry on detrital zircons for ten stratigraphically and spatially arrayed outcrop samples of these two units. This multifaceted

provenance approach is expected to improve stratigraphic control, enhance our understanding of the depositional history of the Turkana Grits and its paleofauna, and elucidate the tectonic evolution of the Turkana Basin. Furthermore, the composite data generated by this study is expected to help test recent hypotheses regarding the initiation and tectonic control on large scale drainage patterns in central Africa during the Late Jurassic-Cretaceous (Stankiewicz and De Wit, 2006; Roberts et al., 2012), and perhaps even during the initiation of the East African Rift System.

4.2 Geologic setting and stratigraphy of the Turkana Basin

4.2.1 Geologic setting

The study area is located in northwestern Kenya within the Turkana Basin (Omo-Turkana Basin). The Turkana Basin covers an area of 131,000 km^2 of northern Kenya and southern Ethiopia, with a mean elevation of ~400 m above sea level and it is bordered by the Omo basins of Ethiopia to the north and the North Lokichar Basin to the west, and to the east is the Kerio Basin (Baker et al., 1972; Fiebel, 2011; Thuo, 2009; Fig. 4-1). The structural and tectonic association of the Turkana Basin to the East African Rift or the Central African Rift systems is still unresolved as some researchers consider it as part of the East African Rift System (e.g. Wolfenden et al., 2004; Charowicz, 2005; Nutz et al., 2017), whereas others (e.g. Browne and Fairhead, 1983; Reeves et al., 1987) view it as part of the Central African Rift System. The Mesozoic component of the Turkana region is generally considered as derived from the Central African Rift System (e.g., Anza Rift – see Fig. 4-13 for location), which was later overprinted by the Cenozoic East African Rift System, although the complexities of these two rift systems suggest their ages may overlap (*see* Bosworth, 1992

for discussion). Many workers have also highlighted the complex interactions between the Mesozoic and Cenozoic rift systems of the Turkana region, including the long-lived structural weakness (e.g. Bosworth, 1992; Le Gall et al., 2005), and the presence of Mesozoic, Paleogene and Neogene strata filling the basin attest to this. However, the tectonic characterization of the Turkana Basin is beyond the scope of this work. In this study the Turkana Basin is considered as part of the East African Rift System.

The East African Rift System is divided into the eastern and western branches that together stretch from the Red Sea to Mozambique (Baker et al., 1972; McConnell, 1972). Rifting in the eastern branch has traditionally been thought to have initiated much earlier than in the western branch (Chorowicz, 2005). The earliest evidence of plume-related volcanism in the East African Rift System, which is heralded as the precursor to rifting, is recorded in the eastern branch in Kenya Rift **(**Turkana Basin: Fig. 4-1) at ~45 Ma (Morley et al., 1992; Ebinger and Sleep, 1998). However, recent findings from the Rukwa Rift Basin within the western branch, suggest that rift initiation may actually have been nearly synchronous between the two branches (Roberts et al., 2012). Updated thermochronology of the Malawi and Albert rift flanks (Bauer et al., 2012; Mortimer et al., 2016; Fig. 4-1) and new geochronologic data from the Kivu Rift (Pouclet et al., 2016) also provide additional support for more synchronous volcanism, rifting and uplift between the two branches.

4.2.2 Stratigraphy of the Turkana Basin

The Turkana Basin is floored by Precambrian and Paleozoic gneisses of the Mozambique Belt (e.g., Feibel, 2011); and filled by up to 7 km of Cretaceous fluvial sandstones, overlain by Oligocene-Miocene volcaniclastic fluvial-lacustrine strata, and capped by Pliocene to Holocene alluvial and lacustrine deposits (Williamson and Savage, 1986; Boschetto, 1988; Feibel, 2011; Fig. 4-2).

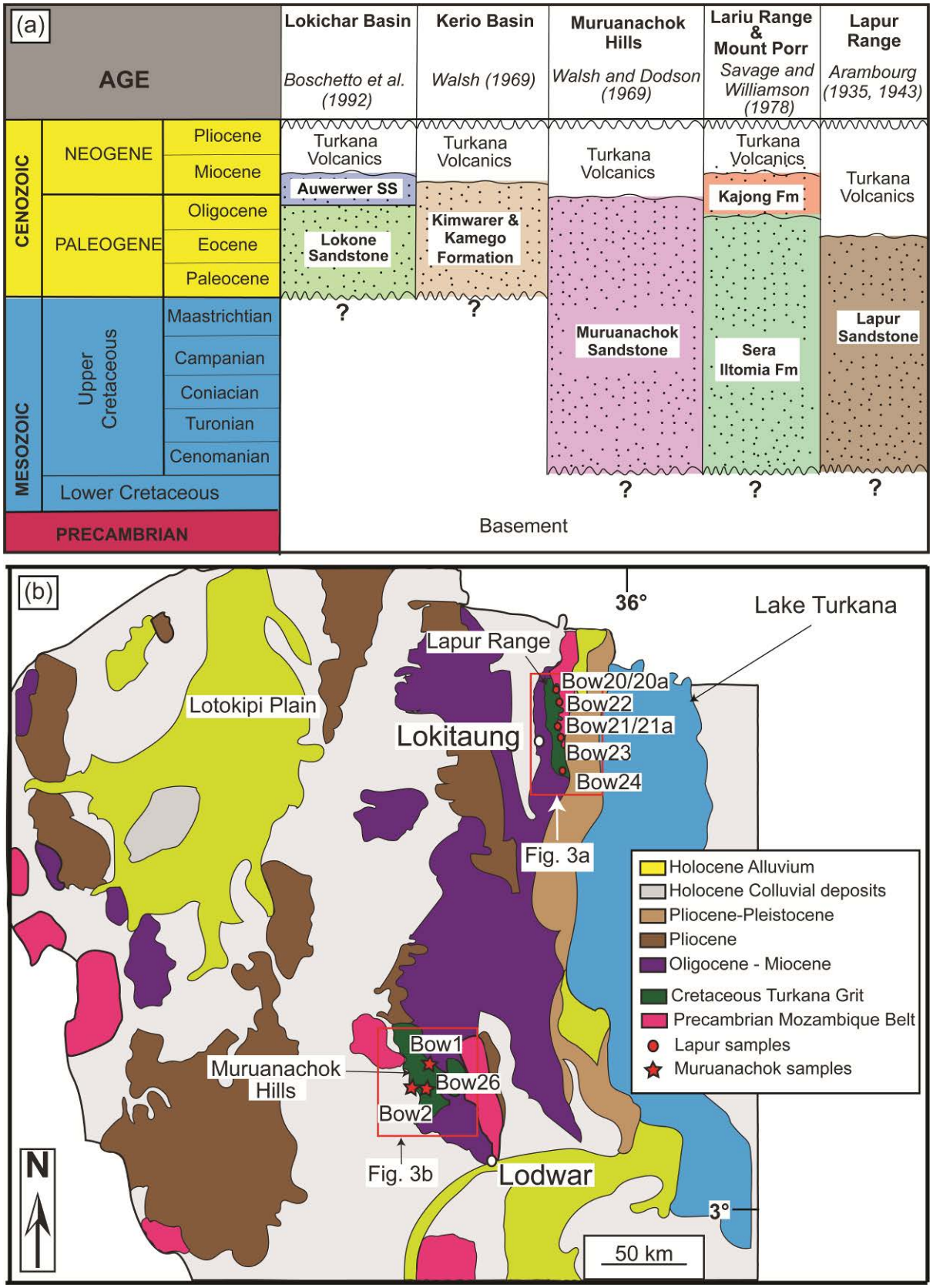

Figure 4-2. Stratigraphic chart and geological map of the Turkana Basin.

(a) Stratigraphic chart of the Turkana Grits showing some of the units previously lumped together. Stratigraphic chart was modified from Tiercelin et al. 2004; 2012 and the references therein. (b) Geological map of the Turkana Basin showing sample areas (Map modified from Ministry of Energy and Regional Development of Kenya, Geological map, 1987).

The Mozambique Belt (Fig. 4-1a) is characterized by exposed supracrustal rocks in northern Kenya and crustal granulite facies rocks in southern Kenya and Tanzania (Cutten et al., 2006). Two distinct domains have been identified within the Mozambique Belt, which have been called the Western Mozambique Belt with bedrock ages between 2970 to 1870 Ma and the Eastern Granulites with metamorphic ages between 841 Ma and 632 Ma (Cutten et al., 2006). The geologic and tectonic evolution of this belt are discussed by Mosley (1993) and others (Holmes, 1951; Key et al., 1989; Kröner, 2001; Grantham et al., 2003; Kröner and Stern, 2004) and the references therein.

Prior to the characterisation of the different lithostratigraphic units in the Turkana Basin by Walsh and Dodson (1969), Williamson and Savage (1986), Boschetto (1988) and others, all clastic deposits in the Kenya Rift were collectively referred to as the Turkana Grits by Murray-Hughes (1933). Detailed discussion on the Turkana Grits can be found in Williamson and Savage (1986), Boschetto (1988), Boschetto et al. (1992), Morley et al. (1992), Wescott et al. (1993), Thuo (2009) and Muia (2015). The age of the 'Turkana Grits' was originally considered to be Oligocene to Miocene based on the presence of the fossil wood genus *Dryoxylon* (Murray-Hughes, 1933), until Arambourg (1943) reinterpreted the fossilised 'wood-bearing sediments' as most likely Eocene and/or Cretaceous in age (also see Boschetto, 1988). Arambourg (1943) proposed two distinct episodes of sedimentation in the Turkana Basin, characterised by a basal Mesozoic event and an overlying Miocene event (Williamson and Savage, 1986).

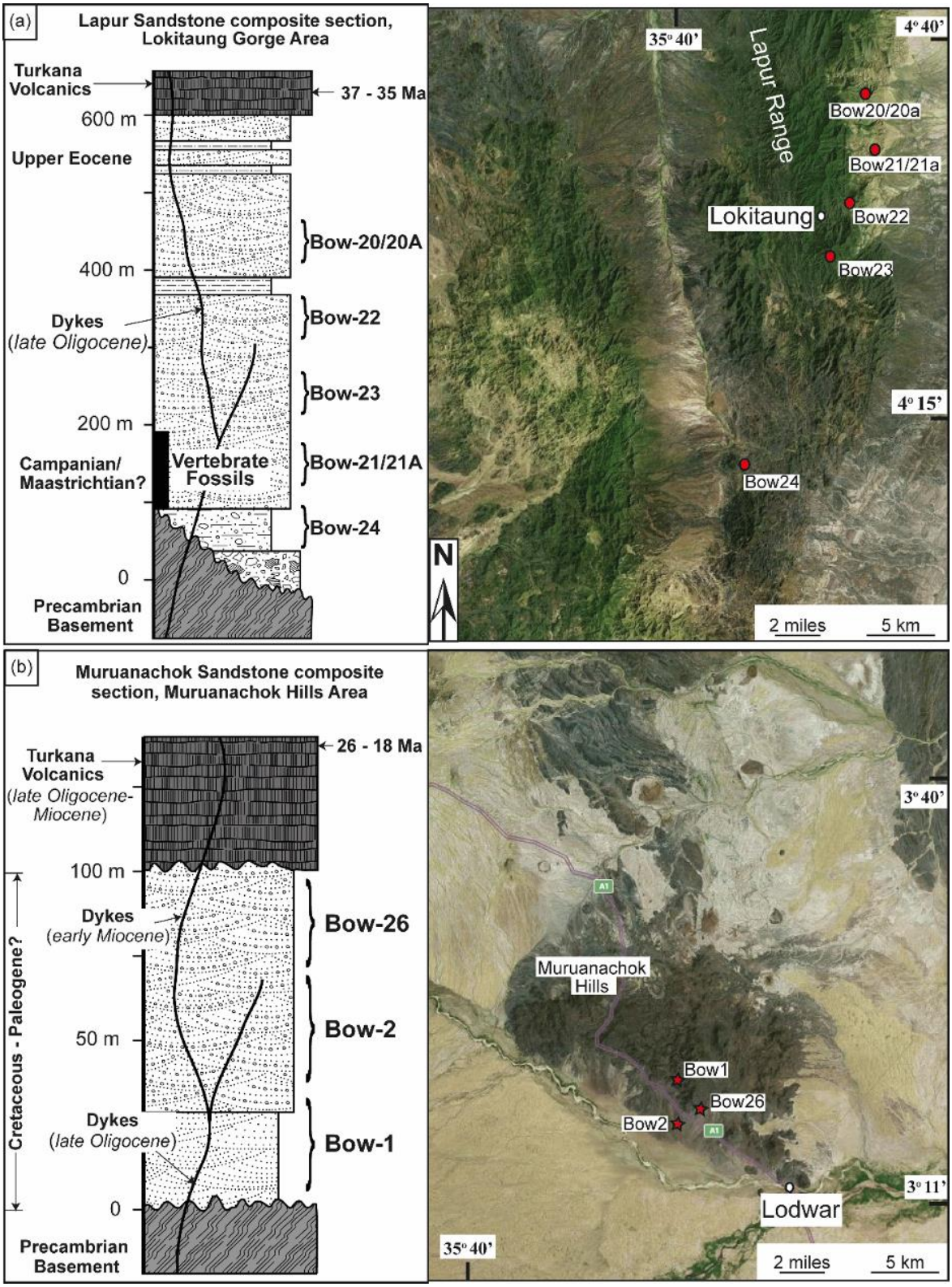

Figure 4-3. Simplified stratigraphy and ariel view of portions of the Kenya Rift within the Turkana Basin

(a) Lapur Sandstones (N = 7), (b) Muruanachok Sandstone (N = 3). (Ariel maps taken and modified from Bing maps – Earthstar Geographics SIO, © 2017).

Subsequently, Williamson and Savage (1986) defined four major lithostratigraphic units in the Turkana Basin (see Boschetto, 1988), which include: (1) the Precambrian and Paleozoic gneisses of the Mozambique Belt; (2) a thick sequence of coarse, immature clastic sedimentary rocks, named the 'Turkana Grits' or Laburr (Lapur) Series (Arambourg (1935); (3) a sequence of Oligocene through Miocene volcanic and interbedded sedimentary rocks; and (4) a thick, heterogeneous assemblage of Pliocene-Pleistocene volcanic and sedimentary rocks (Boschetto, 1988). Subsequent authors have since subdivided the clastic sequences of the 'Turkana Grits' into several distinct lithostratigraphic units, including the Sera Iltomia Formation (Mount Porr), Kajong Formation (Loriu), Kimwarer Formation, Lapur and Muruanachok sandstones (e.g. Tiercelin et al., 2004; G Muia, unpub.Ph.D. thesis, Univ. Rennes 1, 2015; Fig. 4-2a). The stratigraphic relationship between each of these units is poorly understood and in many cases, these units are assumed to be lateral equivalents to one another in different parts of the basin. Complex faulting and the presence of younger volcanic and sedimentary cover across much of the basin make precise stratigraphic and temporal correlations difficult. In general however, the lower part of coarse-grained portion of the 'Turkana Grits' rest nonconformably on basement rocks and are variably overlain by upper Miocene volcanic and sedimentary units. The key exception to this is in the Lapur Range (Fig. 4-2b) where significantly older Oligocene basalts overlie and in some cases appear to interfinger with the presumed Cretaceous age Lapur and Muruanachok sandstones of the 'Turkana Grits' (Walsh and Dodson, 1969; Boschetto, 1988; Tiercelin et al., 2012a).

4.2.2.1 Stratigraphy of the Lapur and Muruanachok sandstones

The Lapur Sandstone is a quartzofeldspathic sandstone dominated unit characterized by abundant metamorphic and sedimentary rock fragments (G Muia, unpub.Ph.D. thesis, Univ.

Rennes 1, 2015). The Lapur Sandstone is composed of pebbly sandstones with clast to matrix supported conglomerates interbedded with thin mudstone and fine grained sandstone horizons (Thuo, 2009). This distinctive unit of the 'Turkana Grits' is located on the northwestern side of Lake Turkana and extends over 60 km in length along the Lapur Range (Figs 4-2b and 4-3a). The lower beds of the Lapur Sandstone are affected by N-S oriented minor faulting (Tiercelin et al., 2012a). Volcanic sills and dyke intrusions of late Oligocene age (Fig. 4-3a) are common within the upper and middle beds of the Lapur Sandstone; a situation that is attributed to a major phase of volcanic activity in the region (Thuo, 2009; Tiercelin et al., 2012a). The Lapur Sandstone has variously been interpreted as between Cretaceous and Eocene (Morley et al., 1992; McDougall and Brown, 2009; O' Connor et al., 2011). The upper beds can be no younger than late Eocene based on dating of the overlying rhyolitic and basaltic lavas called the Turkana volcanics, which are dated between 37-29 Ma (Bellieni et al., 1981; Zanettin et al., 1983). In contrast, the age of the lower to middle portion of the stratigraphy has been assumed to be Lower or 'middle' Cretaceous (Bosworth and Morley, 1994). Palynologic evidence support a Campanian-Maastrichtian age, and fossil indicators of nearshore marine vertebrates (e.g., dyrosaurids, mosasaurs) correlated with proposed marine incursions in the Anza Rift Basin in the Campanian and Maastrichtian (Bosworth and Morley, 1994), are consistent with recent fossil discoveries also suggesting that these beds are Turonian-early Campanian (O'Connor et al., 2011).The depositional environments associated with the Lapur Sandstone have typically been interpreted as fluvial based on the facies and fragmentary nature of the fossils found within it (Walsh and Dodson, 1969). Paleocurrent directions are variable but generally indicated northerly transport direction (e.g. Wescott et al., 1993; Thuo, 2009). Two main paleoflow directions are inferred for the Lapur Sandstone based on paleocurrent analysis, which indicate west-northwest to northeast flow

for the lower and upper parts and south to west-southwest for the middle part of the unit (McGuire et al., 1985; Wescott et al., 1993; Sertich, 2006).

The Muruanachok Sandstone crops out in isolated hills and gullies in the Muruanachok Hills about 45 km northwest of Lodwar town (Figs 4-2b and 4-3b). The Muruanachok Sandstone is estimated at between 100 – 350 m thick, and is composed of coarse-grained sandstones interbedded with minor red-brown siltstones and shales. The petrography of this unit is also charactized as quartzofeldspathic, and the unit has traditionally been considered a lateral equivalent of the Lapur Sandstone (Thuo, 2009). The Muruanachok Sandstone is intruded by upper Miocene dykes and unconformably overlain by the upper Oligocene to Miocene Turkana volcanics (Figs 4-2a and 4-3b; Morley et al., 1992; Muia, 2015). The age of the Muruanachok Sandstone is variously estimated as between Cretaceous and Paleocene, although the top of the sandstone has also been considered to be as young as late Oligocene-early Miocene (Thuo, 2009). Regardless, the top of the Muruanachok Sandstone can be no younger than 25.5 – 18.5 Ma, based on dating of overlying volcanics in the Muruanachok area (McGuire et al., 1985: Figs 4-2b and 4-3b). Paleocurrent directions for the Muruanachok Sandstone are towards north-northwest based on measurements on trough-cross bedding within it (McGuire et al., 1985; Thuo, 2009).

4.2.2.1.1 Paleontology of the Lapur Sandstone

Vertebrate fossils were first recorded in the Lapur Sandstone following the discovery of an isolated sauropod dinosaur humerus in 1968 by F.H Brown and G.G. Eck while in transit to the lower Omo Valley (Figs 4-1b; Arambourg and Wolff, 1969). A subsequent paleontological expedition to the region in 1985 succeeded in locating abundant, but isolated,

vertebrate remains that included dinosaurs and other archosaurs. Though never formally described, notes from the expedition were widely reported (e.g. Jacobs et al., 1996; Weishampel et al., 2004). These expedition notes described fauna that included theropod and sauropod dinosaurs, and resulted in tentative temporal assessments ranging from the Jurassic through the Cretaceous (Williamson and Savage, 1986; Weishampel et al., 2004). In particular, the report of a possible spinosaurid theropod dinosaur suggested a 'middle' Cretaceous age for the deposits, an interval biostratigraphically consistent with assemblages from other northern African and South American localities (e.g. Sereno et al., 1998; Amiot et al., 2010).

More recent paleontological exploration of the Lapur Sandstone has recovered significant, though mostly fragmentary, vertebrate remains. These collections, housed at the National Museums of Kenya in Nairobi and TBI-Turkwel, Kenya, consist entirely of large-bodied vertebrates including dinosaurs, crocodyliforms and turtles. Despite largely fluvial deposition of the Lapur Sandstone, several recovered taxa are consistent with marginal marine settings including an isolated vertebra originally attributed to a pterodactyloid pterosaur (O'Connor et al., 2011) but later re-identified as the caudal vertebra of a mosasaur (Averianov, 2014), and abundant remains of dyrosaurid crocodyliforms. Several marine incursions into the Anza Rift system, notably in the Cenomanian and Maastrichtian (Bosworth and Morley, 1994), could explain the presence of estuarine/marine vertebrate taxa within the fluvial Lapur Sandstone. Dyrosaurid crocodyliforms are currently known only from Maastrichtian-Eocene deposits (Jouve et al., 2008; Hastings et al., 2011) providing weak biostratigraphic support for a Maastrichtian age for the Lapur assemblage.

The Cretaceous-aged vertebrate fossils of the Lapur Sandstone are exclusively located in the lower 200 meters of the section exposed around Lokitaung Gorge (Figs. 4-2b and 4-3a).

The high energy, coarse-grained sandstones and conglomerates typical of the Lapur Sandstone sequence produce a taphonomic bias toward large and robust fossil remains. Among the most common vertebrate fossils recovered from the Lapur Sandstone include large sauropod dinosaur limb bones and caudal vertebrae. More delicate remains, including thin vertebrae and cranial elements, are fragmentary and heavily abraded by transport in a coarse fluvial system. Microvertebrate remains, including teeth and small bones, are virtually absent from collections despite intensive surveys by one of the authors (JS). This bias may explain the absence of small to medium vertebrates typical of most early Paleogene assemblages in upper horizons of the Lapur Sandstone, and possibly the Muruanachok Sandstone.

4.3 Sampling and analytical methods

4.3.1 Sampling

The 'Turkana Grits' in the Lapur Range and the Muruanachok Hills were investigated as part of hydrocarbon exploration program in Block 11b conducted by Adamantine Energy Limited and Bowleven Oil plc during March 2014. Mapping was focussed on identification of lithologic units and key geologic structures and their relationships. Lithologic and sedimentologic characterisation was carried out for both the Lapur and Muruanachok sandstones in an attempt to date and correlate the different stratigraphic units (Figs. 4-2a and 4-3). Detailed stratigraphic logs and paleocurrent data for the Lapur and Muruanachok Sandstones are presented in Thuo (2009) Tiercelin et al. (2012a) and Muia (2015), and are referenced in this study. Sampling was extensive and attempted to represent all major lithologies and sedimentary facies of both the Lapur and Muruanachok sandstones. To

determine the sedimentary provenance of the Lapur and Muruanachok sandstones, hand samples typically weighing 2-2.5 kg each, were collected from the Lapur (N = 7) and Muruanachok (N = 3) for sandstone petrography, U-Pb geochronology, Lu-Hf isotope and trace element analysis of detrital zircons. Sample location details are presented in Table 4-1 and plotted in Figures 4-2b and 4-3.

Table 4-1. Location details of Lapur and Muruanachok sandstone samples

Sample #	Sandstone	Elevation	Northing			Easting		
		(m)	Degree	Minutes	seconds	Degree	Minutes	seconds
Bow-1	Muruanachok	586	3	21.369	3.35615	35	24.278	35.4046
Bow-2	Muruanachok	585	3	21.403	3.35672	35	24.252	35.4042
Bow-26	Muruanachok	590	3	22.299	3.37165	35	24.178	35.403
Bow-20	Lapur	1202	4	23.882	4.39803	35	47.778	35.7963
Bow-20A	Lapur	1202	4	23.882	4.39803	35	47.778	35.7963
Bow-21	Lapur	531	4	19.492	4.32487	35	48.5	35.8083
Bow-21A	Lapur	531	4	19.481	4.32468	35	48.527	35.8088
Bow-22	Lapur	682	4	19.481	4.32468	35	48.527	35.8088
Bow-23	Lapur	674	4	14.767	4.24612	35	48.223	35.8037
Bow-24	Lapur	487	4	11.173	4.18622	35	49.681	35.828

4.4 Analytical methods

Provenance analysis of sedimentary units like the Lapur and Muruanachok sandstones is considered an effective method of understanding basin kinematics, mountain building systems and the tectonic evolution of orogens (e.g. Jorge et al., 2013). An integrated approach rather than a single method to sedimentary provenance can provide comprehensive information on source characteristics, which enhances tracing sediment to their sources (Morton et al., 2012; Jian et al., 2013). Detrital minerals such as zircon in sedimentary rocks can provide useful information on the genesis, transport and deposition of such rocks (e.g., Oliveira et al., 2015). The ubiquitous and refractory nature of zircon is particularly useful as the uranium stored in its crystal structure makes it advantageous for obtaining age of source

rocks in addition to acquiring geologic information on unknown magmatic or metamorphic events (Carrapa, 2010; Cawood et al., 2012). In situ Lu–Hf isotopic data from zircons can also provide additional information about the crustal evolution of the zircon sources to complement the U-Pb geochronology data (Corfu and Noble, 1992; Griffin et al., 2004; Zheng et al., 2007).

4.4.1 Sedimentology and sandstone petrography

Macroscopic observations on hand specimens and microscopic studies on thin sections were performed at James Cook University, Townsville, Australia. This was done in an attempt to infer parent rock characteristics of the 'Turkana Grits' (e.g. Dickinson and Suczek, 1979; Dickinson et al., 1983). Ten thin sections prepared to the standard thickness of 30 μm and impregnated with blue-dyed epoxy resin to highlight porosity were point-counted following the Gazzi-Dickinson method (Ingersoll et al*.,* 1984). The sandstone point-counts consisted of 350 points per sample, which were used to estimate the compositional percentages of quartz (Q), feldspar (F) and lithic (L) grain fragments (Ingersoll et al*.,* 1984; Dickinson, 1985). The point counting was conducted using transmitted-light polarizing Leica DMRXP microscope. Modal parameters were normalized and plotted on ternary diagrams using tectonic discrimination fields as outlined in Dickinson and Suczek (1979) and Dickinson et al. (1983).

4.4.2 U-Th-Pb dating

Ten detrital samples from the Lapur (N = 7) and Muruanachok (N = 3) sandstones were analysed for their U-Pb age dates of the zircons. Detrital zircons separation and U-Pb dating

were conducted following standard procedures outlined by Gehrels et al. (2008) and Slma and Koler (2012), and adapted by Tucker et al. (2013) for Advanced Analytical Centre at James Cook University, where all analyses were conducted. Samples were each crushed, milled, and passed through a Wilfley Table for gravity separation using water. The washed samples from the Wilfley Table were dried in an oven set at ~ 60 °C. A hand magnet was used to extract magnetic minerals from the dried sample. The Frantz magnetic separator set at progressively higher magnetic currents of 0.4, 0.8, 1.0 and 1.2 amperes (A) at a constant side slope of 10° to remove strongly magnetic minerals from the samples. The non-magnetic portion of each sample was then density separated using lithium polytungstate adjusted to a specific gravity of ~2.85 g/cm^3. Subsequently, the heavy mineral separates were washed with distilled water and dried in an oven set at ~ 60 °C. All identified zircons were handpicked (≥ 100 zircons / sample) using an electron microscope and mounted in a 25 mm diameter transparent epoxy resin disc with fragments of zircon standards GJ-1 (609 Ma, Jackson et al*.,* 2004) and Temora-2 (416.8 Ma, Black et al*.,* 2003). The zircons in the epoxy disc were polished to expose the zircons for cathodoluminescence imaging using a Jeol JSM5410LV scanning electron microscope. Steps were taken throughout the sample preparation and mineral separation processes to prevent contamination.

The cathodoluminescence images were used to identify unaltered areas of the zircon grains for U-Pb dating. Dating was conducted using U-Pb laser-ablation inductively coupled plasma mass spectrometry (LA-ICP-MS) via a Coherent GeolasPro 193 nm ArF Excimer laser ablation system connected to a Bruker 820-MS (formerly Varian 820-MS) following methods outlined in Owusu Agyemang et al. (2016). Total analysis time for each zircon grain was 70 seconds; the first 30 seconds was used to measure the background intensities followed by 40 seconds of zircon ablation. Standard bracketing was used to correct for the remaining

elemental fractionation and mass bias (Gehrels et al., 2008). Two analyses each of zircon standards GJ-1 and Temora-2 were conducted before and after analysis of 10-12 unknown zircons from the studied samples. NIST 612 standard glass (50ppm glass USGS working values, 2009) was also analysed before and after each U-Pb laser ablation session (usually 8 hours per session) and at least once between sessions for calibrating thorium and uranium concentrations. Zircon grains were ablated using a 32μm beam diameter.

Data reduction and age determination was performed using the GLITTER 4.0 software (Van Achterbergh et al*.,* 2001). The reduced data was exported to Microsoft Excel with Isoplot/Ex 3.75 (Ludwig, 2012), an excel-based macro for the calculation of discordancy, which is a ratio of $^{206}Pb/^{238}U$ and $^{207}Pb/^{206}Pb$ ages. A discordance cut-off of 10 % was used in this study for all grains older than 300 Ma (Gehrels, 2012). Concordia diagrams (2σ error ellipses) and probability density plots were developed for the U-Pb age dataset using Isoplot/Ex 3.75. Reported uncertainties were propagated by linear addition of the external reproducibility obtained from primary standard zircon GJ-1 during individual analytical sessions.

4.4.3 Lu-Hf isotope analyses

Lu-Hf isotopic compositions of zircons were measured from a subset of detrital zircon grains selected to provide the greatest coverage of different grain-age populations from eight of the U-Pb detrital zircon samples with ≤ 10% discordance. Lu-Hf methods follow those described by Kemp et al. (2009) and Næraa et al. (2012) for the Advanced Analytical Centre at James Cook University. The eight samples include five from the Lapur and three from the Muruanachok sandstones. The Lu-Hf analyses were performed using a GeoLas 193-nm ArF laser and a Thermo Scientific Neptune multi-collector ICP-MS, with a repetition rate of 4 Hz

and power density of sample maintained around 6 – 7 Jcm^{-2} which translates into an estimated ablation rate of ~0.5 μms^{-1} using helium gas for ablation. The Lu-Hf isotopic ratios for each analysis were derived from a 60-second ablation period, comprising 60 cycles of one-second integration time. Background gas was measured for approximately 60 seconds at the beginning of every analysis. The isotopic data was acquired using a uniform laser spot size of 60 µm, usually overlapping the same spot where the zircon grain was ablated for concordant U-Pb age data (Fisher et al., 2014).

The Lu-Hf datasets were subsequently processed offline to check for the homogeneity of all ablated zircons. Correction for the isobaric interference of lutetium (Lu) and ytterbium (Yb) on ^{176}Hf was performed by monitoring ^{175}Lu ($^{176}Lu/^{175}Lu$ = 0.026549) and ^{171}Yb ($^{176}Yb/^{171}Yb$ = 0.897145). Both ^{171}Yb and ^{173}Yb were measured in order to correct for the mass bias, which was subsequently corrected by the exponential law (Fisher et al., 2011). The measured average $^{176}Hf/^{177}Hf$ from two standard zircons; Mud Tank zircon (MTZ) and FC-1 zircon, were used to monitor the instrumental state and analytical accuracy (Fisher et al., 2014). The FC-1 zircon standard was repeatedly measured, for which the normalized $^{176}Hf/^{177}Hf$ value is 0.282178 ± 16 (n = 13) and the 'true' (solution) value is 0.282184 ± 16 (Woodhead and Hergt, 2005), where the uncertainties are two standard deviations. The measured average $^{176}Hf/^{177}Hf$ from MTZ obtained over all analytical sessions is 0.282493 ± 6 (n = 18) and compared with the 'true' (solution) value of 0.282507 ± 6 (Woodhead and Hergt, 2005). Based on the analyses of the MTZ, a $^{176}Hf/^{177}Hf$ normalization factor of *1.000050* was applied to the unknown sample zircons from this study (Næraa et al., 2012; Fisher et al., 2014). The ^{176}Lu decay constant of 1.867 ± 0.008 x 10^{-11} $year^{-1}$ reported by Söderlund et al. (2004) and the Chondritic Uniform Reservoir (CHUR) values of $^{176}Hf/^{177}Hf$

(0.282785) and $^{176}Lu/^{177}Hf$ (0.0336) reported by Bouvier et al. (2008) were used in the calculations.

4.4.4 Zircon trace elements analysis

Zircon trace element composition analysis, following U-Pb dating and Lu-Hf, was employed to provide additional source rock characteristics, as transportation and weathering processes do not modify the trace elemental ratios in zircon (e.g. Pearce et al., 1984; Hoskin and Ireland, 2000; Belousova et al., 2002; Grimes et al., 2007; Yao et al., 2011). Selected grains from the Archean, Proterozoic and the Paleogene zircon populations from both sandstones were analysed for their trace element ratios. The analyses were conducted using laser-ablation inductively coupled plasma mass spectrometry (LA-ICP-MS) with a Coherent GeolasPro 193 nm ArF Excimer laser ablation system connected to a Bruker 820-MS following a similar methodology to that described above for U-Pb geochronology. Laser repetition rate was 10 Hz and laser beam energy at the sample was maintained between 5 and 6 J/cm^2. A spot size of 44 μm was used throughout the analysis. The analysis time for each sample was also 70 seconds, comprising a 30 seconds measurement of background intensities and a 40 seconds sample analysis time. Cathodoluminescence images of the zircons were used to select unaltered spots that were in the same domain on the zircon as where it was analysed previously for the U-Pb age data. Calibration was achieved using standard procedures (Kovacs et al., 2009) that included the use of NIST 610 glass reference material for external standardization and the stoichiometric zircon SiO_2 content for internal standardization. Standard zircon 91500 (Wiedenbeck et al., 2004) was used as a secondary standard to check method for accuracy. Zircon trace element data were processed using SILLS with GeoREM preferred concentration values for NIST610 (Guillong et al., 2008).

4.5 Results and interpretation

4.5.1 Sandstone petrography

Modal quartz-feldspar-lithic (QFL) compositions were used to infer the parent rock characteristics (Dickinson and Suczek, 1979; Dickinson et al., 1983; Ingersoll et al., 1984; Dickinson, 1985). Dickinson and Suczek (1979) proposed that the mean compositions of modal quartz-feldspar-lithic (QFL) grains derived from different source regions controlled by plate tectonic processes are inclined to plot within discrete fields on Q_tFL and Q_mFL_t diagrams. However, these provenance assignations reported herein must be treated with caution due to the high probability of feldspar dissolution related to surficial tropical weathering.

Modal quartz-feldspar-lithic (QFL) compositions of Lapur and Muruanachok sandstones are presented in Figure 4-4. Both the Lapur and Muruanachok samples are dominated by monocrystalline quartz with subordinate polycrystalline quartz and rock fragments. The samples had no visible feldspar grains, except for one Muruanachok (Bow-26) and three Lapur (Bow-20A, Bow-21 and Bow-21A) sandstone samples (Figs 4-3 and 4-4). The lithic rock fragments are dominantly of volcanic and metamorphic sources in both units. Ternary diagrams were plotted to define the petrofacies and identify possible source areas for the two sandstones. The Lapur and the Muruanchok sandstones are comparable in their quartz content, which ranges from 89% to 97%, consistent with the quartz arenite to sub-arkose petrofacies. Assuming that no surficial feldspar dissolution has occurred, both sets of samples plot as recycled and craton interior provenance, following the tectonic discrimination diagrams of Dickinson et al. (1983).

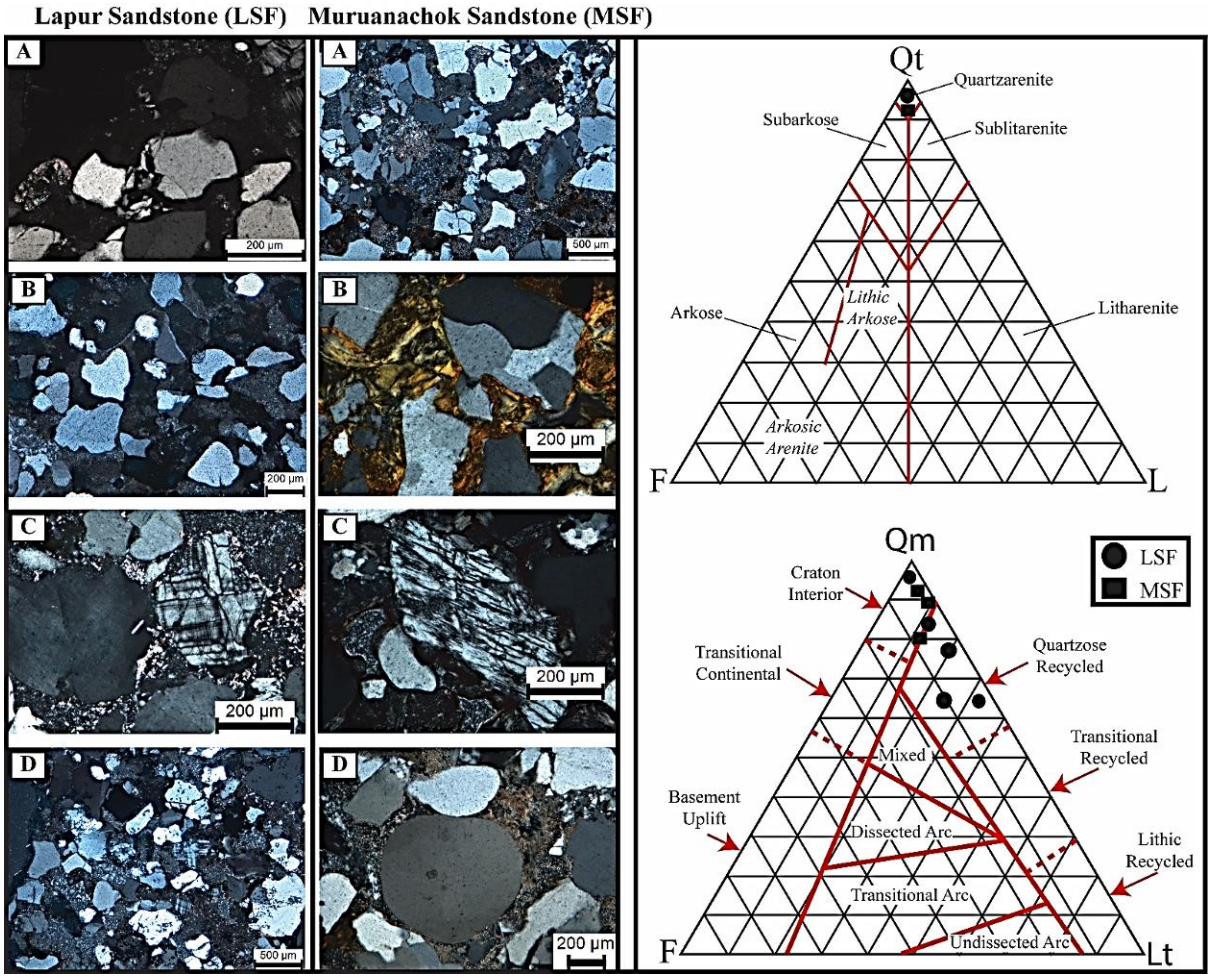

Figure 4-4. Thin section photomicrographs and detrital modes of Lapur and Muruanachok sandstones.

Representative photomicrographs for the two sandstones investigated; Left column is for Lapur samples and right column is for Muruanachok samples. The Lapur samples mostly plot as quartz arenites with mixed provenance suggestive of recycled orogen and craton interior. The Muruanachok samples mostly plot as quartz arenites with craton interior provenance. Tectonic discrimination diagrams are after Dickinson et al. (1983). Qt is total quartz grains, Qm is monocrystalline quartz and Lt is total lithics.

The detrital grains from both sets of samples are sub-angular to sub-rounded, poorly sorted with clay matrix present and abundant calcite, kaolin and hematite cements. Primary porosity is observed mostly in the Lapur samples, although this is quite variable. A number of grains from the two sandstones are elongated with mica inclusions, suggestive of a schistose metamorphic source for those grains (Folk, 1980), which is consistent with sediment derived

from the Eastern Granulite part of the Mozambique Belt underlying most of Kenya and the Turkana Basin (Mosley, 1993). Some monocrystalline quartz grains also contains large vacuoles with rounded corners and embayment suggestive of plutonic and volcanic sources, respectively (Folk, 1980), which is consistent with rocks of the Western Mozambique Belt or possibly from younger, unknown volcanic sources.

4.5.2 U-Pb detrital zircon geochronology

Ten detrital zircon samples were taken from the Lapur (N = 7) and Muruanachok sandstones (N = 3), and analysed for their U-Pb ages. This work yielded 875 concordant U-Pb analyses out of 1106 total analyses using a discordance filter of 10%. U–Pb age results are summarized in Table 4-2 and the complete zircon U–Pb data are presented in 4S1. Detrital zircon grains range from bright to dark with dominantly oscillatory zoning under cathodoluminescence (Fig. 4-5). Zircon grains are mostly clear to light brown predominantly euhedral to sub-rounded with grain lengths ranging from 100-µm to 650-µm and widths between 50-µm to 200-µm, typical of igneous or magmatic source (e.g. Aleinikoff et al., 2006).

High Th/U ratios (Th/U > 0.1) in zircons are typical of magmatic sources, whereas low Th/U ratios (Th/U < 0.1) and variable ratios are characteristic of metamorphic sources (Rubatto, 2002; Hoskin and Schaltegger, 2003). In this study, the majority of zircon grains from the 'Turkana Grits' are characterised by high Th/U ratios except a small fraction (~4%) with Th/U ratios < 0.1 (Fig. 4-6). The high Th/U ratios suggests that most of the detrital zircons in the Turkana Basin were sourced from magmatic/igneous rocks, or more likely in this setting from partially metamorphically overprinted igneous terrains that were unaffected

by resetting. The few grains with metamorphic Th/U ratios were probably affected by localized hydrothermal fluid interactions (for example Bow1-19 zircon grain in Fig. 4-5).

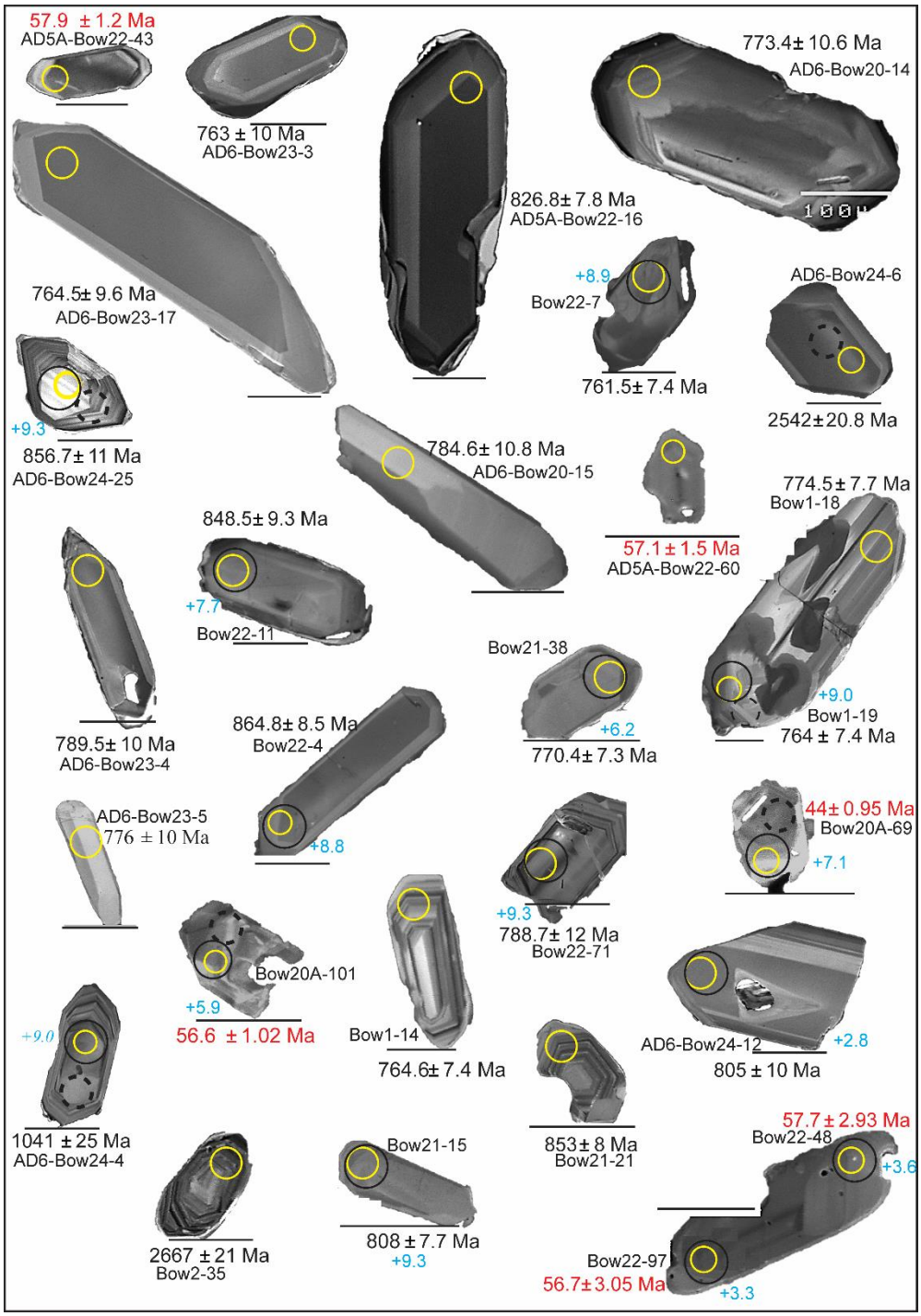

Figure 4-5. Representative cathodoluminescence images of zircons from the Turkana Basin.

Yellow circles show U-Pb age dating spots, black circles show Lu-Hf isotope analysis spots and dashed black circles show trace element analysis spots. The analysis spot size used for the U-Pb, trace element and Hf are 32, 44 and 60 µm in diameter respectively. The scale bar under each zircon is equivalent to 100 µm.

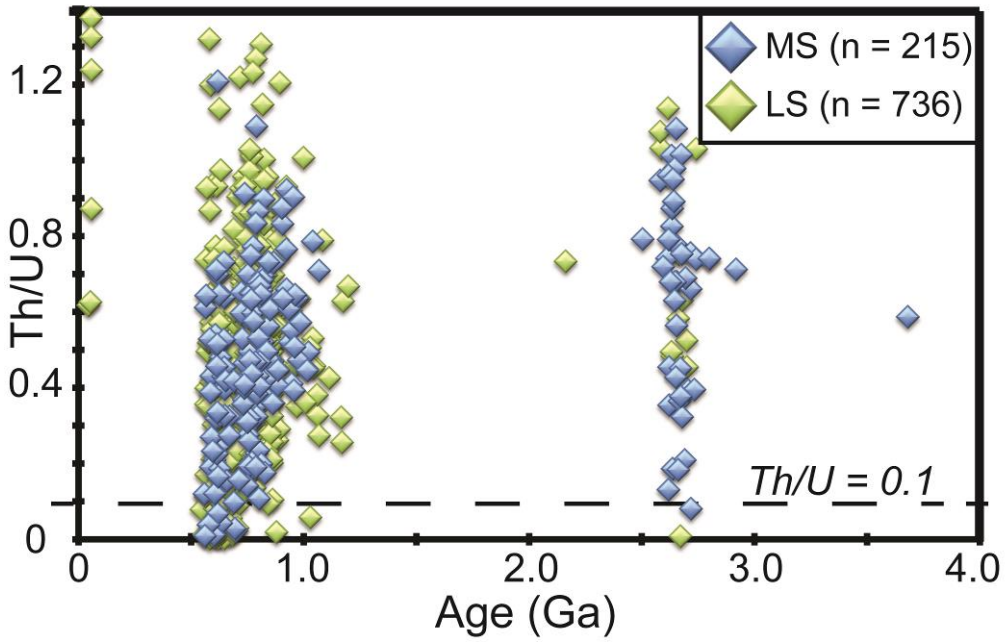

Figure 4-6. Thorium (Th) to Uranium (U) ratios for the Lapur and Muruanachok zircons.

This figure shows the high Th/U ratios for the analysed samples from the Turkana Basin, which suggest that most of the detrital zircons have magmatic provenances. The dash line is Th/U = 0.1.

Table 4-2. Summarized U-Pb detrital zircon results for the Lapur and Muruanachok sandstones.

Unit	Sample	#Analysis	# Concordant	Youngest single grain (Ma)	Oldest single grain (Ma)
Lapur Sandstones	Bow-20	85	61	566	1047
	Bow-20A	183	150	45	969
	Bow-21	141	129	581	1061
	Bow-21A	75	66	604	891
	Bow-22	178	133	57	865
	Bow-23	97	85	587	893
	Bow-24	93	67	570	2741
Muruanachok Sandstones	Bow-1	80	57	589	2717
	Bow-2	94	75	565	2918
	Bow-26	80	52	562	2673
Total		**1106**	**875**		

The seven Lapur samples yielded 691 concordant ages out of 852 grain analyses. The age spectra are similar for all seven samples, and the zircons range in age from Neoarchean (~2700 Ma) to Eocene (~45 Ma). Each of the seven Lapur samples is dominated by Neoproterozoic zircons (1000 – 550 Ma), accounting for ~96% of all concordant analyses (Fig. 4-7). The main exceptions include a population of 11 Archean age zircons from the Lapur sample Bow-24 (base of unit) and six Paleogene age zircons recovered from Lapur samples Bow-20A and Bow-22 (top of the unit; Fig. 4-3a). The Paleogene zircons are particularly significant as the Lapur Sandstone has traditionally been considered to be Cretaceous in age. The Paleogene zircons include one middle Eocene grain (~45 Ma) and a coherent population of five Paleocene grains with a mean age of ~57 Ma.

The three Muruanachok samples yielded 184 concordant grains out of 254 grain analyses, with ages ranging from Mesoarchean (2918 Ma) to Neoproterozoic (562 Ma). The Muruanachok samples are also dominated by Neoproterozoic zircons accounting for ~80% of concordant zircons, followed by ~19% Archean zircons (Fig. 4-8). The Archean grains from the Muruanachok samples, which are clustered around 2800 Ma and 2650 Ma, are similar to the Archean grains from the Lapur sample Bow-24 (Figs 4-7 and 4-8).

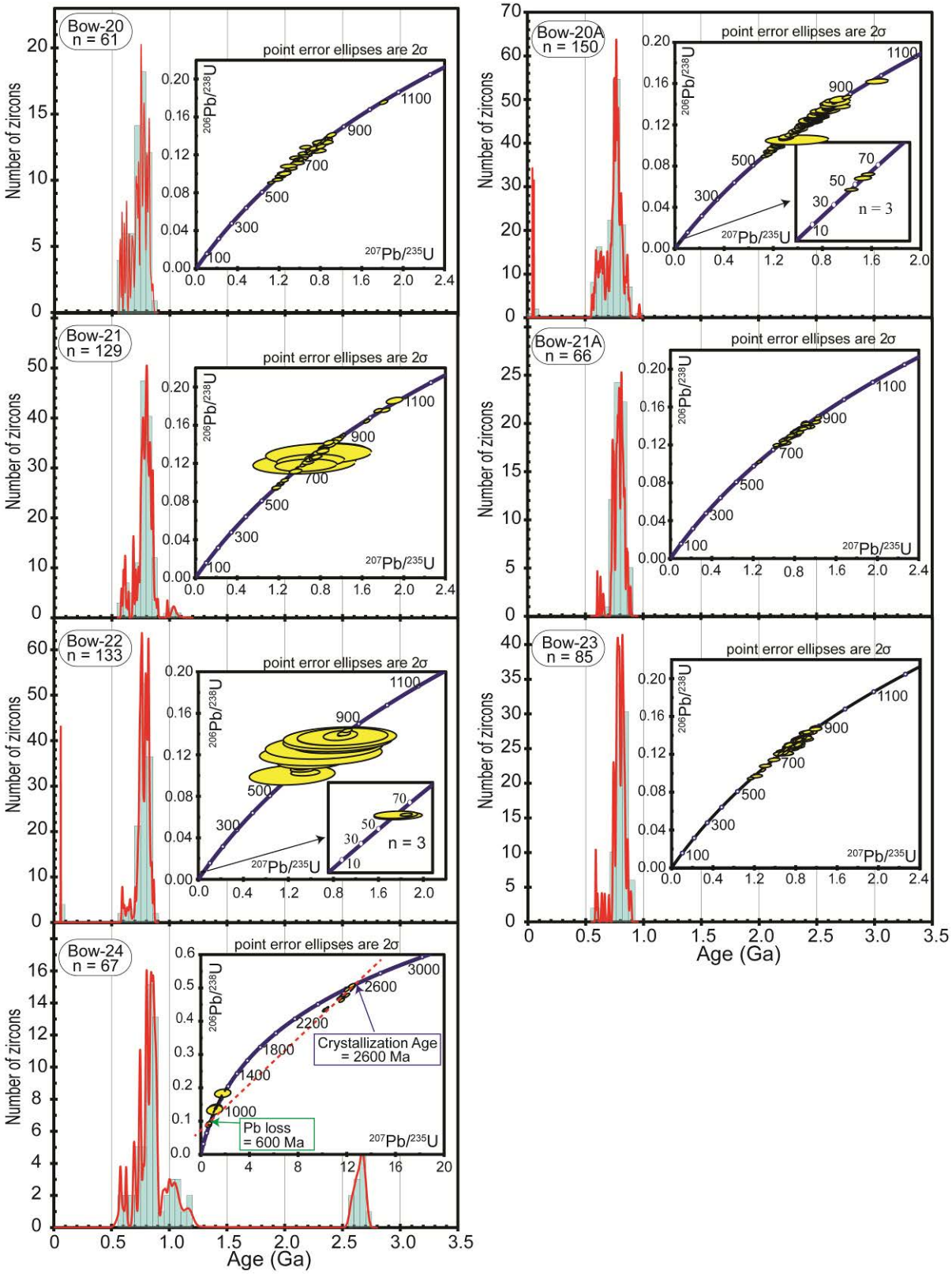

Figure 4-7. Probability density plot and corresponding Concordia plots for the Lapur Sandstone (N = 7).

The plot shows the dominance of Neoproterozoic age zircons for each sample. Reported results are single zircon concordant analyses with the exception of one grain from sample Bow-22 that was analysed twice (The reported

analysis Bow-22-48 and Bow-22-96 is for the same zircon grain, see Fig. 4-5). The $^{207}Pb/^{206}Pb$ age was selected for zircon grains older than 1.0 Ga as they are more reliable for older zircons, whereas the $^{206}Pb/^{238}U$ age was selected for younger zircons with age less than 1.0 Ga, because they are reliable for younger zircons (e.g. Gehrels, 2012). The instrumental parameters and operating conditions are provided in the Appendix 4S1.

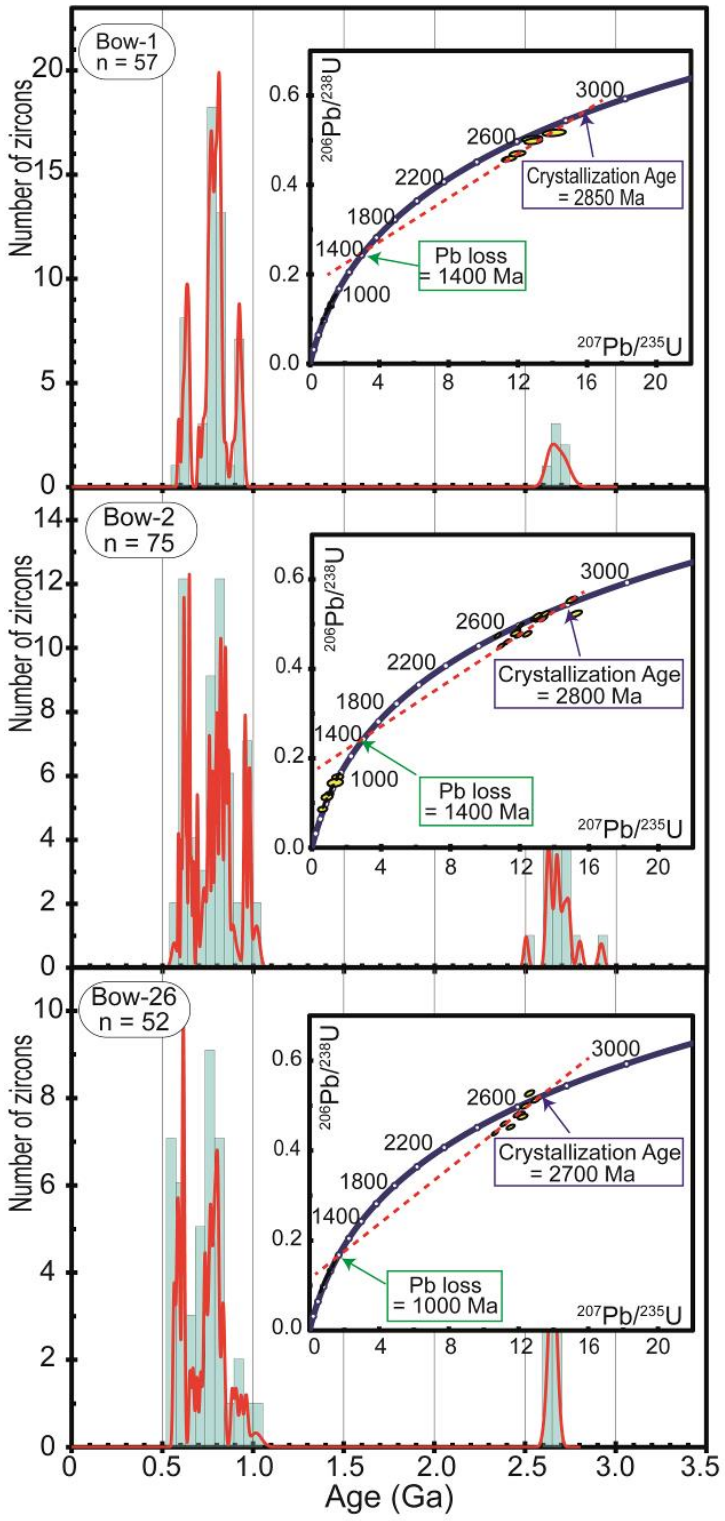

Figure 4-8. Probability density plot and corresponding Concordia plots for the Muruanachok Sandstone (N = 3).

This plot also shows the dominance of Neoproterozoic zircons from Muruanachok Sandstone. Reported results are single zircon concordant analyses exception Bow-1-18 and Bow-1-19, which represent the same grain, see Fig. 4-5).

Kolmogorov-Smirnov (K-S) non-parametric statistical tests were used to compare the age distributions for provenance interpretations. This K-S test compares the maximum probability difference between two cumulative distribution frequency (CDF) curves for two populations and express the probability (P) that the observed difference must exceed *0.05* to be 95% confident that the populations are not different and may have originated from a similar source terrain (Guynn and Gehrels, 2010). The degree of similarity or difference between any two of the samples from this study can be seen in the cumulative distribution frequency plots generated from the K-S test (Fig. 4-9a-c and Table 4-3). The normalized age probability plot (Fig. 4-9d) also highlights the differences and similarities between the two sets of samples. Qualitative comparison of the cumulative frequency distribution plots (Fig. 4-9a-c) for each of the Lapur and Muruanachok samples suggests that both sandstones were sourced from a similar, if not the same Neoproterozoic source, presumably the local crystalline basement rocks of the Mozambique Belt exposed along the rift flanks before the onset of metamorphism around 640 Ma (Hauzenberger et al., 2007) as shown by the dominance of magmatic sources (Fig. 4-6).

The K-S test for Lapur samples (Fig. 4-9a) indicate that six out of seven samples passed the test and are likely to have come from a similar source. The Lapur sample Bow-24, did not pass the K-S test, but does pass a K-S test when compared with Muruanachok samples (Fig. 4-9b). The key provenance difference is the presence of a substantive Neoarchean zircon population in the Muruanachok samples and Bow-24 (from the Lapur), which is not seen in any of the other six Lapur samples. It must be noted that these Neoarchean zircon populations appears to have been affected by Pb loss (Figs 4-7 and 4-8). Additionally, sandstone

petrography confirms a closer similarity between Bow-24 and the Muruanachok Sandstone samples, than with the six other Lapur samples (Fig. 4-4). Although the stratigraphic context of the Bow-24 sample in relation to rest of the Lapur samples is not entirely clear, this sample, which is the southernmost Lapur Sandstone unit samples in this study is reinterpreted herein to be part of the lower Lapur Sandstone (Figs 4-2b and 4-3).

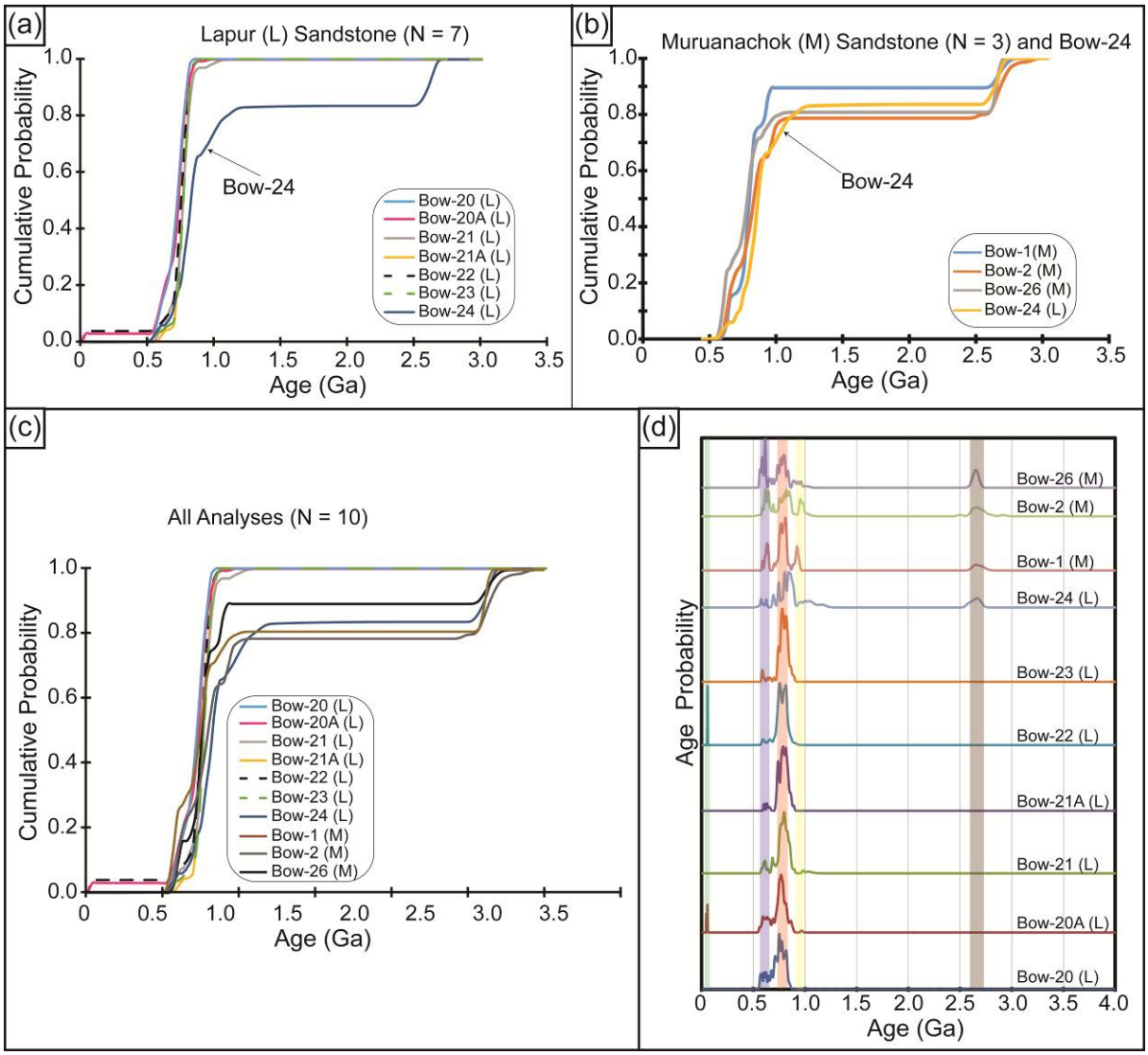

Figure 4-9. Cumulative distribution frequency diagram of the studied samples.

(a) Lapur Sandstone (N = 7). This figure shows that only Bow-24 is different because of the Archean population and hence more similar to the Muruanochok Sandstone. (b) Muruanachok samples (N = 3) and Bow-24 (mapped as Lapur). This plot shows that the three Muruanachok samples have identical provenance to the Lapur Bow-24. (c) All

Analyses. (d) Relative age probability plot of detrital zircon samples (N = 10) from the Lapur (L) and Muruanachok (M) samples showing the similarities and differences in age spectra. Three main Neoproterozoic age populations are also highlighted.

Table 4-3. K-S Test results for Lapur and Muruanachok sandstones

(a) P-values from Kolmogorov-Smirnov test of detrital-zircon age spectra assessing similarities of Lapur Sandstone samples.

	Bow-20	Bow-20A	Bow-21	Bow-21A	Bow-22	Bow-23	Bow-24
Bow-20		**0.973**	0.001	0.003	0.020	0.000	0.000
Bow-20A	**0.973**		0.000	0.002	0.040	0.000	0.000
Bow-21	0.001	0.000		**0.827**	**0.341**	**0.904**	0.000
Bow-21A	0.003	0.002	**0.827**		**0.383**	**1.000**	0.000
Bow-22	0.020	0.040	**0.341**	**0.383**		**0.097**	0.000
Bow-23	0.000	0.000	**0.904**	**1.000**	**0.097**		0.000
Bow-24	0.000	0.000	0.000	0.000	0.000	0.000	

(b) P-values from Kolmogorov-Smirnov test of detrital-zircon age spectra assessing similarities of Muruanachok Sandstone samples and Lapur Bow-24, showing they are similar particularly to Bow-2.

	Bow-1	Bow-2	Bow-26	Bow-24
Bow-1		**0.090**	**0.354**	0.001
Bow-2	**0.090**		**0.201**	**0.365**
Bow-26	**0.354**	**0.201**		0.004
Bow-24	0.001	**0.365**	0.004	

(c) P-values from Kolmogorov-Smirnov test of detrital-zircon age spectra assessing similarities of all samples. The bold p-values indicate that they pass the K-S test and could be from a similar terrane.

	Bow-20	Bow-20A	Bow-21	Bow-21A	Bow-22	Bow-23	Bow-24	Bow-1	Bow-2	Bow-26
Bow-20		**0.970**	0.001	0.003	0.018	0.000	0.000	0.014	0.000	0.020
Bow-20A	**0.970**		0.000	0.002	0.043	0.000	0.000	0.006	0.000	0.008
Bow-21	0.001	0.000		**0.844**	**0.341**	**0.921**	0.000	**0.104**	0.000	0.032
Bow-21A	0.003	0.002	**0.844**		**0.383**	**1.000**	0.000	**0.090**	0.000	0.028
Bow-22	0.018	0.043	**0.341**	**0.383**		**0.085**	0.000	0.034	0.000	0.009
Bow-23	0.000	0.000	**0.921**	**1.000**	**0.085**		0.000	**0.068**	0.000	0.022
Bow-24	0.000	0.000	0.000	0.000	0.000	0.000		0.001	**0.351**	0.004
Bow-1	0.014	0.006	**0.104**	**0.090**	0.034	**0.068**	0.001		**0.091**	**0.327**
Bow-2	0.000	0.000	0.000	0.000	0.000	0.000	**0.351**	**0.091**		**0.207**
Bow-26	0.020	0.008	0.032	0.028	0.009	0.022	0.004	**0.327**	**0.207**	

Considered together, it would seem that two distinct provenance sources exist for the same unit and that sample Bow-24, which is the most basal, southernmost Lapur sample may share both sources or be sourced from the same source as the Muruanochok Sandstone, but not that of the Lapur Sandstone.

4.5.3 Lu-Hf isotope geochemistry

The Lu-Hf isotope ratios were used to estimate the initial εHf (t) values of selected zircon grains, in order to predict their tectonic source. This process provides a targeted approach to sedimentary provenance investigation (e.g. Kinny and Maas, 2003). Zircons yielding positive initial εHf(t) values are indicative of sources of juvenile crustal additions/growth or significant input from new melt from the depleted upper mantle with minimal reworking, whereas negative εHf(t) values indicate crustal reworking (Kinny and Maas, 2003; Condie et al*.,* 2005; Morag et al*.,* 2011). In particular, the focus was gaining a better understanding of the source of sediment for the different populations so subsets from each of the major U-Pb grain-age populations, including the Paleogene grains, were selected to help refine the provenance of the Turkana Grits. The selected populations included 57 Muruanachok and 120 Lapur detrital zircons (Fig. 4-10). The 57 zircon grains were selected from all three Muruanachock samples to represent Proterozoic (mostly Pan-African, n = 46) and Archean populations (n = 11), whereas the 120 Lapur detrital zircons include Paleogene (n = 4), Proterozoic (n = 115) and Archean (n = 1) populations from five of the Lapur samples (see Appendix 4S2).

The results show a wide spread of $^{176}Hf/^{177}Hf$ ratios from 0.281453 to 0.282567 and initial εHf (t) values ranging from –26.4 to + 11.2 (Fig. 4-10), which are dominated by positive

values accounting for 87% of analysis. The main populations with their initial εHf (t) values and inferred sources are shown in Table 4-4. The four Paleogene zircons, including three Paleocene grains (~57 Ma) and a single Eocene grain (~45 Ma), have positive initial εHf (t) values, ranging between +3.3 and +7.4, suggestive of juvenile mantle provenance.

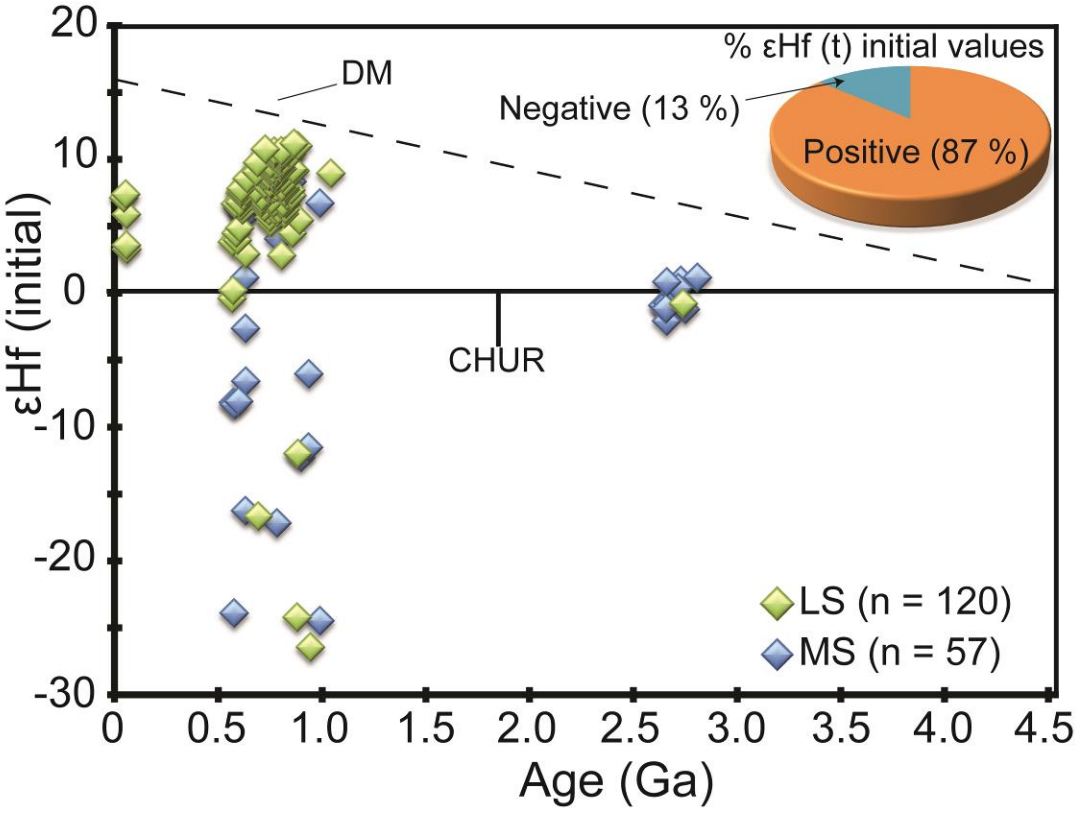

Figure 4-10. Plot of initial εHf(t) vs U-Pb age of Lapur and Muruanachok zircons (n = 177).

This plot shows that most of the zircons in this study were derived from juvenile mantle sources. Note: The depleted mantle (DM) evolution curve is for linear evolution from a Chondritic Uniform Reservoir (CHUR) value at the Earth's formation (i.e., 0 at 4.56 Ga) to εHf (t) = 17 at the present for the DM; Dhuime, Hawkesworth and Cawood, 2011). The mass spectrometer cup configuration for this study is shown in the Appendix 4S2.

The Archean and Proterozoic zircon populations from both sandstones yielded mostly positive initial εHf (t) values ranging from -1.5 to +1.8 and -26.2 to +11.2, respectively (Fig. 4-10). The εHf (t) values from this study indicate mixed provenance with dominant (n = 153) input from the juvenile mantle components and minor contribution (n = 24) from older

reworked crustal sources. The negative initial εHf (t) values are mainly from the more mature Muruanachok and Lapur Bow-24 samples. For example, the εHf (t) values for 590-550 Ma age population (Table 4-4) from the Muruanachok Sandstone are mainly negative, whereas the εHf (t) values for the same age population in the Lapur samples are dominantly positive, indicating different tectonic sources for zircons with similar ages in the two sandstones. Additionally, the two different Archean grain populations at ~2700 Ma and ~2650 Ma from the Muruanachok show distinct positive and negative values respectively, again suggesting different sources for the two Archean grain populations (Table 4-4).

4.5.4 Zircon trace elements results

Summarized detrital zircon trace element analyses are shown in Figure 4-11 and Table 4-5, and complete results are listed in Appendix 4S3. The trace element composition analyses were performed on a subset of 31 grains from the Lapur and 41 grains from the Muruanachok sandstones, representing Paleogene, Proterozoic and Archean zircon populations in a further attempt to better define discrete provenance sources (Taylor and McLennan, 1985; Hoskin, 2005). For example, a single grain-age population may be further queried to look for different populations that may have been formed synchronously, but in different areas that had very different patterns of crustal evolution (e.g. 590-550 Ma population from the two sandstones; see Table 4-4). If this happened, then trace element ratios could potentially shed light on provenance (Taylor and McLennan, 1985); however similarity of REE patterns from different rock types certainly has the potential to make trace element as a provenance indicator problematic (Hoskin and Ireland, 2000).

Magmatic zircons are characterized by heavy rare earth element (HREE) contents, high Th/U ratios and distinct enrichment of HREE (high La_N/Yb_N), positive Ce anomaly and negative Eu anomaly (Hoskin and Ireland, 2000). The trace element composition of

metamorphic zircons in contrast is characterized by the concurrent growth of other minerals, which can be relevant for the identification of metamorphic conditions (Schaltegger et al., 1999; Rubatto, 2002). For instance, garnet incorporates HREE, and its crystallization in a metamorphic environment causes a depletion of HREE in metamorphic zircon (Rubatto, 2002). Plagioclase also acts as a sink for Eu, and zircons without a negative Eu anomaly are usually interpreted as having formed in a plagioclase deficient environments such as kimberlite and syenite (Belousova et al., 2002) and eclogite (Rubatto, 2002).

The Th/U ratios for both sets of samples range from 0.01-1.50 and 0.14-1.55 for Lapur and Muruanachok sandstones, respectively. The strong Ce and Eu anomalies (Fig. 4-11a and Table 4-5) for the different populations from both sets of samples are consistent with the magmatic source (Fig. 4-11b) characterization of Hoskin (2005) as presented in Ce/Ce* vs Sm_N/La_N diagrams. This diagram is also supportive of the Th/U ratios (Fig. 4-6). Plots of Th/Nb – Hf/Th (Fig. 4-11 c-d) for these grains also indicate a dominantly Arc-related orogenic source (Hawkesworth and Kemp, 2006; Yang et al., 2012), for the 'Turkana Grits' zircons.

Felsic igneous rocks are characterised by high LREE/HREE ratios with a negative Eu anomaly (Eu/Eu* < 1), whereas mafic igneous rocks are characterized by low LREE/HREE ratios with little or no negative Eu anomaly (Cullers et al., 1997). Overall, the zircons from the Lapur and Muruanachok sandstones (Turkana Grits) have depleted Gd_N/Yb_N between 0.04 and 0.09, with strong negative Eu (Eu/Eu^* = 0.23–1.0) and positive Ce anomalies (Ce/Ce^* = 25–237), which are all consistent with felsic magmatic sources. This is consistent with presence of felsic dykes and magmatic rocks in the Mozambique Belt within the vicinity of the study area (Key et al., 1989).

Table 4-4. Summarized Lu-Hf isotope analysis for Lapur and Muruanachok

Sandstone	Zircon population	Initial εHf (t) values	Model Age DM	Source
Lapur	60-40 Ma (n = **4**/6)	(+3.3 to +7.4)	588-416.7 Ma	Juvenile mantle
	590-550 Ma (n = **5**/6)	(-0.4 to +6.7)	1171.9-894 Ma	Juvenile mantle
	640-600 Ma (n = **12**/12)	(+2.9 to +8.6)	1078.9-872.2 Ma	Juvenile mantle
	740-680 Ma (n = **12**/13)	(-16.6 to +10.8)	1910.4-858.8 Ma	Juvenile mantle
	800-740 Ma (n = **44**/44)	(+5.3 to +10.6)	1094.9-903.1 Ma	Juvenile mantle
	830-800 Ma (n = **26**/26)	(+2.8 to +10.6)	1242.8-931.8 Ma	Juvenile mantle
	890-840 Ma (n = **10**/12)	(-24.2 to +11.2)	2339.4-963.9 Ma	Juvenile mantle
	2700-2600 Ma	-	-	-
	2800-2700 Ma (n = **1**/1)	(-0.8)	3056.3 Ma	Reworked Crust
Muruanachok	60-40 Ma	-	-	-
	590-550 Ma (n = **4**/5)	(-23.7 to +7.1)	2077-1444.9 Ma	Reworked Crust
	640-600 Ma (n = **8**/11)	(-15.9 to +7.7)	1807.7-886.8 Ma	Juvenile mantle
	740-680 Ma (n = **14**/15)	(-16.9 to +10.5)	1977.2-877.6 Ma	Juvenile mantle
	800-740 Ma	-	-	-
	830-800 Ma (n = **8**/8)	(+5.7 to +10.9)	1138.6-922.8 Ma	Juvenile mantle
	890-840 Ma	-	-	-
	2700-2600 Ma (n = **5**/6)	(-1.5 to -0.1)	3003.4-2893.4 Ma	Reworked Crust
	2800-2700 Ma (n = **4**/5)	(-0.6 to +1.8)	3050.6-2946.8 Ma	Juvenile mantle

Note: This table shows the different detrital zircon populations in the studied zircons from the two sandstones indicating the dominant contributing source of sediment in each population. All populations from the two sandstones except three are dominantly from juvenile mantle sources. The number of analysis for each population is shown as n = a/b; where a, is the dominant number of zircons with either positive or negative initial εHf (t) values. 'b' is the total number of analysis for a particular population. The population is described as sourced from a juvenile mantle or reworked crustal source provenance when 'a' represents positive or negative values respectively.

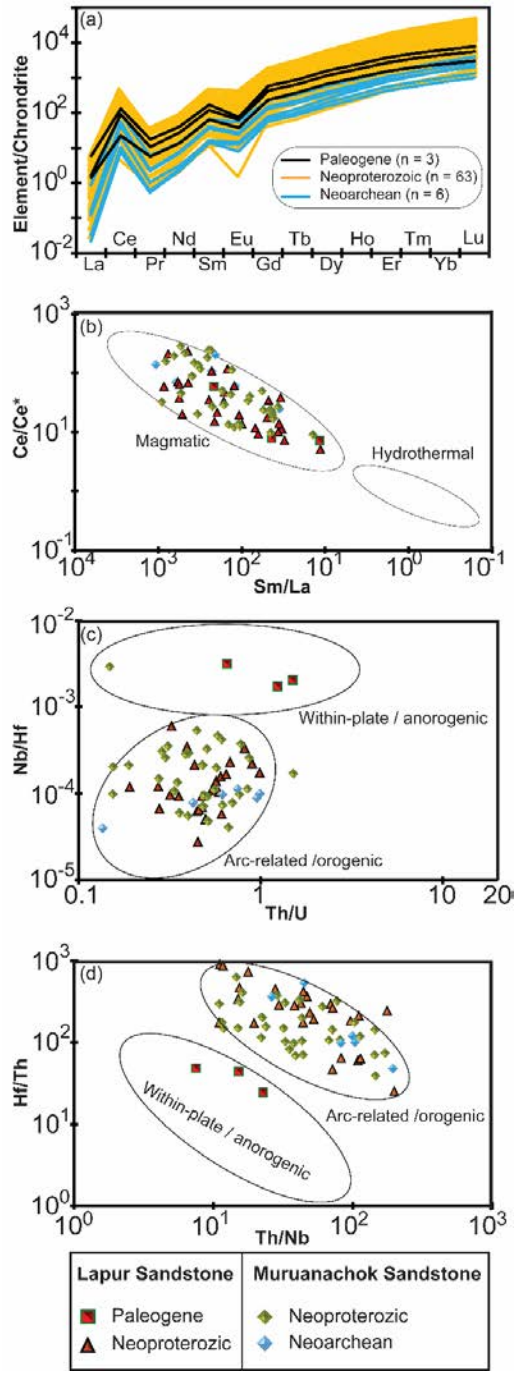

Figure 4-11. (a) Chondrite-normalized rare earth element patterns for the Lapur and Muruanachok (Turkana Grits).

Discrimination plots for (b) magmatic and hydrothermal zircons. Zircons from both sandstone plots within the magmatic domain. The plots (Fig. 4-11 c-d) show a closely clustered zircons in the magmatic domains. (c and d) Plots of trace element ratios showing a dominant Arc-related / orogenic tectonic sources for zircons from the two sandstones except the Paleogene age grains from the Lapur Sandstone, which show trace element patterns suggestive of a within-plate magmatic setting. Chondrite nationalization values from Taylor and McLennan (1985).

Table 4-5. Ratios of chondrite-normalized zircon REE patterns.

Ratio /Population	60-40 Ma	590-550 Ma	640-600 Ma	740-680 Ma	800-740 Ma	830-800 Ma	890-840 Ma	923 Ma	2700-2600 Ma	2800-2700 Ma
(Sm/La)N	**91**	**445**/169	**84**/151	**500**/191	**312**/406	**113**/241	**48**/215	209	359	423
(Lu/Gd)N	**14**	**17**/28	**23**/22	**26**/36	**27**/33	**32**/34	**22**/16	18	21	45
Eu/Eu*	**0.23**	**1**/0.5	**0.72**/0.60	**0.52**/0.43	**0.41**/0.45	**0.50**/0.60	**0.44**/0.41	0.20	0.40	0.38
Ce/Ce*	**25**	**237**/127	**33**/75	**84**/89	**41**/91	**40**/64	**35**/54	38	107	89
(Gd/Yb)N	**0.09**	**0.08**/0.06	**0.08**/0.09	**0.06**/0.04	**0.06**/0.05	**0.05**/0.05	**0.06**/0.09	0.07	0.08	0.04
N	**3**/0	**1**/4	**4**/10	**3**/3	**12**/8	**7**/4	**1**/3	**0**/3	**0**/4	**0**/2

Note: Chondrite normalizing values are from Taylor and McLennan (1985). n = the number of analyses contributing to the mean. The first number in the ratio a/b represent the Lapur Sandstone whereas the second number represent the Muruanachok Sandstone. The numbers presented in this table are the averages of the various ratios. Eu and Ce anomalies were calculated as Ce/Ce* = CeN/(sqrt(LaN * PrN)) and Eu/Eu* = EuN/(sqrt(SmN * GdN)), where 'N' is normalized

4.6 Discussion

4.6.1 Age of the Turkana Grits

Detrital zircon analysis from this study provides new maximum depositional age constraints for the upper Lapur Sandstone, however no new information on the age of the Muruanachok Sandstone was revealed. A population of six Paleogene zircons from middle to upper portions of the Lapur Sandstone (Fig. 4-3) provides confirmation that at least the upper portion of the unit extends into the Paleogene as suggested by some workers (e.g. Thuo, 2009). Of the six Paleogene grains, five were tightly clustered and overlapped at 2-sigma, and was used to calculate a robust Paleocene maximum depositional age with a Weighted Mean $^{206}Pb/^{238}U$ Age of 57.12 ± 0.64 Ma (MSDW = 0.89, probability 0.47; Fig. 4-12). The single ~45 Ma younger grain may indicate that the Lapur Sandstone is even younger than Paleocene. It is worth noting that volcanism of similar age (46 Ma and younger) reported from southern Ethiopia (Bosworth et al., 2015; Bosworth and Stockli 2016), may be coeval to the unknown event in the Turkana region that produced the single 45 Ma grain. However at present, the single grain age lacks reproducibility and must be considered anomalous,

possibly a result of Pb-loss, and should not be considered in maximum depositional age interpretations (see Dickinson and Gerhels, 2009 for further discussion)

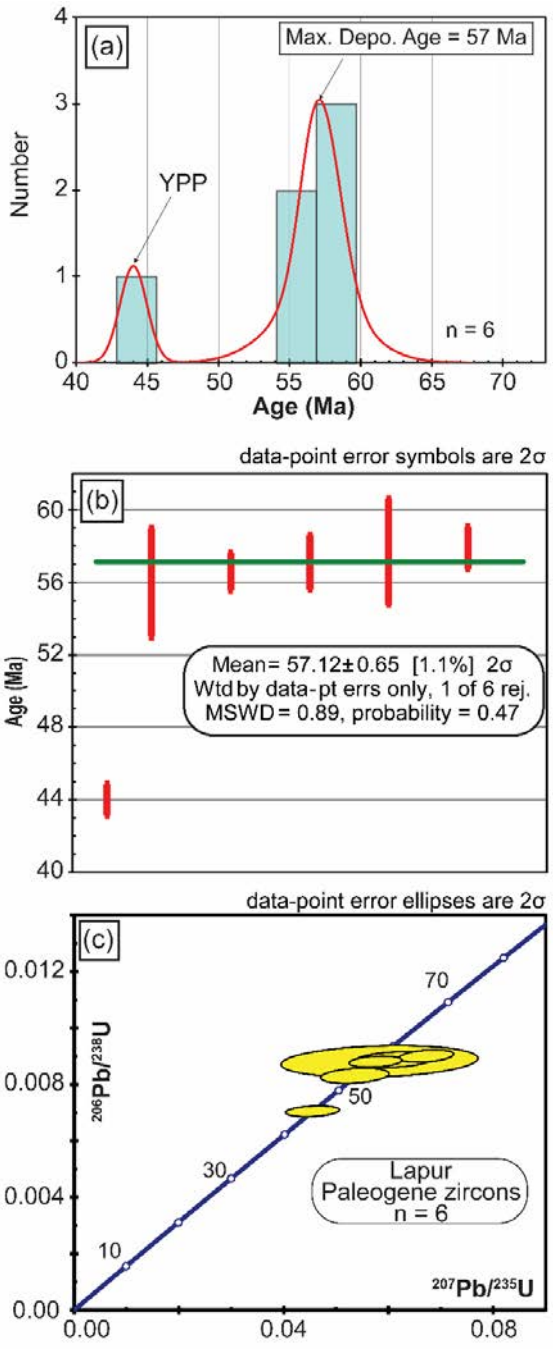

Figure 4-12. Paleogene age zircons recovered from the Lapur Sandstone.

(a) Probability density plot of the Paleogene zircons (n = 6) showing the maximum depositional age. (b) Weighted mean age of the five of the six zircons from Bow-20A and Bow-22, estimated as the Maximum depositional age of the Lapur Sandstone. (c) U-Pb Concordia plot of the six Paleogene zircon grains recovered from the Lapur Sandstone. Seven techniques reported by Dickinson and Gehrels (2009) and Tucker et al. (2013) were used to estimate the

maximum depositional age and they are listed here for comparison. The techniques and their corresponding age estimate are; 1) youngest single grain age (YSG = 44 ± 0.95 Ma); 2) youngest graphical detrital zircon age (YPP = 44 Ma); 3) youngest detrital zircon age (YDZ = 43.92 ± [1.1/0.99] Ma); 4) the weighted mean average age (YC1σ = 57.1 ± 1.2 Ma); 5) Weighted Average (WA = 57.12 ± 0.65 Ma); 6) weighted mean average age (YC2σ = (57.11 ± 0.62 Ma); and 7) TuffZirc (Zircon Age Extractor = 57.1 ± [0.8/1.1] Ma). The different techniques can be accessed via most versions Microsoft Excel with attached Isoplot macro (Ludwig, 2012).

The presence of vertebrate fossils has typically been used as evidence that all of the Lapur Sandstone is of the same Late Cretaceous age (O'Connor et al., 2011). The Paleogene zircons (n = 6) were recovered from the upper Lapur Sandstone (Bow-20A and Bow-22: see Figs 4-2b and 4-3a), well above the vertebrate fossil bearing localities restricted to the lower third of the unit (e.g. Weishampel et al., 2004; O'Connor et al., 2011). Additionally, the ~57 Ma zircon population (n = 5) is consistent with evidence for younger Paleogeone (~37-27 Ma) rhyolitic and basaltic volcanism in the Turkana Rift, including volcanic units capping and possibly interfingering with the upper tens of meters of the Lapur Sandstone (Cahen et al., 1984; Thuo, 2009; Tiercelin et al*.,* 2012a, b). Rather than considering the entirety of the Lapur Sandstone as Paleogene, a significant discontinuity in the middle to upper portions of the stratigraphy that differentiates the underlying Cretaceous depositional succession from the overlying Paleogene depositional succession is suggested. The discontinuity is shown by a prominent intra-Lapur unconformity reported near Lapur samples Bow-20 and Bow-20A and supported by satellite image interpretation of the field area (Approx. 4°23'26.61"N 35°48'42.45"E: see Table 4-1) from Google Earth images (2017). This interpretation is consistent with recent biostratigraphic and sedimentologic data by Thuo (2009), who found evidence that fluvial systems of the Lapur Sandstone may have existed from middle Cretaceous to early Oligocene.

Perhaps what is most interesting about the Paleocene detrital zircon population is that these grains imply that late Paleocene–early Eocene magmatism was underway in or near the

Turkana Basin by 57 Ma. The six Paleogene zircons recovered from the Lapur Sandstone may be associated with a local source or an unknown volcanic source from outside of the Turkana Basin. This unknown volcanic source may be located in the Tibesti Region of Chad (Francis et al., 1973; Permenter and Oppenheimer, 2007), or from the nearby portion the Central African Rift System in the Cameroon Volcanic Line to the southeast of the Benue Trough (Benkhelil, 1989; Wilson and Guiraud, 1998). The southern part of the Benue Trough is known to host Late Maastrichtian to Eocene magmatic rocks (68-49 Ma), which changes from alkaline to tholeiitic with decreasing age (Maluski et al., 1995; Wilson & Guiraud, 1998), and could have sourced the Paleogene zircons in the Lapur Sandstone. Basaltic dykes of K-Ar ages (87-43 Ma) dated from northern Cameroon and southern Chad (Wilson and Guiraud, 1998) is also a potential source for the Paleogene age zircons. The Maastrichtian to Paleocene age basaltic rocks identified in wells drilled in the Mudugh Basin in Central Somalia (e.g. Coffin and Rabinowitz, 1988; Wilson and Guiraud, 1998) is a possible source for the Paleocene Lapur zircons. Sourcing the Paleogene age zircons from the Cameroon Volcanic Line (Benue Trough) or the basin in Central Somalia is inconsistent with the dominantly N-NW paleocurrent data for the Lapur, unless they were transported by paleo-winds as air-fall ash deposits, as may have been the case where zircons were transported from the Parana Basin in South America into the Congo Basin in central Africa by air-fall tuffs (Linol et al., 2016). Alternatively, they could have been brought in by the proposed marine incursions in the Anza Rift Basin (Bosworth and Morley, 1994; Fig. 4-13). This interpretation could also explain the presence of estuarine/marine vertebrate taxa within the fluvial Lapur Sandstone. Other volcanic centres in the region such as from the southwest Egypt (59-46 Ma: Franz et al., 1987), the igneous province from Delgo area in northern Sudan (87-47 Ma: Franz et al., 1993), the Bayuda Desert ring complexes, NE Sudan (74-62 Ma: Barth &

Meinold 1979; Cahen et al., 1984) and Paleocene alkaline volcanic rocks from offshore Guinea plateau, West Africa (59 Ma: Bertrand et al., 1993), are all possible but unlikely sources.

The known volcanic centres/rocks in the vicinity of the study area, for example, the Main Ethiopian Rift (46-34 Ma), the Red Sea Rift (~30 Ma), Dafur (< 23 Ma) and others are significantly younger than the Paleocene zircons recovered from the Lapur Sandstone (e.g. Emerick and Duncan, 1982; Coffin and Rabinowitz, 1988; Bosworth, 1992; Sleep, 1996; Menzies et al., 1997; Ebinger and Sleep, 1998; George, Rogers & Kelley, 1998; Bosworth, 2015; Bosworth et al., 2015; Bosworth and Stockli 2016). Moreover, Paleogene age volcanic rocks have not been dated from the Turkana region and all previous references within Kenya and the East African Rift System have been inferred from subsurface investigations (e.g. seismic), thus, it is difficult to pin-point the exact source of these young zircon grains (Cahen et al., 1984; Boschetto et al., 1992; Morley et al., 1992, 1999; McDougall and Brown, 2009; Feibel, 2011). Paleogene age rocks inferred from various subsurface investigations in the vicinity of the study area includes the Lokone and Auwerwer sandstones in the Lokichar Basin (Paleogene-early Miocene; Vincens et al., 2006), the Kimwarer and Kamego formations from the Elgeyo Escarpment (Paleogene), all to the south of the study area (e.g. Morley et al., 1999; Tiercelin et al., 2004; 2012a), could have sourced the Paleogene age zircons in the Lapur Sandstone. The Lariu Range (Paleogene-Miocene) and the Sera Iltomia Formation (part of the Mount Porr Sandstone) east of the Lake Turkana, considered Mesozoic-Paleocene age (Tiercelin et al., 2004), are all likely sources for the Paleogene zircons in this study. This explanation is supported by Tiercelin et al. (2004) interpretation that the sediments of the Sera Iltomia Formation represents the likely early rifting from either the East African Rift System in northern Kenya (study area) or the Mesozoic-Cenozoic Anza

Rift. This Anza Rift is known to host Cretaceous to Paleogene volcanic rocks and could have sourced the Paleogene zircons (e.g. Reeves et al., 1987; Bosworth, 1992; Mosley, 1993; Ebinger and Sleep, 1998). These southerly sources are all supported by paleocurrent directions from both the Muruanachok and Lapur sandstones.

4.6.2 Sediment provenance of detrital zircons in the Turkana Basin

The results of this sedimentary provenance investigation demonstrates distinct differences in the petrographic and detrital zircon composition of the Lapur and Muruanachok sandstones (Figs 4-5, 4-7 and 4-8). The Muruanachok represents slightly mature sandstone compositions, with discrete Archean provenance source not observed in the Lapur Sandstone (except Bow-24). In addition to this, the young Paleogene zircon population recovered from the upper Lapur Sandstone was not encountered in any of the three Muruanachok samples. Spatially, the Muruanachok Sandstone is located ~140 km to the south/southwest of the southernmost exposures of the Lapur Sandstone (Fig. 4-2b), and hence it is possible that it simply represents a lateral equivalent of the Lapur Sandstone, with point sources to the south of the outcrop area. The southernmost Lapur sample (Bow-24) has a provenance signature identical to that of the Muruanachok Sandstone (see Fig. 4-9b, d), which tends to support this assertion. However, it is also possible that the Muruanachok Sandstone is older and the basal Lapur sample (Bow-24) simply represents the top of the Muruanachok as shown by the significant elevation difference between the Lapur and Muruanachok samples (see Table 4-2) and the maturity of the Muruanachok and Bow-24 samples (Fig. 4-4). Each of the Lapur sandstone except Bow-24 come from higher elevation than any of the Muruanachok samples, which suggests that the Lapur and Muruanachok sandstones may actually just represent distinct stratigraphic units, rather than laterally correlative units.

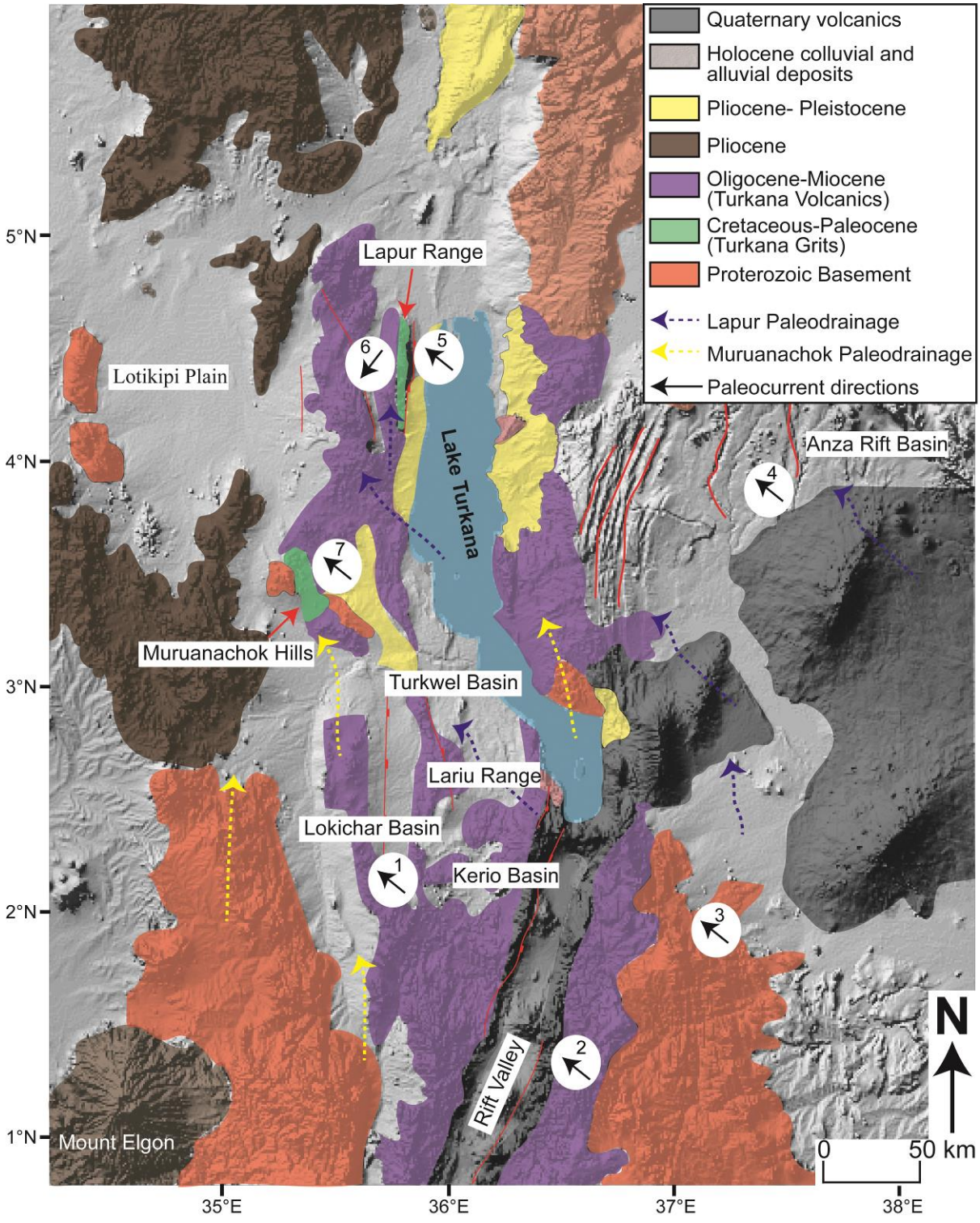

Figure 4-13. Surface geology of the Turkana Basin showing probable source areas for the sediment in the basin.

Paleocurrent directions 1-7 are after McGuire et al. (1985); Williamson and Savage (1986); Wescott et al. (1993); Morley et al. (1999) and Tiercelin et al. (2004). Landsat image taken from the NASA Shuttle Radar Topography Mission collection and modified after Geological map of Kenya interpretations by the Ministry of Energy and Regional Development of Kenya, Geological map, 1987).

Indeed, this hypothesis is supported by the fact that the only Lapur sample with similar provenance to that of a Muruanachok sample is the lowest Lapur sample, Bow-24 (Fig. 4-9b). Hence, this would suggest that the Bow-24 sample is from the top of the Muruanachok Sandstone, rather than the base of the Lapur Sandstone.

4.6.2.1 Archean population

The Archean population from the Muruanachok and the Lapur sample Bow-24 range from 2800-2550 Ma, could have been transported by fluvial systems from the Archean Tanzania Craton (Fig. 4-1) to the west to southwest of the study area as they host grains of similar ages (e.g. Kabete et al., 2012; de Wit and Linol, 2015). This interpretation is consistent with the conclusions of Hepworth and Kennerly (1969) and Hepworth (1972), who found that the western part of the Mozambique Belt in Kenya was underlain by the Archean Tanzania Craton (also see Grantham et al., 2003). In addition, the Archean zircons from this study have similar model ages (Table 4-4) to the Nd model ages of 3100-2700 Ma estimated from the granitoids of the Tanzanian Craton (Maboko, 1995; Maboko and Nakamura, 1996; Möller et al., 1998; Cutten et al., 2006), and could have sourced the Archean detrital zircons in the Turkana Basin.

Alternatively, the Archean detrital zircons could have been sourced from the Archean Congo-Kasai Craton to the extreme southwest of the study area (e.g., Batumike et al., 2009; Kadima et al*.,* 2011). However, the Tanzania Craton is considered a more likely source due to its nearness and a lack of ~1300-1600 Ma grains (Figs 4-9b and 4-13), that would be expected if there was sediment transport from the Congo-Kasai Craton across the Kibaran Belt (Fig. 4-1). Furthermore, the euhedral-subhedral morphology of Archean zircons (Fig. 4-

5) suggests minimal transport or limited recycling of sediment. This interpretation is supported by the dominantly positive initial εHf (t) values of these grains (Fig. 4-10), which suggests that these zircons grains were mainly sourced from juvenile crustal materials. The Archean – Paleoproterozoic granite-greenstones to the southwest of Kenya (Fig. 4-1c) close to the Ugandan border, which is also part of the Tanzania Craton (Cahen et al., 1984) have similar geochemical signatures to the Archean zircons from this study. Moreover, paleocurrent measurements reported for the Muruanachok and Lapur sandstones indicate a dominant northerly paleoflow (Fig. 4-13: Cahen et al 1984; McGuire et al., 1985; Wescott et al., 1993; Fiebel, 2011). Considered together, the Archean basement rocks to the west and south of the Turkana Basin is the most likely provenance source for Archean zircons in both sandstones (Fig. 4-13).

4.6.2.2 Neoproterozoic population

The Neoproterozoic age zircons from both the Lapur and Muruanachok sandstones are consistent with the range of ages assigned to the Neoproterozoic (Pan-African) age basement rocks beneath and forming the rift shoulders of the Turkana Basin (Cahen et al., 1984; Boschetto et al., 1992; Mosley, 1993; Rino et al., 2008; McDougall and Brown, 2009). These basement rocks are part of the Mozambique Belt, which extends across much of eastern Africa (Fig. 4-1; e.g. Grantham et al., 2003; Kroner and Stern, 2004). The basement rocks are extensively exposed in outcrop and under recent volcanic and sedimentary cover throughout the field area, but particularly to the immediate south of Lake Turkana (Fig. 4-13). The Mozambique Belt rocks underlying the Turkana Basin (McDougall and Brown, 2009), and in adjacent areas have magmatic emplacement ages in the range of 980-850 Ma before a later metamorphic overprint around 645-630 Ma (Fig. 4-9d), characterizing the peak of high grade

metamorphism (Mosley, 1993; Hauzenberger et al., 2007). Key et al. (1989) recorded two magmatic emplacement ages of 1200 Ma and 850-800 Ma within the basement rocks of the Mozambique Belt. These authors found evidence of a high proportion of juvenile mantle component within the Mozambique Belt, which is consistent with the findings of dominant contributions from juvenile sources (Fig. 4-10). Harris, Hawkesworth and Ries (1984) also reported juvenile Neoproterozoic protolith rocks age ~860 Ma (Grantham et al., 2003) from within the Mozambique Belt in northwestern Kenya, an interpretation, which collaborates that of Kroner and Stern (2004), who reported similar ages from this belt. This is in agreement with the dominantly (87% of analysis) juvenile mantle signatures for zircons of this age from both the Lapur and Muruanachok sandstones. The magmatic emplacement ages in the Mozambique Belt are also in agreement with the Neoproterozoic ages from both Lapur and Muruanachok sandstones, which ranges from 998 Ma to 558 Ma and 985 Ma to 562 Ma respectively. The high grade metamorphic events recorded in the Mozambique Belt in Kenya (Hauzenberger et al., 2007), appears to have had limited effect on the supposed Cretaceous Turkana Grits in the basin as shown by the few zircons with very low Th/U ratios (Fig. 4-6), indicative of metamorphic provenance.

The findings of this study suggests that the basement rocks of the Mozambique Belt underlying and on the flanks of the Turkana Basin is the primary provenance source for the zircons of both sandstones. Furthermore, the zircons of Pan-African (Neoproterozoic) age yielded initial εHf (t) values between – 25.61 and + 11.2 (Fig. 4-10), suggestive of derivation from a mixture of reworked Pan African crust and juvenile crustal materials, consistent with Mozambique Belt lithologies (Cahen et al., 1984; Harris, Hawkesworth and Ries, 1984; Key et al., 1989; Grantham et al., 2003). Finally, the morphology of Neoproterozoic zircons from both the Muruanachok and Lapur sandstones is typified by subhedral-euhedral grains (Fig. 4-

5), is suggestive of proximal transport from local sources or minimal sediment recycling. Considered together, the provenance of the Lapur and Muruanachok sandstones is interpreted to be localized from the Mozambique Belt.

4.6.3 Tectonics implications

The East African Rift system is believed to have initiated by about 45-35 Ma, based in part on the isotopic dating of oldest volcanic rocks in the rift, which are thought to have formed as a result of the development of the African Superplume beneath eastern Africa (e.g. Ebinger 1989; Ebinger and Ibrahim, 1994; Chorowicz, 2005). The Lapur Sandstone is typically thought to be Cretaceous and hence, its depositional history is usually not tied to the East African Rift System, although some workers have suggested the presence of pre-Cenozoic rifts underneath it (Bosworth, 1992; Morley et al., 1992; Cahen et al., 1984; Boschettoet al., 1992; McDougall and Brown, 2009; Feibel, 2011; Tiercelin et al., 2012a). The recovery of six Paleocene detrital zircon grains from the Lapur Sandstone provides strong evidence for a major disconformity within the Lapur, separating Cretaceous from Paleogene depositional units, which also corroborates the presence of pre-Eocene strata underneath the East African Rift system. This work demonstrates that depositional history of the Lapur Sandstone is more complex than previously thought. The deposition of the upper parts of the Lapur Sandstone may reflect the earliest stages of rift reactivation associated with the development of the East African Rift System in the Paleogene (Thuo, 2009) or the Central African Rift System as suggested by others (e.g. Reeves et al., 1987). Although more work is necessary to confirm this, the presence of a discrete Paleocene population (n = 5) of detrital zircons at ~57 Ma may indicate that initial volcanism associated with the development of the African Superplume beneath eastern African may have started prior to 45 Ma, possibly by as much as 12 Ma

earlier than most accounts. Alternatively, these grains may derive from an unknown volcanic source in central Africa. These young magmatic zircons in the top of the Lapur Sandstone demonstrate the complexities between the two rift systems in the Turkana region, providing support for the presence of pre-Eocene strata beneath the East African Rift System, and in particular, highlighting the need for further geochronological work.

4.7 Conclusions

Based on the integrated approach incorporating framework petrography, U-Pb geochronology, Lu-Hf isotope ratios and zircon trace element geochemistry on outcrop samples from the Lapur and the Muruanachok sandstones in the Turkana Basin, the following conclusions are drawn:

- The Lapur and Muruanachok sandstones are predominantly sourced from felsic igneous rocks as indicated by the chondrite normalized REE patterns, Lu-Hf analysis and U-Pb age data.

- The dominant provenance is attributed to the Neoproterozoic Mozambique Belt, which formed during the Pan African Orogeny. Comparable initial εHf (t) values, an ubiquity of fresh, euhedral zircon grains and paleocurrent orientations in the studied sandstone units point to proximal transport from local sources within the Mozambique Belt of Kenya.

- Sample Bow-24 suggests that parts of Lapur strata may be interfingering the Muruanachok Sandstone or more likely, that the Lapur and Muruanochok sandstones are stratigraphically separated, rather than laterally correlative units. All Lapur

samples show similar provenance to one another except the basal Lapur sample Bow-24, which is indistinguishable from Muruanachok samples, suggesting that the Lapur Sandstone mapped at the Bow-24 location may actually be the upper part of the Muruanachok Sandstone.

- A robust population of late Paleocene zircons from the upper part of the Lapur Sandstone suggest that a major discontinuity, which has been observed in the sandstone by previous workers near the top of the unit, most likely serves as the boundary between two discrete depositional units. Based on this, an informal subdivision of the Lapur Sandstone into lower and upper members of Cretaceous and Paleogene ages, respectively is proposed.

- Paleocene zircons from the Lapur sandstone (~57 Ma) predate the oldest known volcanic rocks in the Turkana Rift (~45 Ma). The presence of these zircons suggest that an older pre-Eocene volcanic source beneath the East African Rift System, which probably is coeval with older volcanism from southern Ethiopia. Alternatively, these grains may have been derived from outside the basin, possibly derived from air-fall ash deposits associated with isolated volcanic centres' somewhere in northern or central Africa. However, the evidence provided in this study points to a south-southeast volcanic source from within the Anza Rift Basin.

5. CHAPTER FIVE

U-Pb detrital zircon constraints on the depositional age and provenance of the dinosaur-bearing Upper Cretaceous Wadi Milk Formation of Sudan

Abstract

Cretaceous continental deposits in Sudan have long been recognized as important archives of continental vertebrate fossils in central Africa. A number of different sedimentary units including the Wadi Milk, Shendi and Kababish formations from northern and central Sudan are known to yield dinosaur and other vertebrate fossils. The ages of these deposits are poorly constrained, and traditionally assumed to be of Albian to Santonian age based on biostratigraphic evidence. However, recent palynological analyses suggest a Campanian–Maastrichtian age for the Shendi Formation. Not only are the ages of these units poorly resolved; but stratigraphic correlations within and between them and similar aged units in central Africa, remains tenuous. To address these issues a detailed sedimentary fingerprinting and provenance analysis was conducted on the putatively correlative Shendi and Wadi Milk formations using sandstone petrography and a multifaceted detrital zircon investigation combining U-Pb geochronology, Lu-Hf isotope analysis and trace element geochemistry. The objective was to provide constraints on the age of deposition, sediment sources and paleofluvial drainage patterns. Based on laser ablation ICP-MS U-Pb detrital zircon geochronology of 18 sandstone samples (~1500 detrital zircons), a population of six Late Cretaceous zircons from the Wadi Milk Formation was identified yielding a maximum depositional age of 79.2 ± 2.4 Ma (MSWD = 0.65, probability 0.62). Specifically, these data constrain the depositional age to Campanian or younger for the Wadi Milk Formation, which significantly improves our understanding of the age of this unit and its fauna. The Lu-Hf-isotope and trace element analyses of the remainder of the dated zircons show a provenance dominated by Neoproterozoic crustal sources and minor Paleoproterozoic and Archean sources for both units, which is interpreted as being sourced from the Arabian-Nubian Shield to the south and southeast of the study area. These findings, coupled with the recently

updated biostratigraphic age for the Shendi Formation, confirm that there is a correlation between them and were probably deposited synchronously by north-north westerly flowing fluvial system draining into the Tethys Sea during the Late Cretaceous.

Keywords: *Wadi Milk, Shendi-Atbara, Detrital zircon geochronology, U-Pb-Lu-Hf, Provenance, Cretaceous volcanism*

5.1 Introduction

Late Mesozoic continental sedimentary deposits are widespread and well exposed in north eastern Africa, particularly Sudan and Somalia, but remain relatively poorly studied (e.g. Mateer et al., 1992). The exploration of these deposits over the last century, including several intensive collecting efforts in the last few decades, have yielded important vertebrate fossil assemblages (Mateer et al., 1992). These fossil finds have significantly increased the understanding of the evolution and paleoecology of the African continent, and provide important insights into the patterns and drivers that set the stage for the development of modern floras and faunas (e.g. Cracraft, 1974). Key localities for which significant late Mesozoic vertebrate fossil collections presently exist from Africa include Tendaguru in coastal Tanzania, the Rukwa Rift Basin in southwestern Tanzania, the Turkana Basin in northwestern Kenya, the Dinosaur Beds of northern Malawi, and the Wadi Milk and Shendi formations of north central Sudan (Klitzsch and Wycisk, 1987; Flynn et al., 1988; Jacobs et al., 1990, 1993; Gomani, 1997, 2005; Heinrich, 1999; O'Connor et al., 2006, 2010; Roberts et al., 2010; Le Loeuff et al., 2012; Gorscak et al., 2014, 2017). These fossil collections from late Mesozoic (Cretaceous) Africa are, however, limited in comparison to other parts of the world, particularly the northern continents; and this limitation has contributed to the poorly known geological, biological and paleontological history of this time period in Africa (Sereno et al., 1994; Widlansky et al., 2018). Moreover, poor age control coupled with the limited abundance, fragmentary nature and isolated occurrences of many Cretaceous continental vertebrates from the central and southern portions of Africa has hampered phylogenetic, taxonomic and paleobiogeographic interpretations for Mesozoic vertebrates from this part of Gondwana (O'Connor et al., 2006; Stevens et al., 2008; Klein et al., 2016).

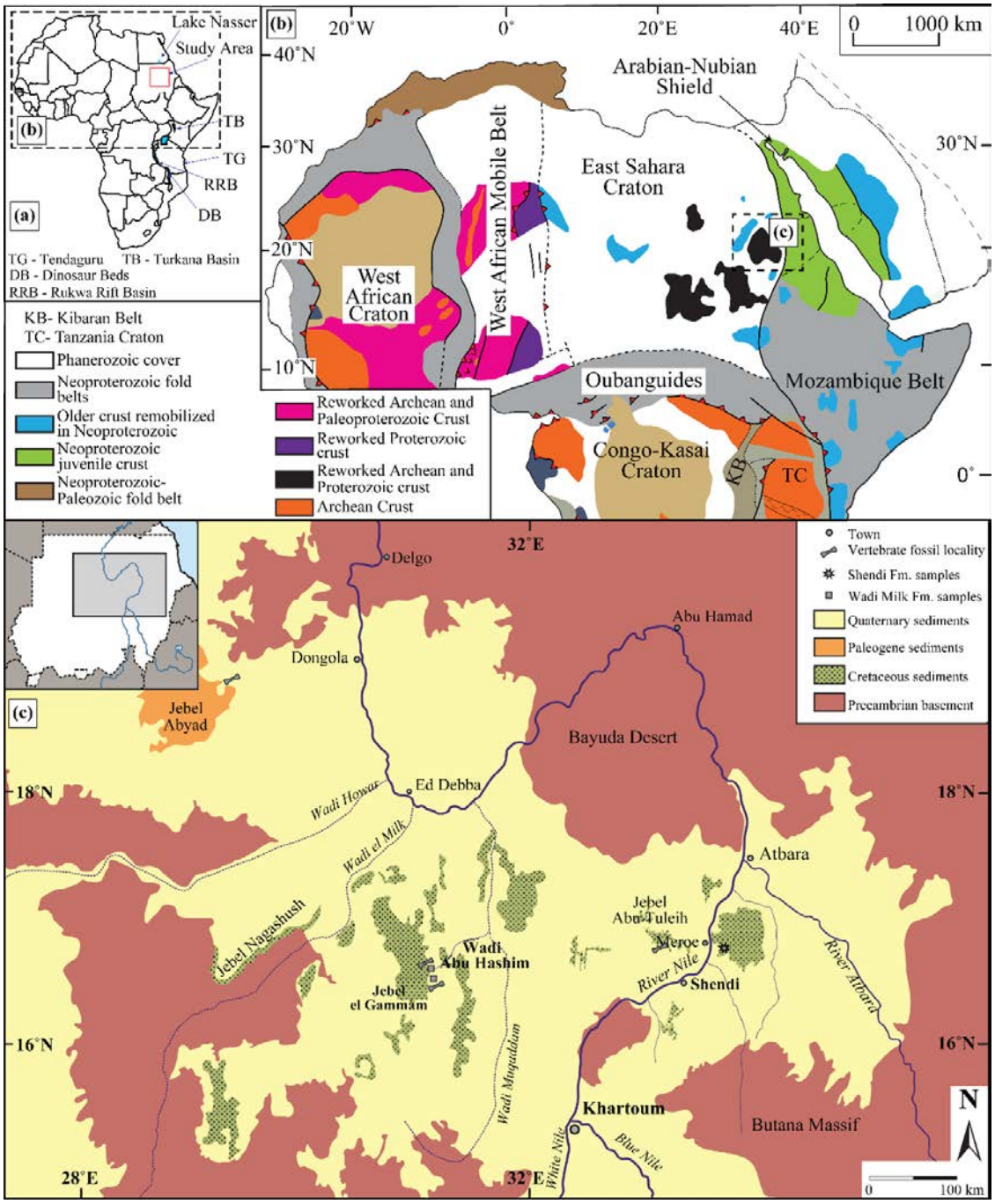

Figure 5-1 Location of study area for Sudan samples.

(a). Map of Africa showing study area. (b). Basement map of northern and central Africa showing the main basement complexes after Begg et al. (2009). (c). Geological map of north and central Sudan showing the sample locations for the Wadi Milk and Shendi formations samples. The map is modified after Klein et al. (2016).

The Wadi Milk and Shendi formations in north central Sudan (Fig. 5-1) are widely exposed in a series of isolated outcrops in the desert region north of Khartoum. These units have yielded some of the richest and most diverse records of Cretaceous continental

vertebrates, including well-preserved remains of lissamphibians, squamates, fishes, turtles, crocodyliforms, sauropod and theropod dinosaurs (Klitzsch and Wycisk, 1987; Buffetaut et al., 1990; Wycisk et al., 1990; Rauhut and Werner 1995; Evans et al. 1996; Rauhut, 1999; Rage and Werner 1999; Klein et al. 2016, Salih et al. 2016). Although fossils have been recovered from the Wadi Milk and Shendi formations, the age of these deposits has remained poorly constrained as middle to Late Cretaceous, based primarily on palynomorphs from nearby water wells and macroflora from outcrops (Schrank 1990, 1992; Werner, 1993, 1994). Both the Wadi Milk and Shendi formations were previously considered as part of the so called Upper Jurassic-Eocene Nubian Sandstone, a lithostratigraphic 'catch-all' describing a variety of quartzose sandstone units covering extensive areas in Chad, Libya, Egypt and Sudan (Pomeyrol, 1968; Schull, 1988; Klitzsch and Squyres 1990; Bussert, 1993; Wycisk, 1991). The Nubian Sandstone has since been subdivided into various regional formations by workers such as Klitzsch (1990) who led this effort. In Egypt and Sudan, Klitzsch (1990) and his team identified over 20 different formations from the so-called Nubian Sandstone ranging in age from Cambrian to Paleocene and comprising many different lithofacies descriptions (Klitzsch and Wycisk, 1987; Klitzsch, 1990; Klitzsch and Squyres, 1990). Stratigraphic correlation between lithologically similar continental units within the former Nubian sandstone, as well as to other continental sedimentary deposits in Sudan and elsewhere in north and central Africa, however, remains tentative in many cases.

Although many of these continental sandstone-dominated successions are lithologically indistinguishable and lack biostratigraphically informative taxa or intercalated volcanics to help constrain their age, advances in sedimentary provenance analysis and dating of detrital mineral grains has provided new possibilities for establishing better age control and refining stratigraphic correlations (e.g. Sickmann et al., 2018). The application of detrital mineral

dating for age control works on the premise that if syn- or nearly syndepositional volcanic, plutonic or metamorphic activity occurred within reasonably close proximity to a basin, there is a chance that erosion and transport of datable minerals, such as zircon, from these sources may have contributed to the sedimentary infill. Magmatic sources associated with volcanic arc systems present the best source of easily eroded, datable detrital minerals; but unfortunately such activity was conspicuously absent during the Mesozoic and Cenozoic across most parts of Africa (e.g. Wilson and Guiraud, 1992). However, recent provenance studies in a variety of sedimentary basins across Africa (e.g. Congo Basin [Roberts et al., 2015; Linol et al., 2016]; Turkana Basin [Owusu Agyemang et al., 2018]) have demonstrated the presence of small populations of syn-depositional, age constraining magmatic zircon populations. These grains have commonly been traced back to a wide range of small, typically alkaline volcanic and plutonic sources spread across Africa. These sources include numerous carbonatites, lamprophyres and kimberlites related to far-field stress reactivation, as well as syenites, phonolites, trachytes and other volcanic rocks related to various forms of intraplate magmatism, including ancient hot-spot tracks (Fairhead, 1988; Jelsma et al., 2009).

The focus of this study was to investigate the potential for applying detrital zircon dating and provenance analysis to the vertebrate fossil-bearing Cretaceous Wadi Milk and Shendi formations in north central Sudan. Sandstone petrography was combined with U-Pb detrital zircon analysis that includes U-Pb geochronology, Lu-Hf isotope analysis and trace element geochemistry on the same grains. The multi-faceted data generated by this study is aimed at refining the age of these units and improving stratigraphic correlations between them, but is also expected to contribute to the on-going discussion on late Mesozoic paleogeography and drainage evolution of central Africa (Stankiewicz and deWit, 2006; Roberts et al., 2012).

5.2 Geological setting and stratigraphy

5.2.1 Geologic setting

The geology of north central Sudan is characterized by Precambrian basement rocks, Paleozoic and Mesozoic anorogenic ring complexes, isolated Upper Cretaceous to Cenozoic volcanics, large Mesozoic to Cenozoic sedimentary basins, and extensive Quaternary cover strata (Whiteman, 1971). The Precambrian basement is mainly comprised of the Neoproterozoic Arabian-Nubian Shield (ANS) to the east of the Nile River and by reworked pre-Neoproterozoic East Saharan Craton (or Sahara Metacraton) rocks west of the Nile River (Fig. 5-1; Schandelmeier et al., 1987, 1994; Stern, 1994). The Arabian-Nubian Shield, which is mainly composed of volcano-sedimentary arc assemblages and ophiolitic sequences, forms the flanks on either side of the Red Sea, extending over 500 km on both sides and stretching from southern Israel to Ethiopia (Stoeser and Camp, 1985; Dixon and Golombek, 1988; Kröner and Stern, 2005). Previous geochemistry and Nd isotopic studies (e.g. Stern, 2002) have helped to characterize the Arabian-Nubian Shield as mainly composed of rocks of juvenile mantle origin, whereas the East Sahara Craton is mostly comprised of older reworked crustal rocks. The East Sahara Craton covers ~5 million km^2 of north central Africa underlying most of Egypt, Sudan, Libya, Chad and Niger; and it is flanked to the west and south by the West African Mobile Belt (Tuareg Shield or Tans-Sahara Orogen) and the Congo Craton, respectively (Fig. 5-1; Abdelsalam et al., 2002; Begg et al., 2009; Iizuka et al., 2013). The exposed parts of the East Sahara Craton are composed of high to medium-grade gneisses and migmatites, granites, schists, quartzites and marbles, with minor intercalations of meta-gabbros and serpentinites (Vail, 1985).

The Precambrian and Paleozoic basement are unconformably overlain by the Upper Jurassic-Eocene fluvial continental deposits collectively referred to as the Nubian Sandstone

(Whiteman, 1971). Deposition of the primarily continental sedimentary rocks is understood to have occurred mainly in intracratonic basins that developed as a result of far-field extensional stresses associated with the break-up of Pangea, the rifting of the Red Sea and the differential opening of the Atlantic Ocean during the Cretaceous (Ward et al., 1979; Schandelmeier et al., 1987; Klitzsch, 1990; Fairhead and Binks 1991). The continental strata north of Khartoum (Fig. 5-1) are divided into different regional formations, including the Wadi Milk, Shendi, Omdurman formations (e.g. Klitzsch, 1990), all of which have been traditionally assumed to be Albian-Santonian in age and are unconformably overlain in places particularly in the Jebel Abyad region of Sudan (Fig. 5-2) by the Turonian-Santonian Wadi Howar Formation (Klitzsch and Wycisk, 1987; Klitzsch and Squyres, 1990; Wycisk et al., 1990; Schrank, and Awad, 1990; Wycisk 1991). The different Cretaceous regional formations in Sudan are lithologically similar and mainly composed of cross-bedded sandstones, minor siltstones and conglomerates, and rare paleosols (Pomeyrol, 1968; Bussert 1993).

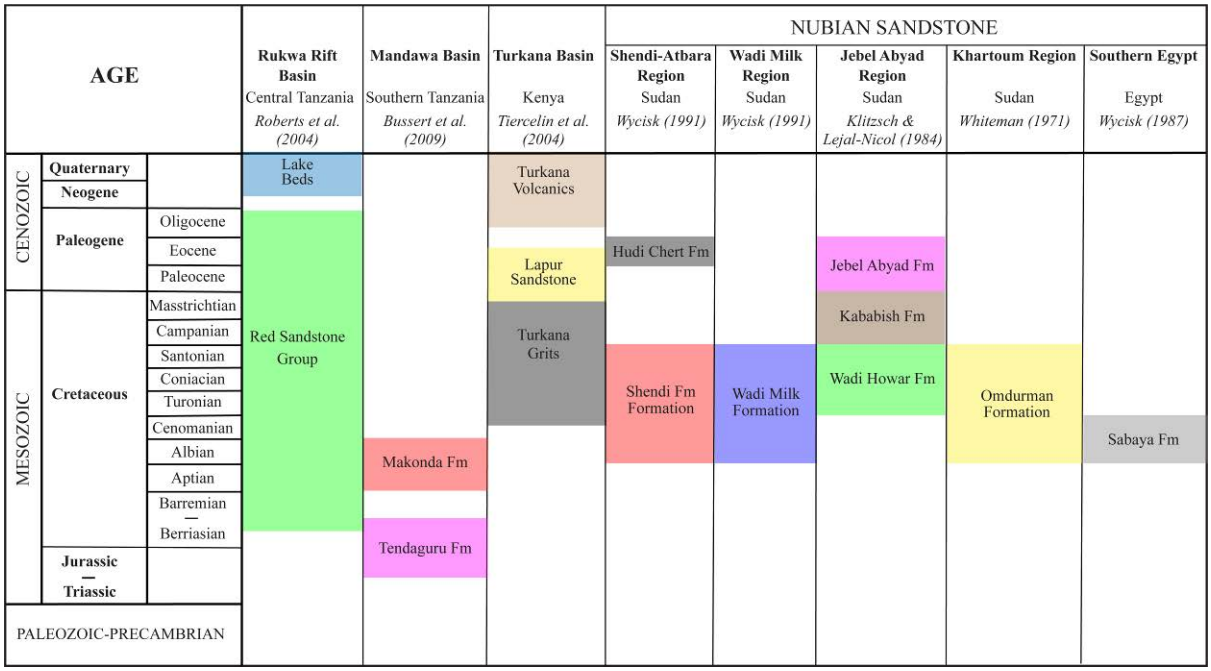

Figure 5-2. Stratigraphic chart of selected late Mesozoic units in central Africa.

The chart shows the correlation of some of the units within the Cretaceous continental strata in Sudan and Egypt (previously "Nubian Sandstone") including the Wadi Milk and Shendi formations. Note: Tendaguru Formation is

mostly Late Jurassic with only the upper portion *Rutitrigonia bornhardti-schwarzi* Member being Early Cretaceous (Valanginian-Hauterivian: Bussert et al., 2009)

5.2.2 Sedimentology and stratigraphy of the Wadi Milk and Shendi

Whiteman (1970) defined the Nubian Sandstone in Sudan as those units sandwiched unconformably between the Precambrian basement rocks or Paleozoic strata and the early Cenozoic Hudi Chert Formation (Fig. 5-2). He assigned to the deposits a wide range of ages from Barremian to Maastrichtian. The two prominent fossil-rich Cretaceous sediment units in Sudan are being defined as the Wadi Milk and Shendi formations, which form the focus of this study (Figs. 5-2 and 5-3).

The Wadi Milk Formation is widely distributed in north-central Sudan, in the region between the Khartoum and Dongola to the west of the River Nile (Fig. 5-1; Wycisk et al., 1990; Bussert, 1998). The formation reaches a thickness of up to 350 m in the Dongola area (Wycisk et al., 1990). Detailed description of the Wadi Milk Formation can be found in Wycisk et al. (1990) and Bussert (1998). The formation unconformably overlies Precambrian basement rocks in the Wadi Milk and Dongola area, and is overlain by the putatively Turonian-Santonian Wadi Howar Formation (Wycisk et al., 1990).

The Wadi Milk Formation is divided into the basal fine-grained Wadi Abu Hashim Member and the upper sand-rich Jebel Abu Tuweiqiya Member (Fig. 5-3; Bussert, 1993, 1998). The age of the Wadi Milk Formation is primarily based on microflora and palynology of water well samples and variably estimated as between Albian to Santonian for the basal fossil-rich Wadi Abu Hashim Member and Turonian to Santonian for the upper Jebel Abu Tuweiqiya Member (Schrank 1990; Wycisk et al., 1990; Wycisk 1991). The presence of putatively Cenomanian sharks (e.g. *Asteracanthus aegyptiacus*) and lungfishes (e.g. *Protopterus protopteroides*) within the Wadi Abu Hashim Member has been reported as correlative to the

Cenomanian Bahariya Formation of Southwest Egypt, where similar fossils were also recovered (Gloy 1997; Rage and Werner 1999; Le Loeuff et al., 2012).

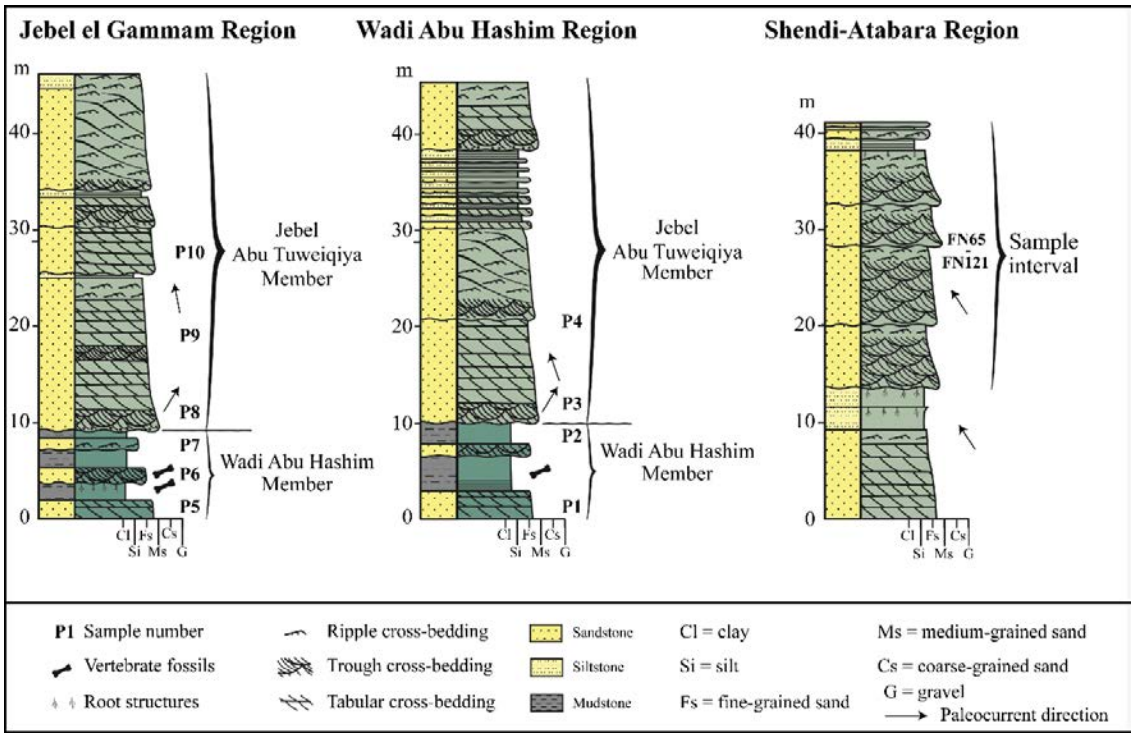

Figure 5-3. Simplified stratigraphic sections of the Wadi Milk and Shendi formations.

Wadi Milk Formation from both Wadi Abu Hashim and Jebel el Gammam regions, and the Shendi Formation from the Shendi-Atbara Region. Both stratigraphic sections are modified after Bussert (1998) and Bussert et al. (2018). Paleocurrent directions are after Bussert (1998).

Two main depositional environments have been identified within the Wadi Milk Formation, which include braidplain deposits and coastal plain deposits, although many depositional environments appear to have contributed to its accumulation (Bussert, 1993). Paleocurrent directions in the Wadi Milk Formation are mainly northward (Bussert 1998).

The Shendi Formation crops out mainly around the town of Shendi in the Shendi–Atbara region ~200 km northeast of Khartoum (Fig. 5-1). The Shendi Formation is composed of a lower and an upper unit, separated by a regional erosive contact (Fig. 5-3; Bussert, 1998). The lower unit consists of fine-grained meandering channel, flood plain, palustrine and lacustrine sedimentary rocks, whereas the upper unit strata range from braided to

meandering river channel sandstones and floodplain fines (Bussert, 1998). The Shendi Formation, originally inferred to be Albian to Santonian age based primarily on plant leaf macrofossils (Schrank, 1990), has been correlated to the Wadi Milk Formation (Wycisk et al., 1990; Wycisk, 1991). Recent palynological work by Eisawi et al. (2012) and Eisawi (2015) on the subsurface part of the Shendi Formation however, indicates a much younger Campanian–Maastrichtian age.

The Campanian to Maastrichtian Kababish Formation overlying the Wadi Howar Formation in the region of the Jebel Abyad in northwestern Sudan is known to contain crocodile and turtle fossils at the eastern rim (Figs. 5-1 and 5-2). The Kababish Formation consists of fine-grained sandstones, siltstones and claystones that were deposited mainly in a shallow marine environment (Barazi, 1985).

5.3 Sampling and analytical methods

5.3.1 Sampling

Eighteen medium- to fine-grained sandstone samples (~2-2.5 kg each) were collected from the Wadi Milk Formation (N = 10) between Khartoum and Ed Debba, and the Shendi Formation (N = 8) in the Shendi–Atbara region (Figs. 5-1, 5-2 and 5-3). The Wadi Milk samples were collected as part of the Sudan-Germany-Canada joint expeditions in January 2014. The Shendi samples were collected on the ancient quarries in Meroe (Fig. 5-1) as part of the Qatar-Sudan Archaeology Project (Mission 037) in joint cooperation with the University College of London (UCL) Qatar. Detailed stratigraphic logs for the two formations are presented by Bussert (1998) and Klein et al. (2016). Sample location details are presented in Table 5-1 (‘a’ and ‘b’) and shown in Figures 5-1 and 5-3.

Table 5-1. Location details for Wadi Milk and Shendi formation samples

(a) Location details 10 Wadi Milk Formation outcrop samples.

Sample number	Location	Lithology	Stratigraphy
	Samples from section north of Wadi Abu Hashim		
P 1	16^0 43‘ 118‘ / 31^0 08‘ 085‘	Cross-bedded, fine-grained sandstone	Wadi Abu Hashim Member (base of outcrop)
P 2	16^0 43‘ 122‘ / 31^0 08‘ 080‘	Cross-bedded, fine-grained sandstone	Wadi Abu Hashim Member (2 m below contact)
P 3	16^0 43‘ 131‘ / 31^0 08‘ 078‘	Cross-bedded, fine- to medium grained sandstone	Jebel Abu Tuweiqiya Member (1 m above contact)
P 4	16^0 43‘ 136‘ / 31^0 08‘ 072‘	Cross-bedded, fine- to medium grained sandstone	Jebel Abu Tuweiqiya Member (10 m above contact)
	Samples from section Jebel El Gammam)		
P 5	16^0 37‘ 931‘ / 31^0 08‘ 398‘	Cross-bedded, fine- to medium-grained sandstone	Wadi Abu Hashim Member (base of outcrop)
P 6	16^0 37‘ 926‘ / 31^0 08‘ 463‘	Cross-bedded, fine- grained sandstone	Wadi Abu Hashim Member (2 m higher)
P 7	16^0 37‘ 415‘ / 31^0 08‘ 467‘	Ripple cross-bedded, fine-grained sandstone	Jebel Abu Tuweiqiya Member
P 8	16^0 37‘ 153‘ / 31^0 08‘ 357‘	Tabular cross-bedded, medium-grained sandstone	Jebel Abu Tuweiqiya Member
P 9	16^0 37‘ 114‘ / 31^0 08‘ 330‘	Tabular cross-bedded, medium-grained sandstone	Jebel Abu Tuweiqiya Member (10 m above contact)
P 10	16^0 37‘ 024‘ / 31^0 08‘ 290‘	Tabular cross-bedded, medium-grained sandstone	Jebel Abu Tuweiqiya Member (20 m above contact)

(b) Location details of the 8 Shendi Formation outcrop samples.

Sample number	Location
FN 65	17^0 01‘ 38‘ / 33^0 44‘ 01‘
FN 77	17^0 02‘ 35‘ / 33^0 43‘ 16‘
FN 92	17^0 02‘ 14‘ / 33^0 42‘ 22‘
FN 100	17^0 01‘ 56‘ / 33^0 45‘ 11‘
FN 104	17^0 01‘ 38‘ / 33^0 44‘ 01‘
FN 110	16^0 55‘ 55‘ / 33^0 45‘ 56‘
FN 113	16^0 55‘ 58‘ / 33^0 45‘ 54‘
FN 121	16^0 55‘ 57‘ / 33^0 46‘ 30‘

Notes: sample location near east of pyramids of Kabushiya/Meroe (Fig. 5-1) region approx. 16^0 56‘ N/$33^0$45‘E

5.3.2 Sedimentology and sandstone petrography

Hand specimens and thin sections were investigated in an attempt to infer parent rock characteristics of the Wadi Milk and Shendi formations (Dickinson and Suczek, 1979; Dickinson et al., 1983). Four thin sections comprising two from the Wadi Milk and two from the Shendi formations were prepared and point-counted following the Gazzi-Dickinson method (Ingersoll et al*.,* 1984) at James Cook University, Townsville, Australia, using transmitted-light polarizing Leica DMRXP microscope. 350 points counted per sample were used to estimate the compositional percentages of quartz (Q), feldspar (F) and lithic (L) grain fragments (Ingersoll et al*.,* 1984; Dickinson, 1985). The modal parameters were plotted on tectonic discrimination fields of Dickinson and Suczek (1979) and Dickinson et al. (1983).

5.3.3 U-Pb detrital zircon geochronology

All detrital zircon separations and U-Pb dating were conducted at James Cook University (JCU) following standard procedures outlined in Gehrels et al. (2008), Slma and Koler (2012) and Owusu Agyemang et al. (2016). Zircons were handpicked (≥ 100 zircons / sample) using stereomicroscope and mounted in a 25 mm diameter transparent epoxy resin disc with zircon standards GJ-1 (609 Ma, Jackson et al*.,* 2004) and Temora-2 (416.8 Ma, Black et al*.,* 2003). The zircons in the epoxy disc were polished to expose the zircons for cathodoluminescence (CL) imaging using a Jeol JSM5410LV scanning electron microscope.

The zircons were dated using U-Pb laser-ablation inductively coupled plasma mass spectrometry (LA-ICP-MS) via a Coherent GeolasPro 193 nm ArF Excimer laser ablation system connected to a Bruker 820-MS (formerly Varian 820-MS) following JCU tuning and operating parameters (Tucker et al., 2013). Details of LA-ICP-MS operating conditions are presented in Appendix 5S1. Total analysis time was 70 seconds; comprising of the first 30

seconds for measuring background intensities followed by 40 seconds of sample ablation, using a 32 μm laser beam diameter. Two analyses each of zircon standards GJ-1 (primary) and Temora-2 (secondary) were conducted before and after the analysis of 10-12 unknown zircons, and used as standard bracketing to correct for remaining elemental fractionation and mass bias (Gehrels et al., 2008). NIST 612 standard glass (50ppm glass USGS working values, 2009) was also analysed before and after each U-Pb laser ablation session for calibrating thorium and uranium concentrations. GLITTER 4.0 software (Van Achterbergh et al., 2001), was used to reduced data and determine the age of individual zircons. Discordance of each grain was also estimated using Microsoft Excel with Isoplot macros (Ludwig, 2012). A discordance cut-off of 15% was used in this study for all zircon grains older than 300 Ma. The U-Pb results were used to assess the age and sedimentary provenance for the two studied units.

5.3.4 Lu-Hf isotopic systematics

A subset of zircons from the Wadi Milk and Shendi formations analysed for their U-Pb ages were subsequently analysed for their Lu-Hf isotopic ratios to help estimate the initial εHf(t) values of each individual zircon grain. The initial εHf(t) values were used as a discriminant tool to predict crustal source of the zircons (Kinny and Maas, 2003). Lu-Hf methods follow those described by Kemp et al. (2009) and Næraa et al. (2012) for the Advanced Analytical Centre at James Cook University. Details on the analytical methods are presented in Appendix 5S2.

5.3.5 Zircon trace elements analysis

A suite of detrital zircons from the Wadi Milk and Shendi formations representing the main age populations, including the Cretaceous grains, were analysed for their trace element ratios following the U-Pb and Lu-Hf analyses. Analyses were interpreted for source rock characteristics using trace elemental ratios in zircon (Pearce et al., 1984; Hoskin and Ireland, 2000; Belousova et al., 2002; Grimes et al., 2007; Yao et al., 2011). Detailed analytical methods for zircon trace element are presented in Appendix 5S3.

5.4 Results and interpretation

5.4.1 Sandstone petrography of Wadi Milk and Shendi formations

The mean modal compositions of quartz-feldspar-lithic (QFL) grains derived from different plate tectonic controlled source regions can plot within discrete fields on Q_tFL and Q_mFL_t diagrams (Dickinson and Suczek, 1979). The QFL compositions of both the Wadi Milk and Shendi formations were plotted and used to infer the parent rock characteristics. Both sets of samples were recovered from outcrops and feldspar dissolution related to surficial tropical weathering is likely to have skewed the results towards quartz. Feldspar grains were generally absent from all the samples except one Wadi Milk sample (P2; Fig. 5-4), where both plagioclase and potassium feldspar were observed. The quartz content of both sets of samples ranges from 60 to 90%, which is consistent with the quartz arenite to sub-arkose petrofacies. The quartz grains are mostly sub-angular but with some rounded grains suggestive of some amount of recycling. Lithic fragments are either of metamorphic or volcanic origin in both sets of samples, with limited sedimentary rock fragments observed.

All samples are poorly- to very well-sorted with both primary and secondary porosity. The samples are also heavily cemented by kaolin and in some cases hematite cement (Fig. 5-4).

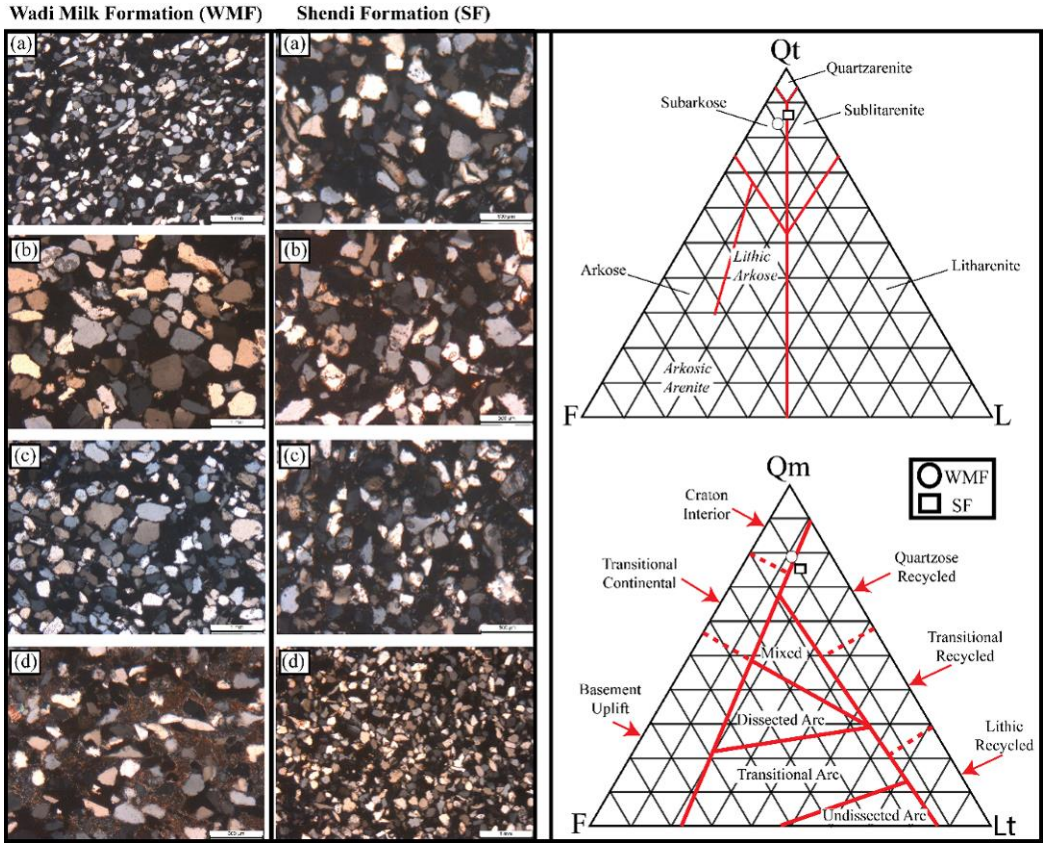

Figure 5-4. Thin section photomicrographs and detrital modes of the Wadi Milk and Shendi formation samples.

Left two columns are photomicrographs from the Wadi Milk and Shendi samples. The right column reveals the quartz-feldspar-lithic (QFL) detrital modes for the Wadi Milk and Shendi formations. All four samples plots as quartzarenite sandstones with quartzose recycled orogeny provenance. Qt = total quartz grains, Qm = monocrystalline quartz, F = feldspar, L = lithics, and Lt = total lithics).

5.4.2 U-Pb detrital zircon geochronology results

The detrital zircon dating of 18 sandstone samples from Wadi Milk (N = 10) and Shendi formations (N = 8) yielded 1246 concordant U-Pb ages out of 1492 total analyses using a discordance filter of 15%. Detrital zircon grains from both formations range from colourless to light pink and from transparent to dark with dominantly oscillatory zoning under cathodoluminescence (Fig. 5-5). Zircons range from euhedral to sub-rounded with grain

lengths ranging from 30-µm to 350-µm and widths between 20-µm to 120-µm, typical of igneous or magmatic sources (e.g. Corfu et al., 2003). This interpretation is supported by the high Th/U ratios observed for most grains, which is consistent with magmatic sources (Fig. 5-6). The ~2% of grains with low Th/U ratios may be effects of fluid induced recrystallization or high grade metamorphism (Vail, 1978). Complete U–Pb zircon age results are shown in Appendix 5S1.

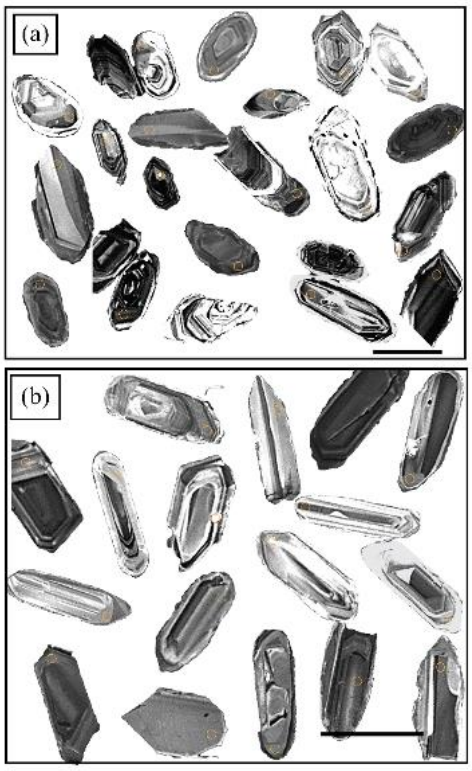

Figure 5-5. Representative cathodoluminescence of Sudan zircons

Images showing internal structure and morphology of detrital zircons from the (a) Wadi Milk Formation and (b) Shendi Formation. The scale bar under each figure is equivalent to 100 µm.

The ten Wadi Milk samples (Fig. 5-7) yielded 692 concordant grain ages out of the 885 grains analysed, with ages ranging from Paleoarchean (3262 Ma) to Cretaceous (77 Ma). However, all ten samples are dominated by Neoproterozoic grain ages that largely coincide with Precambrian terranes associated with the Pan-African orogenic event (850-550 Ma). The

Wadi Milk Formation also yielded a small population of late Paleozoic grains, and perhaps most significantly, a distinct population of six potentially age constraining Cretaceous grains that are evenly distributed through the upper and lower members.

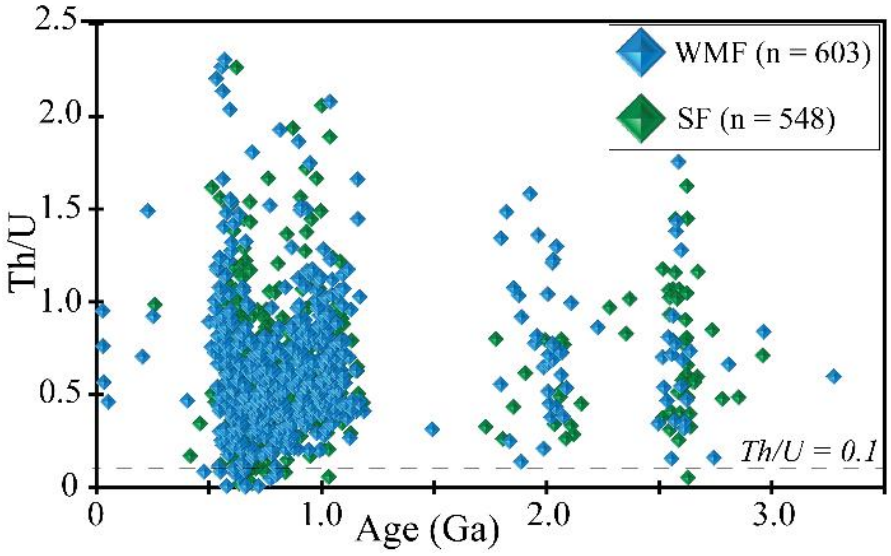

Figure 5-6. Thorium (Th) to Uranium (U) ratios for the Wadi Milk and Shendi formations zircons.

This figure shows high Th/U ratios for most analysed zircons, suggestive of magmatic sources, whereas low (Th/U < 0.1) and variable ratios are suggestive of metamorphic sources (Rubatto, 2002). The dash line is Th/U = 0.1.

The eight Shendi Formation samples (Fig. 5-8) yielded 550 concordant grain ages out of 607 single grain analyses. The grain ages from the Shendi Formation range from Neoarchean (2635 Ma) to Middle Ordovician (462 Ma), with a dominant Neoproterozoic population. Interestingly, no Cretaceous age grains were recovered from this unit.

5.4.3 Lu-Hf isotope geochemistry

The Lu-Hf isotope ratios were used to help to differentiate between similar zircon populations from different crustal sources (e.g. Kinny and Maas, 2003). Zircons yielding positive initial εHf(t) values are indicative of sources of juvenile crustal, whereas negative εHf(t) values indicate sources of crustal reworking (Morag et al., 2011). The selected grains from six Wadi Milk samples (n = 107) included Cretaceous (n = 4), Permian (n = 2),

Neoproterozoic (n = 70), Mesoproterozoic (n = 22), Paleoproterozoic (n = 6) and Archean (n = 3) populations, whereas the selected grains from six Shendi Formation samples (n = 128) included Permian (n = 1), Neoproterozoic (n = 95), Mesoproterozoic (n = 18), Paleoproterozoic (n = 5) and Archean (n = 9) populations. The initial εHf(t) values of detrital zircons from both the Wadi Milk and Shendi samples are plotted in Figure 5-9 (see Appendix 5S2 for detailed information).

The Lu-Hf isotope ratios for the Wadi Milk zircons show a wide spread of initial $^{176}Hf/^{177}Hf$ ratios from 0.280938 to 0.282911 and εHf(t) values ranging from –25.9 to + 13.7, divided into 62% positive and 38% negative initial εHf(t) values (Fig. 5-9). This initial εHf(t) values result is suggestive of mixed provenance from a dominant juvenile mantle and minor reworked crustal sources. All the analysed Cretaceous and Permian zircons from the Wadi Milk Formation have positive initial εHf(t) values, which suggest a juvenile mantle source.

The Lu-Hf isotope ratios for the Shendi Formation zircons also show a wide spread of initial $^{176}Hf/^{177}Hf$ ratios from 0.280844 to 0.282698 and initial εHf(t) values ranging from –24.4 to +13.8, divided into 68% positive and 32% negative initial εHf(t) values (Fig. 5-9). The Shendi Formation results are also indicative of mixed provenance comprising of dominant juvenile mantle components and a minor contribution from reworked crustal sources.

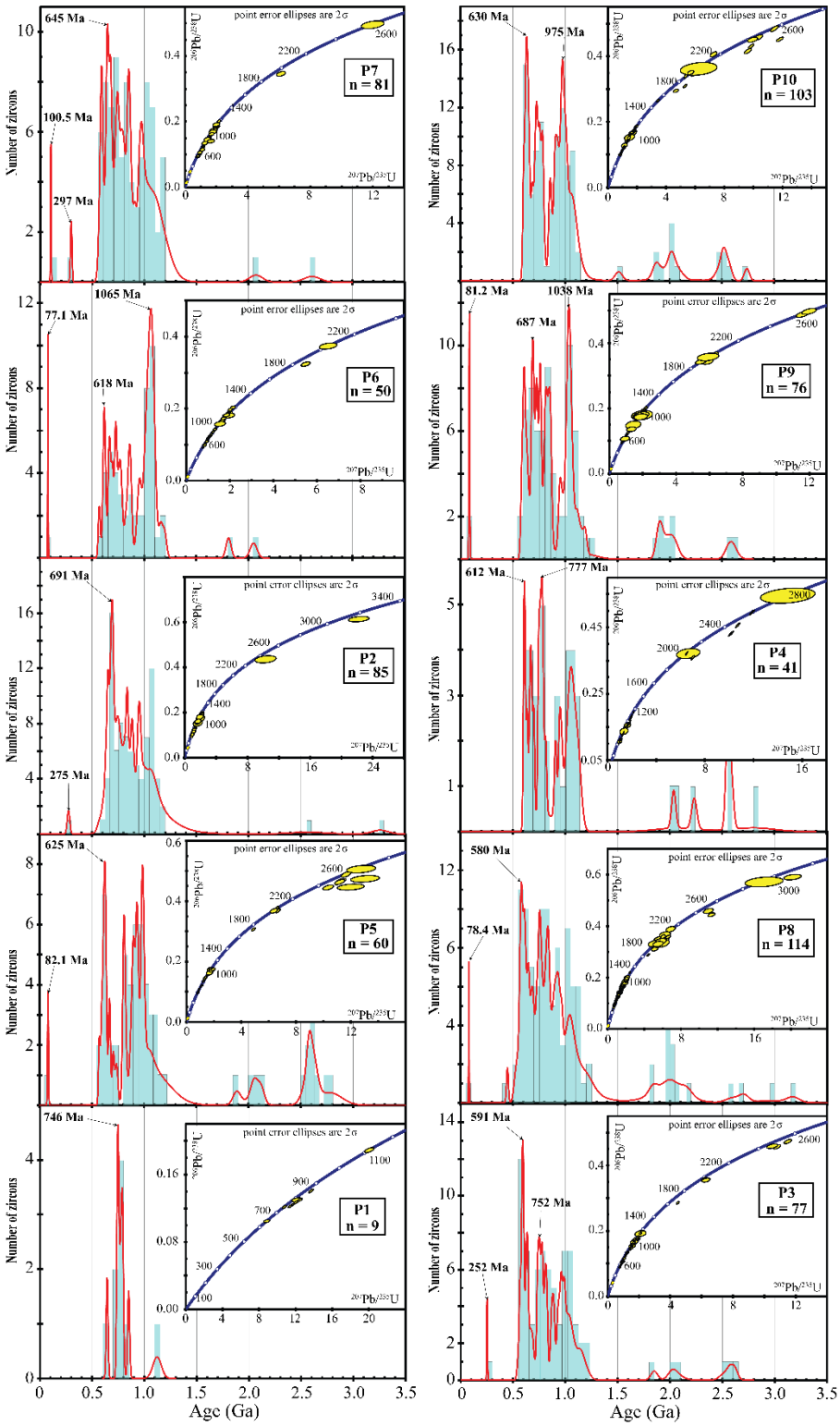

Figure 5-7. Probability density plot and corresponding Concordia plots for the Wadi Milk Formation samples.

The plot shows the dominance of Neoproterozoic to Mesoproterozoic zircons in each sample. Reported results are single zircon concordant analyses. The left column samples are from the Wadi Abu Hashim Member and the right column represent the Jebel Abu Tuweiqiya Member (see Figure 5-3). The $^{207}Pb/^{206}Pb$ age is preferred for zircon grains older than 1.0 Ga as they are more reliable for older zircons, whereas the $^{206}Pb/^{238}U$ age is preferred for

younger zircons with age less than 1.0 Ga, because they are more reliable for younger zircons (e.g. Gehrels, 2012). The instrumental parameters and operating conditions are provided in the Appendix 5S1.

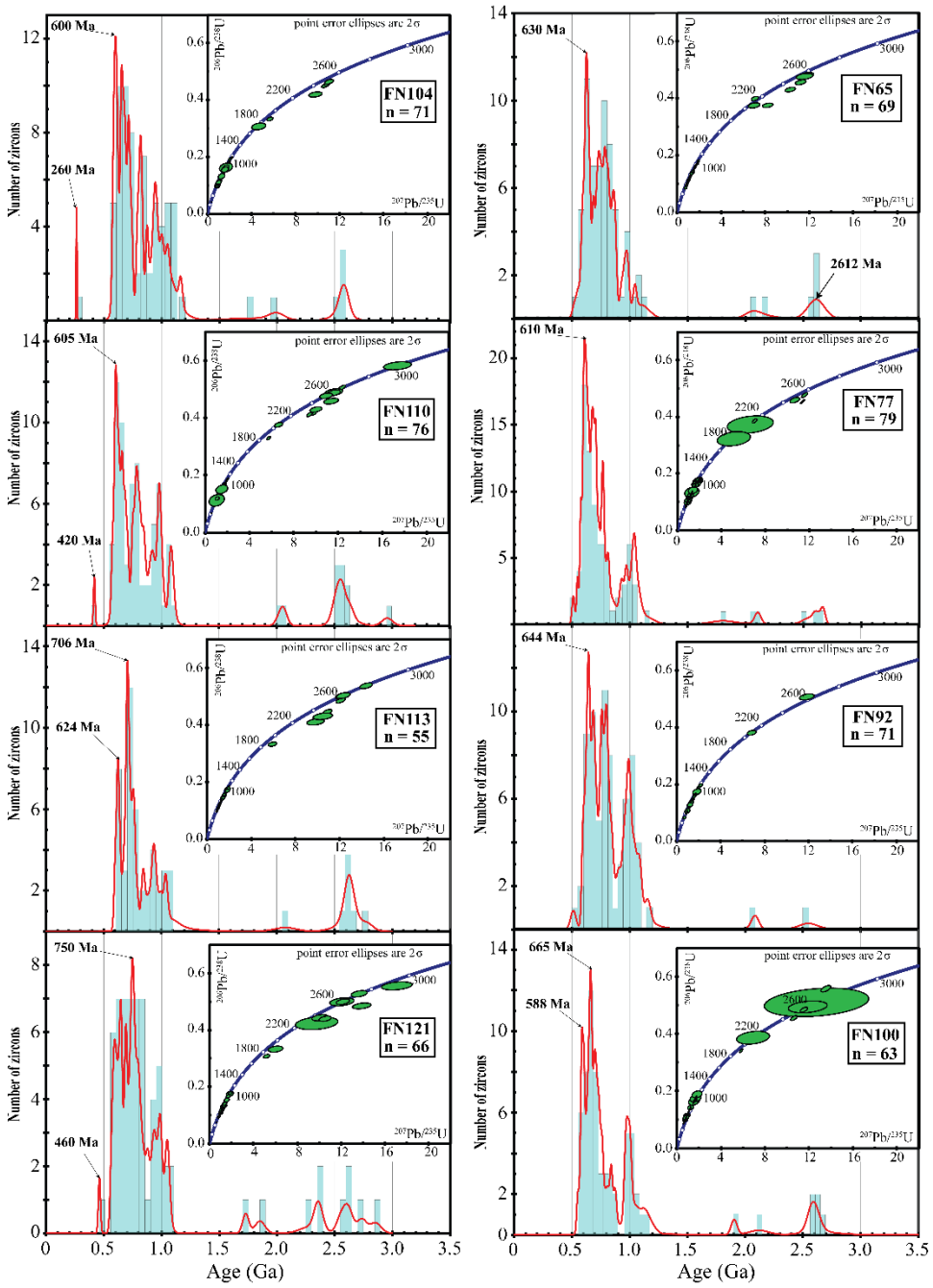

Figure 5-8. Probability density plot and corresponding Concordia plots for the Shendi Formation sample.

This plot also shows the dominance of Neoproterozoic and Mesoproterozoic zircons from the Shendi Formation.

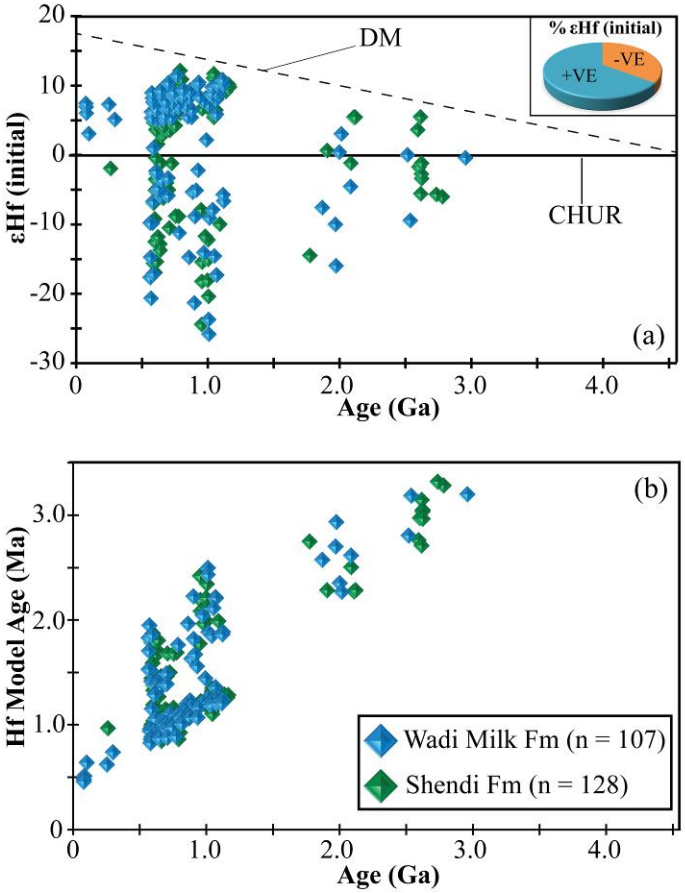

Figure 5-9. Lu-Hf plots for detrital zircon from the Sudan.

(a) Plot of initial εHf values vs U-Pb age of concordant detrital zircons from the Cretaceous Wadi Milk and Shendi formations of Sudan. The plots show that most of the zircons in this study have positive initial εHf(t) values (65%) and were derived from sources with juvenile crust, which we interpret as the Arabian Nubian Shield. (b) Plot of Hf model age vs U-Pb age of the Wadi Milk and the Shendi formations. (The depleted mantle (DM) evolution curve is for linear evolution from a Chondritic Uniform Reservoir (CHUR) value at the Earth's formation (i.e., 0 at 4.56 Ga) to εHf(t) = 17 at the present for the DM [Dhuime et al., 2011]). The mass spectrometer cup configuration for this study is shown in the Appendix 5S2. The ^{176}Lu decay constant of 1.867 ± 0.008 x 10^{-11} year^{-1} reported by Söderlund et al. (2004) and the Chondritic Uniform Reservoir (CHUR) values of ^{176}Hf/^{177}Hf (0.282785) and ^{176}Lu/^{177}Hf (0.0336) reported by Bouvier et al. (2008) were used in the calculation of initial εHf(t) values and model ages.

5.4.4 Zircon trace elements results

Summarized detrital zircon trace element analyses are shown in Figure 5-10 and listed in Appendix 5S3. The trace element composition analyses were performed on a subset of 33 zircons from the Wadi Milk Formation and 52 zircons from the Shendi Formation, representing zircons from the Cretaceous (n = 2), Neoproterozoic (n = 53), Mesoproterozoic (n = 20), Paleoproterozoic (n = 2) and Archean (n = 7) populations in a further attempt to

tighten constraints on sediment sources (Taylor and McLennan, 1985; Hoskin, 2005). The zircon trace element results from the two units show similar chondrite-normalised REE patterns, strongly enriched HREE and depleted LREE, with strong positive Ce and negative Eu anomalies, and plots into the magmatic source field of Hoskin (2005; Fig. 5-10).

The amount of niobium (Nb) in a zircon grain is indicative of the magma source; specifically, zircons are usually depleted in arc-related settings compared to within-plate tectonic settings (Sun and McDonough, 1989; Yang et al., 2012). Zircons from both sets of samples including the Cretaceous grains are suggestive of dominantly from arc-related settings as they have high Th/Nb and low Nb/Hf ratios (Fig. 5-10 e-h) relative to within-plates zircons, assuming magmatic fractionation were similar for both settings (Hawkesworth and Kemp, 2006; Yang et al., 2012). However, the trace element results does not clarify the source of the Cretaceous zircons as there are really no obvious arc-related sources nearby.

5.5 Discussion

5.5.1 Maximum depositional age of the Wadi Milk Formation

Refining the age of a stratigraphic unit can be particularly useful in continental sedimentary basins that lack fossils or have poorly constrained biostratigraphic age estimates (e.g. Jones et al., 2009). The youngest population of U-Pb zircon ages from this study provides important maximum new depositional age constraints for the Wadi Milk Formation, whereas the Shendi Formation did not yield any young, age informative zircons.

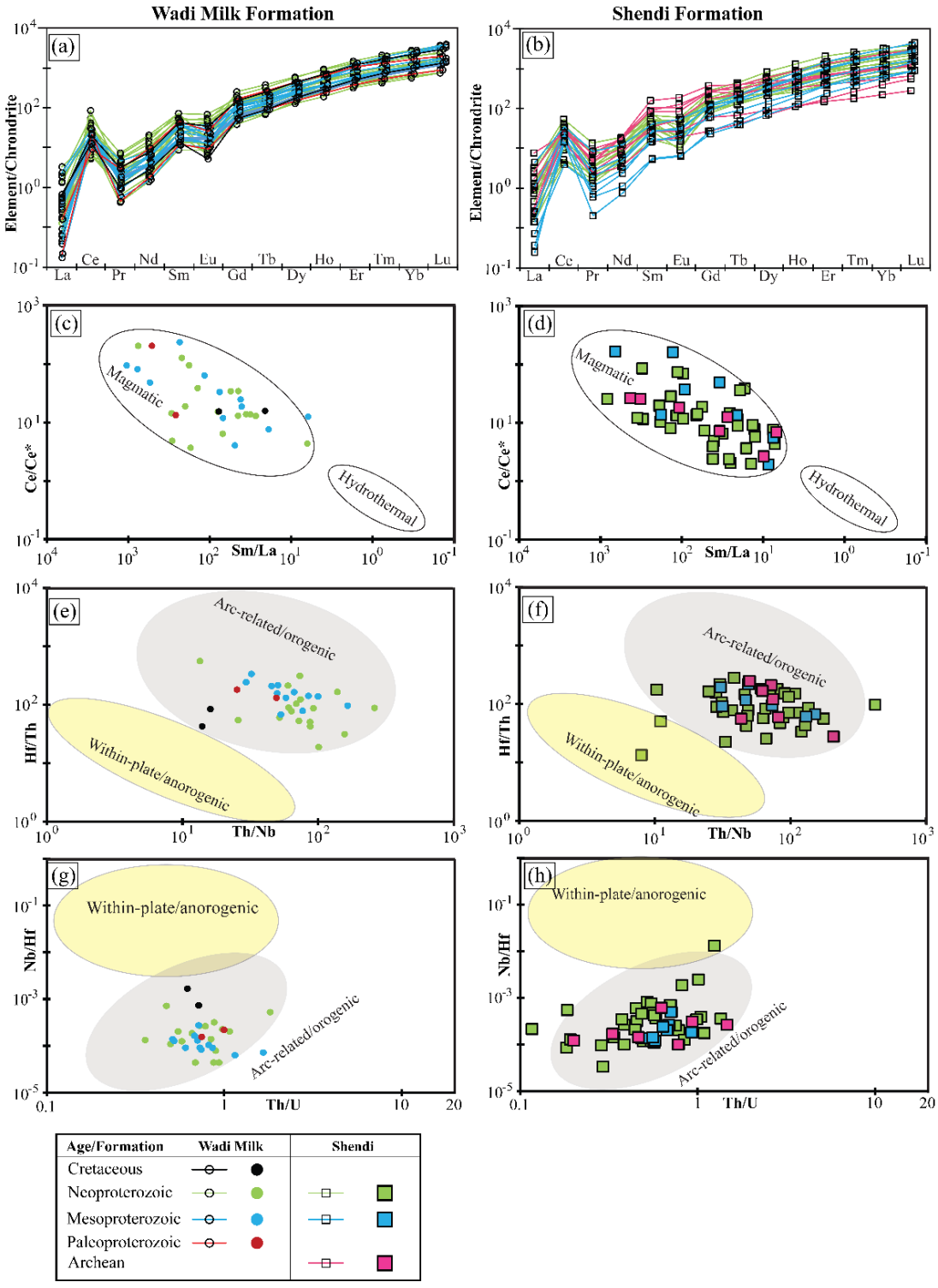

Figure 5-10. Chondrite-normalized rare earth element patterns for the main populations from Sudan samples.

(a) Wadi Milk and (b) Shendi Formation samples. Discrimination plots for magmatic and hydrothermal zircons (c) and (d) are for Wadi Milk and Shendi zircons, respectively. Zircons from both units plot within the magmatic domain of Hoskin (2005). The plots (Fig. 5-10 e-h) show closely clustered zircons within the Arc-related / orogenic tectonic source domain for both units including the Cretaceous grains from the Wadi Milk Formation. Chondrite normalization values are from Taylor and McLennan (1985). Data were processed offline by Signal Integration for Laboratory Laser Systems (SILLS; Guillong et al., 2008) using GeoREM "preferred" concentration values for NIST610.

The ages of the six Cretaceous zircons recovered from the Wadi Milk Formation samples (Figs. 5-7 and 5-11) include one grain at ~100.5 Ma and five tightly clustered grains between 82.1 Ma and 77.1 Ma. The weighted average age (Fig. 5-11 and Table 5-2) for the five coherent clustered grains is 79.2 ± 2.4 Ma (MSWD = 0.65, probability 0.62), and this age falls within the recently suggested biostratigraphic age of Campanian-Maastrichtian reported for the Shendi Formation by Eisawi (2015). However, this maximum depositional age is younger than the Turonian to Santonian age assigned to the overlying Wadi Howar Formation (Klitzsch and Lejal-Nicol, 1984), which is perhaps not that surprising. The new maximum depositional age of 79.2 ± 2.4 Ma presented here (Fig. 5-11) shows conclusively that the age of the Wadi Milk Formation is much younger than the previously suggested Albian-Santonian age assignment. The presence of non-avian dinosaurs from the Wadi Milk Formation (Rauhut, 1999), also tightly refines the age of the unit to the Campanian-Maastrichtian stages. The improved age is particularly important as the Wadi Milk Formation is among the few relatively fossiliferous continental vertebrate bearing succession in northern or central Africa, and this age provides an opportunity to better correlate these rocks and their fossils with other Cretaceous units in the region such as the Shendi Formation.

This new age constraint for the Wadi Milk Formation has important implications in future studies of fossils from this unit and other correlative units in northern Sudan, and beyond. The previously published record of vertebrate fossils from the Wadi Milk Formation has, for example, included notably early occurrences of lissamphibians (e. g., Evans et al. 1996) and snakes (Rage and Werner, 1999). The importance of these fossil occurrences, and others, will need to be re-evaluated in light of the younger geological age estimate for their host rocks. Importantly, the Campanian–Maastrichtian age for the Wadi Milk Formation indicates that this rich fossil fauna now corresponds to a particularly poorly sampled latest

Cretaceous interval in the terrestrial vertebrate record of Africa (e.g., Upchurch et al. 2011; Sallam et al. 2018).

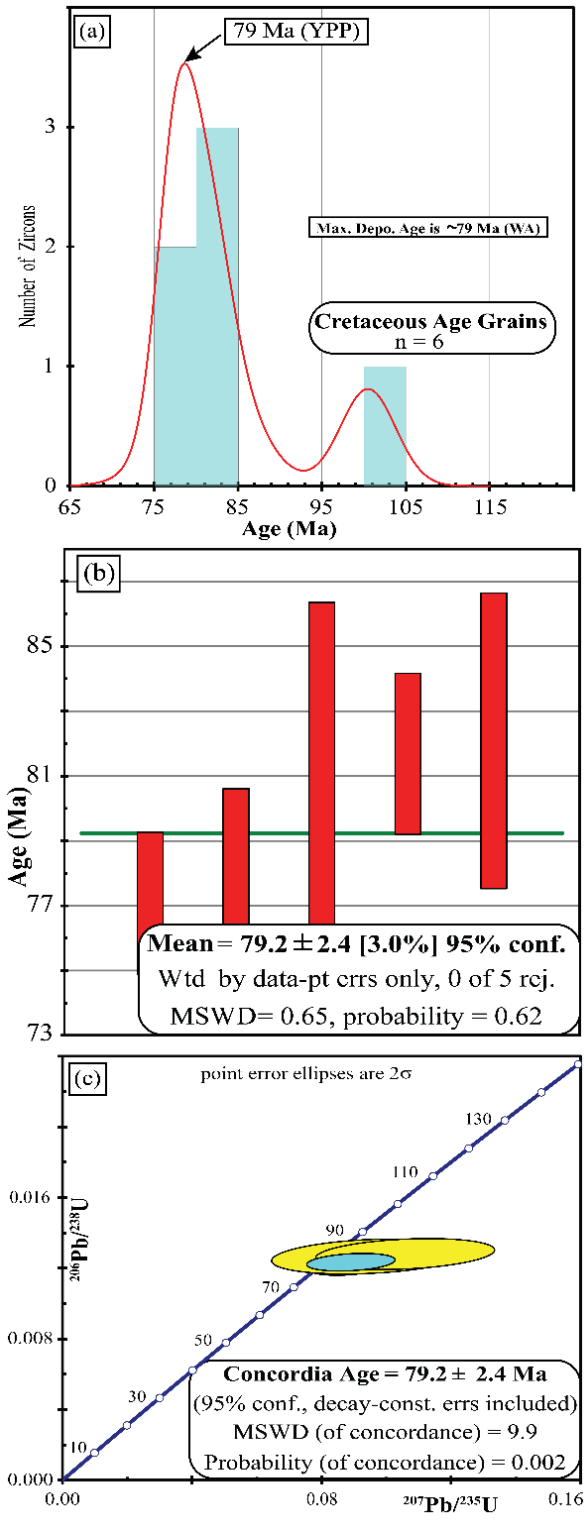

Figure 5-11. Cretaceous age zircon grains recovered from the Wadi Milk Formation (n = 6).

(a) Probability density plot of the Cretaceous grains showing the Youngest Graphical Age (YPP) of 79 Ma. (b). Weighted mean age of a cluster of five Cretaceous zircons from the Wadi Milk Formation. (c). U-Pb Concordia plot of the five coherent Cretaceous grains recovered from the Wadi Milk Formation. The maximum depositional age(s) reported herein were calculated at the 2σ level for the youngest cluster of five zircon grains to meet the conditions for acceptable precision and discordance using $^{206}Pb/^{238}U$ ages (see Dickinson and Gehrels, 2009 for discussion).

Table 5-2. Estimate of the maximum depositional age for the Wadi Milk Formation

Analysis/ Samples		Upper Member	Lower Member	Composite
YSG	Age	78.4	77.1	77.1
	Error	2.23	2.19	2.19
YPP	Age	80	77.5	79
YDZ	Age			77.2
	Range			1.7/2.7
	Confidence			95%
Weighte Average (+3)	Age	80 (± 3.1)	78.0 (± 3.9)	79.2 (± 2.4)
	Confidence	95%	95%	95%
	Rejection	0 of 3	0 of 2	0 of 5
	MSWD	0.52	0.98	0.65
	Probability	0.59	0.32	0.62
TuffZirc (+6)	Age			81.2
	Error			0.90/4.10
	Confidence			93.80%
	Group size			5

Notes: the five techniques used to arrive at a maximum depositional age interpretation have been discussed extensively by Dickinson and Gehrels (2009) and Tucker et al. (2013). All the techniques can be accessed through Microsoft Excel using isoplot macros of Ludwig (2012). The five techniques include (i) youngest single grain age (YSG); (ii) youngest graphical peak age (YPP); (iii) youngest detrital zircon age (YDZ); (iv) the Weighted Average (WA) of a coherent cluster ($n \geq 3$); and (v) TuffZirc (Zircon Age Extractor, (+6 grains).

5.5.2 Correlation of the Wadi Milk and Shendi Formations with other Cretaceous units in Sudan and central Africa

The geological evolution of central and northern Africa has been tied to the extensive late Mesozoic tectonics, particularly the Cretaceous break-up of Gondwana (e.g. Guiraud et al., 2005). However, the ages of most of these Cretaceous units are still poorly constrained,

making stratigraphic correlation very difficult (see Fig. 5-2). A number of recent studies (e.g. Owusu Agyemang et al., 2018; Widlansky et al., 2018) have shown that most of these stratigraphic correlations may require quite significant revision largely due to their over reliance on previously imprecise biostratigraphic age estimates.

In central and northern Sudan and even into southern Egypt (e.g. Wycisk, 1991), the lateral equivalence and lithological similarity between the continental strata has been used as evidence for correlating these units (Mateer et al., 1992). The Wadi Milk and the Shendi formations have previously been assumed to range between Albian and Santonian in age based on microflora, macroflora and vertebrate fauna (Schrank, 1990), one of which have recently been re-evaluated. For example, Eisawi (2015) recently hypothesized a Campanian–Maastrichtian age for the Shendi Formation based on new palynological data. The newly reported age from the Shendi Formation by Eisawi (2015) from palynological analysis and detrital zircons from the Wadi Milk Formation presented herein demonstrate that both units are considerably younger than traditional estimates, and can now be refined to at least Campanian for the Wadi Milk Formation and Campanian – Maastrichtian for the Shendi Formation. The newly reported age for both units provides a significant basis for revising the age for the other units of the so-called Nubian Sandstone. The non-marine fluvial sandstones of the Sabaya Formation in south-western Egypt have been correlated to the Wadi Milk and Omdurman formations (Schrank and Awad, 1990; Wycisk, 1991) in north-western Sudan based on lithological similarity and assumed Cretaceous age. The newly refined Campanian age reported herein for the Wadi Milk Formation provides strong support for the recently revised Campanian–Maastrichtian age for the Shendi Formation (Eisawi, 2015) and suggests that the Sabaya Formation may also be younger than previously accepted. Generally, the new ages from the Shendi and Wadi Milk formations raises doubts about reliability of the Albian

to Santonian biostratigraphic age interpretations for the rest of the previously Nubian Sandstone units, as well as other regionally correlative units in northern and central Africa (Wycisk, 1991; Mateer et al., 1992).

Many other recent examples exist where legacy biostratigraphic age estimates for middle to Upper Cretaceous continental deposits across central Africa have systematically proven to be too old. The advent of detrital zircon geochronology and other dating approaches (e.g., paleomagnetic) have been instrumental in improving age interpretations. For instance, the Lapur Sandstone from the Turkana Basin in northern Kenya was considered to be mid to Upper Cretaceous based on vertebrate fossils (O'Connor et al., 2011). However, detrital zircon geochronology has recently been used to demonstrate that the Lapur Sandstone is partly Paleogene in age (Owusu Agyemang et al., 2018), as suggested Thuo (2009). In southwestern Tanzania, detrital zircon geochronology, tuff dating and improved biostratigraphy have been used to revise the age of the Red Sandstone Group (Roberts et al., 2004; 2010; 2012), which was previously based on broad/imprecise biostratigraphic age estimates. Most recently, Widlansky et al. (2018) applied magnetostratigraphy to demonstrate that the Galula Formation of the Red Sandstone Group extends well into the Upper Cretaceous (Campanian) and is likely correlative with the Wadi Milk Formation. Overall, the results highlight the need for more work to constrain the age of the different units within the so-called Nubian Sandstone and other similar age units for better stratigraphic correlation.

5.5.3 Provenance of Wadi Milk and Shendi Formations

The detrital zircon age spectra from both the Wadi Milk and the Shendi formations are dominated by Neoproterozoic age grains with minor Paleoproterozoic and Archean zircons (Figs. 5-7, 5-8 and 5-12). The only exception is the recovery of six age defining Cretaceous

zircons (Fig. 5-11) from the Wadi Milk Formation discussed in section 5.1. The age spectra of the two units show a trimodal distribution for the Neoproterozoic age zircons between 985-968 Ma, 765-700 Ma and 650-600 Ma, whereas the Paleoproterozoic and Archean zircons are clustered between 2100-2000 Ma and 2700-2500 Ma respectively (Fig. 5-13). The results of the Kolmogorov-Smirnov (K-S) statistical tests (Fig. 5-12 and Table 5-3) for the Wadi Milk (N = 9) and Shendi (N = 8) formations show the samples of the two units pass the K-S tests and could all have a common provenance. Lu-Hf isotope geochemistry of most of the grains (Fig. 5-9) show a dominance of juvenile mantle source for the rocks of both units, whereas the trace element (Fig. 5-10) of the zircons are suggestive of arc-related magmatism for most of the zircons including the Cretaceous age grains. The trace element interpretations are consistent with the findings of Ries et al. (1985), who found most the basement rocks in the northeastern margin of the Bayuda Desert (e.g. Abu Hamad area; Fig. 5-1) are products of arc-related magmatism.

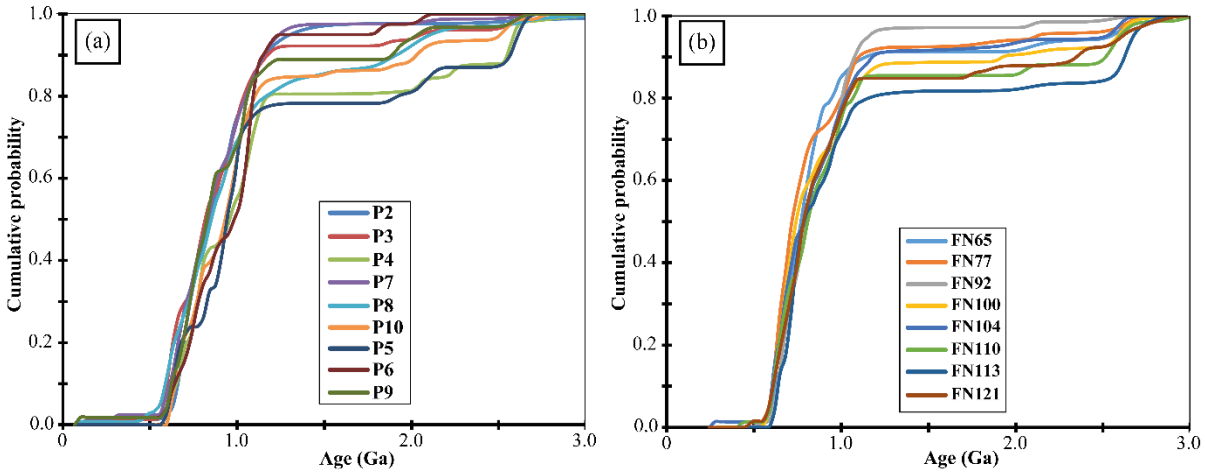

Figure 5-12. Cumulative distribution frequency diagram of the studied samples resulting from the K-S Test.

(a) Wadi Milk Formation (N = 9). This figure shows that all samples passed the K-S statistical test and are likely to have common provenance. One Wadi Milk sample was not included in the K-S Test because the small number of analysis (n ≤ 20) would make the statistical test meaningless (see Guynn and Gehrels, 2010 for discussion). (b) Shendi Formation (N = 8). This plot shows that all eight Shendi Formation passed the test and may share a common provenance.

Table 5-3. K-S Test results for the Wadi Milk and Shendi formation samples

(a).P values for nine Wadi Milk Formation samples

	P2	P3	P4	P7	P8	P 10	P5	P6	P9
P2		**0.182**	**0.221**	**0.834**	**0.282**	**0.288**	**0.110**	**0.108**	**0.946**
P3	**0.182**		**0.213**	**0.965**	**0.758**	**0.296**	**0.099**	**0.120**	**0.767**
P4	**0.221**	**0.213**		**0.250**	**0.565**	**0.758**	**0.818**	**0.632**	**0.406**
P7	**0.834**	**0.965**	**0.250**		**0.411**	**0.175**	**0.052**	**0.135**	**0.954**
P8	**0.282**	**0.758**	**0.565**	**0.411**		**0.465**	**0.159**	**0.340**	**0.962**
P 10	**0.288**	**0.296**	**0.758**	**0.175**	**0.465**		**0.798**	**0.607**	**0.176**
P5	**0.110**	**0.099**	**0.818**	**0.052**	**0.159**	**0.798**		**0.439**	0.046
P6	**0.108**	**0.120**	**0.632**	**0.135**	**0.340**	**0.607**	**0.439**		**0.391**
P9	**0.946**	**0.767**	**0.406**	**0.954**	**0.962**	**0.176**	0.046	**0.391**	

Kolmogorov-Smirnov (K-S) statistical test for nine Wadi Milk Formation samples. The bold p-values are > 0.05, which indicates that these samples passed the K-S test, suggestive of a common provenance for all nine samples.

(b) P values for eight Shendi Formation samples

	FN65	FN77	FN92	FN100	FN104	FN110	FN113	FN121
FN65		**0.469**	**0.747**	**0.679**	**0.592**	**0.324**	**0.289**	**0.676**
FN77	**0.469**		**0.134**	**0.944**	**0.309**	**0.106**	**0.069**	**0.195**
FN92	**0.747**	**0.134**		**0.537**	**0.887**	**0.701**	**0.421**	**0.675**
FN100	**0.679**	**0.944**	**0.537**		**0.972**	**0.551**	**0.356**	**0.727**
FN104	**0.592**	**0.309**	**0.887**	**0.972**		**0.966**	**0.494**	**0.975**
FN110	**0.324**	**0.106**	**0.701**	**0.551**	**0.966**		**0.721**	**1.000**
FN113	**0.289**	**0.069**	**0.421**	**0.356**	**0.494**	**0.721**		**0.984**
FN121	**0.676**	**0.195**	**0.675**	**0.727**	**0.975**	**1.000**	**0.984**	

Kolmogorov-Smirnov (K-S) statistical test for eight Shendi Formation samples. The bold p-values are > 0.05, which indicates that these samples passed the K-S test, suggestive of a similar provenance for all eight samples.

5.5.3.1 Cretaceous zircons

Volcanic or magmatic source rocks associated with the Cretaceous (100 – 77 Ma) age interval in the region are numerous and varied, ranging from northern Egypt through to southern Sudan (*see* Cahen et al., 1984). Volcanic rocks with ages of 119 ± 3 Ma, 87-81 ± 2 Ma and 84-79 ± 3 Ma have been reported for the Lake Nasser area, whereas volcanic rocks in the range of 100-80 Ma are reported from the Wadi Nash-Aswan both in southern Egypt (Bernau et al. 1986; Meneisy and Kreuzer 1974). A large igneous province in the Delgo area in northern Sudan also host Cretaceous volcanic rocks of 87-47 Ma age (Franz et al., 1993).

In southern Sudan, alkaline basalts (105-95 Ma) and dolerite sills (82 ± 8 Ma) have also been reported from the Blue Nile Rift (Fig. 5-1) and the Muglad Trough, respectively (McHargue et al., 1992; Reynolds, 1993). Volcanic activity of ages ~80 Ma and 38 Ma have also been reported from the Blue Nile Rift by Wycisk et al. (1990). In addition, basaltic volcanic rocks of Upper Cretaceous to Paleogene age (74-62 Ma) in the Bayuda Desert could also have sourced the Cretaceous zircons recovered from the Wadi Milk Formation (Barth and Meinold 1979; Cahen et al., 1984).

Bussert (1998) measured the paleoflow direction of the Wadi Milk and Shendi formations and found that flow was generally northward; consistent with sources to the south of the study area, probably from the Blue Nile rift and or the Muglad Trough (Vail, 1978). Interestingly, the Shendi Formation sample area, which lacks the Cretaceous volcanic zircon population, lies >200 km to the east of the Wadi Milk Formation. The lack of Cretaceous population in the putatively correlative Shendi Formation would suggest that the volcanic grains are being sourced from a point source likely to the southwest or south of the Wadi Milk sample area, which points to the Blue Nile rift and the Muglad Trough volcanics as the most likely source.

5.5.3.2 Neoproterozoic zircons

Magmatic source rocks associated with the Neoproterozoic age grains clustering around 985-968 Ma, 765-700 Ma and 650-600 Ma have been documented within the Arabian-Nubian Shield (e.g. Stern, 2002; Avigad et al., 2003, 2007). The initial εHf(t) values for these populations are dominated by positive values suggestive of major contribution from juvenile mantle sources consistent with rocks within the Arabian-Nubian Shield. The Lu-Hf model ages (Fig. 5-9b) show that most of the Neoproterozoic zircon grains were sourced from

Neoproterozoic (1000-800 Ma) source terrain, with only a few being sourced from older rocks (2500-1000 Ma).

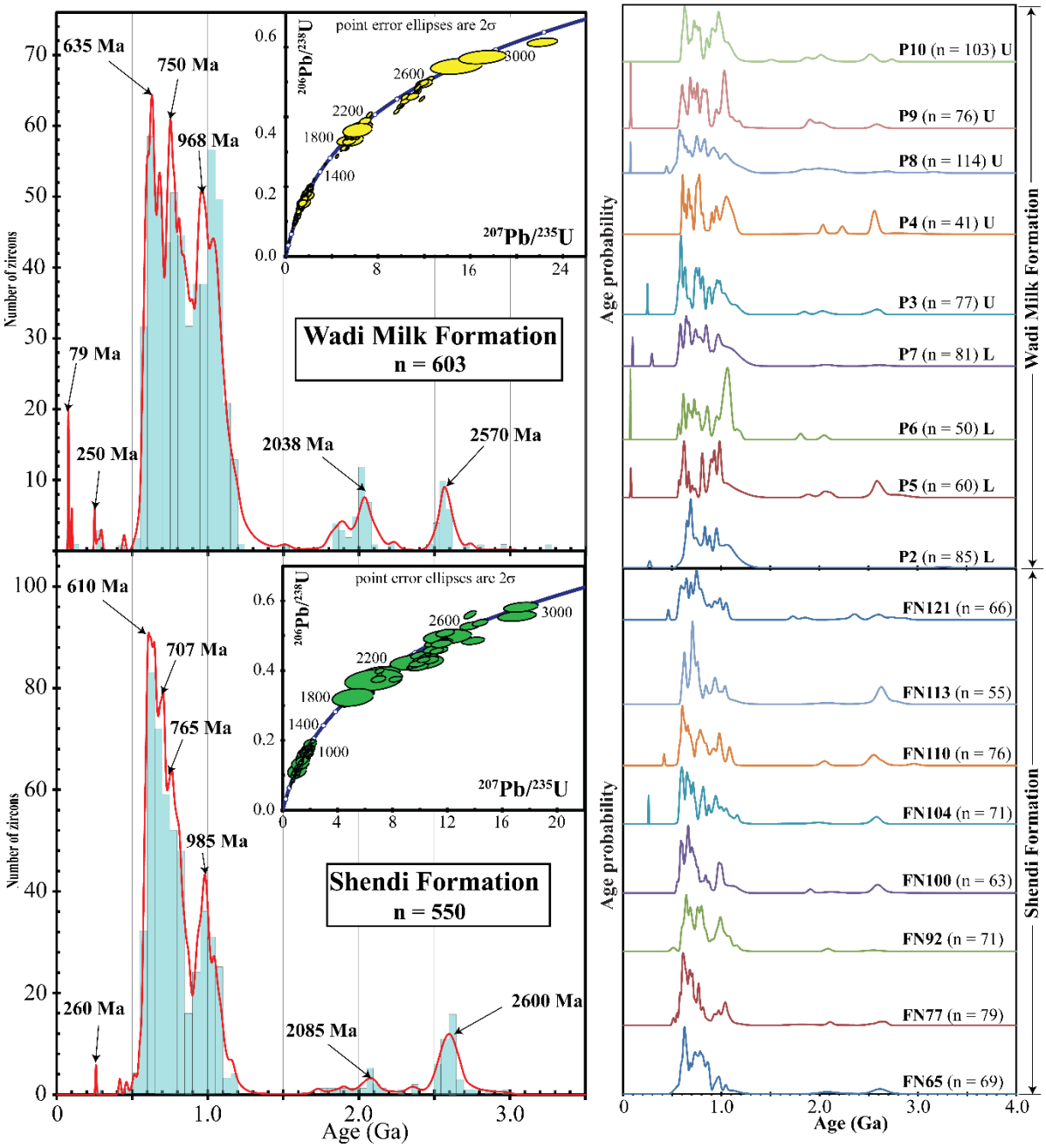

Figure 5-13. Composite probability density plot and corresponding Concordia plots for the Sudan samples.

This plot shows the dominance of Neoproterozoic and Mesoproterozoic zircons from the two units. Relative age probability plot of detrital zircon samples from the Wadi Milk and Shendi formations showing the similarities and differences in age spectra. The letters "L" and "U" means Lower Member and Upper Member respectively.

The age spectra coupled with the Lu-Hf geochemistry suggest that sediment for both units could have come from the Arabian-Nubian Shield and or the East Sahara Craton, respectively. The dominance of angular detrital sand grains with a minor component of rounded sand grains (Fig. 5-4), is supportive of limited recycling. However, the reported presence of pre-Neoproterozoic zircons within the Arabian-Nubian Shield (Bea et al., 2009), permits the possibility that all Neoproterozoic age zircons may be derived from this single source. The most likely Neoproterozoic point source in this scenario would be the Butana Massif (Fig. 5-14), which is part of the Arabian-Nubian Shield along its southern margins, about 100 km east and southeast of Khartoum (Beauchamp et al., 1990; Abu-Alam and Stüwe, 2012) where the Arabian-Nubian Shield comes into contact with the older reworked Mozambique Belt (Kröner and Stern, 2005). This interpretation would be consistent with the dominantly north directed paleocurrents documented in the Wadi Milk and Shendi formations by Bussert (1998).

5.5.3.3 Paleoproterozoic and Archean zircon

The minor Paleoproterozoic and Archean zircon populations were possibly sourced from the East Sahara Craton in Sudan (Schandelmeier et al., 1987, 1994; Stern, 1994). Zircon trace element results, however, indicate that primary Proterozoic-Archean populations are mainly from arc-related source, which is again consistent with the sources within Arabian-Nubian Shield, which resulted from a prolonged accumulation of island-arc terrains (Sultan et al., 1990; Stern and Kröner, 1993; Stern, 1994). These provenance sources were probably uplifted and eroded as a result of the break-up of Pangea, initial rifting of the Red Sea and or the differential opening of the Atlantic Ocean during the Cretaceous (Ward et al., 1979; Schull, 1988).

The drainage of eastern and central Africa, which is largely characterized as young and rift-controlled (Burke et al., 2003) and predominantly north directed is consistent with paleocurrent directions for both the Wadi Milk and Shendi formations. The results likely suggest that both the Wadi Milk and Shendi formations (formerly Nubian sandstones) were sourced from the Butana Massif, which is part of the Arabian-Nubian Shield and were probably deposited synchronously by north-north westerly flowing fluvial system (Fig. 5-14) draining into the Tethys Sea during the Late Cretaceous.

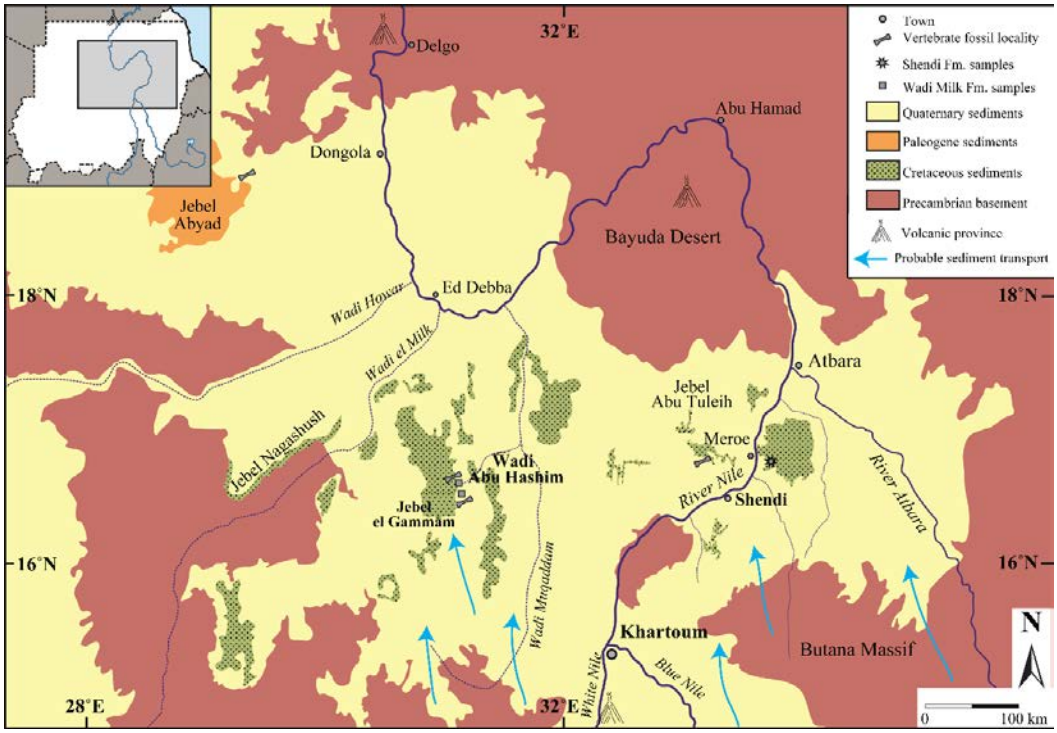

Figure 5-14. Probable sediment pathways or paleofluvial drainage routes for both Wadi Milk and Shendi formations.

5.6 Conclusions

The following conclusions are drawn based on the sandstone petrography coupled with in-situ U-Pb, Lu-Hf isotopes and trace element analysis of detrital zircons from the Wadi Milk and Shendi formations.

- A maximum depositional age of 79.2 ± 2.4 Ma is demonstrated herein for the youngest detrital zircon population in the Wadi Milk Formation, which significantly improves the understanding of the age of this important vertebrate bearing continental succession. These young grains were recovered from both the lower and upper members of the formation, and demonstrate that the formation can be no older than middle Campanian. Moreover, this refined age for the Wadi Milk Formation is consistent with recently refined biostratigraphy suggesting a Campanian-Maastrichtian age for the Shendi Formation. Considered together, the Wadi Milk and Shendi formations are likely correlative depositional units.
- The Cretaceous age detrital zircon population found in the Wadi Milk Formation is likely derived from the Blue Nile rift and the Muglad Trough volcanics.
- Detrital zircon provenance of both the Wadi Milk and Shendi formations is dominated by a range of Neoproterozoic zircon populations with trace element and Hf isotope geochemistry consistent with products of magmatic, arc-related source areas. The Butana Massif portion of the Arabian-Nubian Shield located to the south and southeast of the study area is interpreted as the primary source terrain, which fits with available paleocurrent data from the two formations. Minor Archean and Paleoproterozoic grains are also likely recycled from older terrains within the same Arabian-Nubian Shield basement rocks in this region.

6. CHAPTER SIX

Discussion and synthesis of Jurassic and Cretaceous paleogeography and drainage evolution of central Africa: Insights from U-Pb detrital zircon geochronology and Lu-Hf isotope geochemistry.

6.1 Introduction

The African myth of a lost species of dinosaur—Mokele-mbembe "he who stops the flow of rivers"—that still roams somewhere deep in the Congo Basin (Figs. 2-1 and 6-1), is one of many legends that have long-fanned the flames of exploration and discovery in this inaccessible and difficult to reach part of central Africa. European interests in the headwaters of major river systems, and the drainage and paleogeography of Africa dates back to the 1800s, when explorers like David Livingstone and Mungo Parks mapped the courses of major rivers, like the Congo, Nile and Niger, across the African continent (e.g. Pratt, 2007). Although the interests and focus have changed through time; the fundamental pursuit of understanding the evolution and source of major rivers has remained a topic of great interest. Understanding drainage evolution and provenance is pivotal to understanding uplift histories of continents, the paleobiogeography and evolutionary history of floras and faunas, and the sources of many different economic commodities, such as hydrocarbons, precious metals and gemstones (e.g. Greenhalgh, 1985; Partridge, 1998; De Wit, 1999; Moore and Larkin, 2001; Milesi et al., 2006; Moore, 2009).

Investigations of continental-scale drainage evolution and sediment provenance over the last few decades have proven invaluable for understanding many first order geologic questions. Indeed, tectonics and climate are the main drivers of landscape and drainage evolution, although the changes effected by these drivers usually take millions of years to be appreciable (Whittaker et al, 2008; Armitage et al., 2011). The landscape evolution of Africa has long captured researcher's attention, starting with perhaps best highlighted by the pioneering work of King (1963) in his study of the 'African Surface', associated with denudation and uplift following the break-up of Africa from Gondwana. In northern Africa, Neogene drainage evolution has been investigated to understand the timing of East African

rifting, Afar volcanism, retreat of the Tethys Sea, past climate conditions, and paleodrainage evolution of large rivers like the Nile (e.g. Issawi and McCauley, 1992; Griffin, 2002; Goudie, 2005).

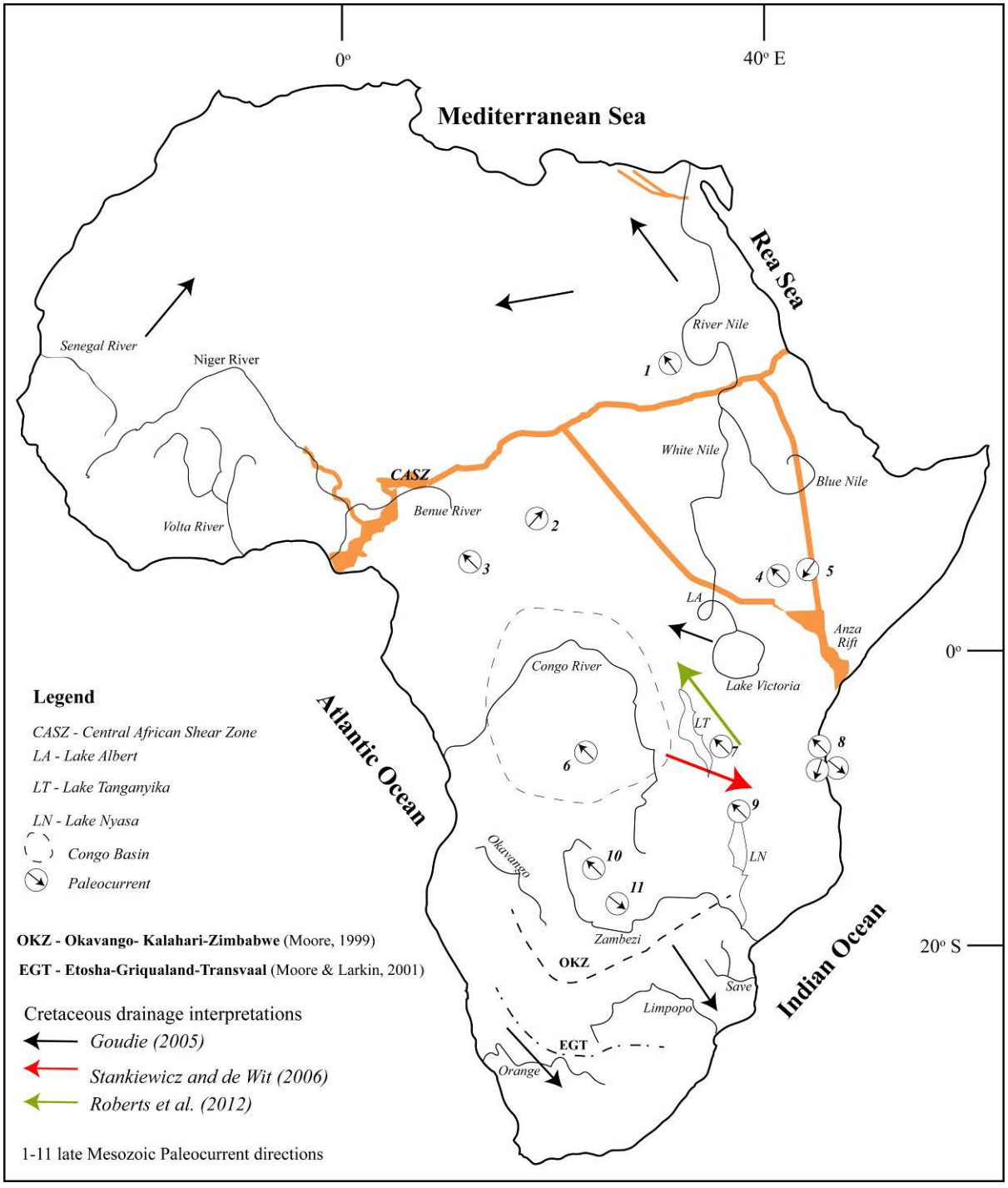

Figure 6-1. Map of Africa showing the Congo Basin, selected paleo-rivers in central Africa.

Paleocurrent directions from the Jurassic-Cretaceous units across central Africa.The data plotted here were all taken from published literature except (*6*), which was recorded in the DRC. The directions are enhanced for visual appreciation. (*1*) Paleocurrent directions from Wadi Milk and Shendi formations are from Bussert (1998). (*2* & *3*) are paleocurrent currents from the Cretaceous Mouka-Ouadda Formation and Carnot Formation as documented by Malibanger et al. (2006) and Censier and Lang (1999). (*4* & *5*) are paleocurrent directions from the Lapur and Muruanachok sandstones in Kenya as published by Morley et al. (1992) and others (see text). (*7* & *9*) are from Cretaceous Galula Formation and Dinosour Beds in Tanzania and Malawi respectively as documented by Roberts et al. (2012). (*8*) paleocurrents for the Tendaguru Formation in coastal Tanzania, published by Bussert et al. (2009). (*10* & *11*) are paleocurrent directions from the Zambezi Rift, Cabora Bassa and Mana Pools basins in Zimbabwe as documented by Shoko (1998). CASZ is after Bosworth (1992).

Considerable work has also been done in southern Africa dedicated to understanding post-Gondwanan tectonics, landscape evolution, and the configuration of modern drainage patterns (e.g. Shaw et al., 1992; Partridge, 1998; Partridge and Maud, 2000; Moore and Larkin, 2001). These researchers have made major progress in understanding the timing and location of drainage divides, and their effects on the configuration and drainage evolution of major African rivers, such as the Zambezi, Limpopo and Orange Rivers, from the Cretaceous to present times (Fig. 6-1).

By comparison with other time periods and portions of the African continent, our understanding of the late Mesozoic (Jurassic-Cretaceous) period of central Africa is much more limited (e.g. Guiraud and Maurin, 1991, 1992; Guiraud et al., 1992; Mateer et al., 1992; Wilson and Guiraud, 1992; Maurin and Guiraud, 1993; Guiraud and Bosworth, 1997; Ebinger and Sleep, 1998; Burke, 1996, 2003 Moore and Blenkinsop, 2002; Bumby and Guiraud, 2005; Guiraud et al., 2005). Drainage evolution and the configuration of late Mesozoic rivers in central Africa remains uncertain, indeed, to date only a few studies have been conducted and these have resulted in two contrasting interpretations (e.g. Stankiewicz and de Wit, 2006; Roberts et al., 2012). Better age control and stratigraphic correlations, in

addition to constraints on drainage patterns in central Africa, are critical to the understanding of the timing and controls on Jurassic-Cretaceous sedimentary basin development, paleoenvironments and drainage evolution in the sub-region. This is also of value for evaluating the potential for working hydrocarbon systems in these sedimentary basins and for improved exploration of placer deposits such as alluvial diamonds (Burke, 1996, 2003; Mathu and Davies, 1996; Censier and Lang 1999). Providing better constraints on late Mesozoic drainage and landscape evolution of central Africa are also important for investigating the ecological, evolutionary and paleobiogeographic significance of Mesozoic floras and faunas, as well as the evolution of modern African clades (Durand, 2005; Jacobs et al., 2009, 2016; Brunet et al., 1990; Mateus et al. 2010, O'Connor et al., 2006, 2010, and 2011).

To address these issues, this chapter synthesises the sedimentary provenance results presented in Chapters 2-5, along with additional new samples presented herein (see Table 6-1). Published Jurassic-Cretaceous paleocurrent data from across central Africa were also incorporated. In total, sixty-three sandstone samples from eight different basins in central Africa were investigated for framework petrography, U-Pb detrital zircon geochronology and Lu-Hf isotope geochemistry. The goal of this chapter was to: (1) summarise existing data and provide new, more robust constraints (where possible) on the age of deposition of key units in central Africa for better stratigraphic and faunal correlation, (2) document the primary provenance sources across central Africa during this timeframe as a proxy for reconstructing regional paleogeography, but in particular paleotopography and timing of uplifts; and (3) utilise this information to model source-to-sink paleo-fluvial drainage patterns of Jurassic-Cretaceous strata in central Africa. A side product and outcome of this chapter/study was the opportunity to compile an extensive database on Hf-isotopes in detrital zircons from central

Africa, and use this data to glean new insights into the tectonic and geologic history of the Precambrian basement rocks in the region, much of which are presently overlain by these cover sequences.

6.2 Background to study

6.2.1 African drainage evolution

The fluvial drainage patterns of Africa, although geologically considered youthful (Post-mid Cretaceous), are generally understood to have undergone significant changes following Gondwana break-up (Goudie, 2005). However, the drainage patterns and landscape evolution of Africa is still not very well understood (De Wit, 1999; Moore and Larkin, 2001; Goudie, 2005; Shaanan and Rosenbaum, 2018). In addition, the northern and southern portions of Africa have received considerably more attention than central Africa. These efforts have mainly been devoted to understanding Mesozoic and Cenozoic drainage evolution, with much of the focus on the relative roles of mantle plumes (hot spots) versus far-field stresses on the development of African paleogeography, landscape evolution and paleo-drainage patterns (e. g. King 1963; Burke and Dewey, 1973; Partridge and Maud, 1987; Thomas and Shaw, 1988; Cox, 1989; White and McKenzie, 1989; Shaw et al., 1992; Ebinger and Sleep, 1998; Burke, 1996: Burke et al, 2003; Partridge, 1998; Moore and Larkin, 2001; Moore and Blenkinsop, 2002; Goudie, 2005; Moore et al., 2009).

During continental breakup (e.g. Gondwana), river systems initially tend to flow away from uplifted domes created by rising mantle plumes (King, 1963; Cox, 1989; White and McKenzie, 1989). The theory of topographic changes resulting from rising mantle plumes and its influence on drainage patterns is largely accepted (e.g. Cox, 1989), however, the

simplification of mantle plume effects on drainage evolution without accounting for the role of tectonics and climate (Summerfield, 1991) is problematic. Moore and Blenkinsop (2002) for instance, argued that modern drainage systems of southern Africa can be better explained by taking into account the structural controls related to far-field stresses of post-Gondwana. The break-up of Gondwana during Mesozoic caused significant changes in many drainage and paleo-river systems in Africa (Moore and Larkin, 2001; Goudie, 2005; Stankiewicz and de Witt, 2006; Moore et al., 2009). The links between the Limpopo River and the Okavango, Cuando and the upper Zambezi rivers in southern Africa for instance, have been argued to have been severed as a result of crustal flexuring due to rifting (Moore and Larkin, 2001).

The source and drainage patterns of Mesozoic to Cenozoic paleo-rivers of in central Africa still remains unresolved (e.g. Stankiewicz and de Wit, 2006; Roberts et al., 2012). Drainage patterns are especially complicated by the interpretations by different researchers. Moore and Larkin (2001) in their work on the drainage evolution of south-central Africa, for example identified three major river systems (Zambezi, Save and Limpopo) that drained the central and southern parts of Africa during the Jurassic and Cretaceous. Of these, one is interpreted to have flowed into the Okavango inland delta and the others into the Indian Ocean via the Save River drainage near the present day Zambezi mouth. The Zambezi and Okavango rivers are also documented to have drained eastward during Mesozoic to Recent times (Moore and Larkin, 2001; Moore et al., 2007). The eastward drainage of both the Zambezi and the Okavango rivers is consistent with the paleodrainage patterns of Central and East Africa identified by Stankiewicz and de Wit (2006). Their investigations of drainage patterns in Central and East Africa, based on tracing of putative Cretaceous peneplains also led them to hypothesize an east draining paleo-Congo River that emptied into the Indian Ocean via the Rufiji delta. Stankiewicz and de Wit (2006) also suggested that this occurred

after the Congo Basin was uplifted above sea level during the Late Cretaceous due to rifting associated with Gondwana breakup and West-Central African Rift systems. They posited that the east flowing paleo-Congo River only changed to its present flow direction (eastward) during the Eocene to Oligocene when uplift from the East African Rift System obstructed its path.

6.2.2 Tectonics, age control and stratigraphic correlation

The age and style of major tectonic and magmatic events are important in plate tectonic reconstructions. Today the East African and Southern African Plateaus are major features of the African landscape, however the timing and origin of these anomalously high tectonic features have been the subject of considerable focus (e.g. Quennel, 1960; Nyblade and Robinson, 1994; Ebinger et al., 1999; Doucouré and de Wit, 2003; Lana et al., 2003; Nyblade and Sleep, 2004; Ebinger, 2005; Burke and Gunnell, 2008; Flowers and Schoene, 2010; Erlanger et al., 2012). Although the timing of uplift is still debated, most researchers have suggested that the landscape of pre-Mesozoic Africa was relatively flat and low-lying with highs associated with Pan-African Orogenesis (e.g. King, 1963; Doucoure and de Wit 2003). Greater differentiation between Africa's geologic history related to mantle plume and those related to plate tectonics is needed to further resolve the evolution of its topography (Doucoure and de Wit 2003). Plate tectonics, climate and landscape evolution share an important relationship and they play an important role in sedimentation, which is directly linked to climate and erosion (Leeder, 1991; Summerfield, 1991; Bishop, 1995). The key events in the development and setting of African drainage systems include the Karoo volcanism (~181 Ma) opening of the Indian Ocean, the opening of the south Atlantic, associated with the Parana-Etendeka volcanism (~120 Ma) and the final separation of Africa

from South America (e.g. Renne et al., 1996; Moore and Blenkinsop, 2002; Goudie, 2005). The mechanics of these events are beyond the scope of this study and have been discussed extensively by other researchers elsewhere, however this study does have the potential to shed light on the timing and location of uplift related to these and other events.

Most of the previous studies on drainage evolution and paleo-river paths in Africa are mainly based on concepts of long-lived erosion surfaces and present-day geomorphology (e.g. King 1963; Partridge and Maud, 1987; Moore and Larkin, 2001; Stankiewicz and de Wit, 2006; Key et al., 2015). The concept of long-lived fluvial drainage patterns and networks has major implications for understanding the evolutionary and ecological history of the African continent. Long-lived fluvial drainage patterns and networks are useful for understanding patterns of paleobiogeography. Such large, long-lived, trans-continental river systems are important because they could have served as migration corridors for the movement of flora and fauna (Moore and Larkin, 2001; Goudie, 2005; Schreve et al., 2007; Roberts et al., 2012). These large river systems are also responsible for long-distance transport of placer minerals including alluvial diamonds (Marshall and Baxter-Brown, 1995; de Wit, 1999; Patyk-Kara, 2002; Moore and Moore, 2004, 2006), as well as the development of hydrocarbon reservoir facies and downstream lacustrine source rocks (Bosworth, 1992; Burke, 1996, Burke et al, 2003). Hence, the reconstruction of ancient river drainages has significant economic implications.

Poor stratigraphic control of many continental sedimentary units in central Africa has limited the ability to trace and correlate Mesozoic beds. Lack of geological data (e.g. detailed facies, detrital zircons, and paleocurrents data) for many areas, the relative inaccessibility, deep surficial weathering and dense vegetation found across much of central Africa has limited our ability to understand its sedimentary provenance (Daly et al, 1992; Giresse, 2005;

Kadima et al., 2011; Buiter et al., 2012; Linol, 2013). This is particularly true for poorly indurated Jurassic and Cretaceous strata, for which exposures are extremely limited, and very little detailed sedimentologic investigation across central Africa has been performed since the early colonial geological survey investigations in the early to mid-1900's (Daly et al, 1992; Giresse, 2005). Over the last few decades however, many new Cretaceous fossil discoveries have been made in places like Cameroon, Angola, Malawi, Kenya and Tanzania (e.g. Jacobs et al., 2009; Brunet et al., 1990; Mateus et al. 2010, O'Connor et al., 2006, 2010, and 2011), and placing these faunas within a more reliable temporal and environmental context will have broad faunal and paleobiogeographic implications.

Thomas and Shaw (1988) conceded the difficulty of directly dating drainage changes. They noted the critical link between drainage development and stratigraphic units, but also highlighted the speculative way ages of sediments are sometime assigned. Advances in U-Pb detrital zircon geochronology over the last two decades have enhanced this approach as a critical tool for solving many geologic problems, particularly in the fields of stratigraphy, sedimentary provenance analysis and tectonics (Fedo et al., 2003; Anderson, 2005; Link et al., 2005; Dickinson and Gehrels, 2009; Carrapa, 2010; Cawood, et al., 2012; Gehrels, 2012; 2014). Many authors have demonstrated the applicability of detrital zircon geochronology for addressing stratigraphic, economic and tectonic questions in Precambrian-Recent strata of southern Africa (e.g. Fildani et al., 2009; Mckay et al., 2015) However, its application to solving similar questions in central Africa largely remains untested.

6.3 Geological overview of Central Africa

Africa was part of Gondwana that also included South America, Arabia, India, Madagascar, Australia and Antarctica, which begun breaking up from 550 Ma up until about

180 Ma (Gratham et al., 2003; Gray et al., 2007). Africa consist of several Archean-Paleoproterozoic cratons (Fig. 6-1), which are mainly surrounded by Proterozoic-early Paleozoic (Pan-African) mobile belts and covered by sedimentary basins of Phanerozoic age in most places (e.g. Kröner and Stern, 2005; Begg et al., 2009; Iizuka et al., 2013). This section summarises the main geologic terranes in central Africa with emphasis on their age and tectonic evolution.

The principal cratonic blocks underlying central Africa are the Congo-Kasai Craton (central & west), Tanzania Craton (eastern) and Zimbabwe Craton (extreme south) as shown in Figure 6-2. These cratons are surrounded by Proterozoic mobile belts. The Congo-Kasai Craton of central Africa, extends from Angola through the Democratic Republic of Congo (DRC) into South Sudan, and is mostly surrounded by Pan-African age mobile belts on its margins (e.g. De Wit and Linol, 2015). The age of the Congo-Kasai Craton ranges from ~4000 Ma to 2200 Ma and is mostly composed of reworked crustal rocks (Cahen et al., 1984; Walraven and Rumvegeri, 1993; De Carvalho et al., 2000; De Wit and Linol, 2015; Jelsma et al., 2015). The Congo-Kasai Craton underlies the Congo Basin, which is one of the largest intracratonic sedimentary basins in the world (Daly et al., 1992; Kadima et al., 2011). The Tanzania Craton, extends from central Tanzania to western Kenya and into southeast Uganda. The Tanzania Craton comprises a high grade metamorphic terrane and a low grade granite-greenstone terrane (Clifford, 1970). The age of Tanzania Craton ranges from ~2900 Ma to 2500 Ma (Borg and Shackelton, 1997; De Waele, 2005).

The Proterozoic belts of central Africa have ages ranging from ~2200 Ma to ~500 Ma, and they are important sources of sediments for basins across the region (e.g. Linol et al., 2016). Episodic deformation on the margins of the cratons have resulted in repeated cycles of uplift and erosion in these belts, which provide semi-continous sediment sources for

Proterozoic-Recent basins (e.g. Milesi et al., 2006; Batumike et al., 2009; Link et al., 2010; Boniface et al., 2012). The Proterozoic belts are grouped into the Paleo- to Mesoproterozoic and Neoproterozoic (Pan-Africa mobile belts). The main Paleo- to Mesoproterozoic belts in central Africa includes; the Magondi Belt (~2200-1660 Ma), Ubendien Belt (1800 Ma), Usagaran Belt (2000-1800 Ma), and Bangweulu Block (1800 Ma), Irumide Belt (1400-1000), Kibaran Belt (1400-1100 Ma) (e.g. Daly, 1986; Leyshon, 1988; Treloar and Kramers, 1989; M ller et al., 1995; Majaule et al., 2001; McCourt et al., 2001; Link et al., 2010; Boniface et al., 2012). The Neoproterozoic mobile belts mainly resulted from the Pan-African orogenesis (Kennedy, 1964), an amalgamation of continental domains between 850 Ma and 550 Ma (Kröner and Stern, 2005). The ages and the tectono-thermal evolution of these Pan-African mobile belts have been documented and summarized by Kröner and Stern (2005) and others (e.g. Begg et al., 2009). There are two broad types of Pan-African mobile belts, (1) mainly supracrustal and magmatic, mostly juvenile mantle derived and 2), polydeformed high-grade metamorphic assemblages, that resulted from the reworking of older Archean to Mesoproterozoic crust (Kröner and Stern, 2005). The main Neoproterozoic belts in central Africa are, the Zambezi Belt (1100 Ma and 550 Ma), the Damara Belt (1000-450 Ma), the Lufilian Belt or Arc (550 Ma), the Mozambique Belt (650-500 Ma), the Arabian-Nubian Shield (1000-600 Ma) and the West Congo Belt (~550 Ma) (e.g. Kröner, 1982; Cahen et al., 1984; Pin and Poidevin, 1987; Hanson et al., 1988; Stern, 1994; Möller et al., 1995; Kröner et al., 1997; Goscombe et al., 2000; Muhongo et al., 2002; Stern, 2002; Kröner and Stern, 2005; Begg et al., 2009).

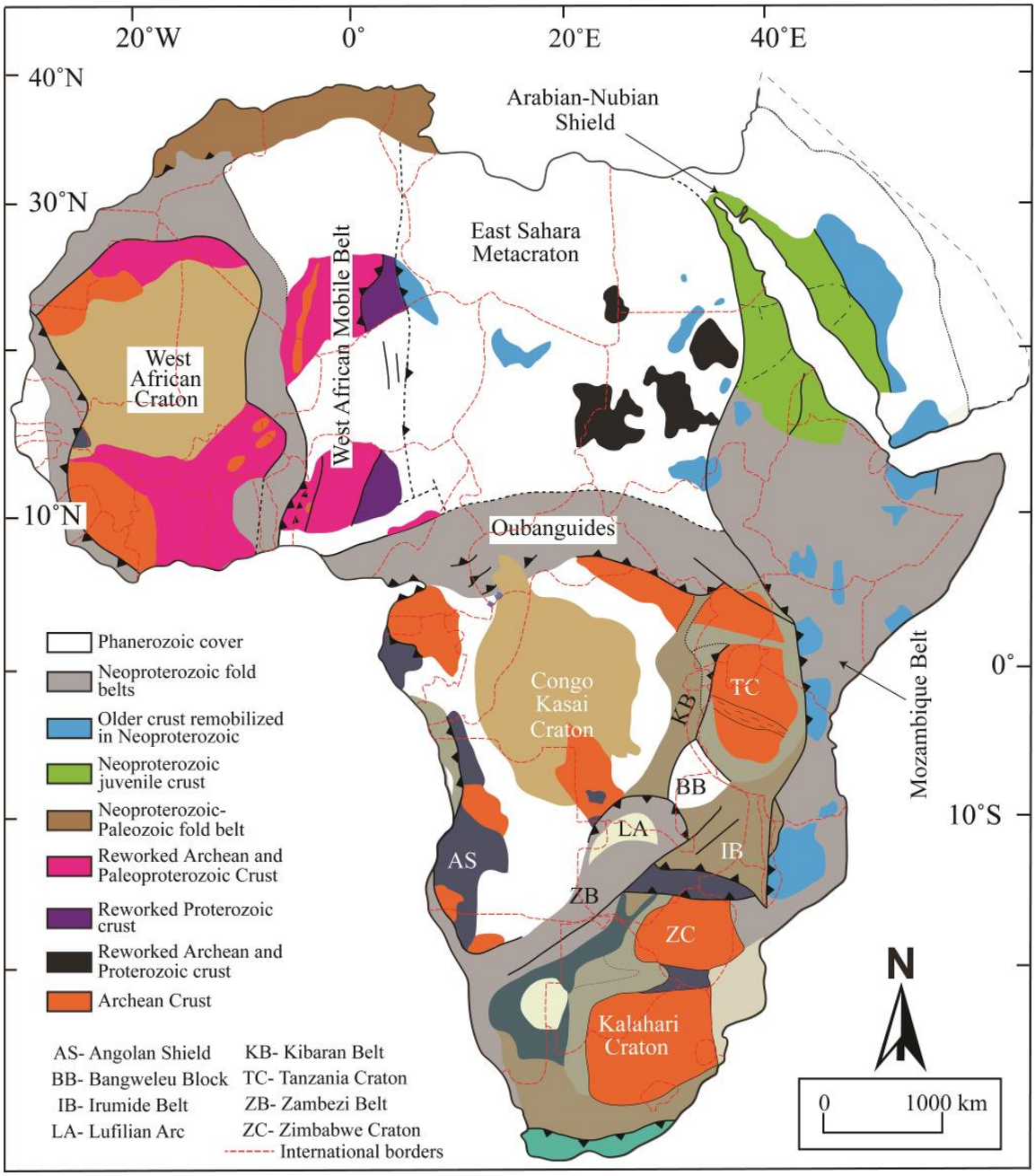

Figure 6-2. Bedrock map of Africa showing the main basement complexes after Begg et al. (2009).

6.3.1 Overview of late Mesozoic tectonics of Central Africa

Different timescales herald different tectonic regimes. The Triassic was predominantly marked by extensional tectonics, climatic warming and epicontinental sea transgression

associated with supercontinent break-up of Panagea. This was followed by rifting and blocks development in the Jurassic (Guiraud et al., 2005). Global transgression of epicontinental seas over Arabia and eastern Africa, possibly extending inland as far as the Congo Basin during Late Jurassic (Sahagian, 1988, 1993; Guiraud et al., 2005; Stankiewicz and de Wit, 2006). Renewed rifting began again in the earliest Cretaceous associated with separation of Africa and South American (Fairhead and Binks, 1992). Far-field stresses during this time led to renewed subsidence within large intracratonic basins across central and western Africa, as well as in smaller rift basins, which were punctuated by periodic compressional tectonic events during the Late Cretaceous times that resulted in folding and basin inversions, followed by renewed rifting through Niger, Chad, the Central African Republic (CAR) and Cameroon (Fairhead, 1988; Bosworth, 1992; Guiraud et al., 2005; Fairhead et al., 2013).

Mesozoic to Cenozoic tectonic history of central Africa is dominated by the breakup of the continents (Fairhead, 1988; Bosworth, 1992; Guiraud et al., 2005). The two main rift systems in central Africa, which are believed to have resulted from the breakup of the continents are the Mesozoic Central African Rift and the Cenozoic East African Rift, although the uniqueness of each system is still debated (e.g. Browne and Fairhead, 1983; Bosworth, 1992; Chorowicz, 2005; Nutz et al. 2017). For example, rift systems from central Sudan to southern Kenya are considered to be part of the same system (Bosworth, 1992; Thuo, 2009). Detailed discussion on the East African Rift System has been presented elsewhere by Chorowicz (2005) and summarized in Chapter four of this thesis. The tectonics of central Africa is documented by widespread and sporadic periods of rifting, compression, subsidence and partial inversion along the Central African Rift System (CARS) (Guiraud et al., 2005). The CARS extends from the Benue Trough in Nigeria through to the Anza Basin in Kenya, and is marked by the deposition of thick continental series under alternatively extensional and trans-

tensional stress fields, which are also believed to have caused the development of the West and Central African shear zones (Fairhead, 1988; Bosworth, 1992). These tectonic episodes are believed to be temporally related to similar tectonic and basin filling events recorded in other parts of central Africa, most notably in the Congo Basin, the Turkana Rift (Kenya), the Rukwa Rift (Tanzania), the Cabora Bassa Basin (Zimbabwe), and the Mid-Zambezi and Mana Pools basins (Zimbabwe), and the Sudan Rifts (Fig. 6-3).

6.3.2 Stratigraphy of key late Mesozoic deposits in central Africa

Continental late Mesozoic sedimentary deposits are common in western, central and north eastern Africa (*see* Mateer et al., 1992 *for discussion*). The separation of Africa from South America led to both uplift and subsidence in many parts of central Africa, thus playing a critical role in: (1) the evolution of intracratonic sedimentary basins; (2) the development of working hydrocarbon systems; and (3) erosion, transport and redeposition of alluvial diamonds from syn-genetic kimberlite sources, making some of these units of great economic importance (e.g. Bosworth, 1992; Mateer et al., 1992; Burke et al., 2003). Some of these sedimentary deposits have also served as important achieves for continental vertebrate fossils, and have provided critical context for understanding the paleobiogeography and evolution of Gondwanan vertebrates, as well as some modern vertebrate clades (e.g. Durand, 2005; Jacobs et al., 2016).

Dinosaur fossils, in particular, have been recovered in central Africa from the Rukwa Rift and Madawa basins (Tanzania), the Sudan Rifts, the Malawi Rift, the Mid Zambezi and Cabora Bassa basins (Zimbabwe), and Turkana Rift (Kenya). Alluvial diamonds and diamondiferous kimberlite diatremes have also been discovered and exploited in the Carnot and Mouka Ouadda formations in the Northern Congo Basin (Central Africa Republic), in the Kwango (southwest) and Kasai (southeast) portions of the Congo Basin (Democratic

Republic of Congo), and in the Cassenge Graben (Angola). Hydrocarbon exploration is also on the increase in the Sudan Rifts, Turkana Rift, Rukwa Rift Basin, Zambezi Rift, and the Cuvette Centrale of the Congo Basin (Furon, 1963; Bosworth, 1992; Morley et al., 1992; Thuo, 2009; Purcell, 2014, 2017).

In summary, the late Mesozoic of central Africa is now well documented in regards to mineral resource and paleontologic significance, however, the stratigraphic and temporal context of these deposits and localities has remained a key impediment to understanding their significance and origins. In this thesis, key Jurassic and Cretaceous sedimentary units of economic or paleontologic significance were selected from across central Africa in an attempt put better constraints on their age and sedimentary provenance. The stratigraphy of the selected sedimentary units in central Africa are presented in Figure 6-3.

6.4 Sampling and Analytical Methods

As discussed above, the selection of study locations and samples in central Africa were based mainly on a reflection of economic or paleontologic significance of the deposits, followed by the availability of sufficient geologic or geochronologic information. Detrital zircon samples were selected from continental sedimentary basins either from borehole core cuttings from Kasai-Congo Basin of DRC (Chapter 2) and from the Cassenge Graben of Angola (Chapter 3), or from outcrop exposures in Turkana Basin of Kenya (Chapter 4), the Sudan Rifts of Sudan (Chapter 5), Mid-Zambezi Basin, Mana Pools Basin, Cabora Bassa Basin (Zimbabwe), Madawa Basin (Tanzania), and Malawi Rift. Detailed sampling, analytical methodology and results are presented in chapters' 2-5 of this thesis. In addition to the samples reported in earlier chapters, additional work is presented below on

Cretaceous/Jurassic samples from the northern Malawi Rift, the Zambezi Valley and coastal Tanzania. The sampling and analytical approaches follow those presented for the other results, and only the locality information and results are presented in this chapter. Additional details and full analytical results are available in the appendices.

Due to the vegetative nature in central Africa, paleocurrent data is limited for many of these study localities. The paleocurrent data presented in this chapter were mostly taken from published literature, where details on the number of measurements and data is commonly limited (e.g. Turkana Basin, Kenya). No paleocurrent data is available on the Calonda Formation (Angola) and only a small suite of paleocurrent directions (n = 9) was recorded in the field on the Kasai Sandstones (DRC). All paleocurrent data are plotted in Figure 6-1.

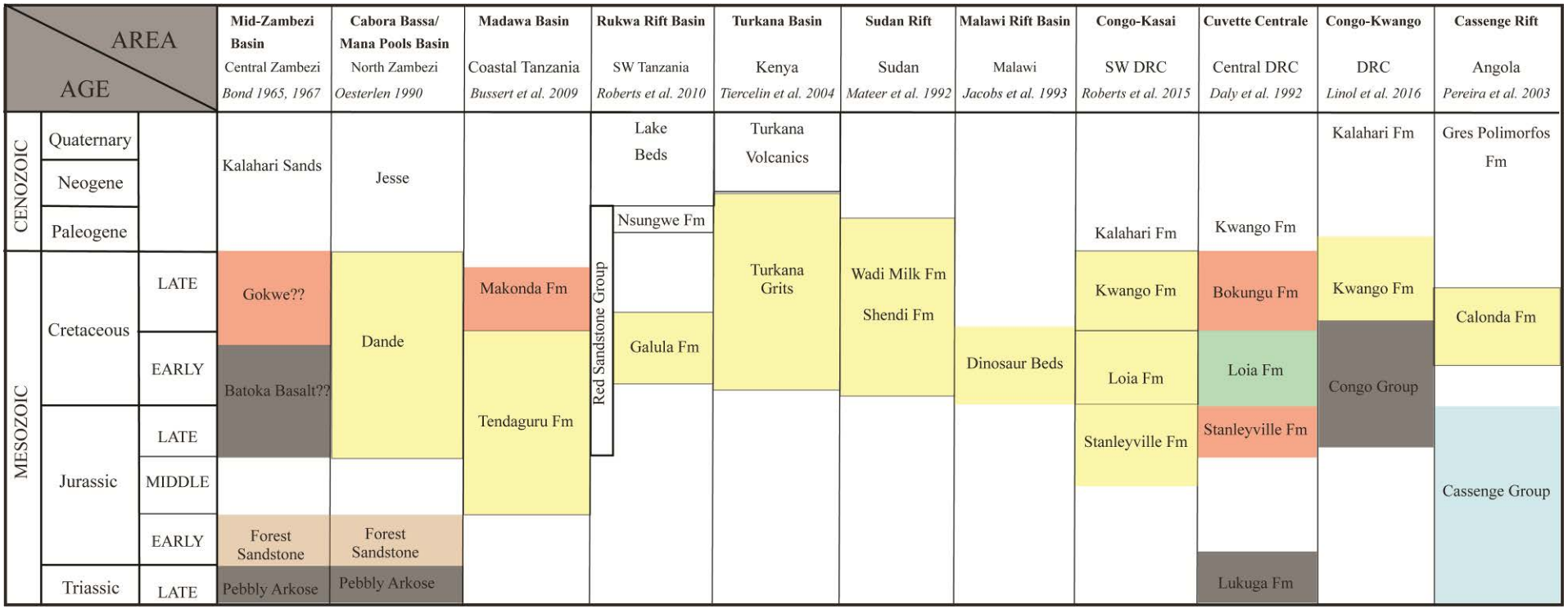

Figure 6-3. Simplified stratigraphic chart of selected late Mesozoic units in central Africa.

Some of the samples were selected from the units highlighted in pale yellow. Additional samples from Cretaceous-Jurassic sedimentary units of the Zambezi Valley in Zimbabwe (x5), the northern Malawi Rift Basin (x1), and from syn-rift deposits along the Tanzania coast (x1). In addition, published sedimentary provenance data from the Rukwa Rift Basin (x4), and Kwango region and Cuvette Centrale of the Congo Basin (x3) added to the data already presented in chapters 2-5 for synthesis.

6.5 Results and interpretations

6.5.1 Provenance data compiled from previous studies

6.5.1.1 Paleocurrent data

Paleocurrent data gleaned from the literature are plotted in Figure 6-1. Published late Mesozoic paleocurrent data were recorded in Cretaceous strata of Central African Republic compiled by Censier and Lang (1999) for the diamond-bearing Carnot Formation in the southwest, and the diamond-bearing Mouka-Ouadda Formation in the northeast of the country (Malibangar et al., 2006). Censier and Lang (1999) documented NNW paleocurrent directions (n = 580) from different lithostratigraphic levels of the Carnot Formation. They interpreted the Carnot Formation as deposited by a north-westerly braided river system that flowed out of the Congo Basin through CAR into the Doba Trough of the Central African Shear Zone (CASZ). Malibangar et al. (2006) also recorded NNE–NE paleocurrent data from the Mouka-Ouadda Formation, which they believed were sourced from rivers flowing out of the Congo Basin from the south. The number of recorded paleocurrents is not available for the Mouka-Ouadda Formation.

In Kenya, paleocurrent directions for the Turkana (Kenya) Rift are those reported by various authors including McGuire et al. (1985), Williamson and Savage (1986), Morley et al. (1992, 1999), Wescott et al. (1993), Tiercelin et al. (2004) and Thuo (2009) from Cretaceous strata. Most of these authors however, did not document the number of measurements. The paleocurrents from Kenya are variable but generally favour north-northwesterly transport (e.g. McGuire et al., 1985; Thuo, 2009; Muia, 2015). The few paleocurrent data from the Turkana Basin with reported number of measurements include the

Lariu Sandstone (n = 18) and the Sera Iltomia Formation (n = 41), and these are dominantly north directed (Williamson and Savage, 1986; Morley et al., 1992; Wescott et al., 1993).

Paleocurrent measurements (n = 278) from the Rukwa Rift Basin presented by Roberts et al. (2012) suggest Cretaceous rivers were mainly flowing in a north westerly direction along the axis of the Rukwa Rift from the highlands in the south. These authors also presented paleocurrent data from the northern part of the Malawi Rift Basin (Dinosaur Beds), which suggest that some flow was directed NE directly out of the Luangwa Rift and converged with a major trunk river system that flowed NW into the Rukwa drainage system. Although a recent study by Key et al. (2015), have found evidence that suggests that the Luangwa maintained a southwesterly flow from upper Permian times (e.g. Banks et al., 1995). These findings suggest the so-called drainage divide may be near the Luangwa Valley area.

Paleocurrent data from the coastal Tendaguru Formation in the Madawa Basin reported by Bussert et al. (2009), are quite variable. This variability in currents is believed by Bussert and Aberhan (2004) to have resulted from a tsunami-related genesis as revealed by the muddled mixture of both marine and continental clasts, and evidence of opposite paleocurrent directions. Paleocurrent data from Mid-Zambezi/ Mana Pools basins (Zimbabwe) and the Cabora Bassa Basin (Zimbabwe/Mozambique) in the Zambezi Valley are quite variable (e.g. Oesterlen & Millstead, 1994; Key et al., 2015). Paleoflow during the Jurassic was primarily directed towards the centre of the Zambezi rift system, possibly into an internally draining lake system, which may have had an outflow to the south, although it has been found to westerly directed during the Triassic (Oesterlen & Millstead, 1994). During the Cretaceous, fluvial systems dominated and it appears that most drainage out of the Mana Pools and Mid –Zambezi rifts was directed southwards, whereas flow in the Cabora Bassa

was more dominantly north (Shoko, 1998; E. Roberts, unpublished data). Paleocurrents (n = 221) taken on Jurassic-Cretaceous aeolianites from the Cuvette Centrale and the Kwango Group in the Congo Basin (DRC) by Linol (2013) and Linol et al. (2016) suggest that paleowind directions during this time were mainly to the southeast and southwest. The few measurements by Linol et al. (2016) from fluvatile deposits indicate that coeval rivers dominantly flowed to the west/northwest at this time.

6.5.1.2 U-Pb geochronology and Age spectra

All the U-Pb detrital zircon results, apart from those presented in chapters 2-5, are summarized in Figure 6-4 and listed in the supplementary tables. Three Cretaceous samples from the aeolian red sandstones of the Lower Kwango Group in the Congo Basin, published by Linol et al. (2016) were incorporated in this study. U-Pb detrital zircon results (n = 167), two from the Dekese core (D470 & D600) in the Cuvette Centrale and one sample (WP19) from the Kwango area of the (Congo Basin, DRC) presented by Linol et al. (2016) were also incorporated (Fig. 6-4a). The ages of zircons from the three samples from Linol et al. (2016) range from Mesoarchean (~3133 Ma) to Late Jurassic (~192 Ma), with a dominant Meso- to Neoproterozoic age population. Cumulative (K-S test, Table 6-1a) and the normalized age probability plots (Fig. 6-4a) show the similarities and differences between the samples.

Three samples analysed from the Jurassic-Cretaceous Tendaguru Formation yielded zircon grains (n = 195) with ages ranging from Neoarchean (~2738 Ma) to late Permian (~258 Ma), with a dominant Meso- to Neoproterozoic age component (Fig. 6-4b). The K-S test results (Table 6-1b) and the normalized age probability plots presented also show the similarities between the samples. The ages of zircon populations from the Tendaguru

Formation are consistent with source rocks with the Mozambique Belt of Tanzania (e.g. Muhongo et al., 2001).

Published detrital zircon data by Roberts et al. (2012) from one sample of the Lower Cretaceous Mtuka Member (TZ2-UT) and three samples (TZ71706, TZ71406 & TZ7/7) from the mid-Upper Cretaceous Namba Member of the Galula Formation in the Rukwa Rift Basin were also included (Fig. 6-4c). The age of zircon grains from the Galula Formation range from Mesoarchean (~2850 Ma) to Late Jurassic (~156 Ma). The K-S test results (Table 6-1c) and the normalized age probability plots presented here (Fig. 6-4c) show similarities between the mid-Upper Cretaceous Namba Member, and is suggestive of a common provenance. A single sample analysed from the Lower to middle Cretaceous Dinosaur Beds of Malawi (Fig. 6-4d), yielded zircon grains with ages ranging from Paleoproterozoic (2483 Ma) to Early Paleozoic (505 Ma), also with a dominant Meso- to Neoproterozoic age component.

Samples from the late Mesozoic strata of Zimbabwe include the Lower Cretaceous Kadzi Formation from the Cabora Basin, the Lower Cretaceous Dande Formation sample from the Mana Pools Basin, the Jurassic Vulcanodon beds and Entumbe Formation samples are from the Mid-Zambezi Rift. The ages of zircons from the Zimbabwe samples (Fig. 6-4e) range from Mesoarchean (2991 Ma) to Early Cretaceous (141 Ma), with a dominant Meso- to Neoproterozoic age component. The cumulative (K-S test, Table 6-1d) and normalized probability plots shows some similarities between samples from Cretaceous Dande and Kadzi formations. Significant differences are also observed between the other samples (Fig. 6-4), which probably support the different paleocurrent directions for this part of the study area.

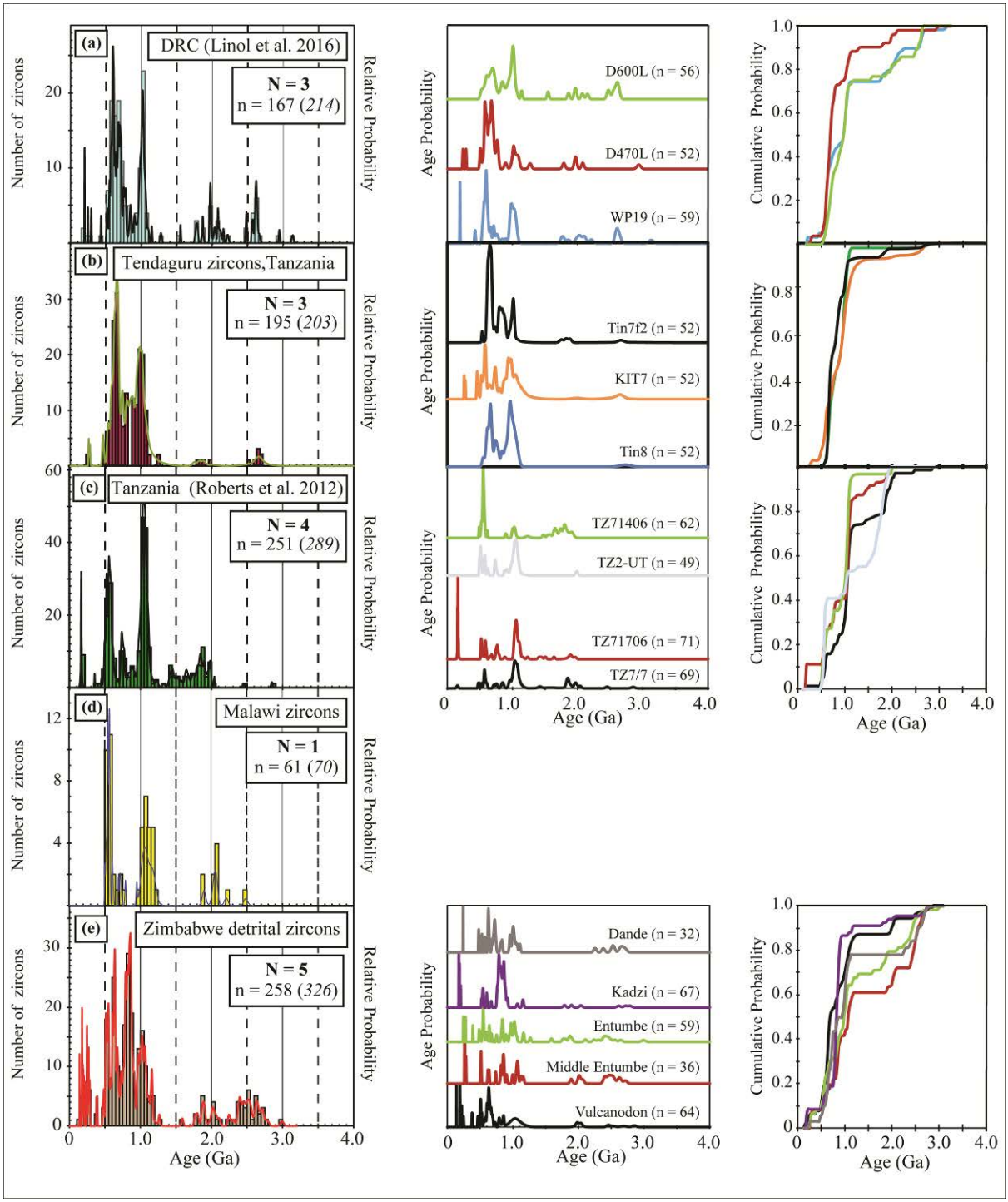

Figure 6-4. Probability density plot and, corresponding age and cumulative probability plots not reported previously. Plots from the U-Pb detrital zircon data not reported in chapters 2-5. N is the number of samples analysed for a particular plot. n = x (*y*) shows the number of analyses for each area. 'x' is the number of concordant analyses, whereas '*y*' is the total number of analyses for each plot. The number shown on the age probability plots are concordant analyses only. Data for these plots are presented in the supplementary tables as digital appendices. (a).

Data from the Cuvette Central and Kwango area of the Congo Basin, published by Linol et al. (2016). (b). Three samples analysed from the Tendaguru Formation as part of this study. (c). Data from the four samples from the Cretaceous Galula Formation from the Rukwa Rift Basin, published by Roberts et al. (2012). (d). One sample analysed from the Cretaceous Dinosaur Beds of Malawi as part of this study. (e). Data from the Zambezi Rift, Cabora Bassa and Mana Pools basins in Zimbabwe (pers comm. E. Roberts).

Table 6-1. K-S Test results for new and published detrital samples incorporated in this study

(a).P values for three samples from the Cuvette Centrale and Kwango areas of the Congo Basin (Linol et al., 2016)

	WP19	D470L	D600L
WP19		0.021	**0.222**
D470L	0.021		0.001
D600L	**0.222**	0.001	

(b).P values for three samples from the Tendaguru Formation

	Tin8	KIT7	Tin7f2
Tin8		**0.272**	**0.075**
KIT7	**0.272**		0.026
Tin7f2	**0.075**	0.026	

(c).P values for four samples from the Galula Formation, Rukwa Rift Basin (Roberts et al., 2012)

	TZ7/7	TZ71706	TZ71406	TZ2-UT
TZ7/7		**0.164**	0.043	0.049
TZ71706	**0.164**		**0.475**	0.002
TZ71406	0.043	**0.475**		0.000
TZ2-UT	0.049	0.002	0.000	

(d).P values for five samples from the Zimbabwe

	Vulcanodon	MiddleNtumbe	Entumbe	Kadzi	Dande
Vulcanodon		0.008	0.034	0.000	**0.209**
MiddleNtumbe	0.008		**0.549**	0.000	**0.201**
Entumbe	0.034	**0.549**		0.000	**0.831**
Kadzi	0.000	0.000	0.000		0.007
Dande	**0.209**	**0.201**	**0.831**	0.007	

Kolmogorov-Smirnov (K-S) statistical test for samples from the Cuvette Central, DRC (Linol et al., 2016), Tendaguru Formation (*this study*), Galula Formation, Rukwa Rift Basin, Tanzania (Roberts et al., 2012) and the Mana Pools and Mid-Zambezi Rift Basins, Zimbabwe (*this study*). The bold p-values are > 0.05, which indicates that these samples passed the K-S test, suggestive of a similar provenance for all eight samples. The p-values < 0.05 means they failed the K-S test.

6.5.1.3 Lu-Hf isotope geochemistry and Crustal Evolution

Limited Lu-Hf data from late Mesozoic central Africa is available, except for data presented in previous chapters from DRC, Angola, Kenya, and Sudan. The initial εHf (t) values of zircons from the Tendaguru Formation (n = 69) analysed as part of this study range from –30.4 to + 11.5, and they are divided into 59% positive and 41% negative values (Fig. 6-5a). The published Lu-Hf data on Africa that is incorporated into this study is from Belousova et al. (2010) and Iizuka et al. (2013). Belousova et al. (2010) studied the evolution of the continental crust on a global scale by continents including Africa, by investigating Hf isotopic data from detrital zircons. The Lu-Hf data of Africa presented by Belousova et al. (2010) have initial εHf (t) values ranging from –41.4 to + 18.9, which are divided into 59% positive and 41% negative values (Fig. 6-5b) shows that the African continental crust is generally dominated by a juvenile mantle. In contrast, the Lu-Hf data from modern river sands from five major African rivers compiled by Iizuka et al. (2013) are dominated by sources of reworked crust, with initial εHf (t) values ranging from –30.5 to + 12.7, which are divided into 39% positive and 61% negative values (Fig. 6-5c). Both data from Belousova and Iizuka were not sourced from late Mesozoic sedimentary units but are included in this study for comparison with the Hf data generated from detrital zircons recovered from late Mesozoic continental sedimentary units in an effort to delineate crustal evolution trends in the African continent.

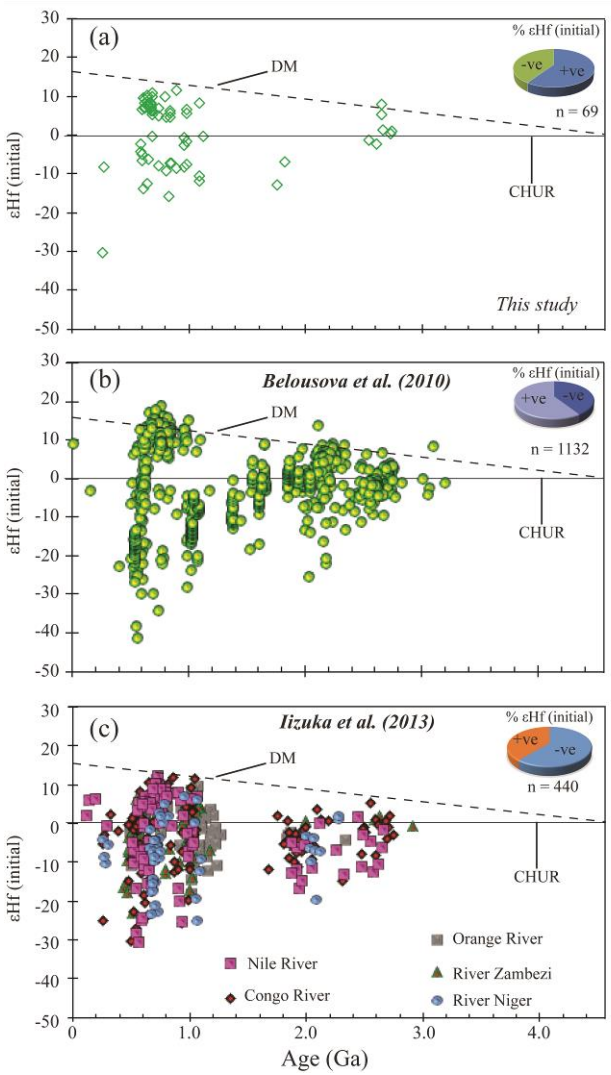

Figure 6-5. Plot of initial εHf values vs U-Pb age of zircons from Africa.

(a). Hf data from detrital zircon grains recovered from the Tendaguru Formation as part of this study. This plot shows that the Tendaguru Formation samples were predominantly sourced from juvenile mantle provenance. (b). Hf data taken from Belousova et al. (2012) on the growth of the continental crust. The results of this plot, which is dominated by positive values is generally consistent with that of Tendaguru Formation of Tanzania. (c). The Hf results from five major African rivers presented by Iizuka et al. (2013) shows that the sources of these modern river sands were mainly from the reworked crust with minor input from the juvenile mantle. (The depleted mantle (DM) evolution curve is for linear evolution from a Chondritic Uniform Reservoir (CHUR) value at the Earth's formation (i.e., 0 at 4.56 Ga) to εHf(t) = 17 at the present for the DM [Dhuime et al., 2011]). The mass spectrometer cup configuration for the Tendaguru Formation sample analyses is shown in the supplementary tables. The ^{176}Lu decay constant of 1.867 ± 0.008 x 10^{-11} $year^{-1}$ reported by Söderlund et al. (2004) and the Chondritic Uniform Reservoir (CHUR) values of ^{176}Hf/^{177}Hf (0.282785) and ^{176}Lu/^{177}Hf (0.0336) reported by Bouvier et al. (2008)

6.5.2 Provenance data from this study

6.5.2.1 Summary of U-Pb geochronology results from Chapters 2-5

A total of 4712 U-Pb analyses are plotted in Figure 6-6 and reported in supplementary sheets as appendices. This data includes those from chapters 2-5 and the new U-Pb age data presented in this chapter in section *4.1.2*. The U-Pb age data presented in the previous four chapters are summarized here and plotted as part of Figure 6-6. The age of zircon grains from 15 detrital samples taken from the Jurassic and Upper Cretaceous samples from the Kasai sandstones (Chapter 2), range from Paleoarchean 3.3 Ga to Late Cretaceous (77 Ma), but dominated by Proterozoic and Archean sources. The ages of zircons from the DRC are grouped into five main populations (Figs. 2-6, 2-8 and 6-6), and the cumulative (K-S test) and the normalized age probability density plots from these samples (N = 9) highlights strong differences between them (Figs. 2-9 and 2-10). The ages of zircons from four middle Cretaceous Calonda Formation samples from Angola (Chapter 3) range from Mesoarchean (3000 Ma) to Late Cretaceous (77 Ma), with a dominant Neoproterozoic and Permian age populations (Fig. 3-11). The cumulative (K-S test) and normalized age probability plots (Fig. 3-7) shows strong similarities between three of the samples, which is suggestive of a common provenance. The ages of zircons from the ten detrital zircon samples from the Turkana Basin in Kenya (Chapter 4) range from Mesoarchean (2918 Ma) to Eocene (~45 Ma), also with a dominant Neoproterozoic population. These sediments were mainly sourced from the Mozambique Belt of Kenya. In Sudan, the ages of the ten Wadi Milk and eight Shendi formation samples (Chapter 5) range from Paleoarchean (3262 Ma) to Cretaceous (77 Ma), with a dominant Neoproterozoic population across all samples (Fig. 6-6). The Sudan samples are interpreted to have mainly sourced from the Arabian-Nubian Shield.

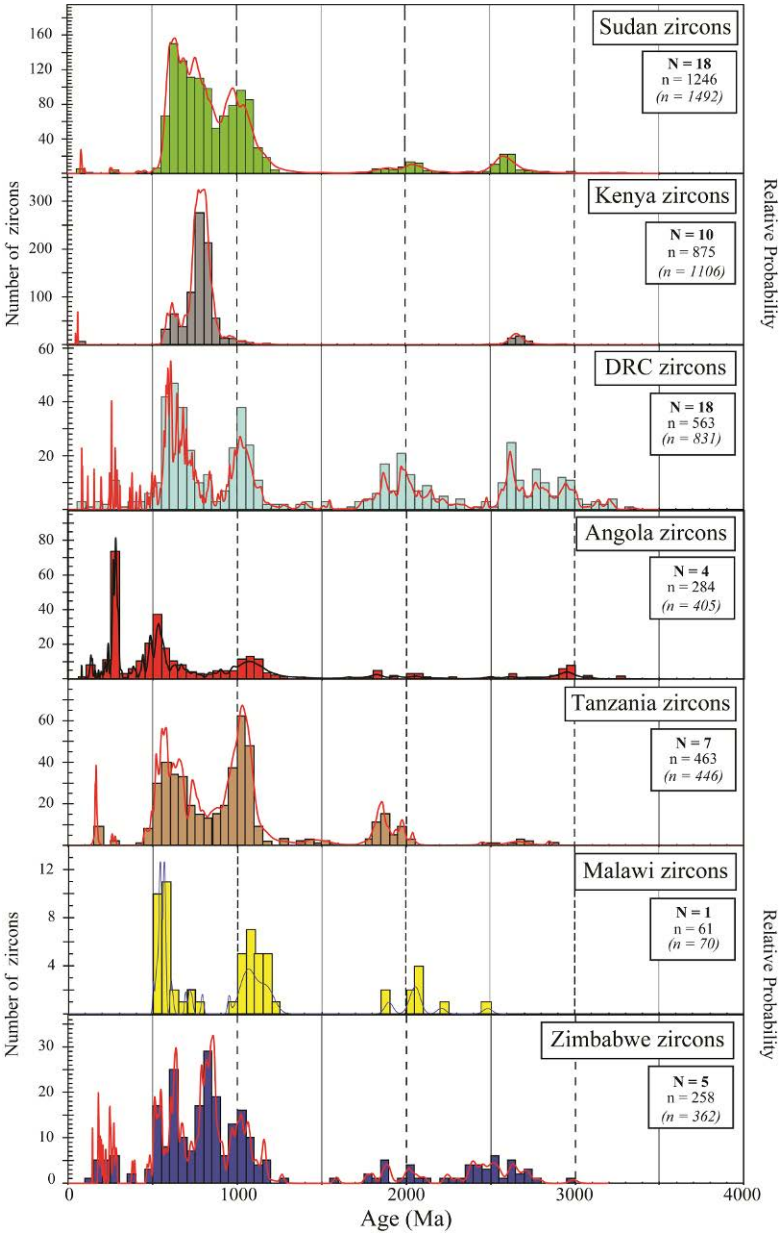

Figure 6-6. Probability density plot for all seven areas investigative in this thesis.

The plot for each area represents a composite of both Jurassic and Cretaceous detrital samples from central Africa. This composite plot is done for visual comparison and delineation of common and missing sources during late Mesozoic of central Africa. N is the number of samples analysed for a particular plot. n = x (*y*) shows the number of analyses for each area. 'x' is the number of concordant analyses, whereas '*y*' is the total number of analyses for each plot.

6.5.2.2 Lu-Hf isotopes and crustal evolution

The Lu-Hf data generated in this study (n = 699) provides one of the first and most comprehensive datasets on the crustal evolution, based on the detrital zircon samples from late Mesozoic sedimentary units across central Africa. The Lu-Hf data presented here is

generally in agreement with and build upon the Hf data database of Iizuka et al. (2013), who sampled modern sands from the Congo, Zambezi, Orange, Niger and Nile rivers to investigate trends in evolution and growth of the African continental crust (Fig. 6-5c). The Hf data are also consistent with the growth and crustal evolution of the continental Africa (Fig. 6-5b) as presented by Belousova et al. (2010). The cumulative Lu-Hf data for primary samples of this study are presented in Figure 6-7. Detailed Lu-Hf isotopic data for DRC, Angola, Kenya and Sudan are presented in their respective chapters, except for the Tendaguru samples from coastal Tanzania, which is presented in Figure 6-5a.. The initial εHf (t) values for DRC zircons (n = 97) range from –28.2 to +9.3 (Fig. 2-7,), shared between 74% negative and 26% positive values. This suggest that source rocks for the DRC samples were predominantly from reworked crustal source rocks from the Congo-Kasai Craton of central Africa. In Angola, the initial εHf (t) values for the Calonda zircons (n = 120) range from –33.5 to + 10.7; divided into 71% negative and 29% positive (Fig. 3-8). Similar to DRC, the Calonda Formation samples from Angola were mainly sourced from a reworked crust of the Congo-Kasai Craton. The initial εHf (t) values of zircons from the Lapur and Muruanachok sandstones from the Turkana Basin of Kenya (n = 177) range from–26.4 to + 11.2, which are divided into 87% positive and 13% negative values (Fig. 4-10). These values unlike those of DRC and Angola are dominated by sources with juvenile mantle, which are consistent with sources with the Mozambique Belt of Kenya. The initial εHf(t) values of the zircons (n = 235) from the Wadi Milk and Shendi formations, range from –24.4 to +13.8, and is divided into 65% positive and 35% negative (Fig. 5-9). The zircons from these Cretaceous Sudan samples are also dominated by sources with juvenile mantle, and they are consistent with sources within the Arabian-Nubian Shield. The complete Lu–Hf isotopic data for DRC, Angola, Kenya, Sudan and Tanzania are listed in the Appendices.

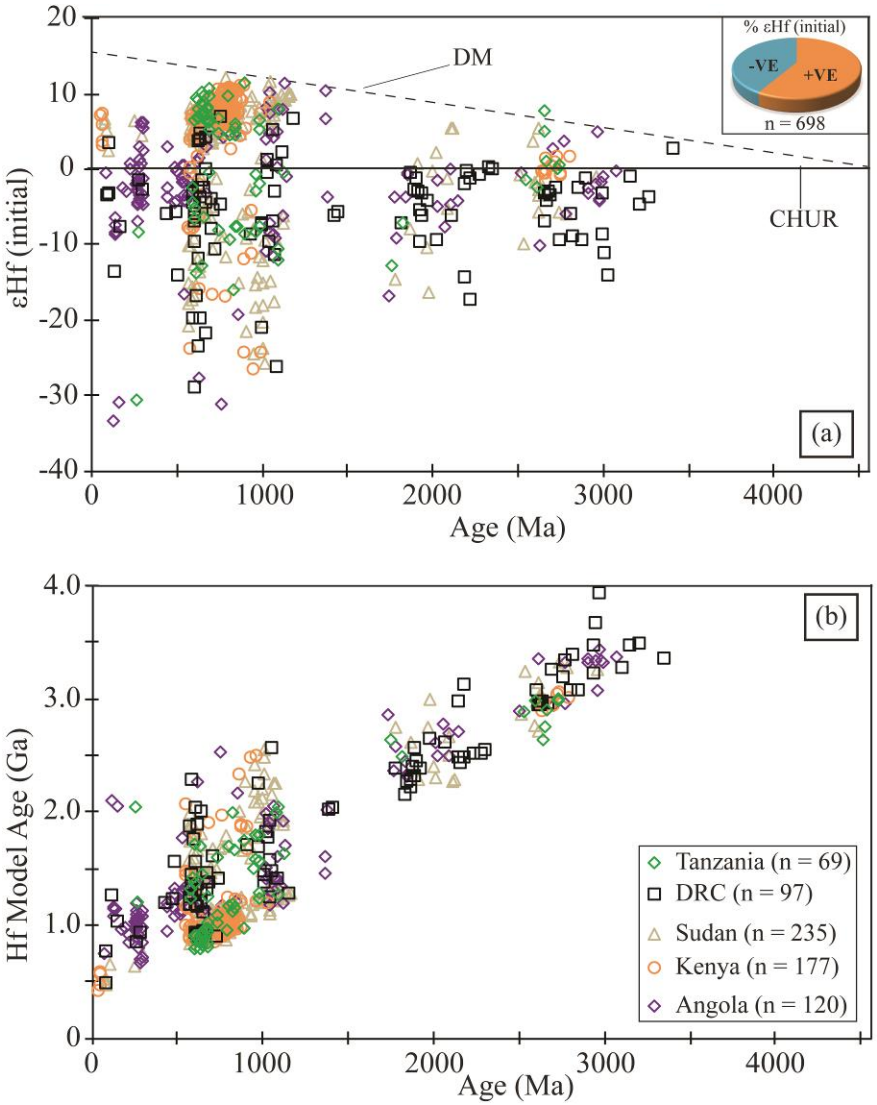

Figure 6-7. Composite plot of initial εHf values vs U-Pb age of zircons from chapters 2-5 and Tendaguru Formation

(a). Plot of initial εHf vs U-Pb age of concordant detrital zircons recovered from Tanzania, DRC, Sudan, Kenya and Angola samples. (b). Estimate of Hf model ages for the same samples. The plot here shows that most of the zircons in the study have juvenile mantle provenances.

6.6 Discussion

6.6.1 Age constraints and stratigraphic correlation of late Mesozoic units

This section summarises age constraints investigations from this study and its implications for late Mesozoic continental stratigraphic correlations in central Africa. The age constraints via maximum depositional age analysis reported in chapters 2-5 routinely

demonstrate the age of many putative Jurassic and Cretaceous units across central Africa are generally younger than previously expected. This situation is not unexpected as most of these units have been previously dated via continental biostratigraphy, often times vertebrate biostratigraphy, which tends to provide fairly imprecise temporal resolution (e.g., Tucker et al., 2013; Wainman et al., 2018a, b).

Increasingly, U-Pb detrital zircon geochronology is proving to be a valuable tool for refining the precision of biostratigraphic ages, which is particularly valuable for regional stratigraphic correlations between basins and for resolving phylogenetic and paleobiogeographic questions of the preserved fossil flora and fauna. In addition, such improved age control is important for understanding regional tectonics and uplift.

The improved age constraint for the Cretaceous Calonda Formation (chapter 3) in Angola and the Kwango Formation in DRC (Chapter 2; Roberts et al., 2015) for example, have raised questions about the reliability of the current age assignment for these important diamondiferous units in central Africa (*see section 3.6.1 for detailed discussion*). The Lapur Sandstone (Kenya, chapter 4) was previously considered to be mid to Upper Cretaceous based largely on vertebrate biostratigraphy (see O'Connor et al., 2011 and references therein); however, a Paleocene (~57 Ma) maximum depositional age constraints (*reported in this study*) for the upper part of the Lapur Sandstone (Chapter 4) suggests that the unit has a more complex stratigraphic history, with at least two discrete periods of deposition. Similarly, in Sudan, the age of the dinosaur-bearing Wadi Milk Formation was dated as Albian-Santonian, but the presence of Campanian (~80 ma) detrital zircons throughout this unit indicate a slightly younger depositional age of Campanian or Maastrichtian, which is more sensible phylogenetically, and more consistent with recent palynological constraints

from the putatively correlative Shendi Formation, which is also considered Campanian-Maastrichtian (Eisawi et al., 2012).

It is interesting that Campanian detrital zircons have now been recovered from units in DRC, Angola, and Sudan, suggesting the presence of a hereto unrecognized regional magmatic event (s), as well as period of regional subsidence during this time. Supporting this notion is the recent stratigraphic revision of Namba Member of the Galula Formation in Tanzania by Widlansky et al. (2018) who identified magnetostratigraphic reversals through this important Cretaceous dinosaur bearing unit in Tanzania that also suggest a Campanian age. Each of these sedimentary units have shown to be younger than published biostratigraphy suggests and are potentially correlative to one another, suggestive that there may be a wider distribution of Campanian or Campano-Maastrichtian sedimentary units in Africa than previously considered. The maximum depositional age assignments derived from this study, and paleomagnetic work presented recently by other workers, provides a strong evidence for the potential and importance of applying additional dating techniques, such as detrital zircon geochronology to help refine the age of other Mesozoic sedimentary units across the continent.

6.6.2 Sedimentary Provenance of late Mesozoic central Africa

The sedimentary provenance interpretations for the new data presented in this chapter are and combined with interpretations from Chapters 2-5 in order to identify key local and regional provenance sources/topographic highs (mountains or uplands) in central Africa, as well as point sources for syn- or near syn-depositional magmatic sources during the Jurassic and Cretaceous in central Africa. The detrital zircon U-Pb age spectra for the composite samples (all analysed samples and published data) shown in Figure 6-8 suggests a wide range

of point sources across central Africa. This interpretation is backed by the Lu-Hf data that confirm a complex assortment of both juvenile mantle and reworked crustal sources even within the same age populations, in some cases (Figs. 6-9 and 6-10). The initial εHf (t) values of detrital zircons from the samples analysed in this study range from -33.5 to +12.2, which are represented by 41.5% negative and 58.5% positive initial εHf (t) values. The positive initial εHf (t) values from this study are dominated Neoproterozoic zircon populations, which serves as the major provenance source for late Mesozoic sediment in central Africa, accounting for ~61% of all analyses (Figs. 6-8 and 6-9b).

The cumulative probability plot generated from the K-S test and the normalized age probability plot of all individual study areas (chapters 2-5 and Fig. 6-4) and for all the composite samples investigated are shown in Figure 6-10. None of the composite samples pass the K-S test (Table 6-2), although test results for the individual study areas are quite different and commonly show a high degree of similarity (see chapters 2-5 and Fig. 6-4). The normalized age probability plot (Fig. 6-10b) at a glance shows some similarities in certain samples in regards to populations that were encountered (e.g. 1100–500 Ma) as well as missing populations (e.g. 1700–1400 Ma). It seems that sediment generation from certain potential source areas were conspicuously absent during the Mesozoic, whereas others were more prominent during the same time period. For instance, the presence of Archean grains derived from cratonic blocks are highly variable in distribution, and are often important for establishing source areas and drainage patterns. The following sub-sections discuss the main detrital zircon populations and compares regional crystalline basements sources in Africa in order to place them in their regional tectonic and paleogeographic context. The discussion hereafter is divided into Archean, Paleoproterozoic to earliest Mesoproterozoic, Late

Mesoproterozoic to earliest Neoproterozoic, mid-late Neoproterozoic, Paleozoic and Mesozoic age provenance sources.

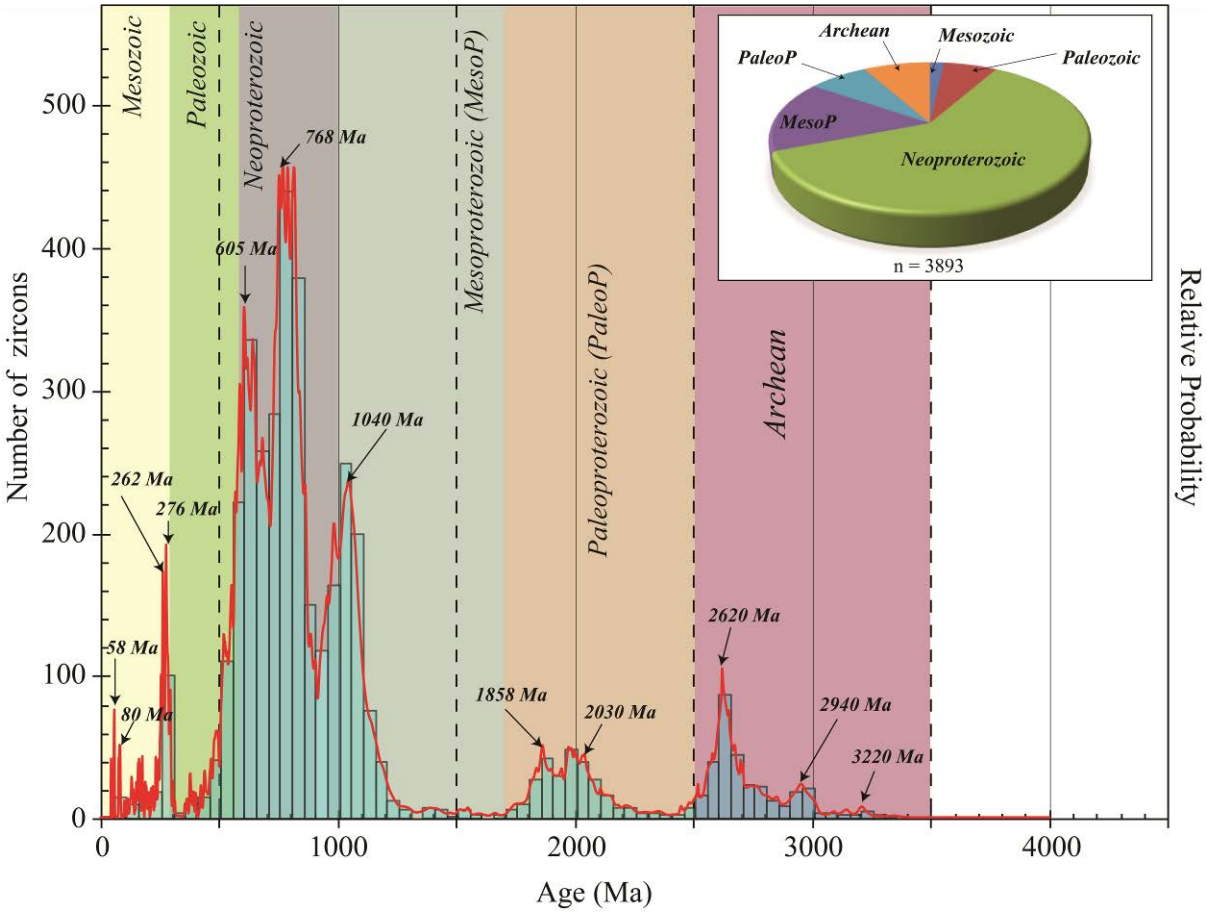

Figure 6-8. Composite probability density plot for all U-Pb age data presented in this thesis

This data includes the data presented in the chapters 2-5 and the new and published data presented in this chapter. The ages on this plot are grouped into Archean, Paleoproterozoic, Mesoproterozoic, Neoproterozoic, Paleozoic and Mesozoic. Selected peak ages are highlighted by arrows. These peak ages point to certain terranes in Africa (see text). Overall, Neoproterozoic age zircons accounted for the largest population followed by Mesoproterozoic age zircons.

Table 6-2. K-S Test results for composite samples for the different areas

	Zimbabwe	Malawi	Tanzania	Angola	DRC	Kenya	Sudan
Zimbabwe		0.043	0.004	0.000	0.000	0.000	0.000
Malawi	0.043		**0.099**	0.000	0.001	0.000	0.000
Tanzania	0.004	**0.099**		0.000	0.000	0.000	0.000
Angola	0.000	0.000	0.000		0.000	0.000	0.000
DRC	0.000	0.001	0.000	0.000		0.000	0.000
Kenya	0.000	0.000	0.000	0.000	0.000		0.000
Sudan	0.000	0.000	0.000	0.000	0.000	0.000	

Kolmogorov-Smirnov (K-S) statistical test for samples from the seven areas investigated in this study. The bold p-values are > 0.05, which indicates that these samples passed the K-S test, suggestive of a similar provenance for all eight samples. The p-values < 0.05 means they failed the K-S test.

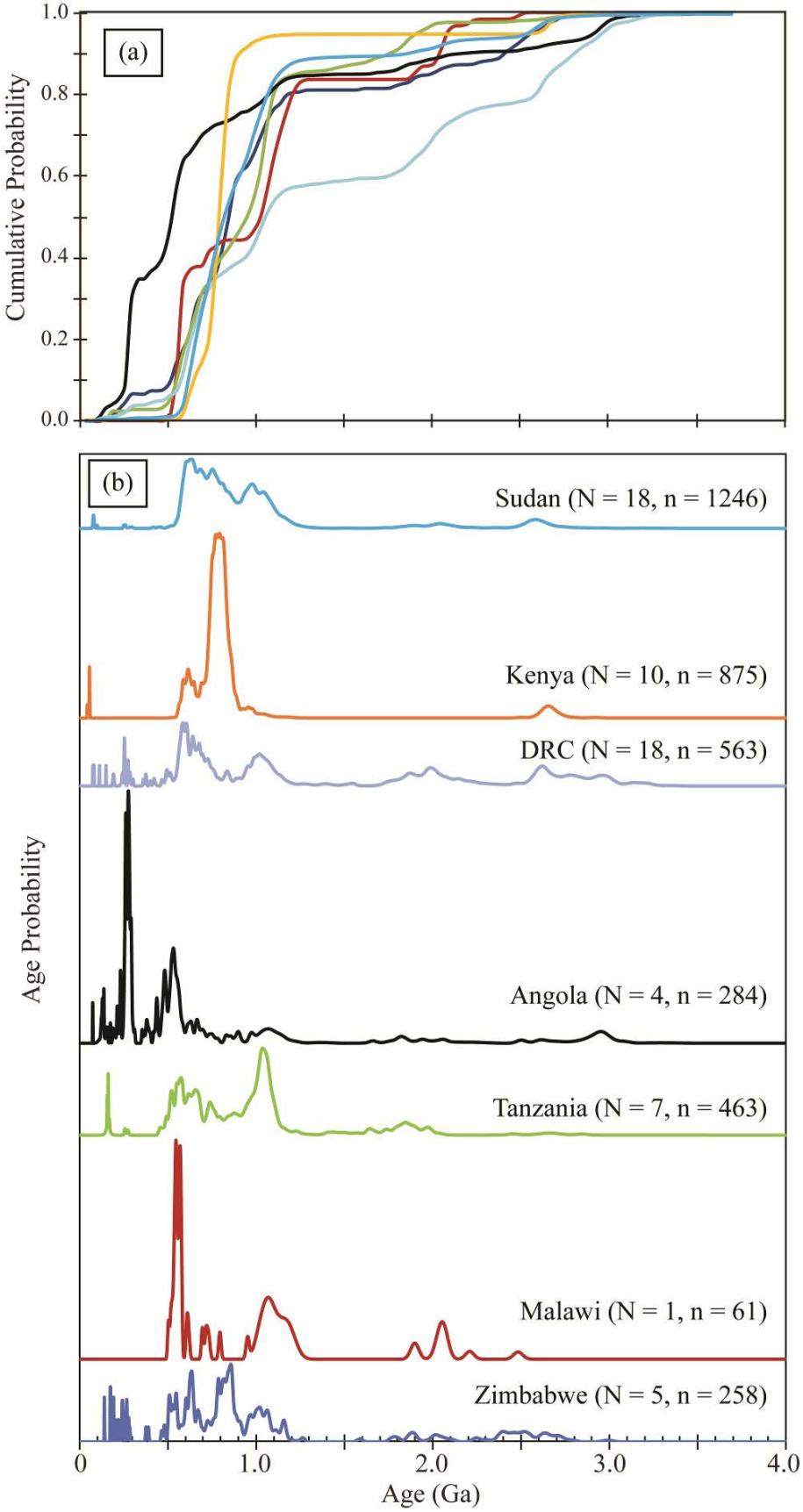

Figure 6-9 Comparison of composite detrital zircon data from all seven areas investigated in this thesis.

(a). Cumulative probability plot from the K-S test. (b). Relative age probability of the all samples showing significant difference and similarities between the different areas.

6.6.2.1 Archean zircon populations

Archean age zircons are present in all samples from the seven study areas, although the proportion is significantly higher in samples from DRC, Angola and Zimbabwe. This is not surprising as the sedimentary basins in these three areas are located adjacent to major sits on Archean cratons. Archean zircons analysed for their Hf isotopic data (n = 65) have initial εHf values ranging from -12.7 to +7.8. This Hf data show a dominance of reworked crustal sources (Fig. 6-5b), accounting for 72% of Archean zircons. The majority of Archean zircons in this study (Figs. 6-4 and 6-6) were recovered from the DRC and Angola samples. The dominant negative initial εHf values from Archean zircons from this study are consistent with composite Hf data from Africa reported by Belousova et al. (2010, Figs. 6-5b and 6-9a). The ages and Hf isotopic data from these samples are consistent with sources within the Congo-Kasai Craton and the Zimbabwe Craton (e.g. Cahen et al., 1984; De Carvalho et al., 2000; De Wit and Linol, 2015). Moreover, the Archean Hf data collected during this study (Fig. 6-9b) is largely consistent with the crustal evolution of the Congo-Kasai and Zambezi cratons, which are known to host an older nuclei (>3500 Ma) that underwent crustal reworking during the Archean, Paleoproterozoic Mesoproterozoic and Neoproterozoic times (Blenkinsop et al., 1997; De Wit, 1998; Batumike et al., 2009; Begg et al., 2009; Jelsma et al., 2015). However, zircons from the Archean Tanzania Craton are conspicuously absent from most Tanzanian samples (e.g., Rukwa, Malawi Rift and Madawa basins), supporting the notion that the East African Plateau did not form a significant topographic feature until sometime in the Paleogene (Baker et al., 1972; Ebinger, 1989; Ebinger et al., 1989; Ebinger and Ibrahim, 1994; Ebinger et al., 2000; Chorowicz, 2005; Ebinger, 2005; Burke and Gunnell, 2008; Corti,

2009; Roberts et al., 2012). Roberts et al. (2012) suggested that flank uplift associated with Rukwa Rift reactivation during the Cretaceous, particularly during the earliest phases (probably during the Early Cretaceous), resulted in deflection of drainages (and sediments) from the Tanzania Craton to the east. The samples from coastal Tanzania (Tendaguru locality) also have limited Tanzanian Craton derived grains, which provides further support to the concept that the Tanzania Craton was not a significant topographic feature at this time. Rather, uplifted Neoproterozoic rift flanks of eastern Africa (Mozambique Belt) associated with rifting of Madagascar during the Jurassic still remained topographically high during this time, which explains the provenance patterns observed.

6.6.2.2 Paleoproterozoic and earliest Mesoproterozoic zircon populations

The Paleoproterozoic to earliest Mesoproterozoic zircon populations (Fig. 6-8) are also spread across all samples except those from the Turkana Basin in Kenya, which did not yield any zircon of this age. The Paleoproterozoic zircons analysed for their Hf isotopic data (n = 50) have initial εHf (t) values ranging from -17.3 to +9.6, with a dominant (~73%) negative component, pointing to reworked crustal source terranes. Reported Paleoproterozoic terranes in central Africa include the Ubendien Belt (~1750-2000 Ma), the Usagaran Belt (~2000-2200 Ma), the Bengwelu Block (~1800 Ma) and the Magondi Belt (~2200-1660 Ma) (Leyshon, 1988; M ller et al., 1995; Majaule et al., 2001; McCourt et al., 2001). Specifically, the Ubendian Belt is interpreted to have been a major provenance source for Cretaceous sedimentary units in the Congo Basin (Chapter 2), and to a lesser extent for the Northern Malawi (presented in this study) and the Rukwa Rift Basin (Roberts et al., 2012). Further to the south in the Zambezi valley samples, the smattering of Paleoproterozoic grains in the 1800-2200 Ma range are likely derived from the Magondi Belt, but may be recycled through

older sedimentary units. The presence of grains of this age in the Sudan samples is interpreted to derive from isolated point sources in the Arabian Nubian Shield (see Chapter 5).

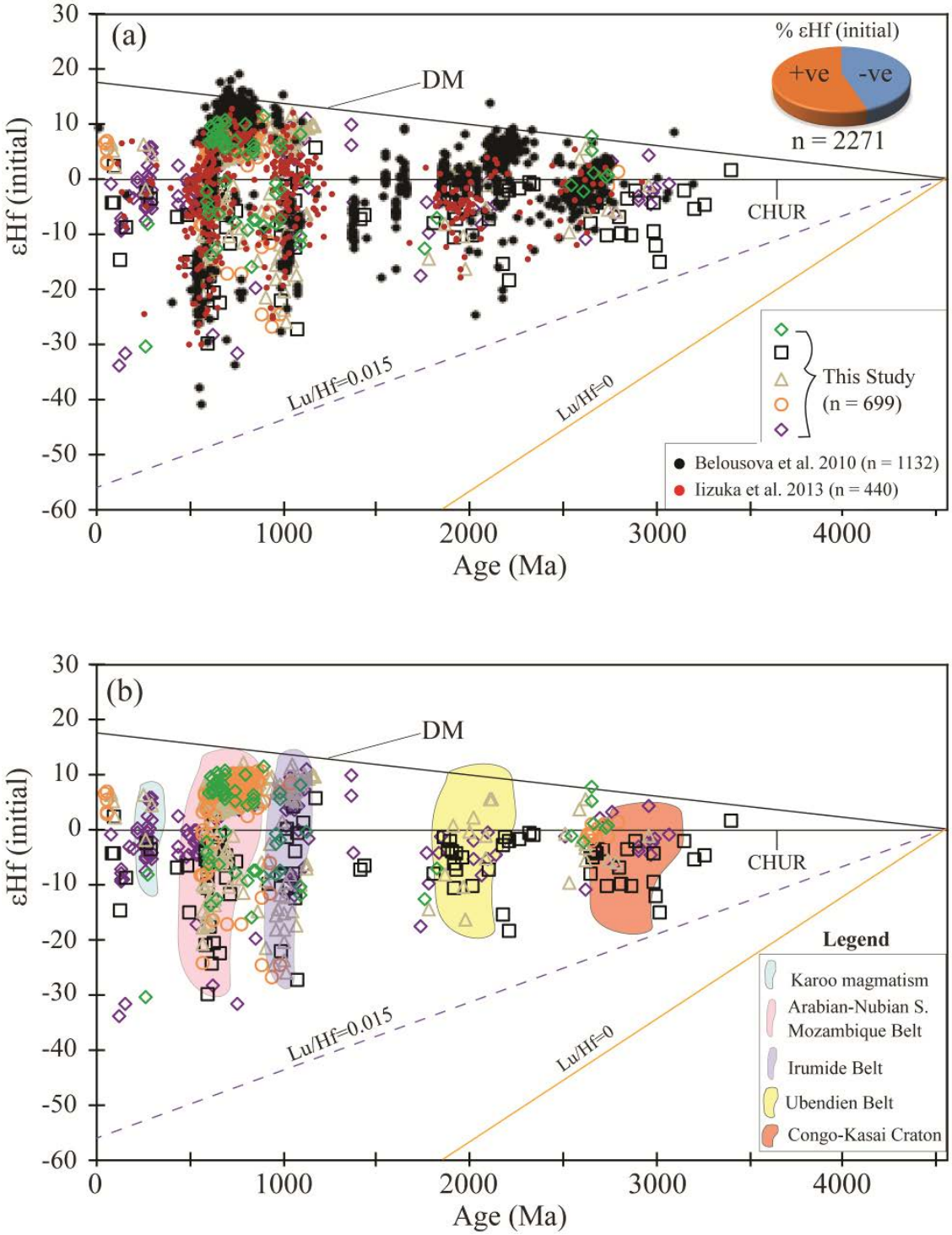

Figure 6-10. Lu-Hf isotopic data from this study compared with published data

(a). Published data of both Belousova et al. (2010) and Iizuka et al. (2013) are incorporated for comparison. Details of all the values from the different areas investigated in this study are listed in the supplementary data tables. (b). Hf data for this study showing the main source for the different cluster populations. Overall, Neoproterozoic age terranes linked to the Pan-African Orogeny are the dominant provenance source for late Mesozoic central Africa. "S" is shield for the Arabian Nubian Sheld.

The general absence of early to middle Mesoproterozoic (1200-1600 Ma, Fig. 6-8) zircon populations from most samples analysed in this study suggest that east-west/west-east drainage patterns across central Africa were uncommon, otherwise significant Kibaran Belt zircon populations would be expected (see Roberts et al., 2012). Similarly, Kibaran grains would be expected in the DRC, Angola, Malawi and Rukwa samples *(see section 6.5.1.22*), if fluvial systems were oriented east-west/west-east across central Africa, but again, this is not observed. Early to middle Mesoproterozoic populations are conspicuously absent from each of the Zimbabwean, Sudanese, Kenyan and coastal Tanzanian samples.

6.6.2.3 Late Mesoproterozoic to earliest Neoproterozoic zircon populations

In contrast, Late Mesoproterozoic to earliest Neoproterozoic zircon (950-1150 Ma) are the next most populous provenance source after the mid-late Neoproterozoic grains, with a peak age around ~1100 Ma (Fig. 6-8). Late Mesoproterozoic-earliest Neoproterozoic zircons are only absent in the Turkana Basin samples (Fig. 6-6), which suggests that sources of this age within the Mozambique Belt of Kenya were not active at this time, and that long-distance transport of sediments across central Africa may have been fairly limited, even if major drainage systems were connected during this time. Indeed, Roberts et al. (2012) noticed a similar phenomenon in the Rukwa Rift Basin, where late Mesoproterozoic to earliest Neoproterozoic Irumide Belt zircon populations were prominent in the southern part of the rift, but much less abundant in the northern part of the rift. These authors demonstrated consistent NW directed paleocurrents from north to south, suggesting that although the rift

provided a conduit for long-distance stream flow, sediment transport distances were more limited.

The late Mesoproterozoic to earliest Neoproterozoic zircons analysed for their Hf isotopic data (n = 100) have initial εHf (t) values ranging from -25.9 to +11.7(Fig. 6-9b), which is divided into ~54% positive and ~46% negative values. The Mesoproterozoic Irumide Belt (1400-1000 Ma) of Zambia, which is known to host rocks of mixed crustal sources (e.g. De Waele et al., 2006) is the main source of zircons of this age from central Africa.

6.6.2.4 Mid-late Neoproterozoic zircon populations

The mid-late Neoproterozoic age zircons forms the largest population in this study and spreads across all samples from the different basins investigated (Figs. 6-4, 6-6, 6-8 and 6-10). The mid-late Neoproterozoic detrital zircon population analysed for their Hf isotopic data (n = 403) is characterised by initial εHf (t) values ranging from -31.3 to +12.2, with dominant (~71%) positive component. Most of the Neoproterozoic age zircons falls within the ages of Pan-African mobile belts (e.g. Arabian-Nubian Shield, the Mozambique Belt the Lufilian and the Zambezi Belts, which formed during the Pan-African orogeny across Africa around ~870 to 550 Ma (e.g. Kröner and Stern, 2005). The dominance of juvenile mantle sources is shown by the Arabian Nubian Shield and the exposed supracrustal rocks of the Mozambique Belt in northern Kenya (Cutten et al., 2006). The crustal evolution of these mobile belts is quite variable; for example, both the Arabian-Nubian Shield and the Mozambique Belt are known to be dominated by juvenile mantle sources, but reworked crustal sources are also present (Fig. 6-9b). Most of the juvenile zircon populations were recovered from samples taken from the eastern side of central Africa (i.e. coastal Tanzania,

Kenya and Sudan) and their initial εHf (t) values are consistent with juvenile mantle source rocks within the Arabian-Nubian Shield and the supracrustal rocks of the Mozambique Belt in northern Kenya (Cutten et al., 2006). The reworked crustal component of the Neoproterozoic zircon populations are also consistent with sources within the Lufilian and Zambezi belts (e.g. Hanson et al., 1994).

6.6.2.5 Paleozoic and Mesozoic zircon populations

The Paleozoic zircon populations (Fig. 6-8) analysed for their Hf isotopic data (n = 54) have initial εHf (t) values ranging from -30.4 to +6.5 with a dominant negative component (~74%). The Paleozoic of Africa saw the formation and breakup of Pangea, with associated reworking of the crust (e.g. Veevers, 2013). The Paleozoic populations from this study are dominated by Permian age zircons with negative initial εHf (t) values and this suggest that these zircon populations were likely sourced from recycled Karoo sedimentary strata and/or intercalated volcanics (e.g. Oesterlen, 1976, 1979; Fildani et al., 2007, 2009) in southern and central Africa. Widespread extension of the crust took place in the Permian, with the development of widespread Karoo-age basins in southern and eastern Africa, but also in parts of central Africa (e.g. Haddon, 2005; Fildani et al., 2009). Interestingly, Permian populations are almost entirely limited to samples from Angola, which record a strong peak, and samples from DRC, which record a much more limited peak. A small population of grains of this age are also observed from the Zimbabwean samples. This suggests that recycling of Karroo age strata was highly localised and presumably limited to local basin inversion in northern Angola.

The Mesozoic (and Cenozoic) detrital zircon population (Fig. 6-8) represents the smallest grain age population in nearly all samples, but may be the most important as it has

provided an opportunity to put constraints on the age of deposition of several key stratigraphic units, including the Wadi Milk Formation of Sudan, Lapur Sandstone of Kenya, the Kwango group in DRC, and possibly the Calonda Formation of Angola. Non age-constraining Jurassic detrital zircons are also present in the Rukwa Rift Basin. The provenance of these Mesozoic age zircons is clearly quite localised, and are most likely sourced from a variety of different alkaline magmatic sources that formed due to the breakup of Gondwana in the Cretaceous. It is also possible that some of the grains were sourced from arc-related volcanic ash transported from South America (e.g. Linol et al., 2016). The Mesozoic age zircons analysed for their Hf isotopic data (n = 27) have initial εHf (t) values ranging from -33.5 to +7.4, divided into ~59% negative and 41% positive values confirming mixed provenance sources zircons of this age group.

6.6.3 Paleodrainage evolution of late Mesozoic central Africa

The drainage of central Africa is considered to be young (Cretaceous-Recent) and controlled by rifting of the continent (Burke et al., 2003; Goudie, 2006). The debate concerning the direction of paleofluvial drainage patterns on the African continent is ongoing, but continues to be refined as more data becomes available (e.g. Goudie, 2005). Continued efforts are largely driven by the economic significance of mineral, hydrocarbon and paleontologic resources resource in these strata. Two principal drainage hypotheses for central Africa currently exist: (1) an east flowing Late Cretaceous-Paleogene paleo-Congo River draining into the Indian Ocean (Stankiewicz and de Wit, 2006); and (2) a northwest flowing transcontinental river system that drained the southern highlands in Zambia and Malawi, which drained into the Congo Basin (Roberts et al., 2012). The probable late Mesozoic drainage patterns for four areas in central Africa has been inferred from sediment

provenance in chapters 2-5. Here, the paleodrainage evolution of late Mesozoic central Africa is discussed from Middle Jurassic through to Paleogene. The objective is to synthesize and infer drainage patterns from provenance of the sedimentary rocks discussed previously. The discussion presented here is based on paleocurrent data, and detrital zircon U-Pb age and geochemistry data, as most of the previous drainage models were largely hinged on geomorphic investigations. The large dataset presented here provides the basis for a robust assessment of earlier models and for the development of a new, more realistic interpretation of late Mesozoic provenance sources and paleofluvial drainage evolution of central Africa.

The Mesozoic and Cenozoic paleogeography of central and southern Africa is believed to have been significantly influenced by a number of key post-Gondwana events including the Parana Plume, Karoo Plumes, the Botswana Dyke Swarm and the Southern Equatorial Divide or the Okavango-Kalahari-Zimbabwe Axis (OKZ) (e.g. Du Toit, 1933; Partridge and Maud, 1987; Moore, 1999; Moore and Larkin, 2001; Moore and Blenkinsop, 2002; Doucouré and de Wit, 2003; Moore et al., 2009). The rifting of South America from Africa resulted in isostatic rebound of the west coast of Africa, creating highlands to the west (e.g. Doucouré and de Wit, 2003). These uplifted continental margins of Africa in Late Cretaceous strongly influenced the direction of river systems at this time (Haddon, 2005). Haddon (2005) contends that drainage patterns were mainly composed of short rivers (Fig. 6-11) that flowed from these uplifted margins towards the sea or into the interior of the continents, terminating in inland deltas.

A model for drainage evolution of south-central Africa post-Gondwana breakup by Moore and Larkin (2001) paint a detailed picture of the paleogeography at the time. This model suggests that the Limpopo River served as conduit for the inland drainage to the Indian Ocean post-Gondwana (e.g. Moore and Blenkinsop, 2002). The OKZ or the Southern

Equatorial Divide, a Late Cretaceous to early Tertiary crustal flexuring of south-central Africa seems to have divided southern from central Africa, as demonstrated by different paleocurrents from the Zimbabwe detrital samples (Shoko, 1998; De Wit, 1999; Moore, 1999; Moore and Larkin, 2001; Haddon, 2005; Moore et al., 2009). In Tanzania, Roberts et al. (2012) have also shown how almost no Archean sediments from the Tanzania Craton entered the Rukwa Rift Basin during the Cretaceous, which suggests that rift reactivation of the Ubendian Belt in the Early Cretaceous probably led to flank uplift along the bounding faults to the west pushing drainage from the Tanzania craton towards the east. Considered together, evidence from the sedimentary provenance investigations presented in this thesis and previous work in central Africa shows a complex interplay of multiple river systems in central Africa during late Mesozoic with the dominant ones from the Zambezi and Malawi rifts and enroute the Rukwa Rift through the Congo Basin and north into the Central African Shear Zone.

6.6.3.1 Jurassic to Paleogene drainage evolution

Paleogeographic reconstructions by Scotese (2012; PaleoMap Project) show that Africa was still part of South America, and the continent was generally tilted to the NE-SW (Figs.6-11 and 6-12). Paleocurrent data from the Upper Jurassic-Lower Cretaceous Tendaguru Formation in Tanzania (Bussert et al., 2009) are variable, generally bi-directional with sources from the east and west, suggesting drainage by fluvial systems into the Indian Ocean. Interestingly, the provenance of this unit also records minimal input from the Tanzanian Craton, suggesting that flank uplift on the east coast of Tanzania due to rifting of Madagascar from eastern Africa probably acted to limit provenance from an uplifted Mozambique Belt. The U-Pb age spectra and Lu-Hf isotope results from Tanzania are consistent with source within the Mozambique Belt of Tanzania, which suggest multiple fluvial sources and

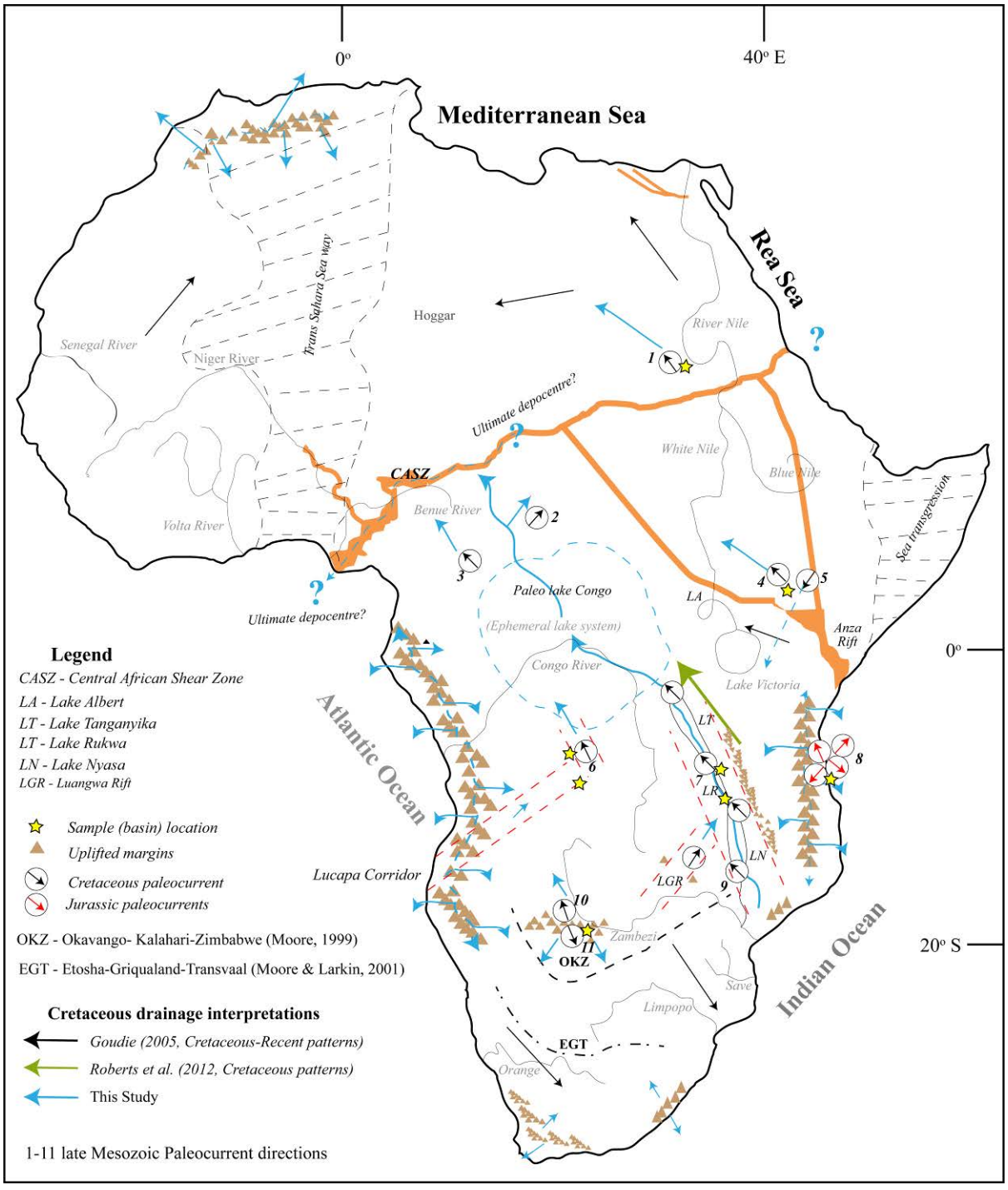

Figure 6-11. Sketch of late Mesozoic drainage model for central Africa.

Paleodrainage evolution of late Mesozoic central Africa inferred from detrital zircon and paleocurrent analysis. This plot shows there were a number of different fluvial systems in late Mesozoic but sedimentary provenance from detrital zircons shows most of the sources were located to the south and thus were transported northwards. Refer to Fig. 6-1 for references (1-11) to the paleocurrent directions.

possibly transgressive seas (Fig. 6-11) or a tsunami may have deposited this formation in coastal Tanzania as indicated by Bussert and Aberhan (2004). Regardless, the Jurassic fluvial systems from the eastern central Africa may have carried on and joined other river systems in central Africa during the subsequent times in central Africa (Fig. 6-11).

The U-Pb age data for most Jurassic and Cretaceous sedimentary deposits (*see* Chapters 2-5) shows that sediment were predominantly sourced from the south, an interpretation consistent with the available paleocurrent data (Fig. 6-1). Detrital samples from the Zambezi Rift were mainly sourced from the Zimbabwe Craton and surrounding mobile belts (e.g. Magondi Belt) to the south, although two contrasting paleocurrent directions seems to support the OKZ axis of Moore (1999). This suggests rivers from the Zambezi Rift were bi-directional flowing either to the north into central Africa or flowing south into the drainage network of southern Africa (see Key et al., 2015 for detailed discussion). Sediments from the Dinosaur Beds (Malawi) and Rukwa Rift Basin (Tanzania) were sourced from the highlands in the Malawi and Zambezi rifts to the south (Roberts et al., 2012), all of which are indicative of north directed flow at this time. Additionally, Cretaceous strata of the Carnot Formation (Censier and Lang, 1999) and Mouka-Ouadda Formation (Malibangar et al., 2006) on the northern margin of the Congo Basin are interpreted to have been deposited by north trending fluvial systems from the Congo Basin. The sources of these Cretaceous sedimentary units strongly suggests they were transported by north directed fluvial systems as theorized by Roberts et al. (2012).

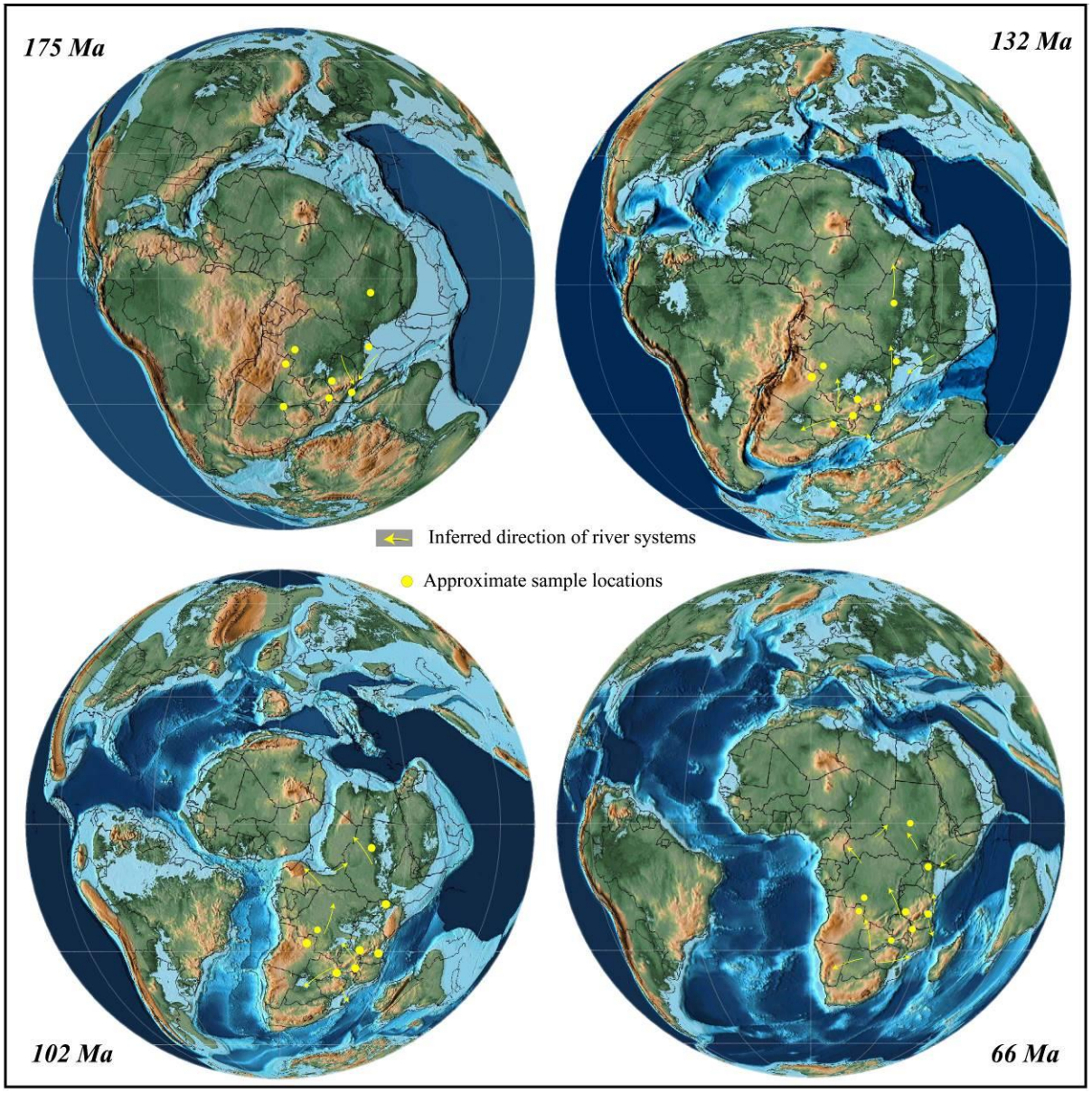

Figure 6-12. Probable drainage directions for Middle Jurassic through to Late Cretaceous Rivers in central Africa. Directions are plotted on paleo reconstruction maps of Scotese (2012).

The data from this study and published literature discussed in this chapter strongly supports and refines the interpretation of northward directed fluvial system during late Mesozoic in central Africa. The data presented here shows that sediments from different study areas were preferentially transported by mainly north directed river systems, which is believed to be a consequence of Africa tilting towards the European continent. (Fig. 6-12).

Overall, paleocurrent directions from both Jurassic and Cretaceous sedimentary units in central Africa present an overwhelming pattern of north-directed river flow, consistent with previous interpretations of a major drainage divide between southern and central Africa in the vicinity of the Luangwa-Rukwa headwaters as suggested by Key et al. (2015). The river systems of continental late Mesozoic central Africa were probably connected and may have formed a series of trunk systems, but that much of the sediments were actually deposited locally, rather than transported across long distances from Zimbabwe to Sudan.

7. Main conclusions

This thesis provides the first detailed detrital zircon investigation of the late Mesozoic strata in the central Africa. The main conclusion of this thesis are:

1. The presence of dominantly north directed paleocurrent data for Late Jurassic-Cretaceous units in central Africa is supportive of a uniform northward continental fluvial drainage patterns throughout late Mesozoic. This also implies that the paleo-Congo drainage system that was likely north flowing, rather than eastward flowing channels out of the basin and into Indian Ocean to the east as previously suggested.
2. Southerly sediment sources from paleo-highlands in Malawi and Zambia, resulting in a major drainage divide between southern Africa and central Africa. This led to dominantly north flowing fluvial systems into central Africa from primarily Neoproterozoic Pan-African uplifts in the Irumide Belt and Lufilian Arc sources.
3. The identificiation of southerly provenance sources for the rich alluvial diamond-bearing Calonda Formation in Angola is particularly important for Kimberlite vectoring in the region. This work suggests that in addition to known kimberlite pipes in the Lucapa study area; there may be additional kimberlite pipes and alluvial diamonds transported from further to the southeast along the Lucapa Coridoor.
4. The dinosaur-bearing Lapur Sandstones in the Turkana Rift have a more complex stratigraphic history than previously appreciated, with at least the upper portion of this regionally extensive unit having been deposited during the Paleogene or later based on maximum depositional ages of the youngest detrital zircons from this study.
5. The Turkana Basin was likely sourced from local provenance sources on the southern Margin of the basin, with paleoflow generally directed northwards; similar to the

patterns observed in Mesozoic of DRC, Angola, western Tanzania, Malawi, Central African Republic, and elsewhere in Central Africa. The ultimate depocentre for sedimentation across the continent remains uncertain, but large transcontinental river systems definitively flowed N-NW across the continent during much of the late Mesozoic, and the anomalously thick sedimentary succession recoreded in the various basins of the Central African Shear Zone (e.g. Muglad and Melut basins in Sudan, Doba Trough in Chad, and Touboro Basin in Cameroon) represent the most likely depocentre.

7.1 Recommendation for future work

The main recommendation is future work should expand the sampling focus to include other areas in central Africa, particularly in the Sudan Rifts, Ethiopia, Central African Republic, Cameroon and others. The second recommendation is to do more Lu-Hf and zircon trace element analysis for the late Mesozoic units in central Africa for better comparison for source provenance.

8. References cited

Abdelsalam, M. G., Liégeois, J. P., and Stern, R. J. (2002). The Saharan Metacraton. Journal of African Earth Sciences, 34(3-4), 119-136.

Abu-Alam, T., and Stüwe, K. (2012). The Butana Region of Central Sudan: Sahara Craton or Arabian-Nubian Shield? In EGU General Assembly Conference Abstracts (Vol. 14, p. 8291).

Aleinikoff, J. N., Schenck, W. S., Plank, M. O., Srogi, L., Fanning, C. M., Kamo, S. L., and Bosbyshell, H. (2006). Deciphering igneous and metamorphic events in high-grade rocks of the Wilmington Complex, Delaware: Morphology, cathodoluminescence and backscattered electron zoning, and SHRIMP U-Pb geochronology of zircon and monazite. *Geological Society of America Bulletin*, *118*(1-2), 39-64.

Amidon, W. H., Burbank, D. W., and Gehrels, G. E. (2005). Construction of detrital mineral populations: Insights from mixing of U-Pb zircon ages in Himalayan Rivers. Basin Research, 17(4), 463-485. Doi:10.1111/j.1365-2117.2005.00279.x

Amiot, R., Buffetaut, E., Lécuyer, C., Wang, X., Boudad, L., Ding, Z., Fourel, F., Hutt, S., Martineau, F., Medeiros, M.A., and Mo, J. (2010). Oxygen isotope evidence for semi-aquatic habits among spinosaurid theropods. *Geology*, *38*(2), 139-142.

Antunes, M. T., Maisey, J. G., Marques, M. M., Schaeffer, B., and Thomson, K. S. (1990). Triassic fishes from the Cassange Depression (RP de Angola). Ciências da Terra (UNL), Número Especial, 1990, 1-64.

Arambourg, C. (1935). Esquisse géologique de la bordure occidentale du Lac Rodolphe. Mission scientifique de l'Omo. 1932–33. Bulletin Muséum National d'Histoire Naturelle, Paris 1(1), 55 p.

Arambourg, C. (1943). Contribution a l'etude geologique et paleontologique du Bassin du Lac Rodolphe et de la Basse Vallee de l'Omo. Mission Scient. Omo. Mus. Netl. Hist. Nat. Paris i, 1(2), 157-230.

Arambourg, C. and Wolff, R. G. (1969). Nouvelles donnees paleontologique sur l'age des "gres du Lubur" (Turkana Grits) a l'Ouest du lac Rudolphe. Compte rendu sommaire des séances de la Société géologique de France 6: 190-202.

Armstrong, R. A., Master, S., and Robb, L. J. (2005). Geochronology of the Nchanga Granite, and constraints on the maximum age of the Katanga Supergroup, Zambian Copperbelt. Journal of African Earth Sciences, 42(1), 32-40. Doi:10.1016/j.jafrearsci.2005.08.012

Averianov, A. (2014). Review of taxonomy, geographic distribution, and paleoenvironments of Azhdarchidae (Pterosauria). ZooKeys 432: 1–107. doi: 10.3897/zookeys.432.7913

Avigad, D., Kolodner, K., McWilliams, M., Persing, H., and Weissbrod, T. (2003). Origin of northern Gondwana Cambrian sandstone revealed by detrital zircon SHRIMP dating. Geology, 31(3), 227-230.

Avigad, D., Stern, R. J., Beyth, M., Miller, N., and McWilliams, M. O. (2007). Detrital zircon U–Pb geochronology of Cryogenian diamictites and Lower Paleozoic sandstone in Ethiopia (Tigrai): age constraints on Neoproterozoic glaciation and crustal evolution of the southern Arabian–Nubian Shield. Precambrian Research, 154(1-2), 88-106.

Baker, B. H., Mohr, P. A., and Williams, L. A. J. (1972). Geology of the eastern rift system of Africa. Geological Society of America Special Papers, 136, 1-68.

Bangert, B., Stollhofen, H., Lorenz, V., and Armstrong, R. (1999). The geochronology and significance of ash-fall tuffs in the glaciogenic Carboniferous-Permian Dwyka Group of Namibia and South Africa. Journal of African Earth Sciences, 29(1), 33-49.

Banks, N. L., Bardwell, K. A., and Musiwa, S. (1995). Karoo rift basins of the Luangwa Valley, Zambia. Geological Society, London, Special Publications, 80(1), 285-295.

Barth, H., and Meinhold, K. D. (1979). Mineral prospecting in the Bayuda Desert. Unpublished Technical Report of the Sudanese–German Exploration Project, Vol. A. BGR, Hannover.

Bata, T., Parnell, J., Samaila, N., and Haruna, K. (2016). Anomalous occurrence of Cretaceous placer deposits: A review. Earth Atmospheric Science, 1, 1-13.

Batumike, J. M., Griffin, W. L., O'Reilly, S. Y., Belousova, E. A., and Pawlitschek, M. (2009). Crustal evolution in the central Congo-Kasai Craton, Luebo, D.R. Congo: Insights from zircon U–Pb ages, Hf-isotope and trace-element data. Precambrian Research, 170(1), 107-115. Doi: 10.1016/j.precamres.2008.12.

Batumike, J. M., O'Reilly, S. Y., Griffin, W. L., and Belousova, E. A. (2007). U–Pb and Hf-isotope analyses of zircon from the Kundelungu kimberlites, D.R. Congo: Implications for crustal evolution. Precambrian Research, 156(3), 195-225. Doi:10.1016/j.precamres.2007.04.002

Bauer, F. U., Karl, M., Glasmacher, U. A., Nagudi, B., Schumann, A., and Mroszewski, L. (2012). The Rwenzori Mountains of western Uganda–Aspects on the evolution of their remarkable morphology within the Albertine Rift. Journal of African Earth Sciences, 73, 44-56.

Beauchamp, J., Omer, M. K., and Perriaux, J. (1990). Provence and dispersal of Cretaceous elastics in northeastern Africa: climatic and structural setting. Journal of African Earth Sciences (and the Middle East), 10(1-2), 243-251.

Begg, G. C., Griffin, W. L., Natapov, L. M., O'Reilly, S. Y., Grand, S. P., O'Neill, C. J., Hronsky, J.M.A., Djomani, Y.P., Swain, C.J., Deen, T. and Bowden, P. (2009). The

lithospheric architecture of Africa: Seismic tomography, mantle petrology, and tectonic evolution. Geosphere, 5(1), 23-50.

Belica, M. E., Tohver, E., Poyatos-Moré, M., Flint, S., Parra-Avila, L. A., Lanci, L., Denyszyn, S. and Pisarevsky, S. A. (2017). Refining the chronostratigraphy of the Karoo Basin, South Africa: magnetostratigraphic constraints support an early Permian age for the Ecca Group. Geophysical Journal International, 211(3), 1354-1374.

Bellieni, G., Justin Visentin, E., Zanettin, B., Piccirillo, E. M., Radicati di Brozolo, F., and Rita, F. (1981). Oligocene transitional-tholeiitic magmatism in northern Turkana (Kenya). Comparison with the coeval Ethiopian volcanism. Bulletin of Volcanology 44, 411–427. http://dx.doi.org/10.1007/BF02600573.

Belousova, E. A., Kostitsyn, Y. A., Griffin, W. L., Begg, G. C., O'Reilly, S. Y., and Pearson, N. J. (2010). The growth of the continental crust: constraints from zircon Hf-isotope data. Lithos, 119(3-4), 457-466.

Belousova, E., Griffin, W. L., O'Reilly, S. Y., and Fisher, N. L. (2002). Igneous zircon: trace element composition as an indicator of source rock type. Contributions to Mineralogy and Petrology, 143(5), 602-622.

Benkhelil, J. (1989). The origin and evolution of the Cretaceous Benue Trough (Nigeria). Journal of African Earth Sciences (and the Middle East), 8(2), 251-282.

Bernau, R., Darbyshire, D. P. F., Franz, G., Harms, U., Huth, A., Mansour, N., Pasteels, P. and Schandelmeier, H. (1987). Petrology, geochemistry and structural development of the Bir Safsaf-Aswan uplift, Southern Egypt. Journal of African Earth Sciences, 6(1), 79-90.

Binks, R. M., and Fairhead, J. D. (1992). A plate tectonic setting for Mesozoic rifts of West and Central Africa. Tectonophysics, 213(1-2), 141-151.

Bishop, P. (1995). Drainage rearrangement by river capture, beheading and diversion. Progress in physical geography, 19(4), 449-473.

Black, L. P., Kamo, S. L., Allen, C. M., Aleinikoff, J. N., Davis, D. W., Korsch, R. J., and Foudoulis, C. (2003). TEMORA 1: a new zircon standard for Phanerozoic U–Pb Geochronology. Chemical Geology, 200, 155–170.

Blenkinsop, T., Martin, A., Jelsma, H. A., and Vinyu, M. L. (1997). The Zimbabwe Craton. Oxford Monographs on Geology and Geophysics, 35(1), 567-580.

Blum, M., and Pecha, M. (2014). Mid-cretaceous to Paleocene North American drainage reorganization from detrital zircons. Geology, 42(7), 607-610. doi:10.1130/G35513.1

Bond, G 1965. Some new fossi l localities in the Karroo System of Rhodesia. Arnoldia (Rhod.), 2 (11), 1 - 4.

Bond, G. (1967). A review of Karroo sedimentation and lithology in southern Rhodesia. In Reviews prepared for the First Symposium on Gondwana Stratigraphy (pp. 173-195).

Boniface, N., Schenk, V., and Appel, P. (2012). Paleoproterozoic eclogites of MORB-type chemistry and three Proterozoic orogenic cycles in the Ubendian Belt (Tanzania): Evidence from monazite and zircon geochronology, and geochemistry. Precambrian Research, 192, 16-33.

Borg, G., and Shackelton, R. M. (1997), The Tanzania and NE Zaire cratons, in de Wit, M., and Ashwal, L. D., eds., Greenstone belts: London, Clarendon Press, p. 608–619.

Boschetto, H. B. (1988). Geology of the Lothidok Range, northern Kenya. Unpublished Doctoral dissertation, The University of Utah, pp. 161.

Boschetto, H., Brown, F. H., and McDougall, I. M. (1992). Stratigraphy of the Lothidok Range, northern Kenya, and K/Ar ages of its Miocene primates. Journal of Human Evolution 22, 47–71.

Bosworth, W. (1992). Mesozoic and early Tertiary rift tectonics in East Africa. Tectonophysics, 209(1-4), 115-137.

Bosworth, W. (2015). Geological evolution of the Red Sea: historical background, review, and synthesis. In The Red Sea (pp. 45-78). Springer, Berlin, Heidelberg.

Bosworth, W. and Morley, C. K. (1994). Structural and stratigraphic evolution of the Anza Rift, Kenya. Tectonophysics 236: 93-115.

Bosworth, W., and Stockli, D. F. (2016). Early magmatism in the greater Red Sea rift: timing and significance. Canadian Journal of Earth Sciences, 53(11), 1158-1176.

Bosworth, W., Stockli, D. F., and Helgeson, D. E. (2015). Integrated outcrop, 3D seismic, and geochronologic interpretation of Red Sea dike-related deformation in the Western Desert, Egypt–The role of the 23Ma Cairo "mini-plume". Journal of African Earth Sciences, 109, 107-119.

Bouvier, A., Vervoort, J. D., and Patchett, P. J. (2008). The Lu–Hf and Sm–Nd isotopic composition of CHUR: constraints from unequilibrated chondrites and implications for the bulk composition of terrestrial planets. Earth and Planetary Science Letters, 273(1), 48-57.

Boyd, F. R., and Danchin, R. V. (1980). Lherzolites, eclogites and megacrysts from some kimberlites of Angola. American Journal of Science, 280(2), 528-549.

Brown, F. H., and McDougall, I. (2011). Geochronology of the Turkana Depression of northern Kenya and southern Ethiopia. Evolutionary Anthropology: Issues, News, and Reviews, 20(6), 217-227.

Browne, S. E., and Fairhead, J. D. (1983). Gravity study of the Central African Rift System: A model of continental disruption 1. The Ngaoundere and Abu Gabra rifts. Tectonophysics, 94(1-4), 187-203.

Buffetaut, E., Bussert, R., and Brinkmann, W. (1990). A new nonmarine vertebrate fauna in the Upper Cretaceous of northern Sudan. Berliner geowissenschaftlische Abhandlungen, (A) 120.1, 183-202.

Bumby, A. J., and Guiraud, R. (2005). The geodynamic setting of the Phanerozoic basins of Africa. Journal of African Earth Sciences, 43(1), 1-12. doi:10.1016/j.jafrearsci.2005.07.016

Burke, K. (1996). The African plate. South African Journal of Geology, 99(4), 341-409.

Burke, K., and Dewey, J. F. (1973). Plume-generated triple junctions: key indicators in applying plate tectonics to old rocks. The Journal of Geology, 81(4), 406-433.

Burke, K., and Gunnell, Y. (2008). The African erosion surface: a continental-scale synthesis of geomorphology, tectonics, and environmental change over the past 180 million years (Vol. 201). Geological Society of America.

Burke, K., MacGregor, D. S., and Cameron, N. R. (2003). Africa's petroleum systems: Four tectonic 'aces' in the past 600 million years. Geological Society, London, Special Publications, 207(1), 21. doi:10.1144/GSL.SP.2003.207.01.03

Bussert, R. (1993). Evolution of Cretaceous continental basins in northern Sudan. In: Thorweihe, U., Schandelmeier, H. (Eds.), Geoscientific Research in Northeast Africa. Balkema, Rotterdam, 415-419.

Bussert, R. (1998). Die Entwicklung intrakratonaler Becken im Nordsudan. Berliner geowissenschaftliche Abhandlungen, (A) 196, 1–329.

Bussert, R., Eisawi, A. A., Hamed, B., and Babikir, I. A. (2018). Neogene palaeochannel deposits in Sudan–Remnants of a trans-Saharan river system? Journal of African Earth Sciences, 141, 9-21.

Bussert, R., Heinrich, W. D., and Aberhan, M. (2009). The Tendaguru Formation (Late Jurassic to Early Cretaceous, southern Tanzania): definition, palaeoenvironments, and sequence stratigraphy. Fossil Record, 12(2), 141-174.

Cahen, L. (1954). Geologie du Congo Belge. H. Vaillant-Carmanne, Liege, pp. 577.

Cahen, L., Snelling, N. J., Delhal, J., and Vail, J. (1984). The Geochronology and Evolution of Africa. Oxford: Clarendon Press, pp. 512.

Cairncross, B. (2001). An overview of the Permian (Karoo) coal deposits of southern Africa. Journal of African Earth Sciences, 33(3), 529-562. doi:10.1016/S0899-5362(01)00088-4

Campeny, M., Kamenetsky, V. S., Melgarejo, J. C., Mangas, J., Manuel, J., Alfonso, P., Kamenetsky, M.B., Bambi, A. C. and Gonçalves, A. O. (2015). Carbonatitic lavas in Catanda (Kwanza Sul, Angola): Mineralogical and geochemical constraints on the parental melt. Lithos, 232, 1-11.

Campeny, M., Mangas, J., Melgarejo, J. C., Bambi, A., Alfonso, P., Gernon, T., and Manuel, J. (2014). The Catanda extrusive carbonatites (Kwanza Sul, Angola): an example of explosive carbonatitic volcanism. Bulletin of Volcanology, 76(4), 818.

Carrapa, B. (2010). Resolving tectonic problems by dating detrital minerals. Geology, 38(2), 191-192. doi:10.1130/focus022010.1

Castillo-Oliver, M., Galí, S., Melgarejo, J. C., Griffin, W.L., Belousova, E., Pearson, N. J., Watangua, M., O'Reilly, S. Y. (2016). Trace-element geochemistry and U-Pb dating of perovskite in kimberlites of the Lunda Norte province (NE Angola): petrogenetic and tectonic implications. Chemical geology, Vol. 426, (2016), p.118-134

Catuneanu, O., Wopfner, H., Eriksson, P. G., Cairncross, B., Rubidge, B. S., Smith, R. M. H., and Hancox, P. J. (2005). The Karoo basins of South-central Africa. Journal of African Earth Sciences, 43(1), 211-253. doi:10.1016/j.jafrearsci.2005.07.007

Cawood, P., Hawkesworth, C., and Dhuime, B. (2012). Detrital zircon record and tectonic setting. Geology, 40(10), 875-878. doi:10.1130/G32945.1

Censier, C. and Lang, J. (1999). Sedimentary processes in the Carnot formation (Central African Republic) related to the paleogeographic framework of central Africa. Sedimentary Geology, 127(1), 47-64. Doi:10.1016/S0037-0738(99)00017-2

Chambel, L., Caetano, L., and Reis, M. (2013) One century of Angolan diamonds. Eaglestone Securities 104p

Chorowicz, J. (2005). The East African rift system. Journal of African Earth Sciences, 43(1), 379-410. Doi: 10.1016/j.jafrearsci.2005.07.019

Clifford, T. N. (1970). The structural framework of Africa. In African magmatism and tectonics (pp. 1-26). Oliver and Boyd Edinburgh.

Coffin, M. F., and Rabinowitz, P. D. (1988). Evolution of the conjugate East African-Madagascan margins and the western Somali Basin. Geological Society of America Special Papers, 226, 1-79.

Condie, K.C., Beyer, E., Belousova, E., Griffin, W. L., and O'Reilly, S. Y. (2005). U-Pb isotopic ages and Hf isotopic composition of single zircons: The search for juvenile Precambrian continental crust: Precambrian Research, v. 139, p. 42–100, doi:10.1016/j.precamres.2005.04.006.

Corfu, F., and Noble, S. R. (1992). Genesis of the southern Abitibi greenstone belt, Superior Province, Canada: evidence from zircon Hf isotope analyses using a single filament technique. Geochim. Cosmochim. Acta 56, 2081–2097.

Corfu, F., Hanchar, J. M., Hoskin, P. W. O., and Kinny, P. (2003). Atlas of zircon textures. In: Hanchar, J. M., Hoskin, P. W. O. (Eds.), Zircon. Reviews in Mineralogy and Geochemistry Vol. 53, pp. 468–500.

Corti, G. (2009). Continental rift evolution: from rift initiation to incipient break-up in the Main Ethiopian Rift, East Africa. Earth-science reviews, 96(1-2), 1-53.

Cox, K. G. (1989). The role of mantle plumes in the development of continental drainage patterns. Nature, 342(6252), 873-877. doi:10.1038/342873a0

Cracraft, J. (1974). Continental drift and vertebrate distribution. Annual Review of Ecology and Systematics, 5(1), 215-261.

Crosby, A., Fishwick, S., and White, N. (2010). Structure and evolution of the intracratonic Congo Basin. Geochemistry Geophysics Geosystems, 11(6) Doi: 10.1029/2009GC003014

Cullers, R. L., Bock, B., and Guidotti, C. (1997). Elemental distributions and neodymium isotopic compositions of Silurian metasediments, western Maine, USA: redistribution of the rare earth elements. Geochimica et Cosmochimica Acta, 61(9), 1847-1861.

Cutten, H. N. C., S. P. Johnson, and B. De Waele. (2006). Tectonic evolution of the Mozambique Belt, Eastern Africa. 21st Colloquium of African Geology. Maputo, Mozambique. 3–5 July (2006), pp. 33-34 Abstracts volume Retrieved from http://citeseerx.ist.psu.edu/viewdoc/download?doi=10.1.1.544.1505andrep=rep1andtype=pdf

Daly, M. C. (1986). The intracratonic Irumide belt of Zambia and its bearing on collision orogeny during the Proterozoic of Africa. Geological Society, London, Special Publications, 19(1), 321-328.

Daly, M. C., Lawrence, S. R., Diemu-Tshiband, K., and Matouana, B. (1992). Tectonic evolution of the Cuvette centrale, Zaire. Journal of the Geological Society, 149(4), 539-539. Doi: 10.1144/gsjgs.149.4.0539

Davis, G. L. (1977). The ages and uranium contents of zircons from kimberlites and associated rocks. Carnegie Institution of Washington Yearbook, 76, 631-654.

De Boorder, H. (1982). Deep-reaching fracture zones in the crystalline basement surrounding the West Congo System and their control of mineralization in Angola and Gabon. Geoexploration, 20(3-4), 259-273.

De Carvalho, H., Tassinari, C., Alves, P. H., Guimarães, F., and Simões, M. C. (2000). Geochronological review of the Precambrian in western Angola: links with Brazil. Journal of African Earth Sciences, 31(2), 383-402.

De Kun, N. (1987). Mineral economics of Africa (Vol. 22). Elsevier Science Ltd.

De Ridder, F., Pintelon, R., Schoukens, J., Navez, J., André, L., and Dehairs, F. (2002). An improved multiple internal standard normalisation for drift in LA-ICP-MS measurements. Journal of Analytical Atomic Spectrometry, 17(11), 1461-1470. doi:10.1039/b207715a

De Waele, B. (2005), The Proterozoic geological history of Irumide belt, Zambia (Unpublished Ph.D. thesis), Curtin University of Technology, Perth, Australia, 358 pp.

De Waele, B., and Mapani, B. (2002). Geology and correlation of the central Irumide belt. Journal of African Earth Sciences, 35(3), 385-397. Doi: 10.1016/S0899-5362(02)00149-5

De Waele, B., Johnson, S. P., and Pisarevsky, S. A. (2008). Palaeoproterozoic to Neoproterozoic growth and evolution of the eastern Congo Craton: its role in the Rodinia puzzle. Precambrian Research, 160(1), 127-141.

De Wit M.J and Linol, B. (2015) Precambrian Basement of the Congo Basin and Its flanking terrains. In De Wit, M., Guillocheau, F., and De Wit, M. C. J. (Eds) (2015). Geology and resource potential of the Congo Basin (pp. 19-37). Dordrecht: Springer.

De Wit, M. C. J. (1999). Post-Gondwana drainage and the development of diamond placers in western South Africa. Economic Geology, 94(5), 721-740.

De Wit, M. J. (1998). On Archean granites, greenstones, cratons and tectonics: does the evidence demand a verdict? Precambrian Research, 91(1-2), 181-226.

De Wit, M., Guillocheau, F., and De Wit, M. C. J. (Eds) (2015). Background to a Punctuated History of Geoscience in the Congo. Geology and resource potential of the Congo Basin (Vol. 1) (pp. xi-xxxix). Dordrecht: Springer, 417pp

Delhal, J., and Liégeois, J. P. (1982). Le socle granito-gneissique du Shaba occidental (Zaïre) - Pétrographie et géochronologie. Annales de la Société Géologie de Belgique 105, 295–301.

Delpomdor, F., Linnemann, U., Boven, A., Gärtner, A., Travin, A., Blanpied, C., and Préat, A. (2013). Depositional age, provenance, and tectonic and paleoclimatic settings of the Late Mesoproterozoic-Middle Neoproterozoic Mbuji Mayi Supergroup, Democratic Republic of Congo. Paleogeography, Paleoclimatology, Paleoecology, 389, 4-34. Doi:10.1016/j.palaeo.2013.06.012

Dhuime, B., Hawkesworth, C., and Cawood, P. (2011). When continents formed. Science, 331(6014), 154-155.

Dickinson, W (1970). Interpreting Detrital Modes of Greywacke and Arkose. Journal of Sedimentary Petrology, Volume 40, No. 2, p. 695-707

Dickinson, W. R. (1985). Interpreting provenance relations from detrital modes of sandstones. In: Provenance of Arenites, Zuffa, G. G. ed., NATO Science Series 148. Reidel Publishing Company: Dordrecht; pp. 333–361.

Dickinson, W. R. and Suczek, C (1979). Plate tectonics and sandstone composition. American Association of Petroleum Geologist Bulletin 63:2164-2182

Dickinson, W. R., and Gehrels, G. E. (2009). Use of U-Pb ages of detrital zircons to infer maximum depositional ages of strata: A test against a Colorado Plateau Mesozoic database. Earth and Planetary Science Letters, 288, 115-125.

Dickinson, W. R., Beard, L. S., Brakenridge, G. R., Erjavec, J. L., Ferguson, R. C., Inman, K. F., Lindberg, F. A., and Ryberg, P. T. (1983). Provenance of North American Phanerozoic sandstones in relation to tectonic setting. Geological Society of America Bulletin, 94(2), 222-235.

Dickinson, W. R., Gehrels, G. E. (2009). Use of U-Pb ages of detrital zircons to infer maximum depositional ages of strata: A test against a Colorado Plateau Mesozoic database. Earth and Planetary Science Letters 288, 115-125.

Dietrich, C. (2000). Inventory of formal diamond mining in Angola. Angola's War Economy: The Role of Oil and Diamonds, 141-72.

Dixon, T. H., and Golombek, M. P. (1988). Late Precambrian crustal accretion rates in northeast Africa and Arabia. Geology, 16(11), 991-994.

Do Toit, AL. (1933). Crustal movements as a factor in the evolution of southern Africa. South African Geographical Journal, 16, 3-20.

Doucouré C. M., De Wit, M. J., and Bowring, S. (1999). New data from the Congo Craton, Central African Shield. CIGCES Annual Report to De Beers Africa Exploration.

Doucouré, C. M., and de Wit, M. J. (2003). Old inherited origin for the present near-bimodal topography of Africa. Journal of African Earth Sciences, 36(4), 371-388. doi:10.1016/S0899-5362(03)00019-8

Downey N. J. and Gurnis, M. (2009) Instantaneous dynamics of the cratonic Congo Basin, Journal Geophysical Research - Solid Earth, 114 (B6), B06401. Doi: 10.1029/2008JB006066

Ducrocq, S., Boisserie, J. R., Tiercelin, J. J., Delmer, C., Garcia, G., Kyalo, M. F., Leakey, M. G., Marivaux, L., Otero, O., Peigné, S., Tassy, P., and Lihoreau, F. (2010). New Oligocene vertebrate localities from Northern Kenya (Turkana Basin). Journal of Vertebrate Paleontology 30 (1), 293–299. http://dx.doi.org/10.1080/02724630903413065.

Dunkelman, T. J., Rosendahl, B. R., and Karson, J. A. (1989). Structure and stratigraphy of the Turkana rift from seismic reflection data. Journal of African Earth Sciences (and the Middle East), 8(2-4), 489-510.

Durand, J. F. (2005). Major African contributions to Palaeozoic and Mesozoic vertebrate palaeontology. Journal of African Earth Sciences, 43(1-3), 53-82.

Ebinger, C. (2005). Continental break-up: the East African perspective. Astronomy & Geophysics, 46(2), 2-16.

Ebinger, C. J., Yemane, T., Harding, D. J., Tesfaye, S., Kelley, S., and Rex, D. C. (2000). Rift deflection, migration, and propagation: Linkage of the Ethiopian and Eastern rifts, Africa. Geological Society of America Bulletin, 112(2), 163-176.

Ebinger, C. J., and Ibrahim, A. (1994). Multiple episodes of rifting in central and east Africa: A re-evaluation of gravity data. Geologische Rundschau, 83(4), 689-702. doi:10.1007/BF00251068

Ebinger, C. J., and Sleep, N. H. (1998). Cenozoic magmatism throughout east Africa resulting from impact of a single plume. Nature, 395(6704), 788.

Ebinger, C. J. (1989). Tectonic development of the western branch of the East African rift system. Geological Society of America Bulletin, 101(7), 885-903.

Ebinger, C. J., Bechtel, T. D., Forsyth, D. W., and Bowin, C. O. (1989). Effective elastic plate thickness beneath the East African and Afar plateaus and dynamic compensation of the uplifts. Journal of Geophysical Research: Solid Earth, 94(B3), 2883-2901.

Ego, J. K. (1994). Sedimentology and Diagenesis of Neogene Sediments in the Central Kenya Rift Valley. Unpublished, M.Sc. Thesis, University of Saskatchewan, pp. 177

Egorov, K. N., Roman'ko, E. F., Podvysotsky, V. T., Sablukov, S. M., Garanin, V. K., and D'yakonov, D. B. (2007). New data on kimberlite magmatism in southwestern Angola. Russian Geology and Geophysics, 48(4), 323-336

Eisawi, A. A. (2015). Palynological evidence of a Campanian-Maastrichtian age of the Shendi Formation (Shendi Basin, central Sudan). American Journal of Earth Sciences, 2, 206-210.

Eisawi, A. A. M., Elbashir, O. M., Babikir, I. A. A., and Ali, O. E. (2012). Palynology and sedimentology of the Campanian-Maastrichtian Shendi Formation, central Sudan: Paleoecological and Paleoclimatical Implications. SAPEG Fifth Conference (Abstract volume), pp. 83–84.

Eley, R., Grutter, H., Louw, A., Tunguno, C., Twidale, J. (2008). Exploration geology of the Luxinga kimberlite cluster (Angola) with evidence supporting the presence of

kimberlite lava. In: 9th International Kimberlite Conference, Extended Abstract, No. 9IKC-A-00166, pp. 3.

Emerick, C. M., and Duncan, R. A. (1982). Age progressive volcanism in the Comores Archipelago, western Indian Ocean and implications for Somali plate tectonics. Earth and Planetary Science Letters, 60(3), 415-428.

Erlanger, E. D., Granger, D. E., and Gibbon, R. J. (2012). Rock uplift rates in South Africa from isochron burial dating of fluvial and marine terraces. Geology, 40(11), 1019-1022.

Evans, S. E., Milner, A. R., and Werner, C. (1996). Sirenid salamanders and gymnophionan amphibian from the Cretaceous of the Sudan. Palaeontology, 39, 77-95.

Fairhead, J. D. (1988). Mesozoic plate tectonic reconstructions of the central South Atlantic Ocean: the role of the West and Central African rift system. Tectonophysics, 155(1-4), 181-191.

Fairhead, J. D., and Binks, R. M. (1991). Differential opening of the Central and South Atlantic Oceans and the opening of the West African rift system. Tectonophysics, 187(1-3), 191–203.

Fairhead, J. D., Green, C. M., Masterton, S. M., and Guiraud, R. (2013). The role that plate tectonics, inferred stress changes and stratigraphic unconformities have on the evolution of the west and central African rift system and the Atlantic continental margins. Tectonophysics, 594, 118-127. Doi:10.1016/j.tecto.2013.03.021

Faure, S. (2010). World kimberlites CONSOREM database (version 3), consortium de recherche en exploration minérale CONSOREM. Université du Québec à Montréal ([WWW Document]. www.consorem.ca).

Fedo, C. M, Sircombe, K. N., and Rainbird, R. H. (2003). Detrital Zircon Analysis of Sedimentary Record, In: Hanchar, J.M., Hoskin, P. W. O. (Eds.), Zircon. Rev. Min. Geochem. 53, 277-303.

Feibel, C. S. (2011). A geological history of the Turkana Basin. Evolutionary Anthropology, 20(6), 206-216. doi: 10.1002/evan.20331

Feibel, C. S., Brown, F. H., and McDougall, I. (1989). Stratigraphic context of fossil hominids from the Omo Group deposits: northern Turkana Basin, Kenya and Ethiopia. American Journal of Physical Anthropology, 78(4), 595-622.

Fernández-Suárez, J., Gutiérrez-Alonso, G., Pastor-Galán, D., Hofmann, M., Murphy, J. B., and Linnemann, U. (2014). The Ediacaran–Early Cambrian detrital zircon record of NW Iberia: possible sources and paleogeographic constraints. International Journal of Earth Sciences, 103(5), 1335-1357. doi: 10.1007/s00531-013-0923-3

Fieremans, C.L. (1996). A brief review of the occurrences of diamonds in the Republic of Zaïre. Special edition of Africa Geoscience Review, 91-94.

Fildani, A., Drinkwater, N. J., Weislogel, A., McHargue, T., Hodgson, D. M., and Flint, S. S. (2007). Age controls on the Tanqua and Laingsburg deep-water systems: New insights on the evolution and sedimentary fill of the Karoo Basin, South Africa. Journal of Sedimentary Research, 77(11), 901-908.

Fildani, A., Weislogel, A., Drinkwater, N. J., McHargue, T., Tankard, A., Wooden, J., Flint, S. (2009). U-Pb zircon ages from the southwestern Karoo basin, South Africa--implications for the Permian-Triassic boundary. Geology, 37(8), 719-722. doi:10.1130/G25685A.1

Fisher, C. M., Hanchar, J. M., Samson, S. D., Dhuime, B., Blichert-Toft, J., Vervoort, J. D., and Lam, R. (2011). Synthetic zircon doped with hafnium and rare earth elements: a

reference material for in situ hafnium isotope analysis. Chemical Geology. 286, 32–47.

Fisher, C. M., Vervoort, J. D., and Hanchar, J. M. (2014). Guidelines for reporting zircon Hf isotopic data by LA-MC-ICPMS and potential pitfalls in the interpretation of these data. Chemical Geology, 363, 125-133.

Fleagle, J., and Leakey, M. (2011). The Turkana Basin introduction. Evolutionary Anthropology, 20(6), 201-201. doi:10.1002/evan.20333

Flowers, R. M., and Schoene, B. (2010). (U-Th)/He thermochronometry constraints on unroofing of the eastern Kaapvaal craton and significance for uplift of the southern African Plateau. Geology, 38(9), 827-830.

Flynn, L. J., Brillanceau, A., Brunet, M., Coppens, Y., Dejax, J., Duperon-Laudoueneix, M., Ekodeck, G., Flanagan, K. M., Heintz, E., Hell, J. and Jacobs, L. L. (1988). Vertebrate fossils from Cameroon, West Africa. Journal of Vertebrate Paleontology, 7(4), 469-471.

Folk, R. L. (1980). Petrology of sedimentary rocks. Hemphill Publishing Company.

Fortelius, M., Zliobaite, I., Kaya, F., Bibi, F., Bobe, R., Leakey, L., Werdelin, L. (2016). An ecometric analysis of the fossil mammal record of the Turkana Basin. Philosophical Transactions of the Royal Society Biological Sciences, 371(1698), 20150232. doi:10.1098/rstb.2015.0232

Foster, D. A., Goscombe, B. D., Newstead, B., Mapani, B., Mueller, P. A., Gregory, L. C., and Muvangua, E. (2015). U–Pb age and Lu–Hf isotopic data of detrital zircons from the Neoproterozoic Damara sequence: Implications for Congo and Kalahari before Gondwana. Gondwana Research, 28(1), 179-190. Doi:10.1016/j.gr.2014.04.011

Francis, P. W., Thorpe, R. S., and Ahmed, F. (1973). Setting and significance of Tertiary-Recent volcanism in the Darfur Province of Western Sudan. Nature, 243(124), 30-32.

Franz, G., Harms, U., Denkler, T., and Pasteels, P. (1993). Late Cretaceous igneous activity in the Delgo uplift (Northern Province, Sudan. In: Thorweihe, U., Schandelmeier, H. (Eds.), Geoscientific Research in Northeast Africa. Balkema, Rotterdam, 227-230.

Franz, G., Puchelt, H., and Pasteels, P. (1987). Petrology, geochemistry and age relations of Triassic and Tertiary volcanic rocks from SW Egypt and NW Sudan. Journal of African Earth Sciences (1983), 6(3), 335-352.

Frimmel, H. E., Tack, L., Basei, M. S., Nutman, A. P., and Boven, A. (2006). Provenance and chemostratigraphy of the Neoproterozoic West Congolian Group in the Democratic Republic of Congo. Journal of African Earth Sciences, 46(3), 221-239. Doi:10.1016/j.jafrearsci.2006.04.010

Frostick, L., and Reid, I. (1989). Is structure the main control of river drainage and sedimentation in rifts? Journal of African Earth Sciences, 8(2), 165-182. doi:10.1016/S0899-5362(89)80022-3

Gaina, C., Torsvik, T. H., van Hinsbergen, D. J. J., Medvedev, S., Werner, S. C., and Labails, C. (2013). The African plate: A history of oceanic crust accretion and subduction since the Jurassic. Tectonophysics, 604, 4-25. doi:10.1016/j.tecto.2013.05.037

Gartner, A., Linnemann, U., and Hofmann, M. (2014). The provenance of northern Kalahari basin sediments and growth history of the southern Congo Craton reconstructed by U–Pb ages of zircons from recent river sands. International Journal of Earth Sciences, 103(2), 579-595. Doi: 10.1007/s00531-013-0974-5

Gehrels, G. (2014). Detrital zircon U-Pb geochronology applied to tectonics. Annual Review of Earth and Planetary Sciences, 42, 127-149. doi:10.1146/annurev-earth-050212-124012

Gehrels, G. E., Valencia, V. A., and Ruiz, J. (2008). Enhanced precision, accuracy, efficiency, and spatial resolution of U-Pb ages by laser ablation–multicollector–inductively coupled plasma–mass spectrometry. Geochemistry, Geophysics, Geosystems, 9(3).

Gehrels, G., Rusmore, M., Woodsworth, G., Crawford, M., Andronicos, C., Hollister, L., Patchett, J., Ducea, M., Butler, R., Klepeis, K., Davidson, C., Friedman, R., Haggart, R., Mahoney, B., Crawford, W., Pearson, D, and Girardi, J. (2009). U-Th-Pb geochronology of the Coast Mountains batholith in north-coastal British Columbia: Constraints on age and tectonic evolution. Geological Society of America Bulletin, 121(9-10), 1341-1361. Doi:10.1130/B26404.1

Gehrels, G.E. (2012). Detrital Zircon U-Pb Geochronology: current methods and new opportunities. In: Busby, C., Azor, A. (Eds.), Tectonics of Sedimentary Basins: Recent Advances. John Wiley and Sons, pp. 47-62.

Genik, G. J. (1993). Petroleum geology of Cretaceous-Tertiary rift basins in Niger, Chad, and Central African Republic. AAPG Bulletin, 77(8), 1405-1434.

George, R., Rogers, N., and Kelley, S. (1998). Earliest magmatism in Ethiopia: evidence for two mantle plumes in one flood basalt province. Geology, 26(10), 923-926.

Giresse, P. (2005). Mesozoic–Cenozoic history of the Congo Basin. Journal of African Earth Sciences, 43(1), 301-315. Doi: 10.1016/j.jafrearsci.2005.07.009

Gloy, U. (1997). Eine Dipnoifauna aus der unteren Oberkreide des Sudan. Unpublished diploma thesis, Department of Palaeontology, Free University, Berlin.

Gomani, E. M. (1997). A crocodyliform from the Early Cretaceous dinosaur beds, northern Malawi. Journal of Vertebrate Paleontology, 17(2), 280-294.

Gomani, E. M. (2005). Sauropod dinosaurs from the early Cretaceous of Malawi, Africa. Palaeontologia Electronica, 8(1), 27A.

Goodwin, A. M. (2013). Precambrian geology: the dynamic evolution of the continental crust. Elsevier. 665 pp.

Gorscak, E., O'Connor, P. M., Roberts, E. M., and Stevens, N. J. (2017). The second titanosaurian (Dinosauria: Sauropoda) from the middle Cretaceous Galula Formation, southwestern Tanzania, with remarks on African titanosaurian diversity. Journal of Vertebrate Paleontology, 37(4), e1343250.

Gorscak, E., O'Connor, P. M., Stevens, N. J., and Roberts, E. M. (2014). The basal titanosaurian Rukwatitan bisepultus (Dinosauria, Sauropoda) from the middle Cretaceous Galula Formation, Rukwa Rift Basin, southwestern Tanzania. Journal of Vertebrate Paleontology, 34(5), 1133-1154.

Goscombe, B., Armstrong, R., and Barton, J. M. (2000). Geology of the Chewore Inliers, Zimbabwe: constraining the Mesoproterozoic to Palaeozoic evolution of the Zambezi Belt. Journal of African Earth Sciences, 30(3), 589-627.

Goudie, A. S. (2005). The drainage of Africa since the Cretaceous. Geomorphology, 67(3), 437-456. Doi:10.1016/j.geomorph.2004.11.008

Grab, S., Knight, J., and SpringerLink (Online service). (2015). Landscapes and landforms of South Africa (1st ed.). S.I.: Springer International Publishing.

Grantham, G. H., Maboko, M., and Eglington, B. M. (2003). A review of the evolution of the Mozambique Belt and implications for the amalgamation and dispersal of Rodinia and Gondwana. Geological Society, London, Special Publications, 206(1), 401-425.

Greenhalgh, P. A. L. (1985). West African Diamonds, 1919-1983: an economic history. Manchester University Press.

Griffin, D. L. (2002). Aridity and humidity: two aspects of the late Miocene climate of North Africa and the Mediterranean. Palaeogeography, Palaeoclimatology, Palaeoecology, 182(1-2), 65-91.

Griffin, W. L., O'Reilly, S. Y., Abe, N., Aulbach, S., Davies, R. M., Pearson, N.J., Doyle, B.J. and Kivi, K. (2003). The origin and evolution of Archean lithospheric mantle. Precambrian Research, 127(1-3), 19-41.

Griffin, W., Belousova, E., Shee, S., Pearson, N., and O'reilly, S. (2004). Archean crustal evolution in the northern Yilgarn Craton: U–Pb and Hf-isotope evidence from detrital zircons. Precambrian Res. 131, 231–282.

Grimes, C. B., John, B. E., Kelemen, P. B., Mazdab, F. K., Wooden, J. L., Cheadle, M. J., Hanghoj, K., and Schwartz, J. J. (2007). Trace element chemistry of zircons from oceanic crust: a method for distinguishing detrital zircon provenance. Geology 35, 643–646.

Grimes, C. B., Wooden, J. L., Cheadle, M. J., and John, B. E. (2015). "Fingerprinting" tectono-magmatic provenance using trace elements in igneous zircon. Contributions to Mineralogy and Petrology, 170(5-6), 46.Grimes, C. B., John, B. E., Kelemen, P. B., Mazdab, F. K., Wooden, J. L., Cheadle, M. J., Hanghoj, K., Schwartz, J. J. (2007). Trace element chemistry of zircons from oceanic crust: a method for distinguishing detrital zircon provenance. Geology 35, 643–646.

Guillong, M., Meier, D. L., Allan, M. M., Heinrich, C. A., and Yardley, B. W. (2008). Appendix A6: SILLS: A MATLAB-based program for the reduction of laser ablation

ICP-MS data of homogeneous materials and inclusions. Mineralogical Association of Canada Short Course Series, 40, 328-333.

Guiraud, R., Bosworth, W., Thierry, J., and Delplanque, A. (2005). Phanerozoic geological evolution of Northern and Central Africa: an overview. Journal of African Earth Sciences, 43(1-3), 83-143.

Guynn, J., and Gehrels, G. (2010), Comparison of Detrital Zircon Age Distributions Using the K-S Test Visualization and Representation of Age-Distribution Data Histograms: Tucson, Arizona, Arizona LaserChron Center, University of Arizona, 16 p., https://sites. google.com/a/laserchron.org/laserchron/.

Haddon, I. G. (2005). The Sub-Kalahari geology and tectonic evolution of the Kalahari Basin, Southern Africa (Unpublished PhD thesis), University of the Witwatersrand, Johannesburg, 360 pp.

Hansen E (2007). Characterization of Cretaceous Age Sedimentary Units from the Kasai Craton, Democratic Republic of Congo, Basin Research. 6:95-113

Hanson, R. E., Wilson, T. J., and Munyanyiwa, H. (1994). Geologic evolution of the Neoproterozoic Zambezi orogenic belt in Zambia. Journal of African Earth Sciences, 18(2), 135-150.

Hargrove, U. S., Hanson, R. E., Martin, M. W., Blenkinsop, T. G., Bowring, S. A., Walker, N., and Munyanyiwa, H. (2003). Tectonic evolution of the Zambezi orogenic belt: Geochronological, structural, and petrological constraints from northern Zimbabwe. Precambrian Research, 123(2), 159-186. Doi:10.1016/S0301-9268(03)00066-4

Harrell, J (1984). Roller micrometer analysis of grain shape sediment PetrolV54, N2, June 1984, P643–645. (1985).International Journal of Rock Mechanics and Mining

Sciences and Geomechanics Abstracts, 22(3), A81-A81. doi:10.1016/0148-9062(85)93360-1

Harris, N. B. W., Hawkesworth, C. J., and Ries, A. C. (1984). Crustal evolution in north-east and east Africa from model Nd ages. Nature, 309(5971), 773-776.

Hastings, A. K., Bloch, J. I. and Jaramillo, C. A. (2011). A new longirostrine dyrosaurid (Crocodylomorpha, Mesoeucrocodylia) from the Paleocene of north-eastern Colombia: biogeographic and behavioural implications for New-World Dyrosauridae. Palaeontology 54: 1095-1116. doi: 10.1111/j.1475-4983.2011.01092.x

Haughton, P. D. W., Todd, S. P., and Morton, A. C. (1991). Sedimentary provenance studies. Geological Society, London, Special Publications, 57(1), 1-11. Doi: 10.1144/GSL.SP.1991.057.01.01

Hauzenberger, C. A., Sommer, H., Fritz, H., Bauernhofer, A., Kröner, A., Hoinkes, G., Wallbrecher, E. and Thöni, M. (2007). SHRIMP U–Pb zircon and Sm–Nd garnet ages from the granulite-facies basement of SE Kenya: evidence for Neoproterozoic polycyclic assembly of the Mozambique Belt. Journal of the Geological Society, 164(1), 189-201.

Hawkesworth, C. J., and Kemp, A. I. S. (2006). Using hafnium and oxygen isotopes in zircons to unravel the record of crustal evolution. Chemical Geology, 226, 144–162.

Heaman, L. M., Bowins, R., and Crocket, J. (1990). The chemical composition of igneous zircon suites: implications for geochemical tracer studies. Geochimica et Cosmochimica Acta, 54(6), 1597-1607.

Heaman, L. M., Kjarsgaard, B. A., and Creaser, R. A. (2003). The timing of kimberlite magmatism in North America: implications for global kimberlite genesis and diamond exploration. Lithos, 71(2-4), 153-184.

Heinrich, W. D. (1999). First haramiyid (Mammalia, Allotheria) from the Mesozoic of Gondwana. Fossil Record, 2(1), 159-170.

Helmore, R. (1984). Diamond mining in Angola. Mining magazine, 150, 530.

Hepworth, J. V. (1972). The Mozambique orogenic belt and its foreland in northeast Tanzania: a photogeologically-based study. Journal of the Geological Society, 128(5), 461-494.

Hepworth, J. V., and Kennerley, J. B. (1969). Photogeology and structure of the Mozambique orogenic front near Kolo, north-east Tanzania. Quarterly Journal of the Geological Society, 125(1-4), 447-479.

Hoefen, T. M., Clark, R. N., Bandfield, J. L., Smith, M. D., Pearl, J. C., and Christensen, P. R. (2003). Discovery of olivine in the Nili Fossae region of Mars. Science, 302(5645), 627-630. Doi:10.1126/science.1089647

Holmes, A. (1951). The sequence of Precambrian orogenic belts in south and central Africa. In 18th International Geological Congress, London, Part (Vol. 24, pp. 254-269).

Horie, K., Hidaka, H., and Gauthier-Lafaye, F. (2008). Elemental distribution in apatite, titanite and zircon during hydrothermal alteration: Durability of immobilization mineral phases for actinides. Physics and Chemistry of the Earth, 33(14), 962-968. Doi:10.1016/j.pce.2008.05.008

Hoskin, P. W. (2005). Trace-element composition of hydrothermal zircon and the alteration of Hadean zircon from the Jack Hills, Australia. Geochimica et Cosmochimica Acta, 69(3), 637-648.

Hoskin, P. W. O., and Schaltegger, U. (2003). The composition of zircon and igneous and metamorphic petrogenesis. Reviews in Mineralogy and Geochemistry 53, 27–62.

Hoskin, P. W. O., and Ireland, T. R. (2000). Rare earth element chemistry of zircon and its use as a provenance indicator. Geology, 28(7), 627-630.

Howarth, R. J. (1998). Improved estimators of uncertainty in proportions, point-counting, and pass-fail test results. American Journal of Science, 298(7), 594-607. Doi:10.2475/ajs.298.7.594

Humphreys, B., Morton, A. C., Hallsworth, C. R., Gatliff, R. W., and Riding, J. B. (1991). An integrated approach to provenance studies: A case example from the upper Jurassic of the central graben, North Sea. Geological Society, London, Special Publications, 57(1), 251-262. doi:10.1144/GSL.SP.1991.057.01.19

Ibrahim, A. E., Ebinger, C. J., and Fairhead, J. D. (1996). Lithospheric extension northwest of the Central African Shear Zone in Sudan from potential field studies. Tectonophysics, 255(1), 79-97. Doi:10.1016/0040-1951(95)00080-1

Iizuka, T., Campbell, I. H., Allen, C. M., Gill, J. B., Maruyama, S., and Makoka, F. (2013). Evolution of the African continental crust as recorded by U-Pb, Lu-Hf and O isotopes in detrital zircons from modern rivers. Geochimica Et Cosmochimica Acta, 107, 96-120. Doi:10.1016/j.gca.2012.12.028

Ingersoll, R. V., Bullard, T. F., Ford, R. L., Grimm, J. P., Pickle, J. D, and Sares, S. W. (1984). The effect of grain size on detrital modes: A test of the Gazzi-Dickinson point-counting method (Holocene, sand, New Mexico, USA). Journal Of Sedimentary Petrology, 54(1), 103-116.

Issawi, B., and McCauley, J. F. (1992). The Cenozoic rivers of Egypt: the Nile problem. The followers of Horus, Studies dedicated to Michael Allen Hoffman, Oxbow Monograph, 20, 121-138.

Jackson, S. E., Pearson, N. J., Griffin, W. L., and Belousova, E. A. (2004). The application of laser ablation-inductively coupled plasma-mass spectrometry to in-situ U-Pb zircon geochronology. Chemical Geology 211, 47-69.

Jacobs, L. L., Mateus, O., Polcyn, M. J., Schulp, A. S., Scotese, C. R., Goswami, A., Buto Neto, A. (2009). Cretaceous paleogeography, paleoclimatology, and amniote biogeography of the low and mid-latitude South Atlantic Ocean. Bulletin De La Societe Geologique De France, 180(4), 333. doi:10.2113/gssgfbull.180.4.333

Jacobs, L. L., Polcyn, M. J., Mateus, O., Schulp, A. S., Gonçalves, A. O., and Morais, M. L. (2016). Post-Gondwana Africa and the vertebrate history of the Angolan Atlantic Coast. Memoirs of Museum Victoria, 74, 343-362.

Jacobs, L. L., Winkler, D. A., and Gomani, E. M. (1996). Cretaceous dinosaurs of Africa: Examples from Cameroon and Malawi. Memoirs of the Queensland Museum, 39(3), 595-610

Jacobs, L. L., Winkler, D. A., Kaufulu, Z. M., and Downs, W. R. (1990). The dinosaur beds of Northern Malawi, Africa. National Geographic Research, 6 (2), 196-204, Washington D.C.

Jacobs, L., Winkler, D. A., Downs, W. R., and Gomani, E. M. (1993). New material of an Early Cretaceous titanosaurid saurepod dinosaur from Malawi. Palaeontology, 36, 523-523.

Janse, A. B., and Sheahan, P. A. (1995). Catalogue of world-wide diamond and kimberlite occurrences: a selective and annotative approach. Journal of Geochemical Exploration, 53(1-3), 73-111.

Jelsma, H. A, Perritt, S. H., Joy, S. and Armstrong, R. A. (2015). Basement architecture of the Central African Kasai Craton revealed using high precision SHRIMP II U-Pb zircon geochronology. Abstract - 35th International Geological Congress, Cape Town.

Jelsma, H. A., and Dirks, Paul H. G. M. (2002). Neoarchean tectonic evolution of the Zimbabwe Craton. Geological Society, London, Special Publications, 199(1), 183-211. Doi:10.1144/GSL.SP.2002.199.01.10

Jelsma, H. A., McCourt, S., Perritt, S. H., and Armstrong, R. A. (2018). The Geology and Evolution of the Angolan Shield, Congo Craton. In Geology of Southwest Gondwana (pp. 217-239). Springer, Cham.

Jelsma, H. A., Perritt, S. H., Armstrong, R., Ferreira, H. F. (2011). Shrimp U-Pb zircon geochronology of basement rocks of the Angolan Shield, western Angola. Abstract, 23rd Colloquium of African Geology, Johannesburg, 8th-14th January.

Jelsma, H., Barnett, W., Richards, S., and Lister, G. (2009). Tectonic setting of kimberlites. Lithos, 112, 155-165.

Jelsma, H., Krishnan, U., Perritt, S., Preston, R., Winter, F., Lemotlo, L., van der Linde, G., Armstrong, R., Phillips, D., Joy, S., Costa, J. (2013). Kimberlites from Central Angola: a case study of exploration findings. Proceedings of 10th International Kimberlite Conference 1. Springer, India, pp. 173–190.

Jian, X., Guan, P., Zhang, D. W., Zhang, W., Feng, F., Liu, R.J., and Lin, S. D. (2013). Provenance of Tertiary sandstone in the northern Qaidam basin, northeastern Tibetan Plateau: integration of framework petrography, heavy mineral analysis and mineral chemistry. Sedimentary Geology 290, 109–125.

Jinnah, Z. A., Roberts, E. M., Deino, A. L., Larsen, J. S., Link, P. K., and Fanning, C. M. (2009). New Ar-40-Ar-39 and detrital zircon U-Pb ages for the Upper Cretaceous

Wahweap and Kaiparowits formations on the Kaiparowits Plateau, Utah: implications for regional correlation, provenance, and biostratigraphy. Cretaceous Research, 30(2), 287-299. doi: 10.1016/j.cretres.2008.07.012

Jones III, J. V., Connelly, J. N., Karlstrom, K. E., Williams, M. L., and Doe, M. F. (2009). Age, provenance, and tectonic setting of Paleoproterozoic quartzite successions in the southwestern United States. Geological Society of America Bulletin, 121(1-2), 247-264.

Jorge, R. C. G. S., Fernandes, P., Rodrigues, B., Pereira, Z., and Oliveira, J.T. (2013). Geochemistry and provenance of the Carboniferous Baixo Alentejo Flysch Group, South Portuguese Zone. Sedimentary Geology 284–285, 133–148.

Jouve, S., Bouya, B. and Amaghzaz, M. (2008). A long-snouted dyrosaurid (Crocodyliformes, Mesoeucrocodylia) from the Paleocene of Morocco: phylogenetic and palaeobiogeographic implications. Palaeontology 51: 281-294. doi: 10.1111/j.1475-4983.2007.00747.x

Kabete, J. M., McNaughton, N. J., Groves, D. I., and Mruma, A. H. (2012). Reconnaissance SHRIMP U–Pb zircon geochronology of the Tanzania Craton: Evidence for Neoarchean granitoid–greenstone belts in the central Tanzania region and the southern east African orogen. Precambrian Research, 216-219, 232-266. Doi:10.1016/j.precamres.2012.06.020.

Kadima, E., Delvaux, D., Sebagenzi, S. N., Tack, L., and Kabeya, S. M. (2011). Structure and geological history of the Congo Basin: An integrated interpretation of gravity, magnetic and reflection seismic data. Basin Research, 23(5), 499-527. Doi: 10.1111/j.1365-2117.2011.00500.X

Kampunzu, A.B., Cailteux, J. (1999). Tectonic evolution of the Lufilian Arc (Central Africa Copper Belt) during Neoproterozoic Pan African orogenesis. Gondwana Research 2 (3), 401-421. http://dx.doi.org/10.1016/S1342-937X (05) 70279-3.

Kemp, A. I. S., Foster, G. L., Scherstén, A., Whitehouse, M. J., Darling, J., and Storey, C. (2009). Concurrent Pb–Hf isotope analysis of zircon by laser ablation multi-collector ICP-MS, with implications for the crustal evolution of Greenland and the Himalayas. Chemical Geology, 261(3), 244-260. doi:10.1016/j.chemgeo.2008.06.019

Kerschhofer, L., Schärer, U., and Deutsch, A. (2000). Evidence for crystals from the lower mantle: Baddeleyite megacrysts of the Mbuji Mayi kimberlite. Earth and Planetary Science Letters, 179(2), 219-225. Doi: 10.1016/S0012-821X (00) 00132-1

Key, R. M., Cotterill, F. P. D., and Moore, A. E. (2015). The Zambezi River: an archive of tectonic events linked to the amalgamation and disruption of Gondwana and subsequent evolution of the African plate. South African Journal of Geology, 118(4), 425-438.

Key, R. M., Charsley, T. J., Hackman, B. D., Wilkinson, A. T., and Rundle, C. C. (1989). Superimposed upper Proterozoic collision-controlled orogenies in the Mozambique orogenic belt of Kenya. Precambrian Research, 44(3-4), 197-225.

King, L.C. (1963). The South African Scenery. Oliver and Boyd, Edinburgh, U.K., pp. 308

Kinny, P. D., and Maas, R. (2003). Lu-Hf and Sm-Nd isotope systems in zircon, in Hanchar, J. M., and Hoskin, P. W. O. (Eds.), Zircon: Mineralogical Society of America Reviews in Mineralogy and Geochemistry 53, p. 327–341, doi:10.2113/0530327.

Klein, N., Bussert, R., Evans, D., Salih, K. A. O., Eisawi, A. A., Nafi, M., and Müller, J. (2016). Turtle remains from the Wadi Milk Formation (Upper Cretaceous) of Northern Sudan. Palaeobiodiversity and Palaeoenvironments, 96(2), 281-303.

Klitzsch, E. (1990). Paleogeographical development and correlation of continental strata (former Nubian Sandstone) in northeast Africa. Journal of African Earth Science, 10 (1-2), 199-213.

Klitzsch, E. H., and Squyres, C. H. (1990). Paleozoic and Mesozoic Geological History of Northeastern Africa Based Upon New Interpretation of Nubian Strata. American Association of Petroleum Geologists Bulletin, 74(8), 1203-1211.

Klitzsch, E., and Lejal-Nicol, A. (1984). Flora and fauna from strata in southern Egypt and northern Sudan. Berliner geowissenschaftliche Abhandlungen, (A) 50, 47-79.

Klitzsch, E., and Wycisk, P. (1987). Geology of the sedimentary basins of northern Sudan and bordering areas. Berliner geowissenschaftliche Abhandlungen, (A) 75.1, 97-136.

Kovacs, R., Schlosser, S., Staub, S. P., Schmiderer, A., Pernicka, E., and Günther, D. (2009). Characterization of calibration materials for trace element analysis and fingerprint studies of gold using LA-ICP-MS. Journal of Analytical Atomic Spectrometry, 24(4), 476-483. doi:10.1039/b819685k

Kroener, A. (1982). Rb-Sr geochronology and tectonic evolution of the Pan-African Damara belt of Namibia, southwestern Africa. American Journal of Science, 282(9), 1471-1507.

Kröner, A. (1985). Ophiolites and the evolution of tectonic boundaries in the late Proterozoic Arabian—Nubian shield of northeast Africa and Arabia. Precambrian Research, 27(1-3), 277-300.

Kröner, A. (2001). The Mozambique belt of East Africa and Madagascar: significance of zircon and Nd model ages for Rodinia and Gondwana supercontinent formation and dispersal. South African Journal of Geology, 104(2), 151-166.

Kröner, A., and Stern, R.J. (2005) Pan-African orogeny: Encyclopedia of geology, v. 1: Amsterdam, Elsevier, p. 1–12.

Kröner, A., Braun, I., and Jaeckel, P. (1996). Zircon geochronology of anatectic melts and residues from a highgrade pelitic assemblage at ihosy, southern Madagascar: Evidence for pan-African granulite metamorphism. Geological Magazine, 133(3), 311-323. doi:10.1017/S0016756800009043

Kröner, A., Sacchi, R., Jaeckel, P. T., and Costa, M. (1997). Kibaran magmatism and Pan-African granulite metamorphism in northern Mozambique: single zircon ages and regional implications. Journal of African Earth Sciences, 25(3), 467-484. doi:10.1016/S0899-5362(97)00117-6

Lana, C., Gibson, R. L., Kisters, A. F., and Reimold, W. U. (2003). Archean crustal structure of the Kaapvaal craton, South Africa–evidence from the Vredefort dome. Earth and Planetary Science Letters, 206(1-2), 133-144.

Lawton, T. (2014). Small grains, big rivers, continental concepts. Geology, 42(7), 639-640. doi:10.1130/focus072014.1

Leeder, M. R. (1991). Denudation, vertical crustal movements and sedimentary basin infill. Geologische Rundschau, 80(2), 441-458.

Le Gall, B., Vétel, W., and Morley, C. K. (2005). Inversion tectonics during continental rifting: The Turkana Cenozoic rifted zone, northern Kenya. Tectonics, 24(2).

Le Loeuff, J., Läng, E., Cavin, L., and Buffetaut, E. (2012). Between Tendaguru and Bahariya: on the age of the Early Cretaceous dinosaur sites from the Continental Intercalaire and other African formations. Journal of Stratigraphy, 36(486), e502.

Leyshon, F. P. (1988). The Proterozoic Magondi mobile belt in Zimbabwe-a review. South African Journal of Geology, 91(1), 114-131.

Link, K., Koehn, D., Barth, M. G., Tiberindwa, J. V., Barifaijo, E., Aanyu, K., and Foley, S. F. (2010). Continuous cratonic crust between the Congo and Tanzania blocks in western Uganda. International Journal of Earth Sciences, 99(7), 1559-1573.

Linol, B. (2013). Sedimentology and Sequence Stratigraphy of the Congo and Kalahari Basins of South-central Africa and Their Evolution During the Formation and Break-up of West Gondwana. (Unpublished PhD thesis), Nelson Mandela Metropolitan University 375 pp.

Linol, B., De Wit, M. J., Barton, E., De Wit, M. M. J., and Guillocheau, F. (2016). U–Pb detrital zircon dates and source provenance analysis of Phanerozoic sequences of the Congo Basin, central Gondwana. Gondwana Research, 29(1), 208-219.

Linol, B., de Wit, M. J., Barton, E., Guillocheau, F., de Wit, M. C., and Colin, J. P. (2015a). Paleogeography and Tectono-Stratigraphy of Carboniferous-Permian and Triassic 'Karoo-Like'Sequences of the Congo Basin. In Geology and Resource Potential of the Congo Basin (pp. 111-134). Springer, Berlin, Heidelberg.

Linol, B., de Wit, M. J., Barton, E., Guillocheau, F., de Wit, M. C., and Colin, J. P. (2015b). Facies analyses, chronostratigraphy and paleo-environmental reconstructions of Jurassic to Cretaceous sequences of the Congo basin. In Geology and Resource Potential of the Congo Basin (pp. 135-161). Springer, Berlin, Heidelberg.

Ludwig, K. R. (2012) User's Manual for Isoplot 3.75-4.15: A Geochronological Toolkit for Microsoft Excel. Berkeley Geochronology Center Special Publication No. 5

Maboko, M. A. H. (1995). Neodymium isotopic constraints on the protolith ages of rocks involved in Pan-African tectonism in the Mozambique belt of Tanzania. Journal of the Geological Society, 152(6), 911-916. doi:10.1144/GSL.JGS.1995.152.01.05

Maboko, M. A., and Nakamura, E. (1996). Nd and Sr isotopic mapping of the Archaean-Proterozoic boundary in southeastern Tanzania using granites as probes for crustal growth. Precambrian Research, 77(1-2), 105-115.

Mahaney, W. C., Krinsley, D. H., Allen, C. C. R., Langworthy, K., Ditto, J., and Milner, M. W. (2012). Weathering rinds: Archives of paleoenvironments on Mount Kenya, east Africa. The Journal of Geology, 120(6), 591-602. doi:10.1086/667805

Majaule, T., Hanson, R. E., Key, R. M., Singletary, S. J., Martin, M. W., and Bowring, S. A. (2001). The Magondi Belt in northeast Botswana: regional relations and new geochronological data from the Sua Pan area. Journal of African Earth Sciences, 32(2), 257-267.

Majaule, T., Hanson, R. E., Key, R. M., Singletary, S. J., Martin, M. W., and Bowring, S. A. (2001). The Magondi Belt in northeast Botswana: regional relations and new geochronological data from the Sua Pan area. Journal of African Earth Sciences, 32(2), 257-267.

Malibangar, A., Lang J., Buoncristiani J. F., Censier, C. (2006). The Mouka-Ouadda Formation; a Cretaceous fluviatile environment in the eastern part of the Central African Republic. Africa Geoscience Review 13(3-4): 301-322 5 Retrieved 10th March 2015 from http://eurekamag.com/research/020/258/020258568.php.

Malibangar, A., Lang, J., and Censier, C. (2001). Use of heavy minerals as indicators of diamantiferous (alluvial) paleo-placers in Central African Republic. Pangea, 35(36), 43-56.

Maluski, H., Coulon, C., Popoff, M. T., and Baudin, P. (1995). 40Ar/39Ar chronology, petrology and geodynamic setting of Mesozoic to early Cenozoic magmatism from the Benue Trough, Nigeria. Journal of the Geological Society, 152(2), 311-326.

Marshall, T. R., and Baxter-Brown, R. (1995). Basic principles of alluvial diamond exploration. Journal of Geochemical Exploration, 53(1), 277-292. doi:10.1016/0375-6742(94)00067-L

Mateer, N. J., Wycisk, P., Jacobs, L. L., Brunet, M., Luger, P., Arush, M. A., Hendriks, F., Weissbrod, T., Gvirtzman, G., Mbede, E., Dina, A., Moody, R. T. J., Weigelt, G., El-Nakhal, H. A., Hell, J., and Stets, J. (1992), Correlation of nonmarine Cretaceous strata of Africa and the Middle East. Cretaceous Research, 13(3), 273-318.

Mateus, O., Jacobs, L., Polcyn, M., Schulp, A. S., Vineyard, D., Neto, A. B., and Antunes, M. T. (2009). The oldest African eucryptodiran turtle from the cretaceous of Angola. Acta Palaeontologica Polonica, 54(4), 581-588. doi:10.4202/app.2008.0063

Mathu, E. M., and Davies, T. C. (1996). Geology and the environment in Kenya. Journal of African Earth Sciences, 23(4), 511-539. doi:10.1016/S0899-5362(97)00016-X

Matteini, M., Dantas, E. L., Pimentel, M. M., and Bühn, B. (2010). Combined U-Pb and Lu-Hf isotope analyses by laser ablation MC-ICP-MS: Methodology and applications. Anais Da Academia Brasileira De Ciencias, 82(2), 479-491. doi:10.1590/S0001-37652010000200023

McConnell, R. B. (1972). Geological development of the rift system of eastern Africa. Geological Society of America Bulletin, 83(9), 2549-2572.

McCourt, S., Armstrong, R. A., Jelsma, H., and Mapeo, R. B. M. (2013). New U–Pb SHRIMP ages from the Lubango region, SW Angola: insights into the Palaeoproterozoic evolution of the Angolan Shield, southern Congo Craton, Africa. Journal of the Geological Society, 170(2), 353-363.

McCourt, S., Hilliard, P., Armstrong, R. A., and Munyanyiwa, H. (2001). SHRIMP U-Pb zircon geochronology of the Hurungwe granite northwest Zimbabwe: Age constraints

on the timing of the Magondi orogeny and implications for the correlation between the Kheis and Magondi Belts. South African Journal of Geology, 104(1), 39-46.

McDougall, I. A. N., and Brown, F. H. (2009). Timing of volcanism and evolution of the northern Kenya Rift. Geological Magazine, 146(01), 34-47.

McGuire, M., Serra, S., and Day, R. (1985). Surface Geological Evaluation Block 10 Concession N. W. Kenya; Amoco Production Company, Houston, Texas, Internal Report

McKay, M. P., Weislogel, A. L., Fildani, A., Brunt, R. L., Hodgson, D. M., and Flint, S. S. (2015). U-Pb zircon tuff geochronology from the Karoo Basin, South Africa: implications of zircon recycling on stratigraphic age controls. International Geology Review, 57(4), 393-410.

Meadows, M. E. (2001). The role of Quaternary environmental change in the evolution of landscapes: Case studies from southern Africa. Catena, 42(1), 39-57. Doi:10.1016/S0341-8162(00)00115-6

Meneisy, M. Y., and Kreuzer, H. (1974). Potassium-argon ages of Egyptian basaltic rocks. Geologisches Jahrbuch D, 9, 21-31.

Menzies, M., Gallagher, K., Yelland, A., and Hurford, A. J. (1997). Volcanic and non-volcanic rifted margins of the Red Sea and Gulf of Aden: crustal cooling and margin evolution in Yemen. Geochimica et Cosmochimica Acta, 61(12), 2511-2527.

Miall, A. D. (1996). The Geology of Fluvial Deposits: Sedimentary Facies, Basin Analysis. Petroleum Geology. Springer-Verlag, New York, 582.

Milesi, J. P., Kampunzu, H. A. B., Nicol, N., Duguey, E., Leistel, J. M., Saint-Martin, M., Moloto-A-Kenguemba, G. (2006). An overview of the geology and major ore deposits of central Africa: Explanatory note for the 1:4,000,000 map “Geology and major ore

deposits of Central Africa". Journal of African Earth Sciences, 44(4), 571-595. Doi: 10.1016/j.jafrearsci.2005.10.016

M ller, A., Appel, P., Mezger, K., and Schenk, V. (1995). Evidence for a 2 Ga subduction zone: Eclogites in the Usagaran belt of Tanzania. Geology, 23(12), 1067-1070.

Möller, A., Mezger, K., and Schenk, V. (1998). Crustal age domains and the evolution of the continental crust in the Mozambique Belt of Tanzania: Combined sm-nd, rb-sr, and pb-pb isotopic evidence. Journal of Petrology, 39(4), 749-783. doi:10.1093/petroj/39.4.749

Moore, A. E. (2009). Type II diamonds: Flamboyant megacrysts? South African Journal of Geology, 112(1), 23-38.

Moore, A. E. (1999). A reappraisal of epeirogenic flexure axes in southern Africa. South African Journal of Geology, 102(4), 363-376.

Moore, A. E., and Larkin, P. A. (2001). Drainage evolution in south-central Africa since the breakup of Gondwana. South African Journal of Geology, 104(1), 47-68. Doi:10.2113/104.1.47

Moore, A. E., Cotterill, F. P., Main, M. P., and Williams, H. B. (2007). The Zambezi River. Large rivers: Geomorphology and Management, 311-332.

Moore, A., and Blenkinsop, T. (2002). The role of mantle plumes in the development of continental-scale drainage patterns: the southern African example revisited. South African Journal of Geology, 105(4), 353-360.

Moore, A., and Moore, J. (2006). A glacial ancestry for the Somabula diamond-bearing alluvial deposit, central Zimbabwe. South African Journal of Geology, 109(4), 625-636. doi:10.2113/gssajg.109.4.625

Moore, A., Blenkinsop, T., and Cotterill, F. (2009). Southern African topography and erosion history: Plumes or plate tectonics? Terra Nova, 21(4), 310. doi:10.1111/j.1365-3121.2009.00887.x

Moore, J. M., and Moore, A. E. (2004). The roles of primary kimberlitic and secondary Dwyka glacial sources in the development of alluvial and marine diamond deposits in southern Africa Elsevier Ltd. doi:10.1016/j.jafrearsci.2003.11.001

Morag, N., Avigad, D., Gerdes, A., Belousova, E., and Harlavan, Y. (2011). Detrital zircon Hf isotopic composition indicates long-distance transport of north Gondwana Cambrian-Ordovician sandstones. Geology, 39(10), 955-958. doi:10.1130/G32184.1

Morley, C. K., Karanja, F. M., Wescott, W. A., Stone, D. M., Harper, R. M., Wigger, S. T., and Day, R. A. (1999). AAPG Studies in Geology# 44, Chapter 2: Geology and Geophysics of the Western Turkana Basins, Kenya. 19-54

Morley, C. K., Wescott, W. A., Stone, D. M., Harper, R. M., Wigger, S. T., Karanja, F. M. (1992). Tectonic evolution of the northern Kenyan Rift. Journal of the Geological Society of London 149, 333–348.

Mortimer, E., Kirstein, L. A., Stuart, F. M., and Strecker, M. R. (2016). Spatio-temporal trends in normal-fault segmentation recorded by low-temperature thermochronology: Livingstone fault scarp, Malawi Rift, East African Rift System. Earth and Planetary Science Letters, 455, 62-72.

Morton, A., Ellis, D., Fanning, M., Jolly, D., and Whitham, A. (2012). The importance of an integrated approach to provenance studies: a case study from the Paleocene of the Faroe-Shetland Basin, NE Atlantic. Geological Society of America Special Papers 487, 1–12.

Mosley, P. N. (1993). Geological evolution of the late Proterozoic “Mozambique Belt” of Kenya. Tectonophysics, 221(2), 223-250.

Mtelela, C., Roberts, E. M., Hilbert-Wolf, H. L., Downie, R., Hendrix, M. S., O’Connor, P. M., and Stevens, N. J. (2017). Sedimentology and paleoenvironments of a new fossiliferous late Miocene-Pliocene sedimentary succession in the Rukwa Rift Basin, Tanzania. Journal of African Earth Sciences, 129, 260-281.

Muhongo, S., Kröner, A., and Nemchin, A. A. (2001). Single zircon evaporation and SHRIMP ages for Granulite-Facies rocks in the Mozambique belt of Tanzania. The Journal of Geology, 1109(2), 171-189. Doi:10.1086/319240

Muhongo, S., Kröner, A., and Nemchin, A. A. (2001). Single zircon evaporation and SHRIMP ages for granulite-facies rocks in the Mozambique Belt of Tanzania. The Journal of Geology, 109(2), 171-189.

Muhongo, S., Tuisku, P., Mnali, S., Temu, E., Appel, P., and Stendal, H. (2002). High-pressure granulite-facies metagabbros in the Ubendian Belt of SW Tanzania: preliminary petrography and P–T estimates. Journal of African Earth Sciences, 34(3-4), 279-285.

Muia, G. (2015). The "Turkana Grits": Potential Hydrocarbon Reservoirs of the Northern and Central Kenya Basins. (Unpublished PhD thesis), University of Rennes 207 pp.

Murray-Hughes, R. (1933). Notes on the geological succession, tectonics and economic geology of the western half of the Kenya Colony. Report of the geological Survey of Kenya No. 3, 8p.

Myers, T., Tabor, N., and Jacobs, L. (2011). Late Jurassic paleoclimate of Central Africa. Paleogeography Paleoclimatology Paleoecology, 311(1-2), 111-125. Doi:10.1016/j.palaeo.2011.08.013

Næraa, T., Scherstén, A., Rosing, M. T., Kemp, A. I. S., Hoffmann, J. E., Kokfelt, T. F., and Whitehouse, M. J. (2012). Hafnium isotope evidence for a transition in the dynamics of continental growth 3.2 Gyr ago. Nature, 485(7400), 627. doi:10.1038/nature11140

Nash, D. J., and Eckardt, F. D. (2015). Drainage development, neotectonics and base-level change in the Kalahari desert, southern Africa. South African Geographical Journal, 1-13. Doi:10.1080/03736245.2015.1028987

Neumaier, M., Tiercelin, J. J., Nalpas, T., and Castillo, J. M. (2014). Basin Analysis and Petroleum Systems Modeling of the Lokichar Basin (Kenya). In AAPG International Conference and Exhibition: The Spirit Between Continents: Energy Geosciences in a Changing World (pp. 1-p).

Nutz, A., Schuster, M., Boës, X., and Rubino, J. L. (2017). Orbitally-driven evolution of Lake Turkana (Turkana Depression, Kenya, EARS) between 1.95 and 1.72 Ma: A sequence stratigraphy perspective. Journal of African Earth Sciences, 125, 230-243.

Nyblade, A. A., and Robinson, S. W. (1994). The African Superswell. Geophysical Research Letters, 21(9), 765-768. Doi:10.1029/94GL00631

Nyblade, A.A. and Sleep, N.H. (2004). Long lasting epeirogenic uplift from mantle plumes and the origin of the Southern African Plateau. Geoscience Africa 2004, Abstracts volume, University of the Witwatersrand, Johannesburg, South Africa, p499.

O'Connor, P. M., Gottfried, M. D., Stevens, N. J., Roberts, E. M., Ngasala, S., Kapilima, S., and Chami, R. (2006). A new vertebrate fauna from the Cretaceous Red Sandstone Group, Rukwa Rift Basin, southwestern Tanzania. Journal of African Earth Sciences, 44(3), 277-288.

O'Connor, P. M., Sertich, J. J., Stevens, N. J., Roberts, E. M., Gottfried, M. D., Hieronymus, T. L., Jinnah, Z.A., Ridgely, R., Ngasala, S.E. and Temba, J. (2010). The evolution of

mammal-like crocodyliforms in the Cretaceous Period of Gondwana. Nature, 466(7307), 748.

O'Connor, P. M., Sertich, J. J. W., and Manthi, F. K. (2011). A pterodactyloid pterosaur from the Upper Cretaceous Lapurr Sandstone, west Turkana, Kenya. Anais Da Academia Brasileira De Ciências, 83(1), 309-315. doi: 10.1590/S0001-37652011000100019

Oesterien, P. M., and Millsteed, B. D. (1994). Lithostratigraphy, palaeontology, and sedimentary environments of the western Cabora Bassa Basin, lower Zambezi Valley, Zimbabwe. South African Journal of Geology, 97(2), 205-224.

Oesterlen, M. (1976). Karoo-System und pra¨kambrische Unterlage imno¨ rdlichen Angola—I. Stratigraphie, Tektonik und Petrographie. Geologisches Jahrbuch, Reihe B, 20, 3-55, Hannover.

Oesterlen, M. (1979). Karoo-System und pra¨kambrische Unterlage imno¨ rdlichen Angola—II. Diagenese und Sedimentologie des Karoo Systems. Geologisches Jahrbuch, Reihe B, 36, 3-41, Hannover.

Oesterlen, P. M. (1990). A further report on the geology of the Dande west area (western Cabora Bassa Basin, mid-Zambezi Valley). Annals of the Zimbabwe Geological Survey, 15, 1-5.

Oliveira, E., McNaughton, N., Windley, B., Carvalho, M., and Nascimento, R. (2015. Detrital Zircon U–Pb Geochronology and Whole-Rock Nd-Isotope Constraints on Sediment Provenance in the Neoproterozoic Sergipano Orogen. From early passive margins to late foreland basins. Tectonophysics, 662, 183-194.

Owusu Agyemang, P. C., Roberts, E. M., and Jelsma, H. A. (2016). Late Jurassic-Cretaceous fluvial evolution of central Africa: Insights from the Kasai-Congo Basin, Democratic Republic Congo. Cretaceous Research, 67, 25-43.

Owusu Agyemang, P. C., Roberts, E. M., Downie, B., and Sertich, J. J. (2018). Sedimentary provenance and maximum depositional age analysis of the Cretaceous? Lapur and Muruanachok sandstones (Turkana Grits), Turkana Basin, Kenya. Geological Magazine, 1-23.

Partridge, T. C. (1998). Of diamonds, dinosaurs and diastrophism: 150 million years of landscape evolution in southern Africa. South African Journal of Geology, 101(3), 167-184.

Partridge, T.C., Maud, R.R. (1987). Geomorphic evolution of Southern Africa since the Mesozoic. South Africa Journal of Geology 90(2), 179– 208.

Pasyanos, M. E., and Nyblade, A. A. (2007). A top to bottom lithospheric study of Africa and Arabia. Tectonophysics, 444(1), 27-44. Doi:10.1016/j.tecto.2007.07.008

Patyk-Kara, N.G. (2002). Placers in the system of sedimentogenesis. Lithology and Mineral Resources, 37(5), 429-429. doi:10.1023/A:1020268115823

Pearce, J. A., Harris, N. B., and Tindle, A. G. (1984). Trace element discrimination diagrams for the tectonic interpretation of granitic rocks. Journal of petrology, 25(4), 956-983.

Pearson, D. G., er, H. S., Harris, J. W., Kjarsgaard, B. A., O'Brien, H., Rao, N. C., and Sparks, S. (2013). Proceedings of 10th International Kimberlite Conference: Volume 2. India: Springer India. Doi: 10.1007/978-81-322-1173-0

Pereira, E., Rodrigues, J., Reis, B. (2003). Synopsis of Lunda geology, NE Angola: Implications for diamond exploration. Comunicações do Instituto Geológico e Mineiro, 90, 189-212.

Permenter, J. L., and Oppenheimer, C. (2007). Volcanoes of the Tibesti massif (Chad, northern Africa). Bulletin of volcanology, 69(6), 609-626.

Perritt, S.H., Jelsma, H.A., and Armstrong, R. (2011). Paleoproterozoic Sedimentation and Tectonism along the Lucapa Fracture Zone, Angola. Abstract, 23rd Colloquium of African Geology, Johannesburg, 8th-14th January.

Pervov, V. A., Somov, S. V., Korshunov, A. V., Dulapchii, E. V., and Félix, J. T. (2011). The Catoca kimberlite pipe, Republic of Angola: A paleovolcanological model. Geology of Ore Deposits, 53(4), 295-308. doi:10.1134/S1075701511040052

Pettijohn, F. J. (1972). Sand and sandstone. Berlin: Springer-Verlag

Pettijohn, F. J., Potter, P. E., and Siever, R. (1987). Sand and sandstone. New York: Springer-Verlag.

Pin, C., and Poidevin, J. L. (1987). U-Pb zircon evidence for a pan-African granulite facies metamorphism in the Central African Republic. A new interpretation of the high-grade series of the northern border of the Congo craton. Precambrian Research, 36(3-4), 303-312.

Pomeyrol, R. (1968). Nubian sandstone. American Association of Petroleum Geologists Bulletin, 52(4), 589-600.

Pouclet, A., Bellon, H., and Bram, K. (2016). The Cenozoic volcanism in the Kivu Rift: Assessment of the tectonic setting, geochemistry, and geochronology of the volcanic activity in the south-Kivu and Virunga regions. Journal of African Earth Sciences, 121, 219-246. doi:10.1016/j.jafrearsci.2016.05.026

Pratt, M. L. (2007). Imperial eyes: Travel writing and transculturation. Routledge

Puetz, S. J. (2018). A relational database of global U–Pb ages. Geoscience Frontiers, 9(3), 877-891.

Purcell, P. (2014). Oil and Gas Exploration in East Africa: A Brief History. [http://www.searchanddiscovery.com/documents/2014/30388purcell/ndx_purcell.pdf] Accessed on 6th December 2017

Purcell, P. G. (2018). Re-imagining and re-imaging the development of the East African Rift. Petroleum Geoscience, 24(1), 21-40.

Quennel, A.M. (1960). The Rift System and the East African Swell. Proceedings Geological Society London, 1581, 78-86.

Rage, J. C., and Werner, C. (1999). Mid-cretaceous (Cenomanian) snakes from Wadi Abu Hashim, Sudan: The earliest snake assemblage. Palaeontologia Africana, 35, 85-110.

Rainaud, C., Master, S., Armstrong, R. A., and Robb, L. J. (2005). Geochronology and nature of the Paleoproterozoic basement in the Central African Copper Belt (Zambia and the Democratic Republic of Congo), with regional implications. Journal of African Earth Sciences, 42(1), 1-31. Doi:10.1016/j.jafrearsci.2005.08.006.

Rainaud, C., Master, S., Armstrong, R. A., Robb, L. J. (2003). A cryptic Mesoarchean terrane in the basement to the Central African Copperbelt. J. Geological Society of London. 160, 11–14.

Rauhut, O. W. M. (1999). A dinosaur fauna from the Late Cretaceous (Cenomanian) of northern Sudan. Palaeontologia Africana, 35, 61-84.

Rauhut, O. W. M., and Werner, C. (1995). First record of the family dromaeosauridae (dinosauria: Theropoda) in the Cretaceous of Gondwana (Wadi Milk Formation, northern Sudan). Paläontologische Zeitschrift, 69(3-4), 475-489. doi:10.1007/BF02987808

Raveloson, A., Nyblade, A., Fishwick, S., Mangongolo, A., and Master, S. (2015) The Upper Mantle Seismic Velocity Structure of South-Central Africa and the Seismic

Architecture of Precambrian Lithosphere Beneath the Congo Basin. In De Wit, M., Guillocheau, F., and De Wit, M. C. J. (Eds) (2015). Geology and resource potential of the Congo Basin (pp. 3-18). Dordrecht: Springer.

Real, F. (1959), Intrusoes kimberliticas da lunda: Service geol. Portugal Mem., ser. 9a, no. 5, 116 p.

Reeves, C. V., Karanja, F. M., and MacLeod, I. N. (1987). Geophysical evidence for a failed Jurassic rift and triple junction in Kenya. Earth and Planetary Science Letters, 81(2-3), 299-311.

Reis, B. (1972). Preliminary note on the distribution and tectonic control of kimberlites in Angola. 24th International Geological Congress, Montreal, Section, 4, 276-281.

Renne, P. R., Glen, J. M., Milner, S. C., and Duncan, A. R. (1996). Age of Etendeka flood volcanism and associated intrusions in southwestern Africa. Geology, 24(7), 659-662.

Reyment, R. A., and Dingle, R. V. (1987). Palaeogeography of Africa during the Cretaceous period. Palaeogeography, Palaeoclimatology, Palaeoecology, 59, 93-116.

Ries, A. C., Shackleton, R. M., and Dawoud, A. S. (1985). Geochronology, geochemistry and tectonics of the NE Bayuda Desert, N Sudan: implications for the western margin of the late Proterozoic fold belt of NE Africa. Precambrian Research, 30(1), 43-62.

Rino, S., Kon, Y., Sato, W., Maruyama, S., Santosh, M., and Zhao, D. (2008). The Grenvillian and Pan-African orogens: world's largest orogenies through geologic time, and their implications on the origin of superplume. Gondwana Research, 14(1), 51-72.

Roberts, E M., Stevens, N. J., O'connor, P M, Dirks, P H G M., Gottfried, M D., Clyde, W C and Hemming S. (2012). Initiation of the western branch of the East African Rift coeval with the eastern branch. Nature Geoscience, 5(4), 289. Doi: 10.1038/ngeo1432

Roberts, E. M., O'Connor, P. M., Stevens, N. J., Gottfried, M. D., Jinnah, Z. A., Ngasala, S., Choh, A. M., and Armstrong, R. A. (2010). Sedimentology and depositional environments of the Red Sandstone Group, Rukwa Rift Basin, southwestern Tanzania: New insight into Cretaceous and Paleogene terrestrial ecosystems and tectonics in sub-equatorial Africa. Journal of African Earth Sciences, 57(3), 179-212.

Roberts, E. M., O'Connor, P. M., Gottfried, M. D., Stevens, N., Kapalima, S., and Ngasala, S. (2004). Revised stratigraphy and age of the Red Sandstone Group in the Rukwa Rift Basin, Tanzania. Cretaceous Research, 25(5), 749-759.

Roberts, E., Jelsma, H. A., and Hegna, T. (2015). Mesozoic sedimentary cover sequences of the Congo Basin in the Kasai Region, Democratic Republic of Congo. In Geology and Resource Potential of the Congo Basin (pp. 163-191). Springer, Berlin, Heidelberg.

Robles-Cruz, S. E., Escayola, M., Jackson, S., Galí, S., Pervov, V., Watangua, M. and Melgarejo, J. C. (2012). U-Pb SHRIMP geochronology of zircon from the Catoca kimberlite, Angola: Implications for diamond exploration. Chemical Geology, 310-311, 137-147. doi:10.1016/j.chemgeo.2012.04.001

Rollinson, H. R., and Whitehouse, M. (2011). The growth of the Zimbabwe Craton during the late Archaean: An ion microprobe U-Pb zircon study. Journal of the Geological Society, 168(4), 941-952. Doi: 10.1144/0016-76492010-156.

Rubatto, D. (2002). Zircon trace element geochemistry: partitioning with garnet and the link between U–Pb ages and metamorphism. Chemical Geology, 184(1), 123-138.

Sahagian, D. L. (1993) Structural evolution of African basins: Stratigraphic synthesis, Basin Res. 5:41–54.

Sahagian, D. (1988). Epeirogenic motions of Africa as inferred from Cretaceous shoreline deposits. Tectonics, 7(1), 125-138.

Salih, K. A. O., Evans, D. C., Bussert, R., Klein, N., Nafi, M., and Müller, J. (2016). First record of Hyposaurus (Dyrosauridae, Crocodyliformes) from the Upper Cretaceous Shendi Formation of Sudan. Journal of Vertebrate Paleontology. DOI: 10.1080/02724634.2015.1115408.

Sallam, H. M., Gorscak, E., O'Connor, P. M., El-Dawoudi, I. A., El-Sayed, S., Saber, S., Kora, M. A., Sertich, J. J., Seiffert, E.R., and Lamanna, M. C. (2018). New Egyptian sauropod reveals Late Cretaceous dinosaur dispersal between Europe and Africa. Nature Ecology and Evolution, 2(3), 445.

Samuelsson, L., Åhäll, K., and Persson, P. (1997). Geochronology and structural setting of the 1.38 Ga Torpa granite; implications for charnockite formation in SW Sweden. GFF, 119(1), 37. doi:10.1080/11035899709546451

Schaltegger, U., Fanning, C. M., Günther, D., Maurin, J. C., Schulmann, K., and Gebauer, D. (1999). Growth, annealing and recrystallization of zircon and preservation of monazite in high-grade metamorphism: conventional and in-situ U-Pb isotope, cathodoluminescence and microchemical evidence. Contributions to Mineralogy and Petrology, 134(2-3), 186-201.

Schandelmeier, H., Klitzsch, E., Hendriks, F., and Wycisk, P. (1987). Structural development of north-east Africa since Precambrian times. Berliner geowissenschaftliche Abhandlungen, (A) 75.1, 5-24.

Schandelmeier, H., Wipfler, E., Küster, D., Sultan, M., Becker, R., Stern, R. J., and Abdelsalam, M. G. (1994). Atmur-Delgo suture: A Neoproterozoic oceanic basin extending into the interior of northeast Africa. Geology, 22(6), 563-566.

Schärer, U., Corfu, F., and Demaiffe, D. (1997). U-Pb and Lu-Hf isotopes in baddeleyite and zircon megacrysts from the Mbuji-Mayi kimberlite: Constraints on the subcontinental mantle. Chemical Geology, 143(1), 1-16. Doi:10.1016/S0009-2541(97)00094-6

Schl ter, T., and Trauth, M. H. (2008). Geological atlas of Africa: With notes on stratigraphy, tectonics, economic geology, geohazards, geosites and geoscientific education of each country. Berlin: Springer. Doi:10.1007/978-3-540-76373-4

Schrank, E. (1990). Palynology of the elastic Cretaceous sediments between Dongola and Wadi Muqaddam, northern Sudan. Berliner geowissenschaftliche Abhandlungen, (A) 120.1 149-168.

Schrank, E. (1992). Nonmarine Cretaceous correlations in Egypt and northern Sudan: palynological and palaeobotanical evidence. Cretaceous Research, 13(4), 351-368.

Schrank, E. and Awad, M. Z. (1990). Palynological evidence for the age and depositional environment of the Cretaceous Omdurman Formation in the Khartoum area, Sudan. - Berliner geowissenschaftliche Abhandlungen, (A) 120.1 169-182.

Schreve, D. C., Keen, D. H., Limondin-Lozouet, N., Auguste, P., Santisteban, J. I., Ubilla, M., Westaway, R. (2007). Progress in faunal correlation of late Cenozoic fluvial sequences 2000–4: The report of the IGCP 449 biostratigraphy subgroup. Quaternary Science Reviews, 26(22), 2970-2995. doi:10.1016/j.quascirev.2007.07.021

Schull, T. J. (1988). Rift basins of interior Sudan: Petroleum exploration and discovery. American Association of Petroleum Geologists Bulletin, 72, 1128 – 1142.

Scotese, C. R. (2014). Atlas of Late Cretaceous paleogeographic maps, PALEOMAP atlas for ArcGIS, volume 2, The Cretaceous, Maps 16–22, Mollweide Projection.

Sears, J. W. (2013). Late Oligocene-Early Miocene grand canyon: A Canadian connection? Geological Society of America Today, 23(11), 4-10. doi:10.1130/GSATG178A.1

Sereno, P. C., Wilson, J. A., Hans C. E. Larsson, Dutheil, D. B., and Sues, H. (1994). Early Cretaceous dinosaurs from the Sahara. Science, 266(5183), 267-271. doi:10.1126/science.266.5183.267

Shaanan, U., and Rosenbaum, G. (2018). Detrital zircons as palaeodrainage indicators: Insights into southeastern Gondwana from Permian basins in eastern Australia. Basin Research, 30, 36-47.

Shaw, P. A., Thomas, D. S., and Nash, D. J. (1992). Late Quaternary fluvial activity in the dry valleys (mekgacha) of the Middle and Southern Kalahari, southern Africa. Journal of Quaternary Science, 7(4), 273-281.

Shaw, P., and Thomas, D. S. G. (1992). Geomorphology, sedimentation and tectonics in the Kalahari Rift. Isreal Journal of Earth-Sciences 41, 87– 94.

Shoko, D. S. M. (1998). Tectono-sedimentary relationships within the Cabora Bassa Basin, with emphasis on the Dande Sandstone Formation. (Unpublished PhD thesis), University of Zimbabwe 312 pp.

Sickmann, Z. T., Schwartz, T. M., and Graham, S. A. (2018). Refining stratigraphy and tectonic history using detrital zircon maximum depositional age: An example from the Cerro Fortaleza Formation, Austral Basin, southern Patagonia. Basin Research 30 (708–729), Doi: 10.1111/bre.12272.

Sláma, J., and Košler, J. (2012). Effects of sampling and mineral separation on accuracy of detrital zircon studies. Geochemistry, Geophysics, Geosystems, 13(5).

Sleep, N. H. (1996). Lateral flow of hot plume material ponded at sublithospheric depths. Journal of Geophysical Research: Solid Earth, 101(B12), 28065-28083.

Smith, B. H. S., Skinner, E. M. W., and Loney, P. E. (1986). The Kapamba lamproites of the Luangwa Valley, eastern Zambia. Kimberlites and Related Rocks: Proceedings of the

Fourth International Kimberlite Conference, Perth 1986. No. 14. Geological Society of Australia, 1989.

Söderlund, U., Patchett, P. J., Vervoort, J. D., and Isachsen, C. E. (2004). The 176 Lu decay constant determined by Lu–Hf and U–Pb isotope systematics of Precambrian mafic intrusions. Earth and Planetary Science Letters, 219(3), 311-324.

Solari, L. A., Ortega-Gutiérrez, F., Elías-Herrera, M., Ortega-Obregón, C., Macías-Romo, C., and Reyes-Salas, M. (2014). Detrital provenance of the Grenvillian Oaxaca complex, southern Mexico: A zircon perspective. International Journal of Earth Sciences, 103(5), 1301-1315. Doi: 10.1007/s00531-013-0938-9

Spencer, C. J., Kirkland, C. L., and Taylor, R. J. (2016). Strategies towards statistically robust interpretations of in situ U–Pb zircon geochronology. Geoscience Frontiers, 7(4), 581-589.

Stankiewicz, J., and De Wit, M. J. (2006). A proposed drainage evolution model for central Africa—Did the Congo flow east? Journal of African Earth Sciences, 44(1), 75-84. Doi:10.1016/j.jafrearsci.2005.11.008

Stern, R. J. (1994). Arc assembly and continental collision in the Neoproterozoic East African Orogen: implications for the consolidation of Gondwanaland. Annual Review of Earth and Planetary Sciences, 22(1), 319-351.

Stern, R. J. (2002). Crustal evolution in the East African Orogen: a neodymium isotopic perspective. Journal of African Earth Sciences, 34(3-4), 109-117.

Stern, R. J., and Kröner, A. (1993). Late Precambrian crustal evolution in NE Sudan: isotopic and geochronologic constraints. The Journal of Geology, 101(5), 555-574.

Stevens, N. J., Gottfried, M. D., Roberts, E. M., Kapilima, S., Ngasala, S., and O'Connor, P. M. (2008). Paleontological exploration of Africa: A view from the Rukwa Rift Basin

of Tanzania. In: J. G. Fleagle and C. C. Gilbert (Eds.), Elwyn Simons: a search for origins pp. 159-180. Springer, New York, NY.

Stoeser, D. B., and Camp, V. E. (1985). Pan-African microplate accretion of the Arabian Shield. Geological Society of America Bulletin, 96(7), 817-826.

Sultan, M., Chamberlain, K. R., Bowring, S. A., Arvidson, R. E., Abuzied, H., and El Kaliouby, B. (1990). Geochronologic and isotopic evidence for involvement of pre-Pan-African crust in the Nubian Shield, Egypt. Geology, 18(8), 761-764.

Summerfield, M. A. (1991). Tectonic geomorphology. Progress in Physical Geography, 15(2), 193-205.

Sun, S. S., and McDonough, W. S. (1989). Chemical and isotopic systematics of oceanic basalts: implications for mantle composition and processes. Geological Society, London, Special Publications, 42(1), 313-345.

Surpless, K. D., Graham, S. A., Covault, J. A., Wooden, J. L. (2006). Does the Great Valley Group contain Jurassic strata? Reevaluation of the age and early evolution of a classic foreland basin. Geology 34, 21–24

Sykes, L. R. (1978). Intraplate seismicity, reactivation of pre-existing zones of weakness, alkaline magmatism, and other tectonism postdating continental fragmentation. Reviews of Geophysics, 16(4), 621-688.

Tack, L., Wingate, M. T. D., De Waele, B., Meert, J., Belousova, E., Griffin, B., and Fernandez-Alonso, M. (2010). The 1375 Ma “Kibaran event” in Central Africa: Prominent emplacement of bimodal magmatism under extensional regime. Precambrian Research, 180(1), 63-84. Doi:10.1016/j.precamres.2010.02.022

Tang, W., Zhang, Z., Li, J., Li, K., Chen, Y., and Guo, Z. (2014). Late Paleozoic to Jurassic tectonic evolution of the Bogda area (northwest China): Evidence from detrital zircon

U–Pb geochronology. Tectonophysics, 626, 144-156. doi: 10.1016/j.tecto.2014.04.005

Taylor, S. R., and McLennan, S. M. (1985). The continental crust: Its composition and evolution: An examination of the geochemical record preserved in sedimentary rocks. Oxford: Blackwell Scientific.

Thomas, D. S. G., and Shaw, P. A. (1988). Late Cainozoic drainage evolution in the Zambezi basin: Geomorphological evidence from the kalahari rim. Journal of African Earth Sciences, 7(4), 611-618. doi:10.1016/0899-5362(88)90111-X

Thomas, W. A. (2011). Detrital-zircon geochronology and sedimentary provenance. Lithosphere 3 (4): 304–308. doi: https://doi.org/10.1130/RF.L001.1

Thuo, P. (2009). Stratigraphic, Petrographic and Diagenetic Evaluation of Cretaceous/Paleogene Potential Reservoir Sandstones of Western Turkana, Kenya. Implications on the Petroleum Potential of Northwestern Kenya. (Unpublished PhD Thesis) University of Western Brittany, Brest, France, 139 pp..

Tiercelin, J. J., Potdevin, J. L., Morley, C. K., Talbot, M. R., Bellon, H., Rio, A., Le Gall, B. and Vétel, W. (2004). Hydrocarbon potential of the Meso-Cenozoic Turkana Depression, northern Kenya. I. Reservoirs: Depositional environments, diagenetic characteristics, and source rock–reservoir relationships. Marine and Petroleum Geology, 21(1), 41-62.

Tiercelin, J. J., Thuo, P., Potdevin, J. L., and Nalpas, T. (2012b). Hydrocarbon Prospectivity in Mesozoic and Early–Middle Cenozoic Rift Basins of Central and Northern Kenya, Eastern Africa. In: Gao, D. (Ed.), Tectonics and Sedimentation: Implications for Petroleum Systems, American Association of Petroleum Geologists Memoir 100, 1-29

Tiercelin, J., Potdevin, J., Thuo, P. K., Abdelfettah, Y., Schuster, M., Bourquin, S., and Ruffet, G. (2012a). Stratigraphy, sedimentology and diagenetic evolution of the lapur sandstone in northern Kenya: Implications for oil exploration of the Meso-Cenozoic Turkana Depression. Journal of African Earth Sciences, 71-72, 43-79. doi: 10.1016/j.jafrearsci.2012.06.007

Treloar, P. J., and Kramers, J. D. (1989). Metamorphism and geochronology of granulites and migmatitic granulites from the Magondi Mobile Belt, Zimbabwe. Precambrian Research, 45(4), 277-289.

Tucker, R. T., Roberts, E. M., Hu, Y., Kemp, A. I., and Salisbury, S. W. (2013). Detrital zircon age constraints for the Winton Formation, Queensland: contextualizing Australia's Late Cretaceous dinosaur faunas. Gondwana Research, 24(2), 767-779.

Tullow Oil Plc. Half-Year Results Presentation 2017. Available at https://www.tullowoil.com/Media/docs/default-source/3_investors/2017-half-year-results/tullow-oil-2017-half-year-results-presentation.pdf?sfvrsn=2 (accessed on 8 January 2018)

Upchurch, P., Mannion, P. D., Benson, R. B., Butler, R. J., and Carrano, M. T. (2011). Geological and anthropogenic controls on the sampling of the terrestrial fossil record: a case study from the Dinosauria. Geological Society, London, Special Publications, 358(1), 209-240.

Vail, J. R. (1978). Outline of the geology and mineralization of the Nubian shield east of the Nile Valley, Sudan. Precambrian Research, 6 (1), A39-A40.

Vail, J. R. (1985). Alkaline ring complexes in Sudan. Journal of African Earth Sciences, 3(1-2), 51-59.

Van Achterbergh, E., Ryan, C. G., Jackson, S. E., Griffin, W. L. (2001). Appendix 3, data reduction software for LA-ICP-MS. In: Sylvester, P. (Ed.), Laser-Ablation-ICPMS in the Earth Sciences-Principles and Applications. Mineralogical Association of Canada, Short Course Series, pp. 239-243.

Van Balen, R. T., Van der Beek, P. A., and Cloetingh, S. A. P. L. (1995). The effect of rift shoulder erosion on stratal patterns at passive margins: implications for sequence stratigraphy. Earth and Planetary Science Letters, 134(3), 527-544.

Veevers, J. J. (2013). Pangea: Geochronological correlation of successive environmental and strati-tectonic phases in Europe and Australia. Earth-Science Reviews, 127, 48-95.

Vincens, A., Tiercelin, J. J., and Buchet, G. (2006). New Oligocene–early Miocene microflora from the southwestern Turkana Basin: Palaeoenvironmental implications in the northern Kenya Rift. Palaeogeography, Palaeoclimatology, Palaeoecology, 239(3), 470-486.

Wainman, C. C., Hannaford, C., Mantle, D., and McCabe, P. J. (2018a). Utilizing U–Pb CA-TIMS dating to calibrate the Middle to Late Jurassic spore-pollen zonation of the Surat Basin, Australia to the geological time-scale. Alcheringa: An Australasian Journal of Palaeontology, 1-13.

Wainman, C. C., McCabe, P. J., and Crowley, J. L. (2018b). Solving a tuff problem: a new chronostratigraphic framework for Middle to Upper Jurassic strata in eastern Australia using U–Pb zircon dates. AAPG Bulletin, 102.

Walraven, F., and Rumvegeri, B. T. (1993). Implications of whole-rock Pb-Pb and zircon evaporation dates for the early metamorphic history of the Kasaï craton, southern Zaïre. Journal of African Earth Sciences, 16(4), 395-404. Doi:10.1016/0899-5362(93)90098-B.

Walsh, J., and Dodson, R. G. (1969). Geology of northern Turkana. Report Geological Survey of Kenya, 82p.

Ward, J. D. (1998). The Geology of the Calonda Formation, North-East Angola. Abstract, Africa Meeting, August 1998.

Ward, W. C., McDonald, K. C., and Mansour, S. E. I. (1979). The Nubia Formation of the Quseir-Safaga area, Egypt. Annals of the Geological Survey of Egypt, 9, 420-431.

Weishampel, D. B., Barrett, P. M. Coria, R. A. Le Loeuff, J. Xing, X. Xijin, Z. Sahni, A. Gomani, E. M. and Noto, C. R. (2004). Dinosaur Distribution. Pp. 571-606 in D.B. Weishampel, P. Dodson, and H. Osmolska, eds. The Dinosauria, 2nd ed. University of California Press, Berkeley.

Werner, C. (1993). Late Cretaceous continental vertebrate faunas of Niger and northern Sudan. In: U. Thorweihe and H. Schandelmeier (Eds.), Geoscientific research in Northeast Africa 401-405.

Werner, C. (1994). Die kontinentale Wirbeltierfauna aus der unteren Oberkreide des Sudan (Wadi Milk Formation). Berliner geowissenschaftliche Abhandlungen E (B. Krebs-Festschrift), 13, 221-249.

Wescott, W. A., Morley, C. K., and Karanja, F. M. (1993). Geology of the “Turkana Grits” in the Lariu range and Mt. Porr areas, southern Lake Turkana, northwestern Kenya. Journal of African Earth Sciences (and the Middle East), 16(4), 425-435.

White, S. H., De Boorder, H., and Smith, C. B. (1995). Structural controls of kimberlite and lamproite emplacement. Journal of Geochemical Exploration, 53(1-3), 245-264.

Whiteman, A. J. (1970). Nubian Group: origin and status. American Association of Petroleum Geologists Bulletin, 54, 526 – 529.

Whiteman, A. J. (1971). The geology of the Sudan republic. Oxford: Oxford Clarendon Press, 290 pp.

Widlansky, S. J., Clyde, W. C., O'Connor, P. M., Roberts, E. M., and Stevens, N. J. (2018). Paleomagnetism of the Cretaceous Galula Formation and implications for vertebrate evolution. Journal of African Earth Sciences, 139, 403-420.

Wiedenbeck, M., Hanchar, J. M., Peck, W. H., Sylvester, P., Valley, J., Whitehouse, M., Kronz, A., Morishita, Y., Nasdala, L., Fiebig, J. and Franchi, I. (2004). Further characterisation of the 91500 zircon crystal. Geostandards and Geoanalytical Research, 28(1), 9-39.

Williamson, P. G., and Savage, R. J. (1986). Early rift sedimentation in the Turkana basin, northern Kenya. Geological Society, London, Special Publications, 25(1), 267-283.

Wilson, M., and Guiraud, R. (1992). Magmatism and rifting in Western and Central Africa, from Late Jurassic to Recent times. Tectonophysics, 213(1-2), 203-225.

Wolfenden, E., Ebinger, C., Yirgu, G., Deino, A., and Ayalew, D. (2004). Evolution of the northern Main Ethiopian rift: birth of a triple junction. Earth and Planetary Science Letters, 224(1), 213-228.

Woodhead, J. D., Hergt, J. M. (2005). A preliminary appraisal of seven natural zircon reference materials for in situ Hf isotope determination. Geostandards and Geoanalytical Research 29 (2), 183-195.

Wycisk, P. (1991). Stratigraphic update of the nonmarine Cretaceous from SW Egypt and NW Sudan. Cretaceous Research, 12(2), 185-200.

Wycisk, P., Klitzsch, E., Jas, C., and Reynolds, O. (1990). Intracratonal sequence development and structural control of Phanerozoic strata in Sudan. Berliner geowissenschaftliche Abhandlungen, (A) 120.1, 45–86.

Yang, J., Cawood, P. A., Du, Y., Huang, H., Huang, H., and Tao, P. (2012). Large Igneous Province and magmatic arc sourced Permian–Triassic volcanogenic sediments in China. Sedimentary Geology, 261, 120-131

Yao, J., Shu, L., and Santosh, M. (2011). Detrital zircon U–Pb geochronology, Hf-isotopes and geochemistry-new clues for the Precambrian crustal evolution of Cathaysia Block, South China. Gondwana Research. 20, 553–567.

Yao, J., Shu, L., and Santosh, M. (2011). Detrital zircon U–Pb geochronology, Hf-isotopes and geochemistry-new clues for the Precambrian crustal evolution of Cathaysia Block, South China. Gondwana Research, 20, 553–567.

Zanettin, B., Justin Visentin, E., Bellieni, G., Piccirillo, E.M., and Rita, F. (1983). Le volcanisme du Bassin du Nord-Turkana (Kenya): Age, succession et évolution structurale. In: Popoff, M., Tiercelin, J.-J. (Eds.), Rifts et Fossés anciens. Bulletin des Centres de Recherches Exploration-Production Elf-Aquitaine 7, pp. 249–255.

Zheng, Y.-F., Zhang, S.-B., Zhao, Z.-F., Wu, Y.-B., Li, X., Li, Z., and Wu, F.-Y. (2007). Contrasting zircon Hf and O isotopes in the two episodes of Neoproterozoic granitoids in South China: implications for growth and reworking of continental crust. Lithos 96, 127–150.

Zimnisky, P (2017). 2017 global natural diamond production forecasted at 142M carats worth $15.6B [http://www.mining.com/web/2017-global-natural-diamond-production-forecasted-142m-carats-worth-15-6b/] Accessed on 5th October 2017

Zuffa, G. G. (1991). On the use of turbidite arenites in provenance studies: Critical remarks. Geological Society, London, Special Publications, 57(1), 23-29. doi:10.1144/GSL.SP.1991.057.01.03

9. Appendices Published Papers

9.1 Appendix 1

Late Jurassic-Cretaceous fluvial evolution of central Africa: Insights fro the Kasai-Congo Basin, Democratic Republic of Congo

9.2 Appendix 2

Sedimentary provenance and maximum depositional age analysis of the Cretaceous? Lapur and Muruanachok sandstones (Turkana Grits), Turkana Basin, Kenya